

eVTOL Emergency Aircraft

Final Report Draft

Group 11

Designing the H₂ERO



eVTOL

Emergency

Aircraft

Final Report Draft

by

Group 11

to obtain the degree of Bachelor of Science
at the Delft University of Technology,

Author:		Student number:
N. M.	van Dam	4552334
P. A.	Elffers	4549783
N. P. E.	Hogenboom	4556267
M.	Klijn	4326814
B. R. W.	Koot	4393635
J.F.	Kronenburg	4439252
J. L. B. M.	Oreman	4558391
M.	Ozols	4537912
M. A.	Saez Ortuno	4541235
A. F.	van de Weijer	4551133

Tutor:	Joost Ellerbroek	TU-Delft
Coaches:	Borrdeephong Rattanagraikanakorn	TU-Delft
	Colin van der Creek	TU Delft

External client: Simon Taylor Fokker-GKN

June 25, 2019

Version 1.0: first draft



Executive Overview

The aim of this report is to present the final design of the H₂ERO, short for Hydrogen (H₂) Emergency Response Operations. The final design is divided into five main subsystems: propulsion, energy system, aerodynamics, geometry and stability & control, and structures. This report is the fourth report in this design process, following the project plan, baseline report and midterm report. The mission need statement for this project is: design an electrical emergency aircraft that can alleviate the noise impact of airborne medical operations. This executive overview gives a summary of the most important parts discussed in this report.

Requirements

The H₂ERO's initial project set up was due to the necessity of reducing the noise produced by emergency aircraft by 25% in loudness levels. Hence, this was considered as one of the most important requirements. Furthermore, strict requirements were set by the customer on the performance, safety, sustainability, engineering budgets and cost of the aircraft. These requirements have been tabulated below:

Code Identifier	Requirement	Type	Compliance
EVTOL-GNOP-141	The aircraft shall be able to perform vertical take off and landing manoeuvres	Driving	Green
EVTOL-GNOP-142	The range of the aircraft shall be at least 250km at a speed of at least 250km/h with at least 75% of maximum payload	Driving	Green
EVTOL-GNOP-143	The aircraft shall be able to operate at minimum 1000 feet of operating altitude	Regular	Green
EVTOL-GNOP-145	The aircraft shall be able to perform at least 10 emergency missions per day	Driving	Green
EVTOL-GNOP-146	The maximum cleared ground area required for safe take off and landing shall not exceed 25x25m	Driving	Green
EVTOL-GNOP-147	The aircraft shall be electrically powered	Driving	Green
EVTOL-GNTR-101	The aircraft shall be able to carry at least five passengers of 90kg each	Driving	Green
EVTOL-GNTR-102	The aircraft shall be able to carry a payload of at least 400kg in addition to the passengers	Driving	Green
EVTOL-GNSA-152	The aircraft shall be able to safely land and take off in populated areas	Driving	Green
EVTOL-GNNO-110	The aircraft shall reach a noise reduction of at least 25% compared to the EC135 emergency helicopter	Driving	Green
EVTOL-COST-001	Total costs of the production of one aircraft shall not exceed €4 million	Driving	Red
EVTOL-TIME-007	The design project shall be finished before July 2nd	Driving	Green

Table 1: Overview of the requirements regarding the customers of the project

It can be seen that the H₂ERO final design fulfills all but one of the requirements set by the customer. Fulfilling these requirements ensures a satisfied customer and a greater confidence in selling the aircraft.

Propulsion

The propulsion subsystem is separated in two. The forward flight propulsion and the Vertical Take Off and Landing (VTOL) propulsion. This separation was made to improve the performance in both flight phases and in the transition phase. The top requirements involving the propulsion subsystem are: the noise generated, and the power required from chapter . These two must always be satisfied, and thus are imposed as constraints during the design of the propulsion system.

The code developed was intended to set a number of possible combinations which will then be used during integration. Some of the parameters that might vary are: the diameter, the RPM, the disk loading, the number of propellers, and the number of blades. The noise requirement and the number of blades is used to calculate the revolutions per minute of the propeller. Furthermore, if the maximum mach tip speed is chosen, in our case 0.8, the diameter of the propeller is merely the division of the linear speed by the angular speed. Once all these values are known, the power available and the power required can be compared, reducing the number of propulsive system combinations. Each of these combinations is feasible in terms of noise and power but it does not take into account the space required.

Once the combination is finally set, after the subsystem integration has been done, the propulsive system takes care of designing the blades. The program used was XROTOR, this program takes as inputs the pro-

peller diameter, the number of blades, the power required, the airspeed, the altitude, the airfoil and the lift coefficient distribution. Using the Blade Element Theory, the program calculates the forces in the whole blade and optimises the design parameters to reduce as much as possible the drag. The design parameters are for example, the thickness to chord ratio, the chord to radius ratio and the twist of the blade. Finally, the program allows to include either a ducted or a free propeller. After subsystem integration, the following propeller values were chosen:

Forward Flight

The final configuration chosen for the forward flight due to space, noise and power constraints is composed of: 1 single-pusher propeller attached to the back of the fuselage. The noise then is reduced because a single propeller increases the diameter, reduces the RPM required and thus the frequency of the blades, reducing the PNL dB values. The propeller accounts the specifications displayed in Table 2:

Vertical Take-off and Landing

The VTOL propulsion system is composed of four propellers. Four propellers were chose for stability and control because a quadcopter is easy to control and manoeuvre. Furthermore, the space in the vehicle is not sufficient to fit more than four propellers since the diameters would become too large. Two propeller VTOL was not consider due to the lower controllability compared to the four propeller. Due to space constraints during integration, the four propellers did not fit on the wing, as originally thought. Thus, the front propeller diameter was reduced and moved ahead of the wing. The VTOL propeller subsystem has the specifications depicted in Table 3:

Table 2: Forward flight propeller parameters.

Parameter	Value	Unit
$N_{\text{propeller}}$	1	-
N_{blades}	2	-
Diameter	1.73	m
Power available	428000	W
RPM	3000	rpm
Efficiency	0.7441	-
Thrust	4590	N

Table 3: VTOL propeller parameters.

Parameter	Value	Unit
$N_{\text{propeller}}$	4	-
N_{blades}	6	-
Diameter Front Prop	2.93	m
Diameter Back Prop	3.59	m
Power available	259610 x4	W
RPM	1600	rpm
Efficiency	0.0747	-
Thrust Front	11984 x2	N
Thrust Back	12930 x2	N

Fuel Cell System

The liquid hydrogen fuel system has been designed to deliver the power required for the propulsion subsystem and the electronics in the aircraft. The fuel system consists of a fuel tank, proton exchange membrane (PEM) fuel cell, an air intake system, cooling system and a battery. The fuel cell is designed to deliver constant power, higher than the cruise required power and lower than the power required during vertical flight. The battery is charged during cruise and used to deliver peak power during vertical flight. The estimations found after a comprehensive analysis are displayed in Table 4.

Table 4: System weights and volume overview

System	Mass [kg]	Volume [m^3]
Fuel Cell	410.1	0.512
Battery	87.7	0.0762
Fuel Tank	90.86	0.54
Air Intake	15	0.0437
Hydrogen Transport	25	0.045
Cooling	20	0.050
Total:	648.7	1.263

Aerodynamics

The first step in the aerodynamic subsystem design is to select a suitable airfoil for wing planform. First, a preselection of airfoils is made based on the design lift coefficient, minimum thickness to chord ratio (driven by other subsystem dimensions) and camber.

Next, XFOIL is used to make an estimation on the preliminary aerodynamic coefficients, since this proved to be the best software to use in the time span given. The limitations of using XFOIL include the fact that it is designed for low Reynolds numbers, making the analysis for the H₂ERO at a Reynolds number of 14 million less reliable. They should be analysed in more detail using CFD and later validated with windtunnel testing. A simple trade-off is done on several NACA 6 airfoils. This series is selected for its optimised performance in laminar flow. The trade off criteria include maximum lift coefficient, lift over drag ratio, lift coefficient for minimum drag coefficient, moment coefficient in cruise and drag bucket length. Eventually, the NACA64210 airfoil is selected for the wing planform.

The next step is to design the wing planform which should generate lift using the span most efficiently, should not provide an excessive bending moment, should have docile stall characteristics and an acceptable roll responsiveness. For this a tapered wing planform is the most optimum design for H₂ERO, because of the near elliptical lift distribution, reasonable stall characteristics and easier manufacture techniques. The driving factors for designing a highwing configuration for the H₂ERO is the door position and sufficient manoeuvre space when on the ground, needed in the mission profile of the emergency aircraft. The wing is set at an incidence angle of 2.5 degrees in order to keep the fuselage as horizontal as possible, but still providing the higher angles of attack needed for the cruise lift coefficient. No twist will be provided, since this has little effect for unswept wings (the quarter chord sweep is zero).

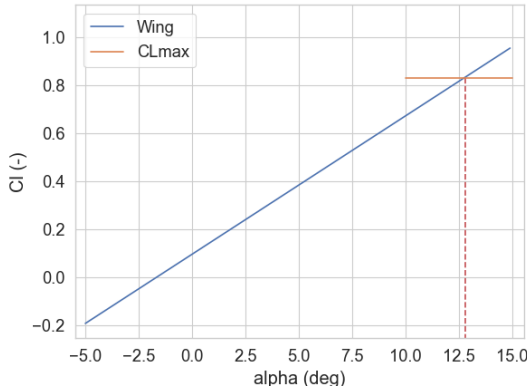
Any aircraft should be designed to have good stall characteristics to ensure safety. It is desired for the wing stall to start at the root and then progress towards the wing tip for increasing angle of attack, else the stall will be unstable and create stability problems. An appropriate wing root fairing should be designed in order to avoid an separation bubble which will increase the drag. Since washout will not be as effective, other ways to keep the wing tips unstalled must be applied. These include applying vortex generators at the leading edge of the wing tip, applying stall fences at the ailerons and a stall strip at the wing root. Additionally a droop leading edge on the wing is applied, delaying stall and aiding in roll stability for high angles of attack.

There are three important aerodynamic aspects of tail design. Firstly, a symmetrical airfoil is chosen for both the horizontal and vertical surface areas, because the net force direction will change. Secondly, the tail has to stall after the main wing in order to ensure that control is still available and the pilot has a chance of moving out of the stall process. Thirdly, the horizontal tail surface area should not be placed in the slipstream in order to avoid tail buffeting, which increases structural fatigue and introduces more noise in the cabin.

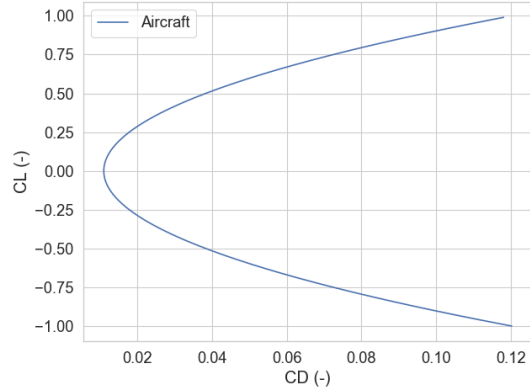
The transition phase from VTOL to forward flight should be correctly designed in order to not loose altitude. This involves keeping the rotors open and producing lift up until the stall speed for the wings is exceeded, so they can take over the full lift needed to carry all the weight. In order to create minimum drag and fly most efficiently, the covering mechanism of the wing integrated rotors must have minimum air flow disturbance. Two mechanisms are considered: an iris shutter mechanism and a linear shutter mechanism, which are positioned such that the airflow sees a thin flat plate, minimising drag.

The main source of airframe noise production for the H₂ERO is the wing trailing edge turning turbulent kinetic energy from the boundary layer into acoustic energy, perceived as noise. This can be reduced by installing porous trailing edge inserts and/or a sawtooth edge which force transition to turbulent flow hence allow the airflow to stay attached longer.

Also, the lift curve slope, maximum lift coefficient, zero lift drag coefficient, drag coefficient and the moment coefficient are converted from 2D to 3D. From these the lift and drag graphs are made, as can be seen in Figure 1a and Figure 1b. Table 5 summarises all the aerodynamic subsystem design results.



(a) Lift coefficient versus angle of attack of the wing



(b) Drag polar of the aircraft

Table 5: Aerodynamic characteristics

Airfoil data			Wing geometry			Wing characteristics		
$C_{l_{des}}$	0.25	[-]	$Sweep_{c/4}$	0	[rad]	C_D at $C_L = 0.25$	0.0169	[-]
$C_{l_{max}}$	1.65	[-]	AR	3	[-]	C_{D_0}	0.0011	[-]
$C_{l_{max\ corrected}}$	1.47	[-]	taper	0.4	[-]	$C_{L_{max}}$ calculation	1.43	[-]
C_{l_a}	6.6842	[1/rad]				$C_{L_{max}}$ calculated	0.83	[-]
C_{l_a} corrected	6.0123	[1/rad]				C_{L_a}	3.3001	[1/rad]
$C_{m_{ac}}$	-0.04	[-]				$C_{m_{ac}}$	-0.04	[-]
α_0	-0.027	[rad]				α_0	-0.027	[rad]
C_{l_0}	0.181	[-]				C_{L_0}	0.0962	[-]

Geometry and Stability & Control

To ensure stability and control of the aircraft throughout all phases of the flight, the specific aircraft geometry definition, as well as the subsequent requirements have to be analysed.

Aircraft Geometry Definition

Once the main aircraft wing planform parameters - wingspan b , surface area S and the main wing aspect ratio A_h had been determined through preliminary sizing methods, the rest of the planform parameters needed to be determined. Firstly, the value of quarter-chord wing sweep angle $\Lambda_{c/4}$ was selected, with the value mainly driven by the desired location of the centre of gravity. The taper ratio λ was selected to achieve the most efficient span-wise lift distribution, also taking the effects of the wing-sweep into account. With definition of these parameters, the trapezoidal wing planform was finalised. The size of the fuselage was mainly driven by the space required within the cabin, as well as by allocating enough space for other aircraft subsystems (e.g. the tank for the energy system) within the fuselage.

The empennage was chosen to feature a double-boom mounted tail configuration, mainly due to its inherent qualities of simpler integration in a combination with a push propeller mounted at the back of the fuselage, as well as the simple structural solution in case the tail arm has to be varied throughout the design, or for a later series of the same aircraft. In order to size the empennage, a detailed approach was performed in the sizing of the horizontal tail, whose surface area was determined by the longitudinal static stability and control requirements, as illustrated in Figure 2. Once the range of the longitudinal centre of gravity was known, a minimum tail size was determined to satisfy both of these requirements. The vertical tail size was based on statistical data on aircraft within the same category and with similar estimated maximum-take-off weight, by selecting a tail-coefficient value $V_v = 0.02$. Consequently, with the vertical tail quarter-chord distance from the most aft centre of gravity and wing geometry known, a total surface area of the vertical tail was estimated. Therefore, a the complete geometry of the aircraft could be defined, as described by Table 6.

Horizontal Flight

Upon identifying layout and main geometrical parameters of the aircraft, the longitudinal weight distribution of the aircraft was assessed to analyse the control and static stability characteristics of the aircraft in

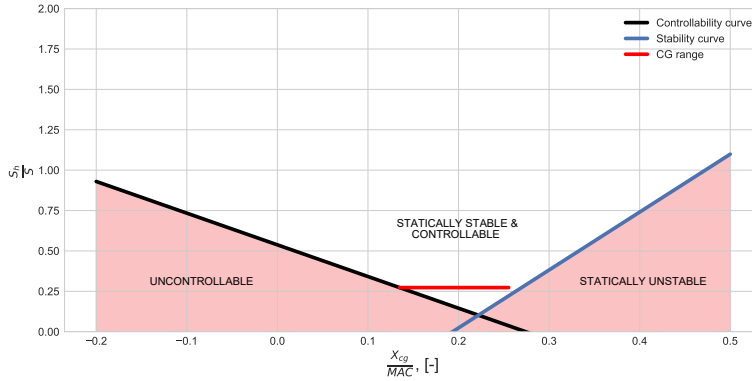


Figure 2: Illustration of the "scissor" plot for horizontal stabiliser sizing for stability and control

Table 6: Geometric definition parameters of the aircraft

Parameter	Value	Parameter	Value
Wing area [m^2]	109.53	Horizontal tail Area [m^2]	29.77
Wingspan [m]	18.13	Vertical tail Area [m^2]	4.21
Wing aspect ratio [-]	3.00	Total aileron area [m^2]	9.87
$\Lambda_{0.25c}$ [-]	0.00	Total rudder area [m^2]	1.01
λ [-]	0.40	Total elevator area [m^2]	6.85
c_r [m]	8.63	Tail arm [m]	9.00
c_t [m]	3.45	Fuselage width [m]	1.50
		Fuselage height [m]	2.10

forward flight. Firstly, the longitudinal centre of gravity and its range was determined. Firstly, the weight of each of the subsystem of the aircraft was estimated either through statistical estimation methods, or through detailed analysis and design of the subsystem, depending on the availability of the information at the stage of longitudinal stability & control assessment. After estimating the position of each subsystem within the aircraft and their weight, an estimate of the longitudinal location of the operational-empty weight of the aircraft was estimated. Assuming that the main contribution to its shift is due to passengers embarking the

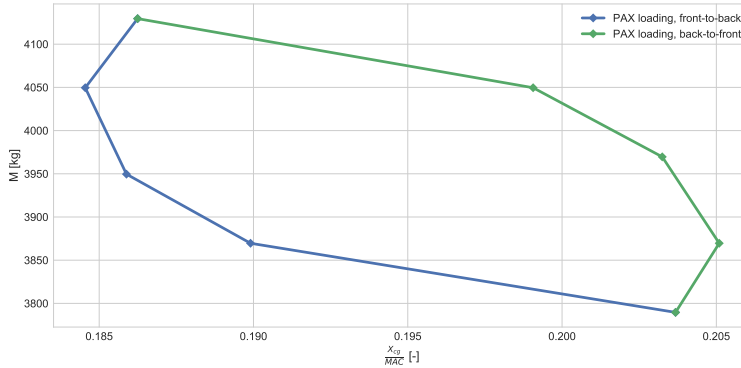


Figure 3: Loading diagram of the aircraft for X_{cg} assessment

aircraft, the range of the centre of gravity was determined, that has been summarised in Figure 3.

By adding a margin to account for unpredicted and unaccounted changes in the centre of gravity of 5% of the length of the mean aerodynamic chord of the aircraft, the centre of gravity location of the aircraft was found to vary between 13% and 26% of the mean aerodynamic chord location of the aircraft. With the longitudinal centre of gravity range known, the horizontal tail surface size is obtained, by estimating the minimum area to satisfy control and static stability requirements shown in Figure 2. Due to time constraints, an assessment of the dynamic stability characteristics under control inputs on the aircraft could not be evaluated, however, an evaluation of control and stability derivatives of the aircraft through e.g. compu-

tational fluid-dynamics model is recommended to analyse the dynamic stability of the aircraft, as well as for its eigenmotion characterisation in forward flight.

Vertical Flight

A thorough analysis is performed to analyse the stability and control aspects of the H₂ERO in vertical flight. Together with advice from an emergency helicopter pilot, the control system requirements are established and these requirements are validated through a numerical simulation of the H₂ERO in vertical flight. Control software is designed to ensure safe, stable operation while still meeting noise requirements to prevent the propulsion system from becoming too loud with the given control inputs. The performance of the control system is such that all centre of gravity positions that can occur during operation still result in a safe, controllable and stable vertical flight.

For vertical flight, the flight control system is an essential component of the aircraft. Without it, vertical flight is not controllable. This is still a safe solution however because both flight controllers as well as sensors that feed into the controllers are working in a redundant system where either one can fail and operation is still guaranteed. These flight control systems have flown on (unstable) aircraft for years already and logged thousands of flight hours. Therefore this is considered a safe way to fly the aircraft.

In the event of a motor failure, the flight control system immediately switches to forward flight mode. This ensures that no pilot inputs get transferred to the remaining 3 motors which could otherwise result in an uncontrollable spinning motion. The four propellers will prevent the aircraft from accelerating too fast by autorotation and the titanium landing gear deforms heavily on impact, absorbing the kinetic energy of the aircraft upon impact. If the pilot thinks there is enough altitude and airspeed for a manoeuvre in which the aircraft is flown to a safe landing spot using the forward propulsion system, there is always the option to try this using the forward flight propulsion system and controls.

Structures & Materials

Due to the configuration of the H₂ERO with two integrated propellers in the wings it is a challenge to make the wings strong enough and capable to withstand all the loads. It is chosen to use two I-beams right beside the propellers to cover the bending moment acting on the wing. The dimensions of the beams can be seen in Table 10.1.

Table 7: Dimensions of the two I-beams given in mm.

Values are in mm.	Root				Tip			
	Height	Flange Width	Flange Thick.	Web Thick.	Height	Flange Width	Flange Thick.	Web Thick.
Beam 1	579	193	35	1.2	233	4	0.5	0.5
Beam 2	771	257	14.5	1.6	311	5.5	0.6	0.6

Furthermore, a wing box with a hole for the propeller is implemented in the wing to cover the torsion and shear of the wing. It is found that the thickness of the wing box skin is 1 mm for the leading edge semi-ellipse and trailing edge part and 0.5 mm for the skin that is behind the propellers.

The fuselage of the aircraft has to be able to withstand the loads from the wings, the propellers, the tail and during landing, from the landing gear. In order to do so, stringers are implemented along the fuselage to carry most of the loads as bending and axial loads. The skin is assumed to withstand all the shear. It was found that 12 stringers will be used in total. The skin thickness is found to be 1.2 mm, while the cabin width is 1.5 m and the height is 2.1 m.

Materials have been chosen for several structures of the H₂ERO. With the eye on the future and noise reduction of this aircraft it seems promising to further investigate the use of Flexfoil for the outer skin of both the main wing and the tail. Concerning the wing box, aluminium is used because of the easy manufacturing and low cost compared to composites. The fuselage will be made out of composites and GLARE in places where impacts can be expected. The propellers will have the same materials as used as the EC135 main rotor blades. This means a core of a foam material, a skin of glass fibre composites and an erosion protection

layer of titanium. Lastly, the landing gear must be able to sustain high impact loads, so therefore titanium will be used.

Subsystem Integration

The method to integrate all the different subsystems consisted of three phases. The first phase was to make sure that all of the subsystems use the same initial parameters. This was done by means of a code able to extract the initial parameters from a common excel file. The second phase made sure that when an input from a subsystem was the output of the other, that there was proper communication between departments. Initially it was done through verbal communication. Using this method during the iterations was not efficient, therefore, a subsystem integration program was developed. As the final sizing process is iterative in nature (due to each change of a subsystem leaving impact on the other subsystem designs), the sizing process has to be performed until characteristic values of the aircraft subsystems directly involved in the data flow within the iteration process converge to their final values, yielding the final parameters of the aircraft. These final parameters can be observed in Table 8 and the final configuration in Figure 5.

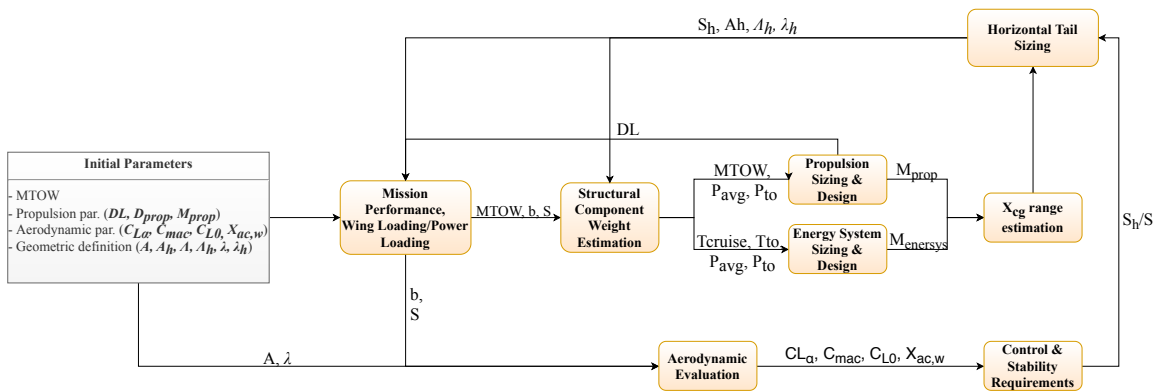


Figure 4: Aircraft balance and sizing process through iteration

Table 8: Initial parameters used for the sensitivity analysis of the propeller.

Paramater	Value	Unit	Paramater	Value	Unit
Wing aspect ratio	3,00	-	MTOW	4150	kg
Wingspan	18,13	m	Back Propeller Diameter	3.59	m
Wing surface area	109,53	m ²	Forward Propeller Diameter	2.93	m
Wing taper ratio	0,40	-	FF Propeller Diameter	1.73	m
Wing Δc/4	0,00	deg	Power Required VTOL	1038	kW
Root chord [m]	8,63	m	Power Required FF	377	kW
Tip chord [m]	3,45	m	Noise VTOL	83,14	dB
XLECr	4,00	m	Noise FF	52	dB
t/c	0,1	-	Payload Mass	628	kg
Tail surface area	29,77	m ²	Number of Passengers	4	-
Range	346	km	Number of pilots	2	-
Speed	82,72	m/s	MAC	6,41	m

Performance

After the subsystems have been integrated, a performance analysis is done to assess performance and check if the design meets all requirements. A payload - range, power available - power required, endurance and load factor analysis have been performed. The maximum range the aircraft is able to fly is 303 km. The maximum endurance 5.5 hours. In terms of power reserve, the aircraft complies with the requirements and meets all mission performance parameters.

Final Design

The final mass and power budget is described in Table 9. The power budget consists of the power required for the rotors and electronic subsystems, described in 'Fuel Cell System' and 'Propulsion' of this executive overview. The final configuration is shown in

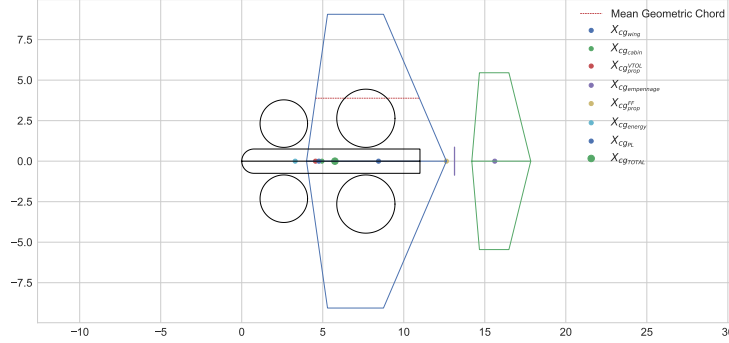


Figure 5: Visualisation of preliminary fully-integrated aircraft

Table 9: Mass budget of the initial design.

Subsystem	Mass [kg]
Wing	335
Figure 9 and Figure 10 Cabin	1511
Empennage	133.92
VTOL Propulsion	467
Energy Source	485
FF Propulsion	187
Flight Controls	48
Electrical	110
Avionics	116
Furnishing	24.7
Hydraulics	43.46
Payload	628
Total	4151

Operations and Logistics

Having a good overview of the operations and logistics is crucial for designing an emergency aircraft. Before taking off the aircraft has to be fuelled within 10 minutes, meaning a minimum fuel rate of 0.063 kg/s. Additionally, the battery is charged in between missions when possible. The operations diagram is shown in Figure 6.

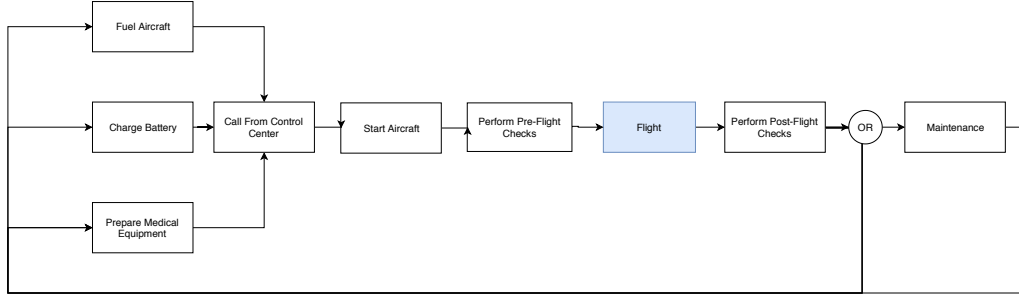


Figure 6: Operations Diagram

Manufacturing, Assembly and Integration Plan

An analysis is done to select which parts of the airframe should be easily accessible and separable from the rest of the aircraft. This greatly reduces maintenance cost because components that likely need service can be replaced and taken apart easily. For all airframe parts their production methods have been chosen such that they can be made to a sufficient standard of quality. Joining methods for the different divisions have been chosen to assemble the whole airframe. Attention has been given to connect carbon fibre composites and aluminium in such a way that galvanic corrosion will not occur, with a layer of titanium in between them. The electrical conductivity of the skin has also been considered to prevent problems when the aircraft is struck by lightning. The requirement that all assembly and production techniques used should be available today is shown to be met. To conclude an analysis is done to give an estimate for the required man-hours during production based on other aircraft manufacturers' data and the expected amount of delivered aircraft. With a slope of 80%, after 100 aircraft delivered the number of man-hours required is already far

below 60000.

Cost Estimate and Market Analysis

The costs of the H₂ERO are determined in three categories. Firstly the expected development and design cost is found to be 10.2 million. Expenses that have been taken into account include engineering costs, tool development, testing costs, quality control and supporting services. Secondly the production cost turns out to be 6.5 million dollars. This is more than 1.5 times the required price by the customer. It is believed that this is mainly caused by the expensive hydrogen technology. But due to the high level of uncertainty of the propulsion system costs, this is not a final figure, more research has to be done. Also the hydrogen technology cost will likely reduce in the coming 15 years, this will require estimation updates through the years. Thirdly the operational cost turned out to be 625.000 dollars per aircraft. Factor considered are fuel cost, battery charged cost, maintenance, overhauls and insurance. Again the biggest cost driver is the hydrogen technology. An emergency helicopter has to have a high availability and fly often around 10 time per day. Taking off and landing that often especially vertically requires a lot of LH₂. The aircraft therefore consumes 35 kg's of LH₂ per hour ¹, while a price of the fuel of 8 dollars and 29 cents per kilogram is only possible using the newest, most cost efficient state of the art hydrolyses technology. Perhaps in the near future new methods can be developed or current methods can be scaled up in order reduce the cost of the fuel. This technology has great potential to drive down the operational cost.

A final remark on the costs found for the H₂ERO regards the quantity of aircraft produced. The Netherlands only requires five aircraft (including one spare) to fully provide its people with Medical Aerial Assistance. Therefore for all three cost categories are calibrated to that figure. The cost and production time exponentially decrease with unit production. This effect is thought to especially decrease the production and maintenance costs.

The current way the Netherlands system is structured, starts by the government. The government provides 4 large hospitals the financial resources to hire an operation company for the Medical Aerial Assistance service. These hospitals chose every 15 years a company for this. In 2018 the "ANWB" was reelected to fulfil this job. The aircraft of choice is the EC-135 Airbus Eurocopter since it had proven itself worthy the last decade. In order for the H₂ERO to take over 15 years from now, the ANWB or rivaling companies have to convinced that this aircraft will be better than the EC-135. These companies are the main target to sell to and the EC-135 is the only significant rival.

The H₂ERO has multiple big advantages. First and foremost is it 25% more quiet. The reason why this design was initiated in the first place is because the current emergency aircraft are under pressure by the public and regulations to fly less, higher or farther from the people because of the nuisance of noise. The H₂ERO alleviates the noise in a densely urbanised country as the Netherlands. Secondly the hydrogen fuel has the potential to reduce the harmful emissions to zero. As this aircraft will be widely seen by the public while doing this thankful job, the companies and the government are really interested in connecting their name to such a vehicle.

The large draw back of this aircraft is its cost. Producing and operating it is more expensive than the known and proven EC-135, which uses cheaper kerosene and conventional turbo shaft engines. This has to be addressed in further design in order to compete with the EC-135. Technology of the propulsive system of the H₂ERO has yet to be tested and improved to reduce its cost and more extensive estimations have to be done to fairly compare the two aircraft. The options are still open.

Risk Management

For the H₂ERO a risk analysis has been done regarding the technical performance, schedule and cost. For any significant risks a risk mitigation has been written. For the technical risks, no significant risks were found that required mitigation. However, many risks were on the limit of requiring mitigation. For the schedule, two risks were dependent on third party organisation. These should be monitored extensively with strong communication. Finally, for the cost risks one risk was identified that required mitigation. This was the risk of an investor leaving the project. Without money, there is no H₂ERO. Good communication should keep the customers satisfied and up to date on design changes

¹still insignificantly small compared to the fuel consumption of the EC-135

RAMS Analysis

The Reliability, availability, maintainability and safety has been assessed for the H₂ERO. A reliability map of all of the subsystems and their failure modes is determined. Furthermore, the H₂ERO is expected to be available 92.4% of the time. A maintainability plan has been set up resulting in three maintenance phases, namely, the daily visual check, the scheduled maintenance and unscheduled maintenance. Finally, the safety of the H₂ERO is assessed as well. All maintenance and safety requirements are complied with.

Sustainability

A sustainable development strategy is developed for the three main categories: environmental, economic and social sustainability. The results of the examined categories are graphically represented in Figure 8. Here end of life (EOL) procedures include repair, reconditioning, remanufacturing and recycling. The technical readiness level (TRL) is estimated for point of entry into service of the H₂ERO, which is set to be in 15 years. If all the scores are added H₂ERO scores 48 and the EC-135 scores 43 (where the maximum would be 12 categories times the maximum score of 5 equals 60). This indicates that H₂ERO is expected to be slightly more sustainable than the EC-135. The main reasons for this are the non-harmful emissions and noise reduction, resulting in a better score on environmental (and to a lesser extent social) sustainability, as visualised in Figure 7.

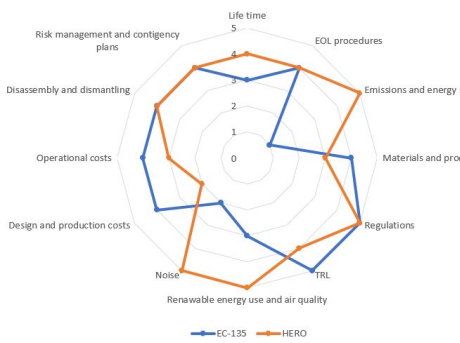


Figure 7: Overview of the sustainability analysis for H₂ERO and EC-135. Starting from the top, environmental, social and economic sustainability factors are indicated in clockwise direction respectively.

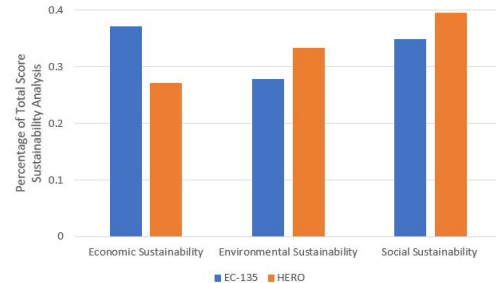


Figure 8: Overview of sustainability analysis for H₂ERO and EC-135 for the main categories

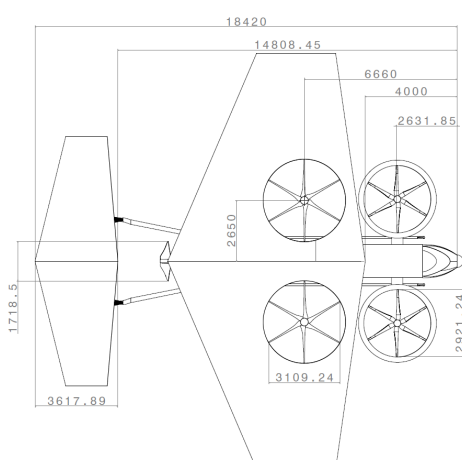


Figure 9: Technical drawing of top view of the aircraft.

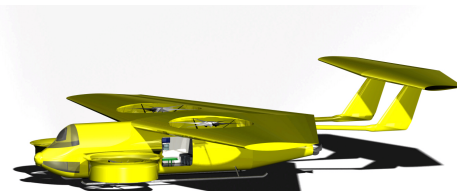


Figure 10: Render with clear view of the door.

List of Acronyms

AoA	Angle of Attack	MTOW	Maximum Take Off Weight
AR	Aspect Ratio	PEM	Proton Exchange Membrane
CAD	Computer Aided Design	PID	Proportional Integral Derivative
CFD	Computational Fluid Dynamics	RPM	Revolutions per Minute
DL	Disk Loading	SPL	Sound Pressure Level
eVTOL	Electric Vertical Take-Off and Landing	STOL	Short Take Off and Landing
ICAO	International Civil Aviation Organisation	TRL	Technology Readiness Levels
MAC	Mean Aerodynamic Chord	VTOL	Vertical Take Off and Landing
MTOM	Maximum Take Off Mass		

List of Symbols

Symbol	Unit	Property
A	m	Aspect ratio
b	m	Wingspan
b_{contr}	m	Span of the control surface
$b_{main\ surface}$	m	Span of the main surface
c_r	m	Root chord
c_t	m	Tip chord
c_{contr}	m	Chord length of the control surface
c_{local}	m	Chord length of the main surface
C_{L_h}	-	Horizontal tail lift coefficient
$C_{L_{A-h}}$	-	Aircraft-less-tail lift coefficient
$C_{L_{a_h}}$	1/rad	Horizontal tail lift curve slope
C_{L_α}	1/rad	Aircraft lift curve slope
$C_{m_{ac}}$	-	Moment coefficient of the aircraft around its aerodynamic centre
N_z	-	Ultimate load factor
(t/c)	-	Thickness-to-chord ratio
K_{door}	-	Door factor for fuselage weight estimation
K_{lg}	-	Landing gear factor for fuselage weight estimation
K_{ws}	-	Wing geometry factor for fuselage weight estimation
C_m	-	Moment coefficient
S	m^2	Wing surface area
S_h	m^2	Horizontal tail surface area
S_v	m^2	Vertical tail surface area
S_{csw}	m^2	Control surface area
X_{ac}	m	Longitudinal position of the aircraft aerodynamic centre
X_{cg}	m	Longitudinal position of the aircraft centre of gravity
$X_{LE_{Cr}}$	m	Longitudinal position of the leading edge of the wing's root chord
W_{dg}	kg	Design gross-weight of the aircraft
α	deg	Angle of attack
$\Lambda_{0.25c}$	deg	Quarter chord sweep of the wing
$\Lambda_{0.25c_h}$	deg	Quarter chord sweep of the horizontal tail
$\Lambda_{0.25c_v}$	deg	Quarter chord sweep of the vertical tail
λ	-	Wing taper ratio
λ_h	-	Horizontal tail taper ratio
λ_v	-	Vertical tail taper ratio
\overline{V}_v	-	Vertical tail volume coefficient

Contents

Executive Overview	xi
List of Acronyms	xii
List of Symbols	xiii
1 Introduction	1
2 Requirements	2
2.1 Customer Requirements	2
2.2 User Requirements	2
2.3 Subsystem Requirements	3
2.4 Technical Requirements	4
2.5 Non-Technical Requirements	6
3 Preliminary Concepts	7
3.1 Energy System Trade-Off	7
3.2 Concept Trade-Off	7
4 Sustainable Development Strategy	9
4.1 Approach to Sustainable Design Engineering	9
4.2 Sustainability Analysis	10
5 Detailed Design: Propulsion Subsystem	11
5.1 Requirements & Constraints	11
5.2 Analysis Description	12
5.3 Configurations	13
5.4 Blade Design	14
5.5 Motor and Motor Controller Selection	14
5.6 Propulsion System Mass Estimation	15
5.7 Requirement Compliance & Feasibility	15
6 Detailed Design: Fuel System	16
6.1 System Overview	16
6.2 Fuel Cell	16
6.3 Reactant Supply System	17
6.4 Fuel System Overview	19
6.5 Fuel System Sizing	19
6.6 Requirement Compliance & Feasibility	22
7 Detailed Design: Electrical System	23
7.1 Electrical System Weight Estimation	23
7.2 Requirement Compliance & Feasibility	24
8 Detailed Design: Aerodynamics	25
8.1 Airfoil Selection	25
8.2 Wing Design	30
8.3 Tail	35
8.4 Transition Phase	35
8.5 Noise Reduction Techniques	35
8.6 Requirement Compliance & Feasibility	36
9 Detailed Design: Geometry Definition, Stability and Control	37
9.1 Aircraft Geometry Definition	37
9.2 Subsystem Weight Estimates	39
9.3 Balancing, Longitudinal Stability and Control	42

9.4 Stability and Control in Vertical Flight	44
9.5 Control Surfaces Actuators	50
9.6 Requirement Compliance & Feasibility	51
10 Detailed Design: Structures and Materials Subsystem	52
10.1 Wing Design	52
10.2 Cabin Design	54
10.3 Fuselage Design	59
10.4 Materials	61
10.5 Requirement Compliance & Feasibility	65
11 Subsystem Integration Method	66
11.1 Initial Parameter Integration	66
11.2 Continuous Integration	66
11.3 Propulsion Subsystem	66
11.4 Fuel Subsystem	70
11.5 Electrical Subsystem	70
11.6 Aerodynamics Subsystem	71
11.7 Structures Subsystem	72
11.8 Configuration Iterations	73
11.9 Final Design	75
12 Performance	77
12.1 Payload Range	77
12.2 Power-Airspeed	77
12.3 Endurance	78
12.4 Manoeuvre and Gust Load Diagram	78
13 Verification and Validation	80
13.1 Verification	80
13.2 Validation	83
14 Sensitivity Analysis	86
14.1 Propulsion Subsystem	86
14.2 Fuel Subsystem	88
14.3 Aerodynamics Subsystem	89
14.4 Structures Subsystem	91
14.5 Integration Sensitivity Analysis	92
15 General Requirements Compliance and Feasibility	94
15.1 Remaining Technical Requirements	94
16 Design Recommendations	96
16.1 Full Aircraft Configuration	96
16.2 Transition Phase	96
16.3 Propulsion	97
16.4 Fuel System	97
16.5 Electronics	97
16.6 Aerodynamics	97
16.7 Structures and Materials	98
16.8 Stability and Control	98
17 Operations and Logistics	99
17.1 Mission Profile	99
17.2 Operations Analysis	99
17.3 Functional Analysis	100
17.4 Requirement Compliance & Feasibility	100
18 Manufacturing, Assembly and Integration Plan	104
18.1 Divisions	104

18.2 Production Process.	105
18.3 Labour Hours and Learning Curve	107
18.4 Requirement Compliance & Feasibility.	107
19 Aircraft Interface Definition	108
19.1 Hardware Interface.	108
19.2 Software Interface	108
19.3 Communication Flow	108
19.4 Data Handling	110
20 Cost Estimate and Market Analysis	111
20.1 Cost Estimate	111
20.2 Development Cost	111
20.3 Product cost	112
20.4 Operation Cost	113
20.5 Market Analysis.	114
20.6 Requirement Compliance & Feasibility Analysis.	116
21 Risk Management	117
21.1 Technical Risk Identification Process	117
21.2 Technical Performance Risks	117
21.3 Schedule Risks	118
21.4 Cost Risks	119
22 RAMS Analysis	120
22.1 Reliability	120
22.2 Availability	121
22.3 Maintainability	121
22.4 Safety	122
23 Sustainability Analysis	123
23.1 Environmental Sustainability	123
23.2 Social Sustainability	125
23.3 Economic Sustainability	127
23.4 Sustainability Overview and Conclusion	128
24 Future steps	129
24.1 Future Project Development	129
24.2 Expectancy	129
25 Conclusion	131
Bibliography	132

Introduction

When a major accident happens, it can be a matter of life and death regarding being at the patient fast, giving treatment and performing transport to a medical institution. A crucial role in transporting a doctor to a site of incident is the emergency helicopter, which flies out over six times a day. These aircraft do not only enable emergency doctors to perform life-saving procedures, they can be used to transport patients to hospitals as well with great speed. Since helicopters do not have to use roads, they can fly more directly and do not have traffic problems, compared to ambulances. Furthermore, they get priority in the air, meaning other aircraft have to wait or fly around them. Even though the necessity of emergency helicopters are unquestioned, problems with performing missions are arising due to their large production of noise. These aircraft are stationed at airports, which have strict noise regulations to adhere to. Contrary to police helicopters, which fall out of the noise legislation, emergency helicopters fall within these rules. An emergency can happen at any time of the day or night, when restrictions are even stricter, and air traffic control can not ground them. However, airports are increasingly less willing to let these helicopters fly away whenever they need to due to these noise regulations, since it reduces the amount of commercial flights they can have. As electric flying is on the rise, a solution for the noise problem can be found in this report. An alternative to the current emergency helicopter, the EC-135, is the H₂ERO (Hydrogen (H₂) Emergency Response Operations), an electric vertical take-off and landing aircraft. This aircraft should be able to adhere to stricter noise regulations while being more sustainable than current helicopters and it should be able to operate missions in multiple situations including densely populated area's.

The aim of this report is to generate a detailed design of the H₂ERO. The subsystems that will be looked into are the propulsion, stability and control, aerodynamics and the structures, which will be integrated into one final design. Furthermore, this report aims to analyse the performance, production, operations, risks and costs to see how the aircraft will perform its missions in different scenario's and how the aircraft can compete with current helicopters. This is the fourth and final report in this design project, following the project plan, the baseline report and the midterm report.

In order to get to a finalised design, several steps are to be taken. In this report, the process to get the detailed design is described in the following way: first, the requirements and preliminary concepts are revisited in chapter 2 and chapter 3 respectively. Secondly, a sustainable development strategy is developed in chapter 4 to use during the designing, which is next. In the detailed design phase, the propulsion, fuel and electric systems are designed in chapter 5, chapter 6 and chapter 7 respectively. chapter 8 describes the aerodynamics, while chapter 9 explains the stability and control of the H₂ERO. Continuing, a structural analysis of the aircraft is performed in chapter 10, as well as the cabin design and the material choice. Afterwards, all subsystems are integrated in chapter 11 and the performance is analysed in chapter 12. The methods are then verified and validated in chapter 13 and a sensitivity analysis is performed in chapter 14. Furthermore, the compliance with the general requirements are checked in chapter 15 and recommendations on the design are given in chapter 16. Then, subsection 11.9.2 describes the mass and power budgets, while chapter 17 elaborates on the operations and logistics of the H₂ERO. The production is analysed in chapter 18. In chapter 19, the interfaces of the aircraft are given. Then, the cost estimates and market analysis is described in chapter 20 and the risk management is given in chapter 21. Additionally, a RAMS analysis is performed in chapter 22 and a sustainable analysis is done in chapter 23. At last, the future steps for the development of this project are stated in chapter 24 and finally, conclusions are drawn in chapter 25.

Requirements

The set up of this project comes from various needs of the customer, being Fokker-GKN, and the stakeholders involved. These needs have lead to requirements that have mostly been established at the beginning of the project. As nothing is certain and change is essentially inevitable through research, the requirements have been considered to be live. Hence, if required due to for example feasibility issues, requirements have been altered in discussion with the customer and stakeholders. However, this does not mean that requirements are always discussed and changed if they are not met but only if they seem greatly unrealistic.

This chapter introduces the requirements as they stand. The requirements have been grouped as follows; customer requirements in section 2.1, user requirements in section 2.2, subsystem requirements in section 2.3, technical requirements in section 2.4 and finally the non-technical requirements in section 2.5.

The customer, stakeholder and user requirements come from a selection of subsystem, technical and non-technical requirements. Hence, it can be possible that these are mentioned more than once as they are relevant for multiple sections. Furthermore, it should be noted that each grouped set of requirements in the following sections is further analysed to determine their compliance with the final design. This is done in each respective chapter in the report. Also, their compliance is verified through one of four means. These are inspection, demonstration, analysis and test. Inspection is the easiest, quickest and cheapest. It is done by the use of the humans one of five senses. Analysis is done when the other means are not appropriate or you can't afford a costly test or demonstration. It is done by collecting data and using your engineering judgement and knowledge to determine if a criteria has been met. Demonstration is done by running at least one test that does not require any costly and special testing equipment. Finally, testing is the most costly verification and requires special testing equipment to be performed. For the requirements of which there are no relevant subsystem design chapters, like the transport and noise requirements, a requirement compliance chapter has been established in chapter 15.

2.1. Customer Requirements

This section touches upon the requirements which are assumed to be important to keep the customer satisfaction and expectations at a high level.

Table 2.1: Overview of the requirements regarding the customers of the project.

Code Identifier	Requirement	Type
EVTOL-GNOP-141	The aircraft shall be able to perform vertical take off and landing manoeuvres	Driving
EVTOL-GNOP-142	The range of the aircraft shall be at least 250km at a speed of at least 250km/h with at least 75% of maximum payload	Driving
EVTOL-GNOP-143	The aircraft shall be able to operate at minimum 1000 feet of operating altitude	Regular
EVTOL-GNOP-145	The aircraft shall be able to perform at least 10 emergency missions per day	Driving
EVTOL-GNOP-146	The maximum cleared ground area required for safe take off and landing shall not exceed 25x25m	Driving
EVTOL-GNOP-147	The aircraft shall be electrically powered	Driving
EVTOL-GNTR-101	The aircraft shall be able to carry at least five passengers of 90kg each	Driving
EVTOL-GNTR-102	The aircraft shall be able to carry a payload of at least 400kg in addition to the passengers	Driving
EVTOL-GNSA-152	The aircraft shall be able to safely land and take off in populated areas	Driving
EVTOL-GNNO-110	The aircraft shall reach a noise reduction of at least 25% compared to the EC135 emergency helicopter	Driving
EVTOL-COST-001	Total costs of the production of one aircraft shall not exceed €3.500.00	Driving
EVTOL-TIME-007	The design project shall be finished before July 2nd	Driving

2.2. User Requirements

This section shows an overview of the various requirements set to ensure users of the aircraft are satisfied.

Table 2.2: Overview of the requirements regarding the users of the aircraft.

Code Identifier	Requirement	Type
EVTOL-GNTR-103	The aircraft dynamics during take off, flight and landing shall ensure that the state of the patient will not deteriorate during transport as a result of vibrations	Driving
EVTOL-GNTR-104	The aircraft shall provide faster transportation from accident site to hospital than an ambulance	Driving
EVTOL-GNSA-153	The aircraft shall be controllable in every stage of flight	Driving
EVTOL-GNSA-156	The aircraft design shall allow for safe entering and exiting of the crew	Driving
EVTOL-GNSA-157	The aircraft design shall allow for safe loading and unloading of the patient	Driving
EVTOL-GNSA-158	The medical equipment shall not interfere with the aircraft avionics	Driving

2.3. Subsystem Requirements

This section shows an overview of the requirements regarding the various subsystems of the aircraft.

2.3.1. Propulsion

Table 2.3: Overview of the requirements regarding the propulsive subsystem.

Code Identifier	Requirement	Type
EVTOL-SRPR-211	The propulsion subsystem shall be fully electrical	Key
EVTOL-SRPR-212	The lift to weight ratio provided by the propulsion subsystem in cruise shall be 1	Driving
EVTOL-SRPR-213	The thrust to drag ratio provided by the propulsion subsystem in cruise shall be at least 1	Driving
EVTOL-SRPR-214	The propulsion subsystem shall not be bigger than 6.5 m in diameter	Regular
EVTOL-SRPR-215a	The propulsion subsystem shall have a maximum power consumption of 460 kW on forward flight	Driving
EVTOL-SRPR-215b	The propulsion subsystem shall have a maximum power consumption of 1120 kW on VTOL	Driving
EVTOL-SRPR-218	The tip velocity of the rotors shall be less than 0.8 Mach	Driving
EVTOL-SRPR-219	The aircraft shall be capable to produce lift at zero total speed	Driving

2.3.2. Electrical

Table 2.4: List of the requirements regarding the electronics subsystem.

Code Identifier	Requirement	Type
EVTOL-SREL-201	The maximum temperature of the battery and electronic subsystems shall be 25 C° during operation	Driving
EVTOL-SREL-202	The minimum battery capacity shall provide power throughout all phases of the aircraft's mission	Driving
EVTOL-SREL-203	The battery system shall be charged during flight	Driving
EVTOL-SREL-207	The energy density of the battery shall be able to fulfil structural sizing constraints while also fulfilling requirement EVTOL-SREL-202	Driving

2.3.3. Power source

Table 2.5: List of the requirements regarding the Fuel Cell subsystem.

Code Identifier	Requirement	Type
EVTOL-SRFC-101	The fuel cell shall be able to provide sufficient power for the complete mission	Driving
EVTOL-SRFC-102	The fuel cell shall be able to provide a constant power level	Key
EVTOL-SRFC-102	The fuel cell shall not be required to be replaced within the first 5 years	Key

2.3.4. Avionics

Table 2.6: List of the requirements regarding the avionics subsystem.

Code Identifier	Requirement	Type
EVTOL-SRAV-251	The aircraft shall allow for communication with the air traffic control tower	Regular
EVTOL-SRAV-252	The aircraft shall allow for communication with the hospitals that can allow for emergency aircraft landing	Regular
EVTOL-SRAV-253	The aircraft shall allow for communication with the emergency control room ('Meldkamer Ambulancezorg')	Regular
EVTOL-SRAV-254	The aircraft shall allow for communication between the people in the cabin	Regular
EVTOL-SRAV-255	The aircraft shall allow for communication between the pilot and the people in the cabin	Regular
EVTOL-SRAV-256	The different communication systems shall not cause any interference.	Regular
EVTOL-SRAV-257	All relevant flight parameters shall be clearly displayed to the pilots	Regular

2.3.5. Aerodynamics

Table 2.7: List of the requirements regarding the aerodynamic subsystem.

Code Identifier	Requirement	Type
EVTOL-SRAE-241	The L/D ratio shall be greater than 8.	Driving
EVTOL-SRAE-242	The wing tip shall not stall before the wing root	Regular
EVTOL-SRAE-243	Airframe noise reduction techniques shall be applied which reduce the noise by 10% compared to a regular airframe where no noise reduction techniques are applied.	Regular
EVTOL-SRAE-244	The transition phase shall be performed such that no altitude is lost.	Regular
EVTOL-SRAE-245	The horizontal tail surface area shall stall after the main wing has stalled.	Regular
EVTOL-SRAE-246	The wing thickness over chord ratio shall allow for enough space to fit the integrated rotors, structural elements, actuators and wiring.	Regular

2.3.6. Stability & Control

Table 2.8: Overview of the requirements regarding the stability & control subsystem.

Code Identifier	Requirement	Type
EVTOL-SRSC-221	The yaw rate provided by the S&C subsystem shall be greater than 45 deg/s.	Driving
EVTOL-SRSC-222	The pitch rate provided by the S&C subsystem shall be greater than 30 deg/s.	Driving
EVTOL-SRSC-223	The wing control surfaces shall not interfere with integration of propulsive system of the wing.	Regular
EVTOL-SRSC-224	The S&C subsystem shall provide stability and control for changes in centre of gravity of 0.773 m.	Driving
EVTOL-SRSC-225	The rotor angular velocity of the S&C subsystem shall not exceed 1600 RPM in order to meet noise requirements.	Driving
EVTOL-SRSC-226	The S&C subsystem shall provide for vertical take-off and landing	Driving

2.3.7. Structures

Table 2.9: Overview of the requirements regarding the structural subsystem.

Code Identifier	Requirement	Type
EVTOL-SRST-231	The structure shall be able to sustain a minimum of 45,000 N originated from the rotor loads	Regular
EVTOL-SRST-232	The structure shall be able to sustain a minimum of 110,000 N originated from the aerodynamic loads	Regular
EVTOL-SRST-233	The structure shall be able to sustain a minimum of 50,000 N originated from the ground loads	Regular
EVTOL-SRST-234	The structure shall be able to sustain a minimum of 80,000 N originated from the impact loads	Regular
EVTOL-SRST-235	The structure shall be able to sustain a minimum of 100,000 N originated from the centrifugal loads	Regular
EVTOL-SRST-236	The structure shall be able to sustain a minimum of 100,000 N originated from the tail loads	Regular

2.4. Technical Requirements

This section provides the requirements that are not related to any specific subsystem but are still considered to be technical.

2.4.1. Transport

Table 2.10: Overview of the requirements regarding the transporting capabilities of the aircraft.

Code Identifier	Requirement	Type
EVTOL-GNTR-101	The aircraft dynamics during take off, flight and landing shall ensure that the state of the patient will not deteriorate during transport	Regular
EVTOL-GNTR-102	The aircraft shall provide faster transportation from accident site to hospital than an ambulance	Regular

2.4.2. Noise

Table 2.11: Overview of the requirements regarding noise produced by the aircraft.

Code Identifier	Requirement	Type
EVTOL-GNNO-110	The aircraft shall reach a noise reduction of at least 25% in loudness compared to the EC135	Key
EVTOL-GNNO-111	The close range EPNL shall be a maximum of 88.5 dB	Driving
EVTOL-GNNO-112	The cruise altitude EPNL shall be a maximum of 80 dB	Driving

2.4.3. Weight

Table 2.12: Overview of the requirements regarding the weight of the aircraft.

Code Identifier	Requirement	Type
EVTOL-GNWE-121	The aircraft shall be able to transport five persons of 90 kg each	Key
EVTOL-GNWE-122	The aircraft shall be able to transport 400 kilograms of medical equipment	Key

2.4.4. Area & Volume

Table 2.13: Overview of the requirements regarding the area and space use within the aircraft cabin.

Code Identifier	Requirement	Type
EVTOL-GNVO-131	The aircraft shall have enough inner surface area to transport five persons, including one patient and at least one pilot	Key
EVTOL-GNVO-132	The aircraft shall have enough inner volume to transport five persons, including one patient and at least one pilot	Key

2.4.5. Operations

Table 2.14: Overview of the requirements regarding the operation and logistics.

Code Identifier	Requirement	Type
EVTOL-GNOP-141	The aircraft shall be able to perform vertical take off and landing manoeuvres	Key
EVTOL-GNOP-142	The range of the aircraft shall be at least 250km at a speed of at least 250km/h with at least 75% of maximum payload	Key
EVTOL-GNOP-143	The aircraft shall be able to operate at minimum 1000 feet of operating altitude	Regular
EVTOL-GNOP-144	The aircraft shall be able to operate at maximum speed of TBD m/s	Regular
EVTOL-GNOP-145	The aircraft shall be able to perform at least 10 missions per day	Driving
EVTOL-GNOP-146	The maximum cleared ground area required for safe take off and landing shall not exceed 25x25m	Key
EVTOL-GNOP-147	The aircraft shall be electrically powered	Driving
EVTOL-GNOP-148	The aircraft shall have a minimum total speed of 0 m/s	Driving
EVTOL-GNOP-149	The endurance of the aircraft shall be a least 2 hours	Driving

2.4.6. Safety

Table 2.15: Overview of the requirements regarding safety of the aircraft.

Code Identifier	Requirement	Type
EVTOL-GNSA-151	The aircraft shall allow for safe storage of the aircraft	Regular
EVTOL-GNSA-152	The aircraft shall be able to safely land and take off in populated areas	Driving
EVTOL-GNSA-153	The aircraft shall be controllable in every stage of flight	Driving
EVTOL-GNSA-154	The passenger shall be transported safely	Regular
EVTOL-GNSA-155	The aircraft shall be able to take off and land on all paved and unpaved surfaces with a minimum hardness of TBD	Regular
EVTOL-GNSA-156	The aircraft design shall allow for safe entering and exiting of the crew	Driving
EVTOL-GNSA-157	The aircraft design shall allow for safe loading and unloading of the patient	Driving
EVTOL-GNSA-158	The medical equipment shall not interfere with the aircraft avionics	Driving

2.4.7. Maintenance

Table 2.16: Overview of the requirements regarding the maintenance of the aircraft.

Code Identifier	Requirement	Type
EVTOL-GNMA-161	Parts that require maintenance shall be accessible for inspection	Regular
EVTOL-GNMA-162	Parts that require maintenance shall be accessible for maintenance operations	Regular
EVTOL-GNMA-163	Part that require maintenance shall be replaceable or allow for maintenance operations to be performed	Regular

2.4.8. Manufacturing

Code Identifier	Requirement	Type
EVTOL-GNMF-171	All designed parts shall be manufacturable with existing manufacturing techniques	Regular
EVTOL-GNMF-172	All designed parts shall allow for assembly with existing assembly techniques	Regular

2.5. Non-Technical Requirements

This section provides an overview of non-technical requirements that are relevant to the project.

2.5.1. Costs

Table 2.17: Overview of the requirements regarding the costs of the project.

Code Identifier	Requirement	Type
EVTOL-COST-001	The total costs of the production of one aircraft shall not exceed €3.500.000,-	Driving
EVTOL-COST-002	The total costs for the structures department shall not exceed TBD % of the total maximum costs	Driving
EVTOL-COST-003	The total costs for the aerodynamics department shall not exceed TBD % of the total maximum costs	Driving
EVTOL-COST-004	The total costs for the electronics department shall not exceed TBD % of the total maximum costs	Driving
EVTOL-COST-005	The total costs for the stability and control department shall not exceed TBD % of the total maximum costs	Driving
EVTOL-COST-006	The total costs for the testing and prototyping process shall not exceed TBD % of the total maximum costs	Driving

2.5.2. Schedule

Code Identifier	Requirement	Type
EVTOL-TIME-001	The total time spent on the design phase shall be less than eleven weeks	Driving
EVTOL-TIME-002	The total time spent on the project planning shall be less than one week	Driving
EVTOL-TIME-003	The total time spent on the general conceptual design shall be less than one week	Driving
EVTOL-TIME-004	The total time spent on the elaborated conceptual design shall be less than three weeks	Driving
EVTOL-TIME-005	The total time spent on the detailed design shall be less than five weeks	Driving
EVTOL-TIME-006	The total time spent on the close out phase of the project shall be less than one week	Driving
EVTOL-TIME-007	The design project shall be finished before July 2nd	Driving

Preliminary Concepts

This chapter functions as a brief summary of the midterm report which includes a trade-off of the energy systems in section 3.1 and of the four preliminary concepts in section 3.2.

3.1. Energy System Trade-Off

Three general approaches to the onboard energy storage system have been considered. These options were analysed and sized for similar performance requirements in terms of energy stored and peak power delivered. As can be seen in Figure 3.1, the results are compiled in a trade-off with different weights assigned to each criteria. The expected system mass and sustainability have the highest weight factor, meaning they are the most important for our design. System mass has been identified as an extremely important parameter, since the aircraft sizing methods are very sensitive, leading to a high weight assigned to this parameter. The result of the trade-off is that a liquid hydrogen system is chosen as the most feasible option.

	Preparation effort (2)	Sustainability (4)	Reliability (3)	TRL (3)	Mass (5)	Volume (3)	Cost (2)
Kerosene-electric	1	-1	0	1	0	1	1
LH2-electric	1	1	0	0	1	0	0
Battery-electric	-1	1	1	-1	-1	1	0

Figure 3.1: Trade-off between the three energy systems.

3.2. Concept Trade-Off

The four concepts that have been identified as the most feasible, realistic and analysable and that have been analysed during the midterm are: the Quadcopter, the Lilium, the eHelicopter and the 'lift + cruise' configuration. These four concepts will be explained below and are visualised in Figure 3.2.

Lift + Cruise Configuration

The 'lift + cruise' configuration (Figure 3.2a) has a blended wing body, two propellers integrated in the wing, and two propellers integrated in a rotating tail to help during take-off and hovering. The forward flight is the most energy consuming flight phase, thus optimisation was required. Therefore, a blended wing body and a mechanism that covers the main wing propellers was introduced. Due to the fact that the forward flight propulsion system is separated from the vertical take-off and landing propulsion system the propellers can be optimised for the different flight phases. Thus making the flight more efficient compared to the other concepts.

Quadcopter

The second concept is the Quadcopter as can be seen in Figure 3.2b. The main difference with a normal drone is that the propellers on the sides are closer to each other, and that the propellers are connected to the tips of the wings. The wings were introduced for several reasons, with the performance in forward flight being the most important.

Lilium

The next concept is the Lilium as can be seen in Figure 3.2c. It has a canard configuration and instead of having four rotors, the Lilium counts with multiple rotors distributed along the span of the wing and the span of the canard surface. In order to transition from vertical take-off to forward flight, the part of the wings containing the rotors is rotated so the propellers are pointed forward.

eHelicopter

The last concept is the eHelicopter (Figure 3.2d), it can be described as a remodelling of the EC135. The EC135 uses fossil fuels to power the engine which turns the propeller to generate lift. The eHelicopter however, will use the energy source established during the energy source trade-off in section 3.1. The advantage of this concept is mainly the technology readiness level and good hover performance, since the helicopters are already widely used.

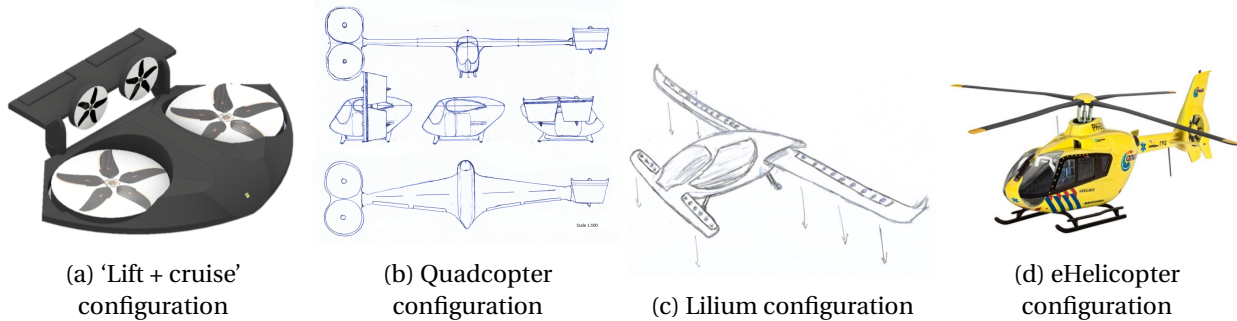


Figure 3.2: The four concept configurations.

The concept trade-off table is depicted in Figure 14.8. Each concept was rated on four different criteria: costs, safety, noise and performance. Two classifications are used for the trade-off: qualitative based and quantitative based. The qualitative based has four criteria: excellent (green), sufficient (blue), correctable deficiencies (yellow) and unacceptable (red). No criterion for any concept proved to be unacceptable, so red is not visible in the table. The quantitative classification again ranges from 1-10 to show in more detail how much better or worse one concept is compared to the others as this is not directly visible from the colours. The reasoning for this is given in the midterm report. [2]

Criterion Concept	Costs (4)	Safety (7)	Noise (10)	Performance (8)	Results
Lilium	8	7	4	9	192
Quadcopter	5	7	6	7	185
'Lift + Cruise' Configuration	4	9	6	7	195
eHelicopter	8	7	8	4	193

	Excellent
	Sufficient
	Correctable Deficiencies

Figure 3.3: Trade-off between the four concepts based on liquid hydrogen as energy source.

In Figure 14.8 it can be seen both from the qualitative based and quantitative based analysis , although close, that the 'Lift + Cruise' configuration is the best design out of these three concepts, based on liquid hydrogen as an energy source. Therefore, this concept was chosen to take into the final design phase.

Sustainable Development Strategy

In this chapter the sustainable development strategy is discussed. This strategy is then used throughout the whole design process. This chapter discusses the general approach, methods and tools, but it does not provide detail yet as chapter 23 will describe how this strategy was implemented in the different subsystem designs and an analysis of the results will be done.

4.1. Approach to Sustainable Design Engineering

The sustainable development strategy is divided into three categories using the triple bottom line, namely environmental, social and economic.

Environmental sustainability is the overall effect of the system¹ on the environment, including the use of renewable resource use, pollution creation, carbon footprint and water usage. Some researches consider energy and resource sustainability a separate key factor, but in this analysis they are merged in the same category as environmental sustainability, where it plays a key factor. Social sustainability refers to the ongoing acceptance of the system's operations by stakeholders and the general public. Generally, employees should also be included in this category, but this is beyond the scope of this engineering project. Also, general human welfare, i.e. human rights and labour standards, are included in this category. Economic sustainability states that the system's business should do well financially and have good governance and risk management. These three categories always interact with each other and cannot be considered independently. They are famously summarised as "people-planet-profit" by John Elkington [14].

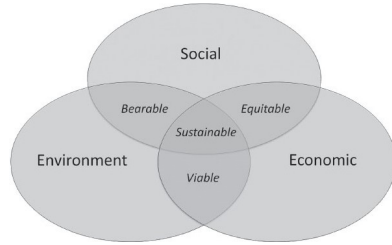


Figure 4.1: The three pillars for sustainability: economic, social, environmental [49].

These three pillars for sustainability are considered for the different phases of the product life time. These phases are narrowed down to development, production, operation and end of life. Hence, the sustainable development strategy does not focus on the product alone, but on the whole process. A number of tools and plans will be used in this process in order to ensure an environmental, social and economic sustainable product. These include:

- Use of a circular economy: a circular economy aims to minimise waste by recycling or reusing the end of life product and by making the product's life as long as possible using proper maintenance planning. The cradle-to-cradle design philosophy is adopted. The aim is that 90-95% of the aircraft can be recycled or reused for other purposes. Therefore, the impact on the environment will be a determining factor in material selection, production plan choices, operation and maintenance choices and end of life procedures. This item focuses on environmental sustainability.
- The design is developed with a client focused mindset. This will not only ensure that the client requirements are met, but also that the aircraft will be accepted and supported by the community it operates in. This item focuses on social sustainability.
- The use of regulations: the Committee on Aviation Environmental Protection of the International Civil Aviation Organisation (ICAO) set standards on, for example, aircraft noise, engine emissions and fuel venting. EASA tries to implement those into EU legislation.² Hence, adhering to the regulations

¹The emergency aircraft seen as the system.

²<https://www.easa.europa.eu/easa-and-you/environment/smart-environmental-standards> [Accessed 17 June 2019]

documented by EASA not only ensure meeting the minimum performance requirements, but also serve as a first tool to a sustainable product. This item focuses both on environmental and societal sustainability.

- This design will aim to reduce noise by at least 25% and reduce emissions by its electric energy source design, as described by the client requirements in chapter 2. Therefore, this will be the main focus in the technical subsystem designs, reflected most dominantly in the propulsion design. This item focuses both on environmental and societal sustainability.
- Apart from a market analysis, a cost budget is made. This financial tool will allow to check if the aircraft design will be profitable and the long-term financial planning. This item focuses on economic sustainability.
- Extensive risk management and contingency planning is done continuously throughout the project. This allows for good organisation and adds to the reliability of the system's processes, currently in the design process and in later phases also the production and operational phases. This item focuses on economic sustainability.

There specific requirements regarding sustainability are mentioned in the chapters where they have an impact on the design method, as mentioning them twice is considered to be unnecessary.

4.2. Sustainability Analysis

In the subsequent chapters this sustainability strategy is implemented while designing the different subsystems. In chapter 23 this sustainability approach and its results will be analysed. Some tools and methods that will be used include:

- In order to measure the sustainable performance, the H₂ERO is compared to the current emergency aircraft, the EC-135.
- A radar diagram and bar chart is made to visualise the final sustainability score of the aircraft.

Detailed Design: Propulsion Subsystem

From various literature and overall general knowledge it can be stated that the propulsive system in any vehicle or aircraft is the main noise producing component. Therefore, regarding the requirements connected to this design, it seems logical to backward engineer the propulsive system. This means that the propulsive system configuration design is started from the noise requirement constraint whereas in [2], the noise production was determined based on an initial predetermined configuration. Remembering the results that were concluded in [2], the initial design did not meet the noise requirements at close range but did fulfil the cruise requirements. Hence, it can be expected that the propulsive subsystem design will have to be altered with respect to the initial configuration.

5.1. Requirements & Constraints

As stated earlier, the propulsive system has been backward engineered with respect to its noise requirements. Before an analysis can be done, the various requirements and constraints set on the configuration design need to be stated.

Requirements

EVTOL-GNNO-110: The aircraft shall reach a noise reduction of at least 25% in loudness compared to the EC135 emergency helicopter

EVTOL-GNNO-112: The overflight PNL_A shall be a maximum of 80 dB

EVTOL-GNNO-113: The close range PNL_A shall be a maximum of 88.5 dB

These requirements have been elaborated on in chapter 2

Constraints

Constraint on the maximum provided power by an individual motor of 500kW

Constraint of the propeller diameter to a maximum of 5.5 meters for the VTOL propulsive system

Constraint of the propeller diameter to a maximum of 3.5 meters for the cruising propulsive system

Constraint on the maximum disk loading of $1000 \frac{N}{M^2}$

Constraint on the maximum number of blades on a propeller system of 6 for the VTOL propulsive system

Constraint on the maximum number of blades on a propeller system of 5 for the cruising propulsive system

Constraint on the maximum number of propellers of 8 for both the VTOL and cruising phase

The above mentioned constraints are a resultant of literature research performed before detailed analysis [2]. The maximum power provided by an individual motor of 500kW is based on the MagniX500 motor¹. The propeller diameter constraint is based on the landing area constraint of 25 by 25 meters. It was expected that if the diameter of propellers would be larger than 5.5 meters, then the aircraft would only contain propellers. Hence, not enough lift producing wing area would be able to be designed which is necessary for this aircraft. Also, larger diameters are mainly only found on larger helicopters. A constraint of $1000 \frac{N}{M^2}$ for the disk loading was determined. A larger disk loading would complicate or even eliminate the possibility of taking off and landing on certain softer ground compositions.

Furthermore, there are also a set of constraints regarding the cruising propulsive system. A constraint of 3.5m is set for the propeller diameter. This is to ensure ground clearance. Also, only a maximum of 5 blades

¹<https://www.magnix.aero/products/> [Accessed 2019-06-18]

per propeller are considered for the cruising propulsive system. This is due to the literature research performed. For horizontal flight, most existing propeller propelled aircraft flying around consist of a maximum of 5 propeller blades. This mainly is due to the interference of each blade with its successor as each blade creates vortices that disturb the airflow behind it.

5.2. Analysis Description

For the individual propeller geometry and dimensional design a python program was initiated. A description of the program input, flow and outputs will be given to inform the reader on the process of the detailed design of the propulsive system. Understanding the process of the program also benefits the readers understanding of certain choices made. These choices are explained in chapter 11 a later stage. A general flow of the python code is shown in Figure 5.1

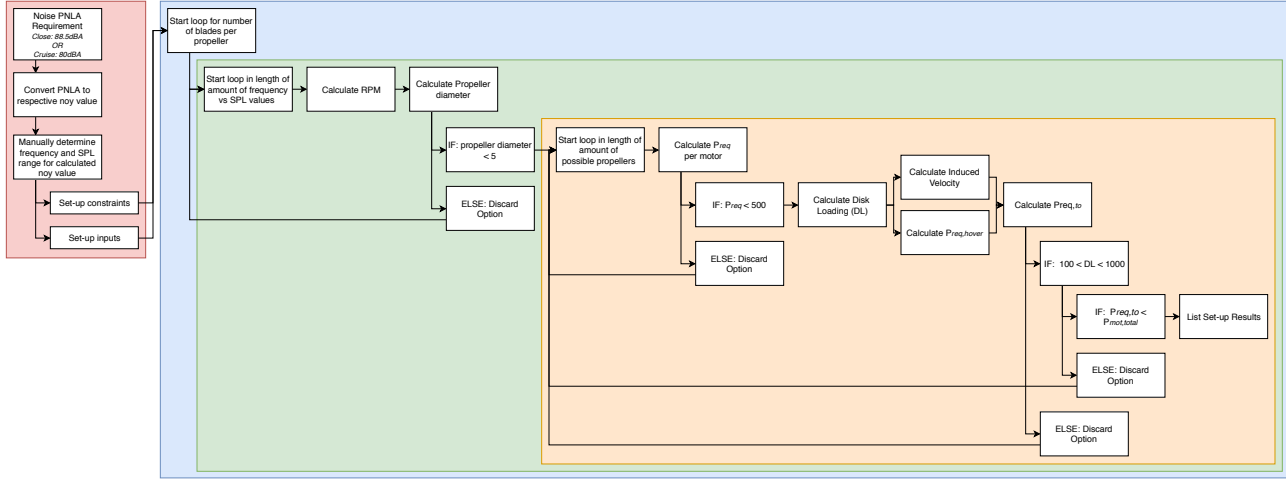


Figure 5.1: General flow of the python code for the propulsion subsystem.

Code Parameters, Formula's & Loop Descriptions

Within the python code, various formula's have been used. In the following section, these will be discussed shortly.

Starting with the formula determining the initial propeller diameter with which an overall loop starts shown in Equation 5.3. This diameter is dependant on the Revolutions per Minute (RPM) given by Ω in Equation 5.2. The f_1 is found from a table in [47] which is dependent on a noy value. This noy value is seen in Equation 5.1 where it is defined in a relationship between the PNL_A requirement stated in section 5.1 and the noy value. PNL_A is the noise level that is perceived by humans as annoying.

$$PNL_A = 54 + 33.3 \cdot \log N \quad (5.1)$$

$$\Omega = \frac{f_1 \cdot 60}{N_{blades}} \quad (5.2)$$

$$D_{prop} = \frac{M_t \cdot c_{sound} \cdot 60}{\pi \cdot \Omega} \quad (5.3)$$

Following the determination of the propeller diameter in Equation 5.3, the constraint of the D_{prop} being below 5 meters is set in the code. Next, the motor power per propeller system is determined. It is calculated using Equation 5.4 and Equation 5.5. The initial P_{mot} is dependent on many variables. These variables are the Sound Pressure Level (SPL), D_{prop} , M_t , N_{blades} , N_{prop} and the distance r from the sound source.

$$P_{mot} = e^{\frac{1}{15.3} \cdot (SPL_{max} - 83.4 + 20 \cdot \log(D_{prop}) - 38.5 \cdot M_{t,max} + 3 \cdot (N_{blades} - 2) - 10 \cdot \log(N_{prop}) + 20 \cdot \log(r))} \quad (5.4)$$

$$P_{mot,propeller} = \frac{P_{mot}}{N_{prop}} \quad (5.5)$$

Next, for all of the configurations that fulfill the set constraints, the Disk Loading (DL), the power required to hover for the specific configuration $P_{req,hover}$, the induced velocity V_h and the power required for take-off $P_{req,to}$ are determined using Equation 5.6 through Equation 5.9.

$$DL = \frac{MTOW \cdot 9.81}{\pi \cdot \left(\frac{D_{prop}}{2}\right)^2 \cdot N_{prop}} \quad (5.6)$$

$$V_h = \sqrt{\frac{DL}{2 \cdot \rho_{trans}}} \quad (5.7)$$

$$P_{req,hover} = \left(\frac{T}{W}\right)_{to} \cdot \sqrt{\left(\frac{DL}{2 \cdot \rho_{trans} \cdot T_i^3}\right) \cdot \frac{MTOW \cdot 9.81}{FoM \cdot 1000}} \quad (5.8)$$

$$P_{req,to} = P_{req,hover} \cdot \left(\frac{0.5 \cdot ROC_{VTOL}}{V_h} + \sqrt{\frac{1}{4} \cdot \left(\frac{ROC_{VTOL}}{V_h}\right)^2} \right) \quad (5.9)$$

5.3. Configurations

The code and implemented formula's as described in section 5.2 resulted in various propulsive configurations which all adhere to the requirements and constraints as they were set in section 5.1. The larger amount of configurations and variation seemed beneficial for the detailed design and overall subsystem integration. This is due to the fact that the propulsive subsystem group can give the choice to the remaining subsystem groups on what suits them most instead of setting in stone what they need to work with. For instance, the results as tabulated in Table 5.1 for the VTOL phase, indicate the possibility of using a configuration with 3 propellers but also a configuration with 8 propellers. Hence, structures can give their preference on rather only having 4 holes for the propellers in the wing, whereas stability and control could argue they need a minimum of 6 to ensure safety. Therefore, good communication and discussions will be key during the subsystem integration determined in chapter 11. Finally, the various configuration ranges examples of the propulsive system for the VTOL phase are tabulated in Table 5.1.

Table 5.1: Configuration Ranges for the VTOL propulsive system.

N _{prop}	RPM (Min – Max)	N _{blades} (Min – Max)	SPL (Min – Max)	D _{prop} (Min – Max)	P _{motor} (Min – Max)	P _{take-off} (Min – Max)	Disk Loading (Min – Max)	Combinations
2	-	-	-	-	-	-	-	0
3	1260 - 1260	3 - 3	127 - 127	4.16 - 4.16	1467.87 - 1467.87	459.82 - 459.82	807.21 - 807.32	1
4	1000 - 1600	2 - 6	121 - 128	3.28 - 5.24	780.98 - 1756.38	327.68 - 501.33	381.33 - 976.21	10
5	960 - 1600	2 - 6	121 - 128	3.28 - 5.46	674.99 - 1971.6	286.93 - 452.38	281.15 - 780.97	12
6	960 - 1920	2 - 6	121 - 128	2.73 - 5.46	486.97 - 1750.12	265.41 - 491.96	234.29 - 937.16	14
7	960 - 2000	2 - 6	119 - 128	2.62 - 5.46	486.47 - 1582.38	248.72 - 475.78	200.82 - 871.62	14
8	960 - 2000	2 - 6	119 - 128	2.62 - 5.46	445.81 - 1450.13	235.29 - 447.49	175.72 - 762.67	14

Furthermore, the same process described in section 5.2 is used to determine the sizing configurations of the propellers used during the horizontal flight phase with respect to noise. These are tabulated in a similar manner in Table 5.2.

Table 5.2: Configuration Ranges for the horizontal cruise propulsive system.

N _{prop}	RPM (Min – Max)	N _{blades} (Min – Max)	SPL (Min – Max)	D _{prop} (Min – Max)	P _{motor} [kW] (Min – Max)	P _{cruise} [kW]	# of Combinations
1	12000 - 1500	2 - 5	108 - 120	0.43 - 3.45	726 - 20126	472	38
2	1500 - 9600	2 - 5	108 - 120	0.54 - 3.45	640 - 12794	472	34
3	1500 - 7560	2 - 5	108 - 120	0.68 - 3.45	664 - 9815	472	30
4	1500 - 7560	2 - 5	108 - 120	0.68 - 3.45	606 - 8133	472	29
5	1500 - 6000	2 - 5	108 - 120	0.86 - 3.45	637 - 7029	472	26
6	1500 - 6000	2 - 5	108 - 120	0.86 - 3.45	672 - 6239	472	25
7	1500 - 6000	2 - 5	108 - 120	0.86 - 3.45	608 - 5641	472	25
8	1500 - 4800	2 - 5	108 - 120	1.08 - 3.45	683 - 5170	472	22

It might seem that the power per motor it is too high, since it is impossible to achieve higher than 560 kW due to engine constraints. But it must be remembered that this is only to adhere to noise constraints, meaning that 20126 kW it is just a maximum but not a minimum.

In chapter 11, when all subsystems will be integrated, a configuration for the VTOL and the cruising phase will be determined.

5.4. Blade Design

The blades for the propellers are designed independently for cruise and VTOL. This is due to the existing differences of flight conditions between the two flight phases.

In Klein [25] different programs for the blade design were compared. It was determined that XROTOR performed better than JavaProp and Adkings & Liebeck scheme. Moreover, XROTOR has been proven to accurately predict propeller performance in Kuijk [57]. XROTOR uses the blade element theory to design the blades composing the propeller. The blade element theory is a mathematical method that predicts the performance of the propeller during flight operations. The blades are divided into different sections along the radius of the propeller. Then, the forces acting on the airfoil (lift, drag, thrust and torque) are determined for each of the sections. Finally, an integration over the full wing is performed to calculate the total lift, drag, thrust and torque over the blade.

Due to the high dependency of the propulsion system with the other subsystems. The actual design will be performed in section 11.3, meaning that, in this chapter, only the process will be explained.

5.4.1. XROTOR Explanation

For both blade designs, the program XROTOR will be used but using different inputs. The first thing that is done in the program is to specify the atmospheric conditions and the airfoil used. In the design, the predefined airfoil of XROTOR is used. This airfoil counts with a CL_{max} of 1.5, a CL_{min} of -0.5, a CD_{min} of 0.013 and a critical mach of 0.8. The atmospheric conditions will be inputted using only the flight altitude using the command "ATMO".

Before specifying the initial propeller diameters the ducted or non ducted option must be selected using the command "DUCT". The vertical propellers will use a ducted system while the forward flight will not. Finally, some propeller parameters must be defined using command "DESI"- "INPU". These are, the number of blades, the propeller radius, the hub radius, the airspeed, the revolutions per minute, the power or thrust required and the lift coefficient of each section of the blade. After the parameters have been inputted, the results can be plotted using the command "PLOT" with number 2 and 3 which will correspond to figures Figure 11.1 and Figure 11.4.

5.4.2. XROTOR Limitations

One of the major limitations of XROTOR is that the lift generated by the section is assumed to be linear from the minimum to the maximum lift coefficient. Stall limits and lift coefficients after stall are also missing. But in contrast with the simple blade element theory they predict better the interactions between the different sections of the blade. Another limitation of XROTOR is that it does not account for blade sweep. Meaning that in theory you could not arrive to the most optimal design. Finally, the slipstream condition can not be modeled, which might cause some differences with real flight applications. These limitations reduce the accuracy of the program.

5.5. Motor and Motor Controller Selection

The selection of a motor that is able to cope with the specifications of the propeller is necessary. The selected motor, must be able to at least match the required Power, the required RPM and the required torque. These values will be found in chapter 11 and will vary per flight stage and propeller. Thus different motors for different propellers might be selected. The possible used motors are shown below.

The Magni250 counts with a continuous torque of 1407 [Nm], a continuous power of 280 [kW], a base speed of 1900 [rpm], a maximum speed of 3000 [rpm] and a weight of 72 [kg]. The Magni500 counts with a continuous torque of 2814 [Nm], a continuous power of 560 [kW], a base speed of 1900 [rpm] a maximum speed of 3000 [rpm] and a weight of 135 [kg]. Both of the motors have a DC Link Voltage (nominal) of 540 [V] and DC Link Voltage range of 450 - 750 [V].

The motor controller used for these motors is the MagniDrive. The MagniDrive has an output power of 170 kW, which means that for the Magni250, two controllers will be used, and for the Magni500, four controllers will be used as stated by the MagniX company. The weight of each of the controllers is 12 kg, with a voltage (HVDC) between 400 and 800 V.

5.6. Propulsion System Mass Estimation

The mass of the whole propulsion system can be estimated using Equation 5.10 from Tyan et al. [54].

$$M_{propulsion} = \left[N_{mot_{Magni500}} \cdot M_{mot_{Magni500}} + N_{mot_{Magni250}} \cdot M_{mot_{Magni250}} + M_{ESC} + M_{propeller} \right] \quad (5.10)$$

M_{motor} is the mass of one motor, which can vary between Magni250 and Magni500, and N_{mot} is the number of motors. M_{ESC} is the total motor controller mass, which will be equal to:

$$M_{ESC} = 4 \cdot N_{mot_{Magni500}} \cdot M_{MagniDrive} + 2 \cdot N_{mot_{Magni250}} \cdot M_{MagniDrive} \quad (5.11)$$

$M_{propeller}$ is the mass per propeller and it can be calculated using Equation 5.12 from Dadone [12]. Where the result is in lbs, that is why is multiplied by 0.453 to transform lbs to kg. K_W is a constant that assumes technology level. D is the propeller diameter in feet. B is the number of blades. AF is the blade activity factor. N is the propeller speed in revolutions per minute. M is the airspeed mach number, and Pbr_{hp} is the shaft power in hp. The values for all the variables and results are listed in Table 5.3.

$$M_{propeller} = K_W \left[\left(\frac{D_{prop}}{10} \right)^2 \cdot \left(\frac{B}{4} \right)^0.7 \cdot \left(\frac{AF}{100} \right)^{0.75} \cdot \left(\frac{\Omega D_{prop}}{20000} \right)^{0.5} \cdot (M+1)^{0.5} \cdot \left(\frac{Pbr_{hp}}{10 \cdot D_{prop}^2} \right)^{0.12} \right] \cdot 0.453 \quad (5.12)$$

Table 5.3: Mass parameters of the propulsion system.

Variable	Value	Unit	Variable	Value	Unit
K_W	180	-	Pbr_{hp_c}	608,40	hp
$D_{propVTOLBig}$	11,78	ft	$N_{mot_{Magni500}}$	1	-
$D_{prop_{VTOLSmall}}$	9.61	ft	$M_{mot_{Magni500}}$	135	-
D_{prop_c}	7.09	ft	$N_{mot_{Magni250}}$	4	-
B	6	-	$M_{mot_{Magni250}}$	72	-
B_c	2	-	$N_{MagniDrive}$	12	-
AF	150	-	$M_{MagniDrive}$	12	kg
Ω_{VTOL}	1600	rpm	M_{motor}	422	kg
Ω_c	3000	rpm	M_{ESC}	144	kg
M	0.22	-	$M_{propeller_{total}}$	132	kg
$Pbr_{hp_{VTOL}}$	361,11	hp	$M_{propulsion}$	698	kg

Some of these values were extracted from the report in [12] while the others were calculated in chapter 11 during the propulsion system design. As explained before, K_W is a technology level, for composite materials is between 160 and 180 thus an average was selected. AF was determined in the same way, from a range of 100-200 the average was selected.

5.7. Requirement Compliance & Feasibility

Table 5.4: Requirements for propulsion subsystem.

Code Identifier	Requirement	Type	Verification	Compliance
EVTOL-SRPR-211	The propulsion subsystem shall be fully electrical	Key	Inspection	
EVTOL-SRPR-212	The lift to weight ratio provided by the propulsion subsystem in cruise shall be 1	Driving	Analysis	
EVTOL-SRPR-213	The thrust to drag ratio provided by the propulsion subsystem in cruise shall be at least 1	Driving	Analysis	
EVTOL-SRPR-214	The propulsion subsystem shall not be bigger than 6.5 m in diameter	Driving	Analysis	
EVTOL-SRPR-215a	The propulsion subsystem shall have a maximum power consumption of 460 kW on forward flight	Driving	Analysis	
EVTOL-SRPR-215b	The propulsion subsystem shall have a maximum power consumption of 1120 kW on VTOL	Driving	Analysis	
EVTOL-SRPR-218	The tip velocity of the rotors shall be less than 0.8 Mach	Driving	Analysis	
EVTOL-SRPR-219	The aircraft shall be capable to produce lift at zero total speed	Driving	Analysis	

As it can be observed in the table, all the requirements are met. Analysis is used for all of them, since the tool to design the subsystem is a code.

Detailed Design: Fuel System

In this section, the hydrogen fuel cell system and battery will be designed. Firstly, an overview of the system used will be provided. Then, the fundamentals of a fuel cell will be discussed. Finally, the system is sized to match the concept's power requirements. In a previous analysis performed in [2], the decision was made to go for a hydrogen proton exchange membrane fuel cell, with liquid hydrogen stored in an internal tank.

6.1. System Overview

As discussed in [2], a hydrogen-electric power supply system will be designed to power the aircraft. During take-off, the rotors require maximum power, much more than the power required for cruise. The fuel-cell will generate a constant average power, as this will increase the lifetime of the fuel cell and means that it can be designed to have optimum efficiency for a set operating point [8]. In Figure 6.1, P_1 is the maximum power during vertical take-off. P_2 is the cruise power. The average power, or P_{FC} , is the power the fuel cell is constantly generating. The average power is higher than the cruise required power. The excess power, $P_{FC} - P_2$ is used to charge the battery.

A fuel-cell is not capable of delivering the peak power necessary for vertical take-off. Therefore the battery supports the fuel cell during this power intense phase, and afterwards the fuel cell recharges the battery for the next vertical take-off. During cruise, the electro-motors are driven by the fuel cell directly.

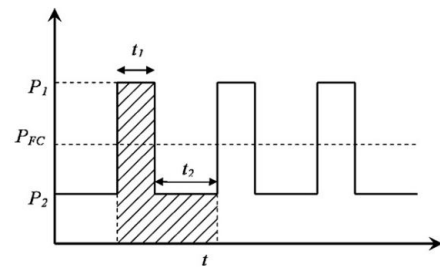
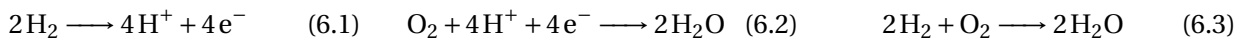


Figure 6.1: Generic Power Profile [8].

6.2. Fuel Cell

The fuel cell used is a Proton Exchange Membrane (PEM). A PEM fuel cell is an electro-chemical cell that is fed hydrogen, which is oxidised (Equation 6.1) at the anode, and oxygen that is reduced (Equation 6.2) at the cathode.



The goal of a fuel cell is to generate electricity from the chemical reaction of the fuel with oxygen to power the aircraft. The rest product of the overall reaction (Equation 6.3) is pure water. The reactants are hydrogen and oxygen.

6.2.1. Fuel Cell Components

A PEM fuel cell consists of 7 different layers as depicted in Figure 6.2¹. There is a membrane electrode assembly layer in the middle, which enables the chemical reaction to take place. Then, there is a cathode and an anode, often called catalyst layers, where both the half-reactions take place. Next, there are two gas-diffusion layers, which allow for diffusion of the reacting substances before reacting at the PEM. Additionally, they control the proper diffusion of the reactants. Two electrically-conducting bipolar plates are installed which connect the anode of one cell to the cathode of another cell, enabling the system to expand and consist of multiple cells. Finally, two current collectors or terminal plates are added, through which the electrons flow. The aforementioned plates are compressed together by two support blocks. Hydrogen and oxygen are supplied through these support blocks and water is expelled [36]. The PEM chosen is a Nafion-117 membrane. This is mainly due to its high conductivity and durability compared to alternatives.

¹<https://www.peakoil.net/renewable/hydrogen-fuel-cell> [Accessed 2019-06-18]

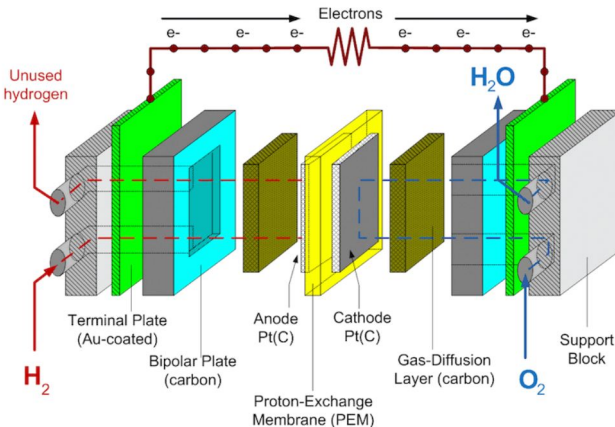


Figure 6.2: PEM Fuel Cell.

The catalyst layers are both made of Platinum Carbon (Pt(C)), as other materials are not fully developed yet and would introduce uncertainties. For the gas-diffusion layers, carbon is used due to its low density and high permeability. The bipolar plates are made out of carbon mixed with graphite to make it conducting. The terminal plates are really thin and coated with gold (Aurum). The support blocks are made out of expanded graphite. The oxygen and hydrogen flow channels can be easily created in expanded graphite and has a relatively low density.

Now that the PEM's materials are known, an initial estimation of the fuel cell mass and costs can be performed as displayed in Table 6.1.

Table 6.1: Fuel cell properties.

Plates	Material	Weight [g/m ²]	Thickness [mm]	Costs [\$/m ²]
PEM	Nafion 117	360	0.183	400
Catalyst layer anode	Platinum carbon	0.5	Neglegible	21
Catalyst layer cathode	Platinum carbon	4	Neglegible	169
Gas-diffusion layers (x2)	Carbon	132	0.35	300
Bipolar plates (x2)	Carbon	160	0.4	350
Terminal plates (x2)	Aurum	135.1	0.07	5809
Support Blocks (x2)	Expanded Graphite	1000	1	50
Total:		3218.7	3.823	13608

6.3. Reactant Supply System

The reactants used for the reversed electrolysis (Equation 6.3) are hydrogen and oxygen. They are supplied through the flow system in the support blocks. Oxygen is retrieved from the surrounding atmosphere, while hydrogen is stored in an internal tank.

6.3.1. Oxygen

As the aircraft is flying at a relatively low altitude, oxygen is chosen to be retrieved from the aircraft's surroundings. Another option would be to store pure oxygen (liquefied or pressurised) in a tank in the aircraft. This tank would take a lot of volume, mass and energy, which makes it a non-viable and, due to the low altitude, an unnecessary option. The air intake system consists of multiple functions which have been listed below;

- An intake with filter, making sure the right amount of air flows into the system and does not contain unwanted particles or animals.
- A fan, able to draw air into the system during vertical flight.
- A compressor, compressing the air to the desired pressure.
- A heater, heating the air to the right temperature.
- A humidifier, humidifying the airflow to the desired level of humidity before going into the PEM.

A schematic visual representation of the air intake system is shown in Figure 6.3. Note that not all air goes into the fuel system, a part is also used to control the cabin environment. An air intake slows the incoming

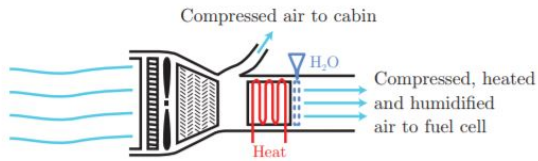


Figure 6.3: Schematic air intake system [36].

airflow significantly with respect to the free-stream velocity. The higher the initial velocity, the more energy it takes to slow the airflow down, the more drag produced. Placing an air-intake in free-stream air induces a lot of drag, especially in cruise conditions. This reduces the overall aircraft efficiency. The air intake should thus be designed to introduce the minimal amount of drag while still fulfilling its function. The region of interaction between the free-stream airflow and the wing body surface is called the boundary layer. Because of this inevitable interaction, the air velocity is close to zero. The air intake is designed to take air from the boundary layer, minimising the amount of drag induced. Using this technique, the intake airspeed is on average $0.58V_\infty$ [56].

6.3.2. Hydrogen

Contrary to oxygen, hydrogen is stored in a tank. In the midterm report [2], both gaseous and liquid hydrogen were considered as options. In gaseous form, the pressure in the tank needs to be approximately 700 bar. Storing hydrogen like this is advantageous regarding simplicity, cost and maturity of the technology. However, the infrastructure of compressed hydrogen is still underdeveloped. A compressed hydrogen tank can only store 6.4% of its structural weight, while for a liquid hydrogen tank this is 70% [2]. Therefore, hydrogen is chosen to be stored as a liquid. However, due to its low boiling point and small heat of vaporisation, liquid hydrogen is a cryogenic fuel and vaporises quickly. Once it is mixed with air it can burn and explode. Hence, it is necessary to have sophisticated thermally insulated storage and tube systems for its transport. The liquid hydrogen tank has a double wall construction to contain the ultra low temperature. The technique used is called vacuum multi layer insulation (VMLI) with foam in between the layers (Figure 6.4). One of these layers is a thin metal sheet preventing thermal irradiation between the multiple layers [61].

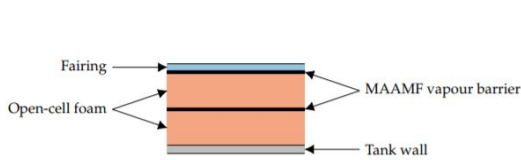


Figure 6.4: Insulation layers fuel tank [61].

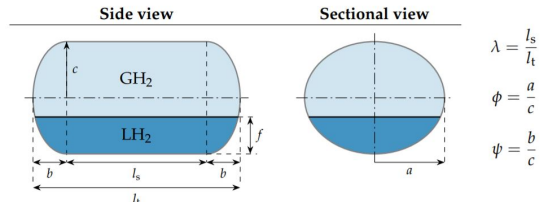


Figure 6.5: Fuel Tank [61].

The latest liquid hydrogen storage tank has a capability of limiting the flow of heat to only a few watts per second. This results in the liquid evaporation of only a few percent per day. This loss is inevitable [32]. Hence, this means that there is always a part of the hydrogen changing to gaseous form as can be seen in Figure 6.5 [61] in which GH₂ represents the gaseous hydrogen. LH₂ represents the liquid hydrogen. The pressure in the tank rises as more of the hydrogen becomes gaseous. The tank is therefore designed to withstand and to release pressure once in a while. The material used for the tank is the aluminium alloy 2219, as it fulfils the requirements best, compared to other metals investigated.

The hydrogen is transferred to the fuel system by an electric pump. Another consideration [36] is using a shaft drive that is connected to a gearbox, but this is not applicable for this concept as there is no gearbox. The main advantage of using an electric pump, is that it can be regulated independently of the other sub-systems. A pressure regulator regulates the pressure of the liquid hydrogen and allows the right amount of liquid hydrogen to flow before it is gasified by a heat exchanger. The heat exchanger also adjusts the temperature of the gas to the optimal working temperature for the fuel cell.

The tube connecting the tank with the fuel cell should be designed to allow at least the flow rate required for the fuel cell to operate at desired power. Liquid hydrogen vaporises quickly because of its low boiling point and small heat of vaporisation as explained before. Once mixed with air, it may explode rapidly [11]. Hence, the fuel tank and the transport tubes need to be insulated properly. An often used technique is insulating the tube using a vacuum layer around it as can be seen in Figure 6.6. According to [36], only 1 out of 2.8

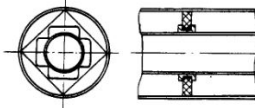


Figure 6.6: Vacuum hydrogen transfer tube [11].

molecules passing through the fuel-cell react and are thus efficiently used. Therefore a circulation system is present to feed the unused hydrogen back into the fuel-cell, optimising the overall fuel usage, which can range between 84% and 98% according to [36].

6.3.3. Cooling

The fuel cell is not 100% efficient and produces excess heat. The cabin, hydrogen heat exchanger and oxygen heater use the excess heat from the fuel cell. However, there will be more excess heat which can not be used effectively and has a negative effect on the low optimum operating temperatures of the fuel cell [16]. Therefore, there needs to be an active cooling system integrated into the fuel system. There are multiple ways to cool the fuel cell, namely air cooling, liquid cooling and phase change cooling. For each of these methods, a radiator has to be installed. The bigger the radiator frontal area, the bigger the drag. It was found that the radiator frontal area can be reduced up to 27% compared to conventional liquid cooling methods by changing from liquid to evaporative cooling (Figure 6.7), provided an aluminium condensing radiator is used. The primary reason for the improvement is due to phase change within the radiator tubes [16].

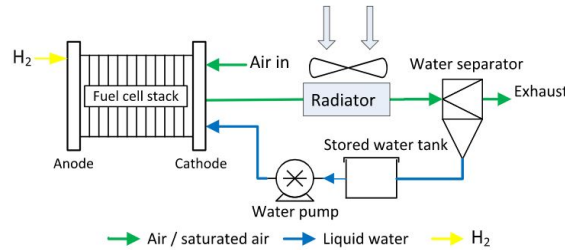


Figure 6.7: Evaporate Cooling System [16].

The hot air coming out of the fuel cell is cooled by the radiator, which then cools the water flow going into the fuel cell. This reduces the overall system temperatures. Next to cooling, water can also be used to humidify air at the oxygen intake. As the fuel cell is operating at temperatures lower than the boiling point of water, and thus no water evaporates, more water is produced than necessary. The excess water is expelled from the aircraft and safely released into the surrounding atmosphere.

6.4. Fuel System Overview

In Figure 6.8, an overview of the fuel cell system is presented. The arrows present the flow of either oxygen, hydrogen, water or power through the system. The fuel cell is connected to the battery and the engines directly, which enables it to deliver power simultaneously with the battery to deliver peak power to the engines. Furthermore, the air-intake system, the hydrogen transport system and the cooling system are powered by the fuel cell directly. The excess hydrogen is recirculated and the excess water is used to humidify the air at the intake or to cool the fuel cell.

6.5. Fuel System Sizing

The benefit of a fuel system can only be extracted when properly sized and designed. In this subsection, a comprehensive design process will be conducted. The final results will be presented in chapter 11.

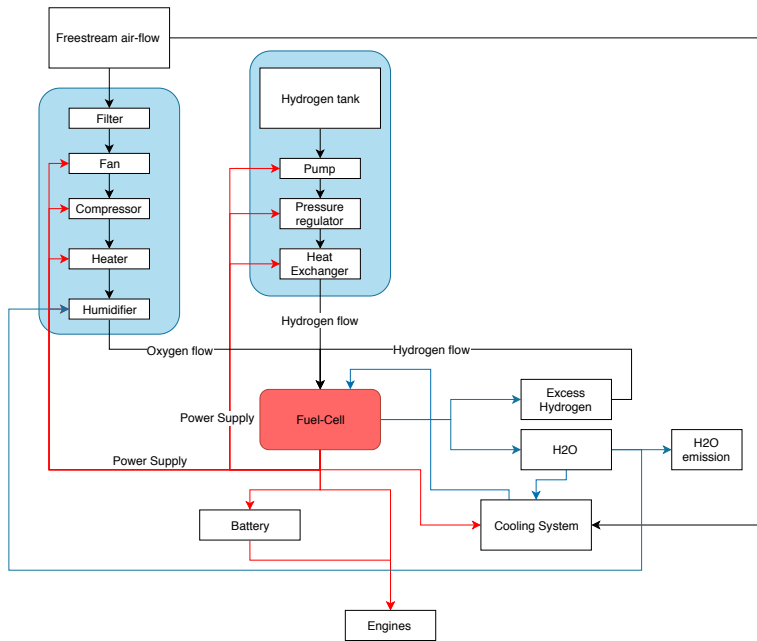


Figure 6.8: Fuel Cell System Overview.

6.5.1. Fuel Cell Sizing

The sizing of the power system starts with the power requirements as defined by 5.2. The fuel cell is designed such that it exactly delivers the average power required for the mission. During take-off, together with the battery, the fuel cell delivers maximum output power to the engines and hence the battery charge decreases. However, during cruise, the fuel cell generates more power than required and hence the battery is charged. This ensures enough combined power, to ensure a safe landing and to be able to take-off again for a next mission. Referring back to Figure 6.1, the average power is calculated using Equation 6.4.

$$P_{FC} = \frac{P_1 \cdot t_1 + P_2 \cdot t_2}{t_1 + t_2} \quad (6.4)$$

A PEM fuel cell stack consisting of multiple cells has a power density (ρ_{WPEM}) of 1500 W/kg, with a volume density (ρ_{VPEM}) of 1200 W/L [32]. To be able to deliver the average power required, the PEM mass and volume are calculated through Equation 6.5 and Equation 6.6 respectively.

$$M_{PEM} = \frac{P_{FC}}{\rho_{WPEM}} \quad (6.5)$$

$$V_{PEM} = \frac{P_{FC}}{\rho_{VPEM}} \quad (6.6)$$

6.5.2. Battery Sizing

During a mission, the battery is required to deliver peak-power three times during vertical take-off of various sections of the mission. The fuel cell, delivering constant power, is designed such that it provides power equal to $P_1 - P_{FC}$. Additionally, the battery is designed to be fully charged during cruise flight by $P_{FC} - P_2$ Watts. The energy discharged from the fuel cell during take-off can be calculated via Equation 6.7 with n being the number of cycles during the mission.

$$E_s = n \cdot (P_1 - P_{FC}) \cdot t_1 \quad (6.7)$$

Depending on the power profile, either the charge or discharge time will be the fastest. The characteristics of fastest process are used to identify the capabilities of the battery and the efficiency of the process at the required rate. To determine which process is faster, Equation 6.8 is used.

$$P_{cd} = P_2 + \frac{1}{2} \cdot (P_1 - P_2) \quad (6.8)$$

If P_{FC} is bigger than P_{cd} , the charge time is the fastest. If P_{FC} is smaller than P_{cd} , the discharge time is the fastest. For the power profile of this design, the discharge time is the fastest process.

Now this information can be taken into the battery sizing process. Battery energy density is a critical limiting factor for flying electric. Also, for hybrid systems, attention should be given to the right battery selection. The best battery in terms of high energy density combined with safety available today has a density of 350 kWh/kg [2]. This is a lithium ion battery. A lithium ion battery has an efficiency of 90% and a discharge efficiency of 80% [8]. With this information, the name plate energy capacity can be calculated using Equation 6.9. This is the intended full-load sustained output of the battery.

$$NPEC = \frac{1}{\eta} \cdot \frac{1}{\eta_{discharge}} \cdot E_s \quad (6.9)$$

From NPEC in Equation 6.9, the battery weight and volume can be calculated with Equation 6.10 and Equation 6.11. Note that the battery weight is multiplied by a factor of 1.15. This is done to have some redundancy and to store excess energy to power other subsystems.

$$M_s = \frac{NPEC}{E_{specific}} \cdot 1.15 \quad (6.10)$$

$$V_s = \frac{NPEC}{\rho} \cdot 0.001 \cdot 1.15 \quad (6.11)$$

The specific energy density ($E_{specific}$) was discussed to be 350 kWh/kg and the density (ρ) to be 360 kWh/L.

6.5.3. Fuel Tank Sizing

The fuel cell consumes oxygen and hydrogen. The hydrogen is stored in liquid form. As previously discussed, thermal insulation is key to achieve high efficiency rates. Therefore, the tank needs to be properly designed. Before sizing the tank, the volume and weight of the hydrogen used need to be determined. As previously discussed, the fuel cell will generate a constant power (P_{FC}). Therefore, the fuel tank has to be designed to be able to supply a constant hydrogen flow to meet the power requirements. Afterwards, a 15% factor will be applied to have some excess fuel used to power the flight control systems, drive the compressors and have excess fuel in case of a deviation of the nominal mission or an emergency situation. The hydrogen mass is calculated via Equation 6.12. Where $\eta_{fuelcell}$ is the fuel cell efficiency, estimated at around 60% [8]. $E_{hydrogen}$ is the hydrogen energy density, which is 33.3 $\frac{kWh}{Kg}$ ². In Equation 6.13, the hydrogen volume is calculated. Where ρ is the density of hydrogen, being 70.8 kg/m^3 ³.

$$M_H = \frac{P_{FC} \cdot (t_1 + t_2)}{\eta_{fuelcell}} \cdot 1.15 \quad (6.12)$$

$$V_H = \frac{M_H}{\rho} \quad (6.13)$$

In [62], a linear approximation has been performed to estimate the sizing of the fuel tank. According to this analysis, for a liquid hydrogen mass in our range, a liquid hydrogen tank maximally stores 70% of its structural mass worth of liquid hydrogen. This means that the tank mass, including the maximum amount of hydrogen filled within, can be calculated using Equation 6.14.

$$W_T = \frac{M_H}{0.7} + M_H \quad (6.14)$$

The volume of the hydrogen tank is approximately $1.02 \cdot V_H$ [62]. The geometry of the fuel tank is yet to be determined. The benefit of using a liquid hydrogen fuel tank is that it does not necessarily have to be cylindrical. It can also be constructed in rectangular form [9]. The geometry will be altered to fit in the aircraft in the integration chapter.

6.5.4. Air Intake Sizing

Looking at the air intake system, a filter, a fan, a compressor, a heater and a humidifier are to be designed. The fuel mass mentioned is 115% of the fuel needed to perform a nominal mission. To design the intake system, we assume that the whole 115% is being used, so there is always plenty of oxygen to react with the hydrogen.

²<https://hypertextbook.com/facts/2005/MichelleFung.shtml> [Accessed 2019-06-18]

³2

The mission duration designed for is 3804 seconds. This is from take-off to final touch-down. However, the engine is on for a longer period of time (e.g. before take-off to power the electronics), so for the flow rate calculations we assume the engine to operate for 3900 seconds. In the integration chapter it is calculated that the hydrogen mass used is 37.4 kg. It is already used here to support the description of the oxygen intake sizing. The average fuel flow rate is $\frac{37.4}{3900} = 0.0096 \frac{\text{kg}}{\text{s}}$. From Equation 6.3, for every two molecules of hydrogen, there is one molecule of oxygen necessary to react with. One hydrogen atom weighs $1.67 \cdot 10^{-24}$ grams. Per second, $\frac{0.96}{1.67 \cdot 10^{-24}} = 5.748 \cdot 10^{23}$ molecules per second. This means that the fuel cell thus requires $\frac{5.748 \cdot 10^{23}}{2} = 2.87 \cdot 10^{23}$ molecules O_2 per second. The weight of one molecule O_2 is $2.66 \cdot 10^{-23}$ grams. So the oxygen inflow should be $2.87 \cdot 10^{23} \cdot 2.66 \cdot 10^{-23} = 7.645 \frac{\text{g}}{\text{s}}$. For this flow rate, the air intake components can be selected. The weights and volumes are summarised in Table 6.2 and obtained from [43] and [21].

Table 6.2: Intake system sizing.

Component	Weight [kg]	Volume [m^3]
Filter	0.8	$2.5 \cdot 10^{-4}$
Fan	1.4	0.0062
Compressor	10	0.021
Heater	5	0.016
Humidifier	0.8	0.0003

Next to these components, insulated tubes have to be added to transfer the air from component to component. The mass and volume of these components are negligible as they will be made to fit in the aircraft.

6.5.5. Hydrogen Transport System and Cooling Sizing

The hydrogen is transported from the tank to the fuel cell by an insulated tube (Figure 6.6). Additionally, there is a pump, a pressure regulator and a heat exchanger to alter the liquid hydrogen to a gas. This is then ready to go into the fuel cell. The weight of these systems combined is equal to 5% of the tank and fuel cell mass [11]. The results are presented in chapter 11.

6.6. Requirement Compliance & Feasibility

The power system has been designed such that it can deliver the required power during the mission with a given constant power level. Therefore, the first two requirements have been met. As the fuel cell delivers constant power and a PEM fuel cell typically has a lifetime of up to 3000 hrs[10], it is also expected that the third requirement is met. For comparison, a single EC-135 has about 400 hrs flight hours a year⁴.

Table 6.3: List of the requirements regarding the Fuel Cell subsystem.

Code Identifier	Requirement	Type	Verification	Compliance
EVTOL-SRFC-101	The fuel cell shall be able to provide sufficient power for the complete mission	Driving	Analysis	
EVTOL-SRFC-102	The fuel cell shall be able to provide a constant power level	Key	Analysis	
EVTOL-SRFC-102	The fuel cell shall not be required to be replaced within the first 5 years	Key	Analysis	

⁴Data retrieved from ANWB pilot

Detailed Design: Electrical System

An electrical system of an aircraft can be described as "a system of components which will generate, transmit, distribute, utilise and store electrical energy."¹ The complexity of an electric system varies staggeringly between a small drone and a complex modern passenger aircraft. However, they both share the same basic electrical components. In Figure 7.1, an overview of the principle individual electrical systems and their relationships is presented. Each block represents an electrical function which contributes to the overall de-

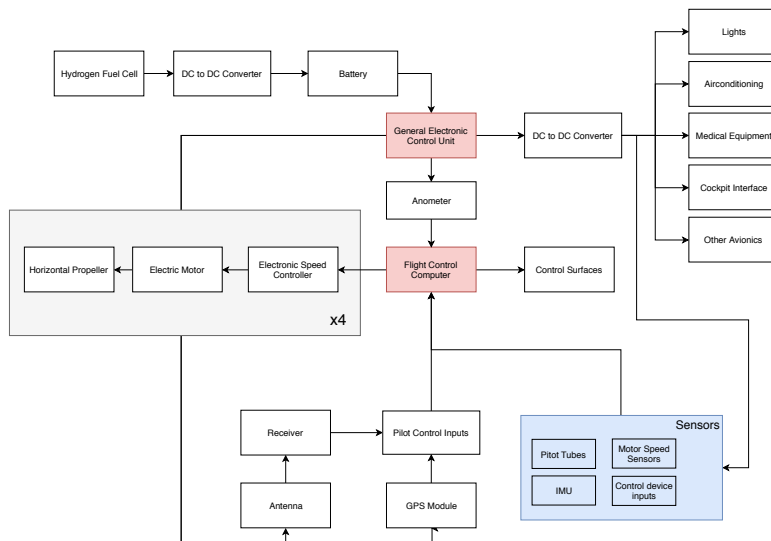


Figure 7.1: Electrical Block Diagram.

sign to meet the mission requirements. The electricity generated in the hydrogen fuel cell will be stored in the battery. The electronic control unit directs the right amount of energy to the important systems such as the antenna, medical equipment, cockpit interface and the flight control computer. The flight control computer distributes the energy to the control surfaces and propulsion systems, indicated with the grey block. The flight control computer is programmed to translate the inputs, i.e. pilot control inputs and sensor inputs, to the right control actuation individual propeller thrust to maintain stability and control.

7.1. Electrical System Weight Estimation

The overall electrical system will be split into two groups. One is the hardware electrical group containing the cabling, screens and other equipment and secondly, the avionics group. This method is based on FLOPS, a flight optimisation program developed by NASA for rapid conceptual aircraft design and weight estimations. The weight estimation equations are based on 42 different aircraft data that have been curve fit based on physical characteristics [59].

7.1.1. Electrical Hardware System

Firstly, the electrical hardware system. The large amount of electrical cabling, screens and equipment contributes a fair amount to the overall aircraft mass. Especially for smaller aircraft, the percentage of the electrical system weight with respect to the overall weight is more significant than larger aircraft. Various initial weight estimation tools have been developed. In the tool that Nasa developed, Equation 7.1 is used to approximate the electrical system weight[59]. In this equation W, L, b and N indicate the weight (kg), length

¹https://www.skybrary.aero/index.php/Aircraft_Electrical_Systems [Accessed 2019-06-19]

(m), width (m) and amount (N) of their respective subscripts. Equation 7.1 is related to the electrical system estimation of aircraft. It should be noted that the electrical hydrogen system weight estimation has been performed in section 6.5 and is not taken into account here. This formula can hence be used as it is expected that the amount of cabling, screens and equipment should not necessarily differ from any other aircraft.

$$W_{ELEC} = 12.72 \cdot L_{fuselage}^{0.4} \cdot b_{fuselage}^{0.14} \cdot N_{fuselages}^{0.27} \cdot N_{engines}^{0.69} \cdot \left(1 + \frac{11}{250} \cdot N_{flight\ crew} + \frac{3}{2000} \cdot N_{passengers} \right) \quad (7.1)$$

Equation 7.1 gives an estimated electrical system weight of 121.55kg. This is based on a fuselage length of 11.0m, a fuselage width of 1.5m, one fuselage, 5 engines, 3 flight crew and 2 passengers.

7.1.2. Avionics Subsystem

The avionics system contains all of the systems required for navigation, communication, displays and the management of the various systems used to perform individual functions. In order to know the weight of the avionics, the minimum required equipment for the EC135 was investigated [1]. The components in Figure 7.2 are required for the EC135 helicopter. Some of the avionic components in Figure 7.2 are already

Minimum required equipment for Avionics Solution 8 and 11					
Document reference	Commercial reference	Title	Weight (margin 2-3 %) kg lb		
05-03007-C	L2562-001-00	First aid kit ¹⁴	1.3 2.9		
05-22008-C	L2621-001-00	Engine fire extinguishing system	3.6 7.9		
05-33001-B	L3113-001-00	Slant panel	0.8 1.8		
05-33002-B	L3113-004-00	Center console	2.2 4.9		
05-34002-B	L2576-001-00	Avionics compartment	4.2 9.3		
05-37016-C	L6701-001-00	Copilot flight controls	6.0 13.2		
05-38010-B	L3111-001-04	7" copilot instrument panel with glare shield	2.7 6.0		
05-39006-B	L2514-003-01	Map case in copilot door	0.5 1.1		
05-39007-B	L3111-001-10	Map case on instrument panel glare shield	0.6 1.3		
05-39008-B	L3113-004-10	Illuminated chart holder for pilot side	0.9 2.0		
05-41004-C	L2104-100-00	Bleed air heating system ¹⁵	6.6 14.6		
05-61010-B	L2433-006-00	Battery, type (Saft) ULM, 40 Ah, 24 V instead of standard battery	16.8 37.0		
 ¹⁴ Reinforced landing gear cross tube instead of standard generator					
¹⁵ Landing & search light, 450 W					
¹⁶ ELT C406-N HM (ArteX) incl. NAV. opt.					
¹⁷ Avionics Solution 8 or Avionics Solution 11					
¹⁸ Radar Altimeter KRA 405B (Honeywell)					
¹⁹ MEGHAS Sensor kit					
²⁰ Copilot pilot static system					
²¹ IFR SAS (IFR pitch/roll Stability Augmentation System)					
²² Digital Automatic Flight Control System - DAFCS					

Figure 7.2: Avionics used in EC135 and incorporated in the aircraft.

accounted for in other subsystems. Components 05-61010-B and 05-63003-B are estimated in the fuel system. Taking the other required components for the avionics system as shown in Figure 7.2 results in the final weight of the avionics to be 100 kg. Scaled for the final weight of the H₂ERO with respect to the EC135 $\frac{MTOW}{MTOW_{EC135}} \cdot 100$ would be 118 kg for the avionics system.

7.2. Requirement Compliance & Feasibility

Regarding the requirements set for the electronics subsystem, it has been determined that the electronics subsystem design fulfils all of the predetermined requirements that were established.

Table 7.1: List of the requirements regarding the Electronics subsystem.

Code Identifier	Requirement	Type	Verification	Compliance
EVTOL-SREL-201	The maximum temperature of the battery and electronic subsystems shall be 25°C during operation	Driving	Analysis	
EVTOL-SREL-202	The minimum battery capacity shall provide power throughout all phases of the aircraft's mission	Driving	Analysis	
EVTOL-SREL-203	The battery system shall be charged during flight	Driving	Analysis	
EVTOL-SREL-207	The energy density of the battery shall be able to fulfil structural sizing constraints while also fulfilling requirement EVTOL-SREL-202	Driving	Analysis	

Table 7.2: List of the requirements regarding the Avionics Subsystem.

Code Identifier	Requirement	Type	Verification	Compliance
EVTOL-SRAV-251	The aircraft shall allow for communication with the air traffic control tower	Regular	Analysis	
EVTOL-SRAV-252	The aircraft shall allow for communication with the hospitals that can allow for emergency aircraft landing	Regular	Analysis	
EVTOL-SRAV-253	The aircraft shall allow for communication with the emergency control room ('Meldkamer Ambulancezorg')	Regular	Analysis	
EVTOL-SRAV-254	The aircraft shall allow for communication between the people in the cabin	Regular	Analysis	
EVTOL-SRAV-255	The aircraft shall allow for communication between the pilot and the people in the cabin	Regular	Analysis	
EVTOL-SRAV-256	The different communication systems shall not cause any interference.	Regular	Analysis	
EVTOL-SRAV-257	All relevant flight parameters shall be clearly displayed to the pilots	Regular	Analysis	
EVTOL-SRAV-258	All the relevant flight parameters according to TBD legislation shall be recorded	Regular	Analysis	

Detailed Design: Aerodynamics

In this chapter, the aerodynamic subsystem of the H₂ERO will be analysed and designed. First, an airfoil selection is done, followed by the wing planform design. Next, a brief analysis of the tail design, transition phase and noise reduction techniques is given. Finally, this subsystem is checked for requirement compliance and feasibility.

An attempt has been made to perform a complete analysis of the aerodynamic subsystem. However, this is only a preliminary design of the aerodynamics of the aircraft as more time is required for a more extensive analysis. Therefore, the estimation methods are not the most advanced methods available which makes it difficult to do a fully quantitative analysis. As a result some important aerodynamic factors have only been assessed quantitatively.

In chapter 11 the final values and aerodynamic performance (lift curve and lift drag polar) is specified. In chapter 16 recommendations are given on how to further proceed with the aerodynamic analysis of the H₂ERO.

8.1. Airfoil Selection

A design is chosen that is not exactly a blended wing body, but does have an airfoil design for the fuselage as well, in order to minimise drag and create some extra lift.¹ Therefore two airfoils must be selected of which the process will be illustrated in this chapter.

8.1.1. Preliminary Selection

In order to make the airfoil selection process more efficient, only a limited amount of airfoils will be analysed in detail using software tools. Therefore, a number of airfoils are selected based on required thickness over chord ratio, design lift coefficient and airfoil group. To perform this preliminary selection in an efficient manner and to verify the eventual analysis, it was chosen to use NACA airfoil series. These series were chosen because the name of the airfoil gives an indication of certain important characteristics of the airfoil. This approach improves the fast optimisation of the process given the limited time. Additionally, it was chosen to opt for these NACA series as an extensive amount of experimental data is available. This is beneficial as the data can be used to validate the results of the software used to analyse the airfoils, as described in subsection 13.1.4. The NACA 6-series is used because they are designed to maximise the laminar flow (which will be the case for H₂ERO because of the low cruise speed), has good stall characteristics and a low profile drag [27].

Design Lift Coefficient

The design lift coefficient is calculated using Equation 8.1, for 2D analysis to know what lift coefficient the airfoil should provide in cruise flight. The parameters needed to perform this calculation were obtained from the preliminary estimations described in the midterm report [2].

$$C_{L_{des}} = \frac{L}{\frac{1}{2} \rho S V^2} \quad (8.1)$$

The final value for the design lift coefficient is 0.25.

¹This design choice is later on changed section 11.6, resulting in a conventional fuselage design.

Thickness to Chord Ratio

The thickness to chord ratio is a driving factor of the airfoil selection, especially for the fuselage part, because it is determined by the minimum cabin dimensions. The cabin needs to fit inside the fuselage section in order to have a feasible design. All the different structural elements and subsystem components, usually fuel tanks, stored in the wing should fit as well. Initial estimates of the cabin dimensions were: a height of 1.5 meters and a length of 9 meters. This results in a minimum $\frac{t}{c} = 0.17$ for the fuselage section. Because the rotors take up a large part of the wing and will not allow for larger tubes connecting other subsystems to the cabin, it is designed that little to no subsystem components are stored in the wing. Only some electronics and connections for the lights at the wing tips and control surfaces will be present. Therefore, a minimum $\frac{t}{c} = 0.08$ should be sufficient for the wing part.

A higher t/c will result in a lower structural weight due to the higher moment of inertia. However, it will also increase friction drag, because of earlier separation. The location of maximum thickness is closely related to the airfoil maximum pressure position. Thus the further aft, the lower the minimum drag but also the lower the maximum lift coefficient. Also there is a lower maximum pressure peak, resulting in a higher critical Mach number.

Camber

The most important feature of cambered airfoils is that lift is generated at zero angle of attack. This is favourable for the wing and fuselage section, since they are designed to produce lift (and no down force, like the tail). Therefore, a cambered airfoil is chosen for both the wing and fuselage section.

What should also be taken into account for cambered airfoil is the fact that cambered airfoils create a quarter chord pitching moment which tends to rotate the airfoil leading edge down. Also, the general airfoil's pitching moment is increased with increasing camber. This will require a larger counteracting force from the tail in order to trim the aircraft. This will be taken into account for the stability and control of the aircraft. Additionally, camber increases the maximum lift coefficient and produces higher values for the lift coefficient in correspondence with lower angles of attack, both favourable. The lift curve slope is unaffected with a change in camber. The camber position is also of influence. Moving the camber further towards the nose, results in a higher maximum lift coefficient but unfavourable stall characteristics. Moving the camber more aft decreases the maximum lift coefficient, but results in a more gradual stall transition (which is more favourable).

Reynolds Number

A change in Reynolds number influences the aerodynamic behaviours of the airfoil. With increasing Reynolds numbers the friction coefficient is lower as long as the flow is laminar. As soon as the transition to turbulent flow takes place, the friction increases suddenly. Afterwards the friction drag decreases again with increasing Reynolds numbers. High values of the Reynolds number allow the flow to stay attached longer, as the boundary layer has more energy and is therefore less influenced by the adverse pressure gradient. Therefore, the drag due to flow separation is decreased and the maximum lift coefficient increased. The change in lift coefficient with changing angles of attack is unaffected by a change in Reynolds number, hence the lift curve slope stays the same.

Mach Number

The Mach number for the mission of H₂ERO is 0.2 at cruise; With a cruise speed of 69 m/s and at 366 meters of altitude, where the speed of sound is 339 m/s, the H₂ERO Mach number ($M = \frac{V}{A}$) equals 0.2. In this incompressible region ($M < 0.3$) the lift is almost constant. However, the local Mach number at the wing can be higher, and if it is higher than 0.3, compressibility should be taken into account. Due to the additional flow acceleration lift starts to increase. At critical Mach number the first point on the (upper surface) of the airfoil reaches $M=1$ and further increasing the Mach number will result in supersonic flow. This will not happen for the H₂ERO, however, because of the low flight speed. Therefore, the effects of critical Mach number will not be of importance for the design.

Reflexed and Symmetrical Airfoils

In contrast to cambered airfoils, symmetrical airfoils can generate negative and zero lift. This makes them very suitable for tail surfaces, which should be able to generate a down force. However, for the wing and fuselage sections a cambered airfoil is preferred since it creates more lift and less drag as discussed before.

For a reflexed (cambered) airfoil shape, the trailing edge is bent upwards, influencing the moment coefficient. Adding reflex to the camber line moves the moment coefficient towards positive values, which helps for longitudinal stability. However, the lift drag polar is shifted down, thus the (maximum) lift is decreased. This leads to higher stall and approach speeds, which is not favourable. For the initial design of the wing, non-reflexed airfoils are chosen, in order to maximise lift and minimise drag. Also, less validation data is available for reflexed airfoils which makes the analysis more unreliable. However, should the moment coefficient of the airfoil pose severe problems for the stability and control of the aircraft, this airfoil selection is revisited and reflexed airfoils are taken into consideration as well.

The analysis of the above parameters resulted in the following airfoils to be analysed.

- Fuselage section: NACA64421, NACA65318, NACA65321, NACA66418,
NACA64221, NACA65218, NACA65221, NACA66218
- Wing section: NACA65209, NACA63210, NACA64210, NACA65212, NACA65215

8.1.2. Analysis of Airfoil Characteristics

For the analysis of the airfoils several software options were considered. The first option that was considered was JavaFoil. The biggest limitation of this software is its ability to model viscous effects as it uses complementary formulations to estimate the drag and the stall characteristics[40]. The second option that was considered was Xfoil. This software performs better in modelling of these viscous effects, however it is still not perfect. Additionally, the interface of Xfoil gives the ability to automate the analysis process in a simple manner. This increases the speed and efficiency of the process. The last option that was considered was Computational Fluid Dynamics (CFD). Although this is the most accurate method, it is also the most time consuming method. Additionally, one has to be careful when using CFD as small errors in for example boundary conditions or initial values will result in faulty results while the perception is that the results are correct. Eventually, it was chosen to use Xfoil due to the time-efficient process while having a better accuracy as JavaFoil.

However, another limitation of Xfoil (the same is true for Javafoil) is that it is designed and developed for low Reynolds numbers. Due to the large chord, the airfoils needed to be analysed for Reynold numbers up to 42 million. This means that the eventual results might not resemble reality. After consultation with multiple professors of the Aerospace Faculty of the University of Technology in Delft, it was recommended to nevertheless use Xfoil and validate the results using test data, since no other software tools or analytical methods are available. The Reynolds number predominantly affects the boundary layer shape, and therefore the maximum lift coefficient. Therefore, these values are only used as a preliminary estimate and should be validated using CFD and wind tunnel testing in future research.

Moreover, convergence plots were made to see the effect of increasing Reynolds number. These were used to verify Xfoil and to choose the aerodynamic coefficients correctly. Since Xfoil will not converge correctly for each angle of attack, these plot serve as a check that the selected parameters are not outliers, but indeed follow the general trend. This is further illustrated in the paragraphs below.

An example is given in Figure 8.1. As can be seen here the maximum lift coefficient does converge for higher Reynolds numbers. The peaks in this convergence plot for maximum lift coefficient can be explained by the way Xfoil works. If Xfoil does not converge after four iterations it will break. This can occur both for the panels (the airfoil geometry) and for the angle of attack. Xfoil takes the previous input and iterates on that value to calculate the aerodynamic properties. If the paneling does not converge, no outputs are given. Thus, the peaks in the figure are caused by non convergence for higher angles of attack, causing the program to quit early and thus a lower maximum lift coefficient.

The lift curve slope should not change with Reynolds number. However, the top left plot in Figure 8.1 does

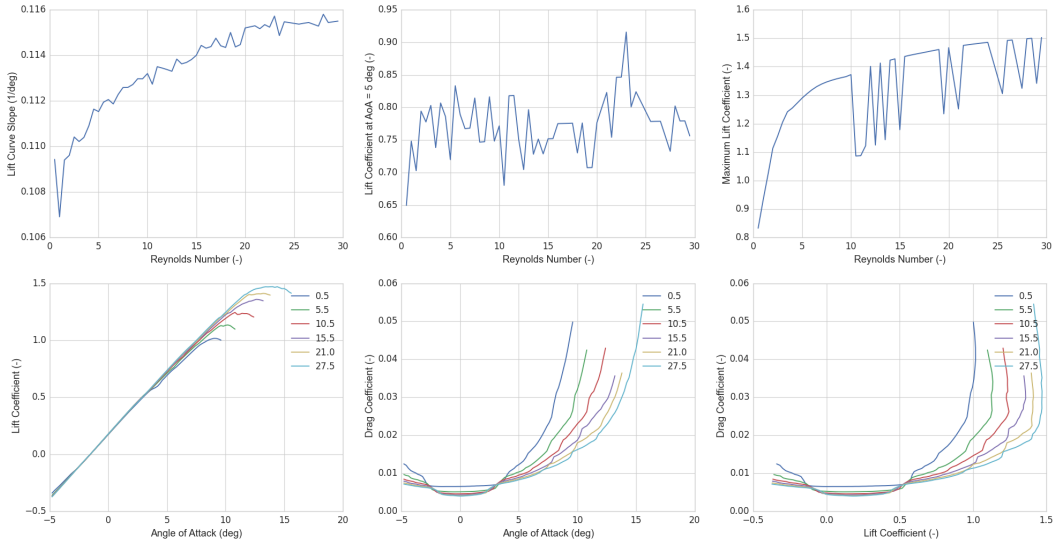


Figure 8.1: Overview of XFOIL analysis for the NACA64210 airfoil for different Reynolds numbers at $M=0.2$.

show a increase of the lift curve slope, with a difference of 7%. For the Reynolds number that the aerodynamic coefficients are analysed for, $14 \cdot 10^6$, this difference is just below 5%. This is considered an acceptable value for this initial analyses, but it should be noted that the lift curve slope will be less reliable for higher Reynolds numbers.

The lift coefficient at the arbitrary angle of attack of 5 degrees shows fluctuations for different Reynolds numbers as well. The value for Reynolds number 23 is clearly an outlier, and hence this specific Reynolds number should not be used to determine the aerodynamic coefficients. When the outlier is taken out, the difference in lift coefficient per Reynolds number is just 6%. This makes sense, since it is on the linear part of lift curve, which is approximately the same for changing Reynolds numbers. Hence, this curve serves as an extra check for outliers.

Note: not all airfoils gave sensible results in XFOIL, even after changing the number of iterations or the paneling of the airfoil geometry. If this was the case, these specific airfoils were removed from the preliminary selection, since no sensible aerodynamic data could be used for these.

Boundary Layer Analysis

The wing contains a hole which eventually is covered up, as a consequence the surface of the wing at this area small bumps and holes. This will cause the boundary layer to make the transition of laminar to turbulent at an earlier stage. Eventually, this influences the lift curve and thus this phenomena required to be investigated. An attempt has been made by using XFOIL to analyse this by setting this transition phase at the most forward position where disturbances of the surface will occur (start of the covered up hole). Unfortunately, the results of this were not expected as the polar is almost identical to the analysis as can be seen in Figure 8.2. As no sensible results were obtained, it is highly desired to investigate this further with more advanced software.

8.1.3. Airfoil Trade Off

All the parameters for the airfoil trade off influence the the performance of the airfoil, and therefore of the wing and aircraft in general. They are given in Table 8.1 and Table 8.2 where it also indicated what the desired value is. The trade off criteria are based the approach as written by Gudmundsson [18] and are chosen since they all influence the performance of the airfoil, and thus the wing. Since this airfoil analysis only provides a rough estimation of the aerodynamic characteristics, the airfoils can only be compared relative to each other. Therefore a simple trade off is performed, where a 0 is given for the least favourable score(s), and a 1 is given for the most favourable score(s). These are then added to see which airfoil performs best. All criterion

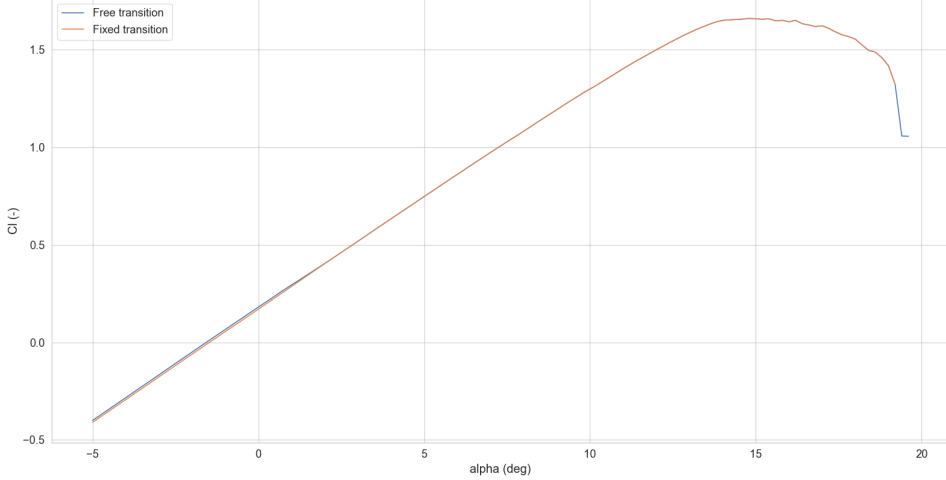


Figure 8.2: Lift curve for free boundary layer transition point and fixed point.

have equal weights.

Table 8.1: Airfoil trade off for fuselage section.

Parameter	Desired Outcome	Fuselage Airfoil					Trade Off Score [0 or 1]				
		NACA64421	NACA65318	NACA65321	NACA66418	NACA64221	NACA64421	NACA65318	NACA65321	NACA66418	NACA64221
Thickness Ratio [-]	High is best	0.21	0.18	0.21	0.18	0.21	1	0	1	0	1
Cl for AoA = 0 [-]	Close to Clcruise is best	0.33	0.25	0.20	0.36	0.17	0	1	1	0	0
AoA for Cl=0 [deg]	-2.69	-2.27	-2.26	-3.23	-1.33						
Clmax [-]	High is best	1.23	0.96	1.07	0.90	1.09	1	0	1	0	1
AoA of Clmax [deg]	High is best	8.3	6.5	9.0	5.0	7.8	1	0	1	0	0
Cdmin [-]	Low is best	0.0043	0.0035	0.0036	0.0037	0.0039	0	1	1	0	0
Cl of Cdmin [-]	Close to Clcruise is best	0.18	0.27	0.29	0.46	0.22	0	1	1	0	1
(Cl/Cd)max [-]	High is best	163	124	134	127	120	1	0	0	0	0
Cl of (Cl/Cd)max [-]	Low is best	0.78	1.1	0.53	0.48	1.07	0	0	1	1	0
Cruise Cm [-]	Close to zero is best	-0.080	-0.063	-0.062	-0.087	-0.042	0	0	0	0	1
Drag bucket length [-]	Large is best (within operational range)	0.53	0.29	0.36	0.49	0.33	1	0	0	1	0
Cl cruise inside drag bucket? (Y/N)	Yes; else not feasible	No	Yes	Yes	Yes	Yes	no go	1	1	1	1
							Som	6	5	9	4
											6

Table 8.2: Airfoil trade off for wing section.

Parameter	Desired Outcome	Wing Airfoil				Trade Off Score [0 or 1]				
		NACA65209	NACA63210	NACA64210	NACA65212	NACA65209	NACA63210	NACA64210	NACA65212	
Thickness Ratio [-]	High is best	0.09	0.10	0.10	0.12	0	0	0	1	
Cl for AoA = 0 [-]	Close to Clcruise is best	0.18	0.18	0.18	0.19	0	0	0	1	
AoA for Cl=0 [deg]	-1.61	-0.00055	-1.55	-1.62						
Clmax [-]	High is best	1.52	1.75	1.74	1.25	0	1	1	0	
AoA of Clmax [deg]	High is best	13.2	16.2	16.2	11.9	0	1	1	0	
Cdmin [-]	Low is best	0.0043	0.0039	0.0041	0.0036	0	0	0	1	
Cl of Cdmin [-]	Close to Clcruise is best	0.16	0.18	0.23	0.21	0	0	1	0	
(Cl/Cd)max [-]	High is best	132	133	133	128	0	1	1	0	
Cl of (Cl/Cd)max [-]	Low is best	1.01	1.23	1.23	1.17	1	0	0	0	
Cruise Cm [-]	Close to zero is best	-0.042	-0.043	-0.043	-0.043	1	1	1	1	
Drag bucket length [-]	Large is best (within operational range)	0.15	0.23	0.36	0.59	0	0	1	1	
Cl cruise inside drag bucket? (Y/N)	Yes; else not feasible	No	Yes	Yes	Yes	no go	1	1	1	
						Som	2 (no go)	5	7	6

As can be seen from Table 8.1 and Table 8.2, the NACA65321 and NACA64210 are chosen as airfoils for the fuselage and wing section respectively.

Trade-Off Sensitivity Analysis

It should be noticed that because this trade-off uses the equal weights it is very sensitive. If one airfoil behaves slightly better or worse than expected, this will change a zero into a one or the other way around. In contrast to the wing airfoil section, there is a large difference between the final score of fuselage section winner and the other airfoils. Therefore, the wing airfoil selection is more sensitive to change than the

fuselage airfoil selection. For the wing airfoil selection, all the scores are very close to each other, so no a solid conclusion can be drawn. For now the airfoil with the highest score is chosen.

8.2. Wing Design

8.2.1. 2D to 3D

After the airfoil had been chosen and its characteristics had been estimated, the airfoil characteristics had to be transformed into wing characteristics. Characteristics which have been translated or an effort is made to this are: the lift curve slope $C_{L\alpha}$, maximum lift coefficient $C_{L_{max}}$, the zero lift drag coefficient C_{D0} , the drag coefficient C_D and the moment coefficient $C_{M\alpha}$

Lift Curve Slope

For the approximation of the 3D lift curve slope, Equation 8.2 has been used [18]. This equation is used as it takes into account the Aspect Ratio (AR), compressibility, deviations from the theoretical 2π lift curve slope, sweep angle (λ) and the taper ratio. The latter is not directly visible as the sweep angle and the taper ratio substituted by the half chord sweep ($\lambda_{0.5c}$).

$$\frac{dC_L}{d\alpha} = C_{L\alpha} = \frac{2\pi AR}{2 + \sqrt{4 + \left(\frac{AR\beta}{C_{l\alpha}/2\pi}\right)\left(1 + \frac{\tan^2 \lambda_{0.5c}}{\beta^2}\right)}} \quad (8.2)$$

where β resembles the Prandtl-Glauert compressibility factor which can be calculated using the following equation.

$$\beta = \sqrt{1 - M_\infty^2} \quad (8.3)$$

Maximum Lift Coefficient

For the approximation of $C_{L_{max}}$ several numerical or semi-empirical methods have been analysed. The conditions required for each of these methods can be seen in Table 8.3. In this table one can see that for all the considered methods, not all required conditions are satisfied. However, it was chosen to still use the method that fits the conditions best in order to get an initial estimation. The method that was chosen was the Phillips and Alleys method as the require conditions matched best with the aircraft's wing characteristics.

Table 8.3: $C_{L_{max}}$ estimation methods.

Method	Description	Conditions
α -method	Apply corrections to the Angle of Attack (AoA) of inviscid 3D analysis by using 2D experiments or CFD tools	No 3D inviscid analysis & No 2D experiments or CFD
ESDU 89034	Table look-up method with empirically derived data	Only for Re up to 12 million & Tables not accesible to the author.
USAF DATCOM	Empirical table look-up method	High AR
Phillips and Alley	Correction of classical lifting line theory for sweep, twist and aspect ratio	AR of 4 or higher

To calculate this maximum lift coefficient, the Phillips and Alley's method uses Equation 8.4. $\kappa_{L\Omega}$ and $\kappa_{L\Lambda}$ are correction factors to account for the sweep angle and twist angle respectively. The values of these can be calculated by using data which is read out of graphs. The exact equations and graphs of these values do not add to the understanding of the reader and therefore they will not be discussed further. The interested reader find the exact calculations and graphs on page 901 - 904 in [42]

$$C_{L_{max}} = \left(\frac{C_L}{C_{l_{max}}} \right)_{\substack{\Omega=0 \\ \Lambda=0}} \kappa_{L\Lambda} (C_{l_{max}} - \kappa_{L\Omega} C_{L,\alpha} \Omega) \quad (8.4)$$

After the calculations had been performed it turned out that the predicted maximum lift coefficient was very close to the maximum lift coefficient only had a difference of .04 compared to the 2D airfoil. The moment this was discovered and the computation was verified, it was decided to discard the calculation

and to use a more arbitrary method for the prediction. For aircraft with low aspect ratios it is common that the maximum lift coefficient is reduced by 30%. This 30% reduction has also been applied to the airfoil maximum lift coefficient to obtain the maximum lift coefficient of the wing.

Drag Coefficient

For the drag coefficient no direct translation method from the 2D to 3D was found. Therefore, a method is used which isn't directly linked to the airfoil data. The equation used to approximate the drag coefficient is Equation 8.5[39]. C_{D0} represents the zero lift drag while the second part represents the lift induced drag. In order to estimate this lift induced drag coefficient, the Oswald efficiency factor needs to be estimated. For unswept wings the Oswald efficiency factor can be established using Equation 8.6. For swept wings a different equation should be used, however the very small leading edge sweep and small AR causes equation for swept wings to go above 1. Therefore, the equation for unswept wings is used.

$$C_D = C_{D0} + \frac{C_L^2}{\pi AR e} \quad (8.5) \quad e = 1.78(1 - 0.045 AR^{0.68}) - 0.64 \quad (8.6)$$

C_{D0} is estimated by using Equation 8.7. For every component c, the respective value for C_{Dc} is multiplied by their corresponding area. For the wing, the reference area should be used, whereas for the fuselage, the frontal area of the fuselage should be used. $C_{D_{misc}}$ is a drag increment for interference, roughness and excrescence. For this value 15% of C_{D0} is used. The values for C_{Dc} that are used are obtained from[39].

$$C_{D0} = \frac{1}{S_{ref}} \sum_c C_{Dc} A_c + C_{D_{misc}} \quad (8.7)$$

Moment Coefficient

For the moment coefficient the most important parameter is to estimate the pitching moment coefficient for the 3D wing. Once this C_{M_α} has been determined, this can be translated into the the moment coefficient itself.[18] C_{M_α} can be calculated using Equation 8.8.

$$(C_{M_\alpha})_{3D} = C_{L_\alpha} \frac{C_{m_\alpha}}{C_{l_\alpha}} \quad (8.8)$$

8.2.2. Aspect Ratio

The H₂ERO has a relatively small aspect ratio which is most dominantly determined by the maximum wing span of 15 meters, the positioning of the rotors and the weight reduction. In addition, it is beneficial for the structural design because of the stiffness requirements are easier met. Generally a higher aspect ratio is desired since this results in a higher L/D ratio and therefore a higher aerodynamic efficiency. However, the lower aspect ratio is compensated by the smaller wetted area of the this design, since the fuselage will generate lift as well (even though this is to a limited extent)². Hence, even though the induced drag is higher because of a small aspect ratio, the skin friction drag is much smaller because of the aerodynamic fuselage design. A parameter that illustrates this effect is the wetted aspect ratio.

$$AR_{wet} = \frac{b^2}{S_{wet}} = \frac{AR}{S_{wet}/S} \quad (8.9)$$

Both Roskam and Torenbeek showed that even though the configuration is very different, performance is very similar for aircraft with the same AR_{wet} [26].

²As mentioned before, this design is later changed to a non lifting fuselage. Therefore, the wing surface area had to be enlarged in order to allow for enough lift being produced

8.2.3. Wing Planform

The most important considerations for which the wing planform should be designed include [18]:

- Generate lift using the span efficiently
- No excessive bending moment
- Docile stall characteristics
- Acceptable roll responsiveness

Wing planforms can be categorised into a number of categories as shown in Table 8.4. These different types have been researched and the main advantages and disadvantages are described in the table. As can be seen, the delta planform is not relevant, since a low subsonic speed range is considered. Furthermore, the formation of shock waves and critical Mach number considerations are not relevant due to the low Mach number ($M = 0.2$). Also, there is no need for thick airfoils in the wing, since they are not used for storage. The large chord length close to the root allows for sufficient thickness at lower t/c ratio's to store the propellers. Therefore, the crescent planform loses its main advantage. Since a low aspect ratio is considered, wing tip flex will be non existent or very small. Therefore, a Schuemann planform is undesired since it requires extreme wash out to be able to counteract the wing tip stall. Swept wings are most suitable for aircraft flying at the high end of the subsonic range and are hence less applicable to this aircraft, flying at $M = 0.2$. Constant chord planforms will add unused wing area, hence increasing the weight unnecessarily. Elliptical planforms will need countermeasures against stall and more advance manufacturing techniques. Hence, the straight tapered or semi tapered wing planform is the most optimum design and will be used for the H₂ERO.

Table 8.4: Overview of the main advantages and disadvantages of different types of wing planforms; based on the findings by Gudmundsson[18].

Planform Type	Advantages	Disadvantages
Constant chord (rectangular)	Favourable stall characteristics (slow progression; root stall before tip stall) Lower manufacturing costs (constant thickness; same rib geometry)	Inefficient use of wing span (wing tip contributes less to lift generation than root)
Elliptical	Uniform distribution of section lift coefficients: efficient use of span Least amount of lift-induced drag of all planform types	Manufacturing issues: complex compound surfaces Entire wing stalls at once (when using constant airfoil over the span): need decisive washout or solve with different airfoil selection
Straight Tapered	Reduction in bending moments: structural benefits Less lift-induced drag: efficient use of wing span Improved efficiency (wing tips produce more lift) compared to constant chord Easier to manufacture than elliptical	Taper compromises stall characteristics: need washout or airfoil at tip that regulates stall Manufacturing complications (different geometry each rib)
Straight LE/TE edges (tapered)	Easy solution to shifting the CG position Improved structural and aerodynamic efficiency compared to constant-chord configuration	Challenging to use single-piece spar (caps will be curved) FW sweep angle for hinge line control surfaces: less efficient more complicated control system
Aft-swept	Delays formation of shockwaves to a higher Mach number Less susceptible to flutter Easy solution to shifting the CG position aft	Deterioration airflow close to tip with increasing AOA Increase in wing torsion (increasing weight airframe) Nose pitch-up moment when approaching stall Deterioration in roll stability and aileron effectiveness (when approaching stall)
Forward swept	Inboard wing stalls first: great roll stability at stall Ailerons effective at high AoA also Reduced bending moments (center lift closer to line of symmetry) compared to aft swept Early flow separation prevented by fuselage acting as border Easy solution to shifting the CG position forward	Divergent aeroelastic deformation (countermeasures will increase weight)
Cranked: semi tapered	Section lift coefficients of outer wing increased: more efficient use of span Aileron effectiveness increased (except when hingeline becomes highly swept)	More complex to manufacture (no constant thickness or rib geometry)
Crescent	Allows use of thick airfoils without introducing early shock formation at high Mach numbers Improved aileron control authority and reduced tendency tip stall nose pitch-up	More complex to manufacture (no constant thickness or rib geometry)
Schuemann	Approximates elliptical lift distribution; limits lift-induced drag efficient use of span	Early wing tip stall (sharp outboard taper); Can be solved by wing tip flex at high AOA: makes center part wing stall first or by applying extreme wash out
Delta	Intended for high-subsonic or supersonic aircraft (not relevant for this project)	Requires high approach speed

8.2.4. Wing Position

Three wing positions are considered: a high, mid and low wing configuration. The most dominant reason pleading for a low wing configuration is better ground manoeuvring because of the wider wheel track possible. Since the H₂ERO will land and take off vertically, this is not an added advantage. Other advantages of a low wing configuration is the lower interference drag, only at the upper fuselage part. Also, it benefits more from the ground effect. However, the lift generation is disturbed by the fuselage intersection, the rolling moment is destabilising and there is less ground clearance [27]. This makes it also harder to manoeuvre around the aircraft when on the ground.

A mid wing configuration generally has a lighter structure due to less wing root fairing being necessary. It may also have a neutral rolling moment. However, it suffers from a high interference drag, both at the upper and lower fuselage parts. Also, the lift generation is interfered with the presence of the fuselage, similar to low wing [27]. The largest disadvantage for the H₂ERO, however, is the amount of fuselage taken up for the wing attachment, not leaving sufficient room to place the door and potentially rotors outside of the wing configuration.

In contrast, a high wing configuration allows for better ground clearance and allows the fuselage to be closer to the ground, which benefits loading and unloading. Both are advantages for H₂ERO since the pilot is dependent on visibility and a stretcher should be able to manoeuvre in- and outside of the aircraft. In addition, high wing aircraft have a stabilising rolling moment. Also, the high wing configuration has a better lift generation and lower interference drag due to the clean upper surface. The under-wing fuselage corner does create extra drag, however. Another disadvantage of the high wing configuration is the heavy reinforced structure needed to suspend the fuselage [27].

Thus, all configurations have their advantages and disadvantages for lift, drag and structures. These can all be designed for, however. The driving factors for the H₂ERO is the door position and sufficient manoeuvre space when on the ground, needed in the mission profile of the emergency aircraft. The aircraft needs to land in civil neighbourhoods and allow for loading a patient on a stretcher. Therefore, a high wing configuration is chosen for the H₂ERO.

8.2.5. Wing Incidence Angle and Twist

The wing can be set at a certain pitch angle with respect to the fuselage which will make the fuselage pitch angle smaller. This will limit higher angles of attack needed in the mission profile which is beneficial in case a patient is transported in the aircraft. For the H₂ERO, the wing incidence angle is set at 2.5 degrees, since this angle of attack provides the most design lift in cruise, as shown in Figure 11.8.

Twist is generally used to prevent the wingtip region from stalling before the wing root does (geometric washout) and to modify the spanwise lift distribution to achieve minimum drag, and is optimised for cruise conditions. However, for unswept wings, twist is of very little influence [26]. This is also visualised in Figure 8.3 where the twist angle will go to infinity for zero sweep.

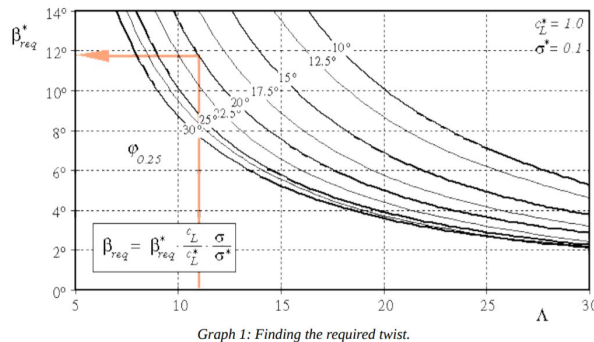


Figure 8.3: Twist angle required for certain sweep angle (the orange arrow is not relevant here) [6].

Since the H₂ERO has unswept wings (quarter chord sweep), twist will not be applied, and therefore favourable stall characteristics should be obtained by other design parameters.

8.2.6. Stall Characteristics

Any aircraft should be designed to have good stall characteristics to ensure safety. Flow separation is only dependent on aircraft geometry and hence measures can be taken in order to avoid this. It is desired for the wing stall to start at the root and then progress towards the wing tip for increasing angle of attack, else the stall will be unstable and create stability problems. Ideally the wing tip should always be un-stalled to ensure roll stability [44]. Separation can both be caused by high angles of attack, which is unavoidable, and by poor geometry on wing/fuselage juncture (where stall will occur for low angles of attack as well). This can be solved by designing an appropriate wing root fairing in order to avoid an separation bubble which will increase the drag.

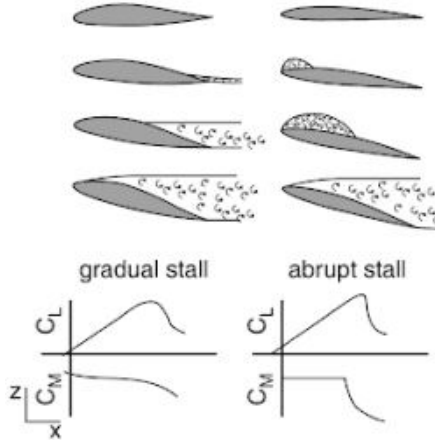


Figure 8.4: Abrupt and gradual stall pattern [27].

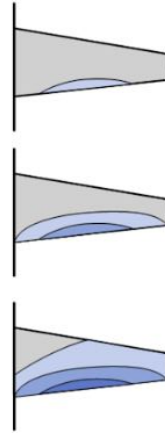


Figure 8.5: Stall pattern over tapered wing [18].

As can be seen in Figure 8.4 and Figure 8.5 the stall pattern for a tapered wing does not necessarily start at the root, but instead starts mid wing and then progresses both to the wing root and wing tip. Since washout will not be as effective, other ways to keep the wing tips unstalled must be applied. These include applying vortex generators at the leading edge of the wing tip. They disturb the airflow into turbulent flow, meaning they the airflow will stay attached to the surface longer. In addition, a stall fence can be place inside the ailerons. They form a barrier to stalled airflow, such that the pilot can use the ailerons to control the aircraft even when the main wing area has stalled. A stall strip works in the exact opposite way of vortex generator, because they encourage stall. These could be placed at the root of the wing, to make sure it stalls before the wing tip does.

Also, gradual stall is desired over abrupt stall. For gradual stall separation starts at the trailing edge of the airfoil such that remainder area can maintain the pressure differential. Separation will now move slowly towards the leading edge, so the aircraft approaches stall gradually, giving the pilot enough time to move out of this stall procedure. Gradual stall is experienced by airfoils with a larger radius of the airfoil's leading edge. For abrupt stall, separation starts at the leading edge. This creates a small bubble that either moves downstream or bursts abruptly. This results in a sudden increase of nose-down moment, as indicated by Figure 8.4. The wing section airfoil, NACA 64210, is not a thin airfoil, but also does not have a very blunt leading edge. Since H₂ERO is flying at subsonic speeds, a leading edge flow separation bubble (vortex) should be avoided. This can be done by changing the angle of attack range such that the stagnation point occurs on the sharp edge.

Additionally a droop leading edge on the wing is applied. They work similar to a leading edge slat. This lowers the nose of the airfoil so that the stagnation point is at the round nose and not below the nose section. Therefore, the suction pressure peak near the nose of the upper surface is reduced and recompression towards the trailing edge will occur more easily. This will delay flow separation, and thus stall. In addition, a drooped nose will also aid in roll stability for high angles of attack. A disadvantage of a drooped nose is the increase in viscous drag. This may reduce the maximum speed the aircraft can achieve, but does not dominate over the advantages of the drooped airfoil leading edge.

8.3. Tail

The tail design and sizing is done for the subsystem stability and control in chapter 9. Aerodynamically there are a few important aspects of empennage design. Firstly, the horizontal stabiliser needs to produce down force, and hence a symmetrical airfoil should be used. The same is true for the vertical fins, the net force direction will change according to the rudder deflection. NACA0009, NACA0010, and NACA0012 are commonly used airfoils for tail sections³.

Secondly, the tail has to stall after the main wing in order to ensure that control is still available and the pilot has a chance of moving out of the stall process. Some measures to make sure this happens include: a lower aspect ratio for the tail than the main wing,⁴, since this benefits the stall angle of attack. Also, the main wing is installed at an incidence angle, so it will always see a higher angle of attack compared to the horizontal tail surface area, which will make the wing stall first. In addition, vortex generators, such as zig-zag stripes, can be placed to the low-pressure side of the airfoil. They introduce higher speed airflow into the slowly moving boundary layer, creating turbulent flow and delaying stall.

Also, the horizontal tail surface area should not be placed in the slipstream in order to avoid tail buffeting (turbulent air hitting the tail surface). Buffeting will increase structural fatigue and introduces more noise in the cabin [26].

8.4. Transition Phase

During vertical take off and landing all lift will be generated by the four rotors. In forward flight all lift will be generated by the main wing, in order to fly more efficiently and not use (hydrogen) fuel for lifting purposes during cruise, in contrast to conventional drone designs. Therefore, the transition phase from VTOL to forward flight should be correctly designed in order to not loose altitude. This involves keeping the rotors open and producing lift up until the stall speed for the wings is exceeded, so they can take over the full lift needed to carry all the weight. This will be further dealt with when integrating all the different subsystems and in the design recommendations, as described in chapter 16.

With open rotors, the wing section from wing root up to 1.1 times rotor diameter is considered to not produce any lift. This assumption has been made to account for the air that the rotor sucks in at the edges of the rotor. Therefore, to calculate the minimum speed for transition, only the clean wing surface area should be taken into account(excluding the rotor parts). This is further quantified after subsystem integration and the final vehicle configuration is known, and can be found in chapter 16.

In order create minimum drag and fly most efficiently, the covering mechanism must have minimum air flow disturbance. Two possible mechanisms are considered. The first one involves multiple sections that can open and close, similar to a linear shutter mechanism. They are positioned such that the airflow moving from the leading to the trailing edge of the wing sees a thin plate cross-section, hence minimising drag. The second option involves a blade shutter mechanism, also called iris mechanism with (overlapping) blades. A combination of these (one on upper and one on lower surface) is also possible. Also, it should be taken into consideration that the rotors should first be turned off and only then can be covered up. Else the force of the moving air will create too high stresses in the material causing it to yield or break. Of course the time needed for this should be minimised and therefore the fastest closing mechanism, that will still allow for a clean wing surface area, will be selected.

8.5. Noise Reduction Techniques

The noise reduction is focused on the propulsive subsystem design for this design phase. In addition, some aerodynamic noise optimisation techniques can be applied as well. The main factors contributing to this airframe noise includes the wing trailing edge turning turbulent kinetic energy from the boundary layer into acoustic energy, perceived as noise. Other contributors to airframe noise are landing gear noise and flow

³https://www.fzthamburg.de/pers/Scholz/H00U/AircraftDesign_9_EmpennageGeneralDesign.pdf [Accessed 2019-06-21]

⁴During subsystem integration this was reflected upon and proved to be non feasible. Therefore the other options stated to avoid early stall will be implemented.

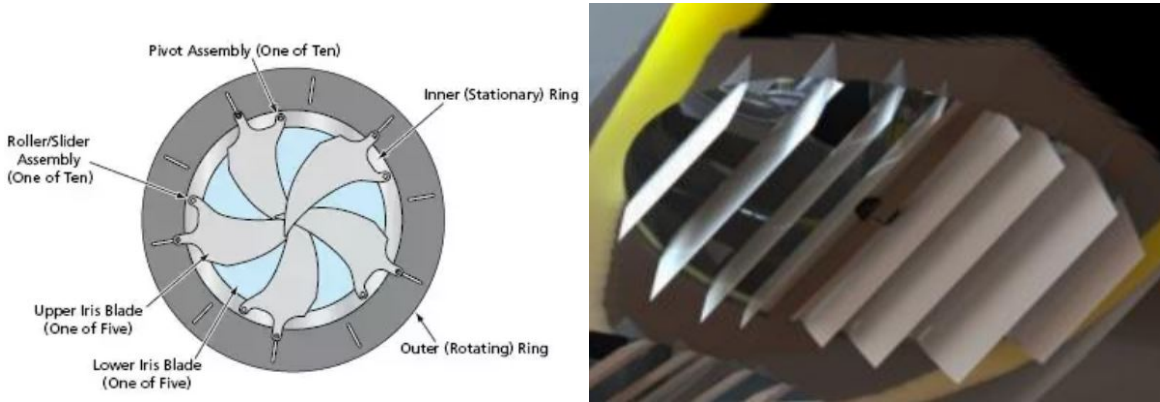


Figure 8.6: Left: mechanism of a iris shutter mechanism [20]. Right: mechanism of linear shutter mechanism [22].

unsteadiness or vortex shedding from slats and flaps. The H₂ERO uses skids as landing gear and not wheels, which produce far less noise because of the smaller surface area and less blunt shapes. Also, the H₂ERO is not designed for slats and flaps. Therefore, only the trailing edge measurements may give significant noise reduction.

Porous Trailing Edge Inserts

Porous trailing edge inserts is a new technique still in phase of research and development, also at the faculty of Aerospace Engineering in Delft, but with some very promising results. It consists of a porous material parts inserted in the trailing edge. They can reduce noise up to 11 dB [46]. The permeability, allowing for air crossflow, lowers the turbulent intensity. This decrease in velocity fluctuations is believed to drive the reduction in (low frequency) noise [46]. However, the porous inserts also decrease the aerodynamic performance slightly, because of the decrease in boundary layer thickness due to the increased skin friction of the rough (porous) surface. Before this technique can be implemented in the H₂ERO more research needs to be done to the effect of porous trailing edge inserts in asymmetrical airfoils at higher Reynolds numbers.

Sawtooth Edge

Another technique to decrease trailing edge noise is the sawtooth edge. They reduce noise up to 13 dB because of the attenuation of vortex shedding at the trailing edge, thus influencing the turbulent field [31]. For this serration wavelength should be smaller than the boundary layer thickness or the root-to-tip distance should be larger than the boundary layer thickness.

8.6. Requirement Compliance & Feasibility

Table 8.5: List of the requirements regarding the aerodynamic subsystem

Code Identifier	Requirement	Type	Verification	Compliance
EVTOL-SRAE-241	The L/D ratio shall be greater than 8.	Driving	Analysis	
EVTOL-SRAE-242	The wing tip shall not stall before the wing root	Regular	Analysis	
EVTOL-SRAE-243	Airframe noise reduction techniques shall be applied which reduce the noise by 10% compared to a regular airframe where no noise reduction techniques are applied.	Regular	Analysis	
EVTOL-SRAE-244	The transition phase shall be performed such that no altitude is lost.	Regular	Analysis	
EVTOL-SRAE-245	The horizontal tail surface area shall stall after the main wing has stalled.	Regular	Analysis	
EVTOL-SRAE-246	The wing thickness over chord ratio shall allow for enough space to fit the integrated rotors, structural elements, actuators and wiring.	Regular	Analysis	

The L/D ratio for the H₂ERO is 14 so the first requirement is easily met. The procedures for stall are designed according to the requirements, so they are considered to be met. However, further research is needed to fully prove this, as explained in chapter 16. The current design provides enough wing surface area to not lose altitude during transition. The thickness over chord is designed according to the subsystems dimensions that are to be integrated in the wing.

The only requirement that is not met is the noise reduction of 10%, because the noise reduction cannot be quantified at this point in the design. A qualitative approach to this noise reduction has been described and a quantitative analysis is recommended for further design.

Detailed Design: Geometry Definition, Stability and Control

To determine and ensure stability and control of the aircraft throughout all phases of flight, the requirements on geometry of the aircraft components, the centre of gravity and the control surface sizes, amongst others, are taken into account in the early design stage of the aircraft. This will be elaborated on in this chapter.

9.1. Aircraft Geometry Definition

During the initial sizing of the aircraft in the conceptual design phase, the basic sizing parameters of the aircraft like the wing surface area S , the wing aspect ratio A and the wingspan b were determined. These parameters were used as the building blocks to determine the final geometry of the wing planform. Additionally, the requirements on the cabin size, required space for aircraft subsystems (e.g. energy source, avionics, instrumentation), ground clearance, take-off and landing area are some of the driving factors in sizing of the fuselage of the aircraft. Last but not least, the empennage, its surface area and other relevant geometry is determined. All while taking the stability and controllability requirements closely into account.

9.1.1. Wing Planform Design

During the initial sizing process of the aircraft, the values of the wingspan b , wing surface area S and aspect ratio A were determined. They were based on performance constraints coming from various flight conditions, the desired mission performance and the corresponding power requirements. At the current stage of the wing design, a trapezoidal planform is assumed. This is believed to be the best approximation of the actual wing planform (small deviations might arise due to, e.g. integration of the VTOL propulsive system). The next step in the design of the wing planform is the selection of the sweep angle.

Sweep Angle

Typically, the sweep angle in aircraft is used to delay the onset of supersonic flow along the wing profile to avoid the associated drag increase. As the nominal cruise Mach number (as fixed by the cruise speed and altitude requirement) is around 0.2, this effect can be safely ignored. However, the sweep angle can also be used to affect the longitudinal position of the centre of gravity of the aircraft, which is the primary consideration in a choice for the quarter-chord wing sweep angle $\Lambda_{0.25c}$. As described in the aerospace design course AE1222-II by J. Melkert, a positive value of wing sweep is chosen due to the favourable effect on the gust and aero-elastic stability. This means that an increase in lift would cause a nose-down torsional deformation of the wing, lowering the local angle of attack and, hence, decreasing the local lift coefficient [58]. A positive sweep angle drawback is the danger of tip-stall, which can render outboard control surfaces ineffective.

Taper Ratio

Taper ratio is selected to shape the wing planform to closely resemble elliptical lift distribution, which is aerodynamically the most efficient, that yields a value close to $\lambda = 0.4$ for an unswept wing, as described in the AE1222-II course material by J.Melkert [58]. However, the chosen sweep angle of the wing also has to be taken into account due to its effect on the span-wise lift distribution. Therefore, after selection of appropriate wing sweep angle, the empirical relationship of Equation 9.1 is used to estimate the best value of taper ratio [58] and shown in Equation 9.1:

$$\lambda = 0.2 \left(2 - \Lambda_{0.25c} \frac{\pi}{180} \right) \quad (9.1)$$

Chord Distribution

Once the wing surface area S , wingspan b , aspect ratio A and the taper ratio λ all have been determined, the trapezoidal wing planform is fully determined by these parameters. This allows to determine the chord length at a given span-wise location along the wing. The root and tip chords are then determined by using the geometric relations in Equation 9.2 and Equation 9.3 respectively.

$$c_r = \frac{2S}{(1 + \lambda)b} \quad (9.2)$$

$$c_t = \lambda c_r \quad (9.3)$$

9.1.2. Fuselage

Central considerations in the geometric design of the fuselage are, firstly, making sure that enough space is allocated for the pilot, the passengers, the patient and all of the necessary equipment, as well as the integration of the avionics and energy source system, amongst others. Secondly, as quick loading and unloading of the passengers is of utmost importance, accessibility of the cabin is an additional important fuselage design criteria. With these considerations, the fuselage geometric layout and structure is designed to comply with all of the necessary requirements. These have been described in detail in chapter 10.

9.1.3. Empennage

To ensure that the empennage, consisting of the horizontal and vertical stabiliser(s), can fulfil its main function which is to ensure stability and control for pitch and yaw of the aircraft, its configuration, size and geometrical definition are of utmost importance to satisfy the requirements.

Empennage Configuration

The selection of empennage design in this design case was mainly driven by integration considerations. The empennage configurations considered were a conventional tail, T-tail, V-tail and a boom-mounted tail. The boom tail was chosen to be the best option, as it allows for the simplest integration of the forward flight propulsive system. As described in section 11.3, a single pusher propeller is chosen for the forward flight propulsion, located at the back of the fuselage. A boom configuration, consisting of a large horizontal and two vertical stabilisers (see Figure 9.1¹), allows to facilitate the propeller between the two booms in a structurally-simple manner. Additionally, the booms connecting the empennage with the fuselage, allows for relatively simple adjustment of the tail arm without significant adjustments necessary in the structural design. Hence, limiting the complexity of the aircraft balancing process for control and stability.

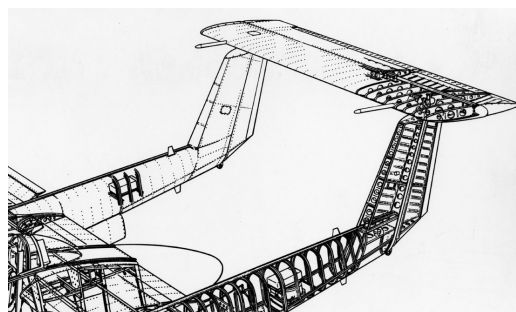


Figure 9.1: Double-boom empennage configuration.

Horizontal Tail Surface

To ensure the aircraft remains statically stable and controllable during the forward flight phase, the horizontal tail is sized accordingly by taking the requirements on the centre of gravity and the aerodynamic centre of the aircraft into account. Detailed procedure on empennage sizing is discussed in subsection 9.3.2

¹<https://www.combatreform.org/killerbees2.htm> [Accessed 2019-06-22]

Vertical Tail Surface

Since the horizontal tail is used for longitudinal stability and control of the aircraft, the vertical tail is used for the directional stability of the aircraft. To size the vertical tail properly, directional stability and control should be analysed in depth, as it is done for the horizontal tail in subsection 9.3.2. However, due to time constraints limiting the scope of the subsystem design, the vertical tail sizing method resorts to preliminary tail sizing estimates based on the vertical tail volume coefficient \bar{V}_v and is computed by using Equation 9.4.

$$\bar{V}_v = \frac{(X_v - X_{aftcg}) S_v}{S_b} \quad (9.4)$$

By consulting aircraft preliminary sizing books (Raymer [44], Torenbeek [52]) and referring to aircraft with a similar maximum take-off weight and similar functionality (i.e. transport/cargo aircraft), a vertical tail coefficient value of $\bar{V}_v = 0.02$ was selected. Rearranging Equation 9.4 to solve for the vertical tail surface area S_v , an area of $S_v = 4.21 \text{ m}^2$ was found. It should be noted that a closer analysis and investigation of desired directional control and stability characteristics should be made at a later design stage, after which the size of the vertical tail area should be reassessed.

Control Surface Sizing

Manoeuvrability of the aircraft has to be ensured around the pitch, roll and yaw axes of the aircraft to be able to actively control the attitude of the aircraft during all phases of flight. During vertical flight, this is provided by the VTOL propulsive system, generating differential thrust and torque. In forward flight, the attitude change is to be provided by aerodynamic surfaces, whilst ensuring compliance with manoeuvrability requirements. Typically, sizing of the control surfaces is achieved through dynamic analysis of the effectiveness of the control system, accounting structural deformations (e.g. to avoid phenomena such as aileron reversal). However, this is out of the scope of this design phase due to the limited time resource. Therefore, the control surface sizing method described in Chapter 6.5 of Raymer is used to size the ailerons, rudders and the elevator for roll, yaw and pitch manoeuvrability respectively [44]. The design parameters used and final size of all aerodynamic control surfaces have been summarised in Table 9.1, where $\frac{c_{contr}}{c_{local}}$ is the ratio of control surface chord to the local main surface chord (e.g. rudder-vertical tail chord ratio), and $\frac{b_{contr}}{b_{main surface}}$ is the span ratio between the control and main surface.

Table 9.1: Control surface sizing variables.

Control Surface	Number of surfaces	$\frac{c_{contr}}{c_{local}}$ [-]	$\frac{b_{contr}}{b_{main surface}}$ [-]	Control surface area (total) [m^2]
Ailerons	2	0.29	0.38	9.87
Rudders	2	0.40	0.80	1.01
Elevator	1	0.30	0.90	6.85

Geometric Parameter Definition

Once the configuration has been selected, both the horizontal and vertical stabilisers are geometrically fixed by selecting the sweep angles $\Lambda_{0.25c_h}$ and $\Lambda_{0.25c_v}$, aspect ratios A_h and A_v , and taper ratios λ_h and λ_v , summarised in Table 9.2. The values of these parameters are mainly selected through trial and error until the stability and controllability requirements of the aircraft are satisfied. However, the limits described by Raymer [44] of the aspect and taper ratios of both the horizontal and vertical tail are only adhered to when determining the final parameter values during systems integration in chapter 11. Additionally, Raymer [44] mentions that the exact values of the tail geometrical parameters (besides the surface areas S_h and S_v) are not critical in low-speed aircraft design. At least until more in-depth aerodynamic experimental analysis is performed. They also show very little variation between a wide range of aircraft across different categories.

9.2. Subsystem Weight Estimates

As the X_{cg} range estimate is already necessary in the early detailed-design stage, initial weight estimates of the aircraft subsystems are required before their respective detailed-design development. The aircraft was divided into 7 groups being the wing group, fuselage group, VTOL propulsion group, empennage group,

Table 9.2: Tail geometric parameters.

Geometric Parameter	Value
$\Lambda_{0.25c_h}$ [deg]	9.46
$\Lambda_{0.25c_v}$ [deg]	30.00
A_h [-]	4.00
A_v [-]	1.50
λ_h [-]	0.50
λ_v [-]	0.50

forward-flight propulsion group, energy source group and finally, the payload group. An estimate of their mass and longitudinal positioning along the aircraft's axis was established to start assessing the possible X_{cg} range of the aircraft. It should be noted that the X_{cg} locations and the subsystem masses are updated throughout the detailed design phase once more precise estimates on weight and position of the respective subsystems is established to allow for proper assessment of the aircraft weight distribution.

9.2.1. Wing Group

The longitudinal position of the wing is set with respect to the previously defined fuselage length of the aircraft. From accessibility requirements, a constraint of longitudinal position of the leading edge of the root chord of $X_{LEC_r} = 2.0$ m was set. The longitudinal position of the wing is one of the parameters that is varied in the process of balancing the aircraft to find the optimum aircraft weight distribution to size the horizontal tail surface area. To determine the weight of the wing, a statistical estimation method for transport and cargo aircraft from Raymer's aircraft conceptual design handbook was used:

$$W_{wing} = 0.0051 (W_{dg} N_z)^{0.557} S_w^{0.649} A^{0.5} (t/c)_{root}^{-0.4} (1 + \lambda)^{0.1} (\cos \Lambda)^{-1.0} S_{csu}^{0.1} \quad (9.5)$$

where W_{dg} is the design gross-weight of the aircraft (in lbs), N_z is the ultimate load factor, S_w is the wing area (in ft^2), A is the aspect ratio of the aircraft, $(t/c)_{root}$ is the thickness-to-chord ratio at the root of the wing, λ is the wing taper ratio, Λ is the quarter-chord sweep, and S_{csu} is the control surface area of the aircraft. However, it is crucial to point out that the final design configuration chosen features a large cutout in the wing to house one of the VTOL propellers within the wing. This has a substantial impact on the weight on the wing. Whilst a portion of area is removed from the wing, implying lower weight, additional structural reinforcements are needed around the cutout to account for the stress concentrations induced by the cutout. In turn, this will increase the weight of the wing. As this design feature significantly differs from a typical wing design from statistical data used in Equation 9.5, it was expected that the wing weight estimate obtained from Equation 9.5 will differ considerably from the final weight obtained after detailed design of the wing. Therefore, the uncertainty of the initial wing group weight was taken into account when assessing the centre of gravity range and the longitudinal stability and control by adding static stability margins addressed in section 9.3.

9.2.2. Fuselage Group

Longitudinal position of the centre of gravity of the fuselage is assumed to be located at 45% of the fuselage length, as suggested by Oliviero [37]. For initial weight estimations, the method described by Raymer [44] for transport and cargo aircraft was used:

$$W_{fuselage} = 0.3280 K_{door} K_{Lg} (W_{dg} N_z)^{0.5} L^{0.25} S_f^{0.302} (1 + K_{ws})^{0.04} (L/D)^{0.10}, \quad (9.6)$$

where $K_{door}=1.06$ is the coefficient accounting for door amount, $K_{Lg} = 1.0$ is the coefficient account for landing gear positioning, L is the length of the fuselage (in ft), S_f is the fuselage wetted area (in ft^2), K_{ws} the geometry factor taking into account the taper ratio, fuselage width and the sweep angle of the wing, and $\frac{L}{D}$ is the lift-to-drag ratio of the aircraft.

9.2.3. VTOL Propulsion Group

As selection of the longitudinal and lateral positioning of the propulsion system is done during systems integration ensuring that the VTOL system can be fully integrated within the wing structure, its longitudinal

position is only fixed during integration process. To estimate the mass of the subsystem before the detailed design phase had been carried out, the same method was used as described in the Class II sizing and weight estimation methodology based on the power requirements that have to be delivered by the VTOL propulsion system, as described in the Midterm report [2].

9.2.4. Empennage Group

The empennage group consists of the horizontal stabiliser, both vertical stabilisers, and the connecting boom elements between the vertical stabilisers and the fuselage. A couple of simplifying assumptions had to be made due to the time constraint when determining the mass and the centre of gravity of the empennage. It was assumed that the longitudinal position of the centre of gravity of the vertical stabilisers coincides with the X_{cg} position of the horizontal stabiliser. This assumption is considered to be valid, as difference between the actual X_{cg} positions is expected to be less than 5% of the overall fuselage length, therefore considered negligible at this stage. To estimate the weight of the horizontal stabiliser, an adjusted version of estimation relationship was user as described by Raymer:

$$W_{horizontal} = 0.0379 K_{uht} (1 + F_w / B_h)^{-0.25} W_{dg}^{0.639} N_z^{0.10} S_{ht}^{0.75} L_t^{-1.0} K_y^{0.704} (\cos \Lambda_{ht})^{-1.0} A_h^{0.166} (1 + S_e / S_{ht})^{0.1}, \quad (9.7)$$

where $K_{uht} = 1.0$ is a factor taking into account fixed/movable tail, $\frac{F_w}{B_h}$ is the ratio between fuselage width and the horizontal tail span, S_{ht} is the horizontal tail surface area (in $f t^2$), L_t is the tail length (in $f t$), K_y is the pitching radius of gyration (in $lb - ft^2$), as estimated by being equal to 30% of the fuselage length, Λ_{ht} is the sweep angle of the horizontal tail, A_h is the horizontal tail aspect ratio, and $\frac{S_e}{S_{ht}}$ is the ratio of elevator and horizontal tail area. The weight of the vertical stabilisers was determined using a similar relation described by Raymer. To estimate the centre of gravity location of the horizontal stabiliser (which was also assumed to be the centre of gravity location of the empennage group), the estimate provided by Oliviero in lecture material on aircraft balancing and weight estimates, placing it at 42% of the chord located at the 38% of the half-span (see Figure 9.2).

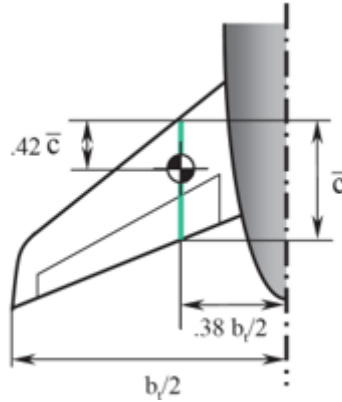


Figure 9.2: Estimation of the X_{cg} location of the horizontal tail [37].

9.2.5. Forward Flight Propulsion Group

Before detailed design stage has been done, the procedure to estimate the mass of the forward flight propulsion group was exactly the same as for the VTOL propulsion group, by using the required power estimates described in the Midterm report, in turn obtaining the mass of the motor, propeller, electric speed controllers, as well as other components.

9.2.6. Energy Source Group

The energy source group consists of the fuel (liquid hydrogen), battery for power-intensive phases of the flight, fuel tanks, feed systems, compressors, valves, etc. As with the previous subsystems, the estimates described in the midterm report were used to calculate the weight of each of the components of the subsystem - refer to the midterm report for a more detailed description of the method [2]. Depending on how well each of the components can be integrated within the fuselage and the wing (in terms of the shape, required

Table 9.3: Longitudinal positioning of the pilot, passengers and the medical equipment.

Position	X_{cg}/l_{fus}
$X_{cg,pilot}$	0.14
$X_{cg,pax1}$	0.14
$X_{cg,pax2}$	0.41
$X_{cg,pax3}$	0.57
$X_{cg,patient}$	0.49
$X_{cg,equipment}$	0.58

volume, etc.), the centre of gravity of this subsystem is expected to vary between 40%-55% of the fuselage length before the detailed design of the energy system.

9.2.7. Payload Group

The payload group consists of the weight of the 3 passengers, each weighing in at 80 kg (weight of the pilot is included in the operational empty weight of the aircraft), the patient with an allocated weight of 100 kg, as well as for the necessary medical equipment, weighing 208 kg. It is assumed that the sequential loading of the passengers will be the main contributor of the shifting of aircraft centre of gravity. By defining the positions within the cabin, as seen in Table 9.3 of each passenger and the patient, a loading diagram is generated (see Figure 9.3), indicating the induced shift of centre of gravity with each passenger embarking the aircraft.

9.2.8. Other Aircraft Systems

The remaining aircraft systems, which have not been developed in high-level of detail, are, nevertheless, crucial to account for in the weight estimate of the aircraft, as they make-up a substantial fraction of the maximum take-off weight of the vehicle. The most relevant remaining subsystems were identified to be the engine control systems, hydraulics, electric system, avionics, and the furnishings of the aircraft. As precise estimation of the longitudinal centre of gravity location of the aforementioned subsystems is out of the scope of this design phase, the weight of these systems was assumed to act through the centre of gravity of the fuselage, which has been determined previously in subsection 9.2.2. The mass of the systems was estimated by using statistical methods. The mass-estimation relationships for avionics and electrical subsystems are discussed more in detail in section 7.1, which illustrates the underlying principle of these statistical relationships: the parameters influencing the mass of a subsystem are scaled appropriately to obtain the best fit for the subsystem weight of already known and existing systems of a specific aircraft group with their mass already known. As the methods involve an exhausting list of relevant parameters and statistical approximation relationships influencing the mass, only the results (the individual masses of the components) are discussed and displayed within the report (refer to subsection 11.9.2). To view the used relations in detail, please refer to Chapter 15 of Aircraft Design: A Conceptual Approach book by Raymer [44]. It is important to note that the aircraft systems under consideration are expected to make up a non-negligible part of the aircraft maximum take off weight, however, they are subjected to a high level of uncertainty in their mass, as no detailed design of these is performed as part of the project, therefore introducing uncertainty in the X_{cg} location of the aircraft, consequently altering the whole design process. To investigate this effect, mass of these components were included as system parameters within the sensitivity analysis of the design process to assess the effect and quantify its influence of the design outcome, as discussed in chapter 14.

9.3. Balancing, Longitudinal Stability and Control

As described in the earlier and subsequent chapters, aircraft weight distribution goes hand in hand with the stability and control characteristics of the vehicle both in forward and vertical flight phases. Therefore, longitudinal positioning of the aircraft centre of gravity as well as determining the expected range thereof are integral parts of the aircraft design process.

9.3.1. Passenger Loading, Centre of Gravity Range

Once longitudinal positions of the payload group have been established, the centre of gravity range can be fully established by generating a loading diagram, as illustrated in Figure 9.3, where the longitudinal centre of gravity shift is captured with each passenger (including patient) embarking the aircraft. It is important to consider that the larger shift in the centre of gravity visible in Figure 9.3 is caused by loading of the patient, with a 20kg additional mass accounted for comparing to the rest of the passengers of the vehicle, hence logically, causing a larger shift in the centre of gravity. From the figure, it is concluded that the X_{cg} range

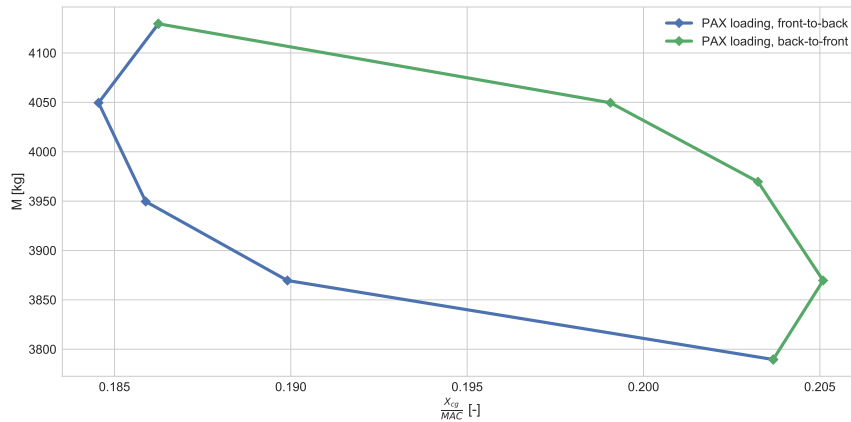


Figure 9.3: Loading diagram of the aircraft for X_{cg} assessment.

varies between and $X_{cg,front} = 13\%$ and $X_{cg,aft} = 26\%$ of the mean aerodynamic chord, taking a 5% margin into account to account for uncertainties of the weights of aircraft subsystem groups and the unaccounted changes in the centre of gravity during flight. It should be noted, however, that only loading of the passengers are considered in the loading diagram - the pilot, as well as the medical equipment have been included in the operational empty weight of the aircraft. Additionally, it should be noted that liquid hydrogen will be consumed during the flight, however, during the initial sizing of the aircraft, the mass of the hydrogen made up less than 1% of the maximum take-off weight of the aircraft, therefore it is assumed to have negligible effect on the shift of the centre of gravity during flight.

9.3.2. Longitudinal Stability and Control

The surface area of the horizontal stabiliser is determined through an iterative process, closely linked with the weight-distribution of the aircraft. The method to determine the required surface area of the horizontal stabiliser will be briefly summarised below, based on the control and stability requirements. The main assumptions made in the longitudinal stability and control analysis in the H₂ERO design are that the influence of drag, thrust, vertical placement of the components, compressibility and aero-elasticity effects are negligible. These assumptions were made to keep the analysis as simple as possible when estimating the first-order longitudinal stability and control characteristics. As the magnitude of the moment generated by the drag and thrust forces is considered to be small when compared to the aerodynamic moments generated by the lift of the main wing and the tail around the centre of gravity, these assumptions are considered to be valid for first-order analysis to include the most important stability and control characteristics of the aircraft for horizontal tail surface sizing. In order to assess the required area, the so called "scissor plot" is generated, where the most forward and most aft limits of the aircraft are restricted by the controllability and stability requirements respectively. The control requirement is determined from being able to achieve a pitch moment equilibrium during flight by having a certain combination of aerodynamic lift coefficients of the wing/fuselage, horizontal stabiliser lift coefficients, and the aerodynamic pitching moment. If equilibrium for this certain combination is achieved, the required horizontal stabiliser/wing area ratio can be found, also constraining the most forward X_{cg} location, as can be seen in Equation 9.8.

$$\bar{x}_{cg} = \bar{x}_{ac} - \frac{C_{m_{ac}}}{C_{L_{A-h}}} + \frac{C_{L_h}}{C_{L_{A-h}}} \frac{S_h l_h}{S_c} \left(\frac{V_h}{V} \right)^2 \quad (9.8)$$

The stability requirement is analysed, firstly, from the longitudinal static stability requirement: $\frac{dC_m}{da} < 0$, which can be shown to impose a static margin requirement - that the aircraft centre of gravity is to be located in front of the aerodynamic centre of the aircraft to ensure static stability - $X_{cg} - X_{ac} < 0$. It should be noted that the longitudinal stability is analysed in stick-fixed condition (to eliminate the tail lift coefficient dependency on the elevator deflection). As described by Oliviero in the stability requirement analysis, the stick-free condition is also typically accounted for if a stability margin of 5% Mean Aerodynamic Chord (MAC) is taken into account within the stability requirement described by Equation 9.9. If the aircraft centre of gravity is located at the neutral point of the aircraft, by definition, the aircraft has neutral longitudinal static stability, hence derivative $C_{m_{alpha}}$ is equal to zero. By expressing the change in local lift values of the wing/fuselage and the horizontal tail, the dimensionless moment equation can be found around the aerodynamic centre. Differentiating it with respect to the angle of attack and rearranging the equation, an expression for the required area ratio $\frac{S_h}{S}$ can be obtained for a given X_{cg} location, as Equation 9.9 describes.

$$\bar{x}_{cg} = \bar{x}_{ac} + \frac{C_{L\alpha_h}}{C_{L\alpha}} \left(1 - \frac{d\epsilon}{d\alpha} \right) \frac{S_h l_h}{Sc} \left(\frac{V_h}{V} \right)^2 - S.M., \quad (9.9)$$

where S.M. denotes the stability margin - distance between the neutral point of the aircraft and X_{cg} . The aerodynamic parameters, such as $C_{L\alpha_h}$, $C_{L\alpha}$, $C_{m_{ac}}$, $C_{L_{A-h}}$, C_{L_h} and $C_{L_{A-h}}$ are initially estimated using either statistical data from other aircraft, or estimation methods based on the current known configuration of the aircraft-to-be-designed. Once more thorough aerodynamic analysis has been performed on the aircraft (e.g. CFD analysis or wind-tunnel testing), these parameters can be further refined. The wing-to-tail velocity ratio $\left(\frac{V_h}{V} \right)^2$ is set to 0.85, a value recommended by Oliviero in AE3211-I lecture material on stability [38], as it is assumed that the incoming airflow of the horizontal stabiliser will be highly perturbed by the wing/fuselage body. The downwash gradient $\frac{d\epsilon}{d\alpha}$ from the main wing is estimated by the method described by Slingerland [51]. In order to estimate the location of the aerodynamic centre of the wing \bar{x}_{ac} , the contributions of from the wing and fuselage were taken into account, based on estimation methods described by Oliviero [38], depending on the geometric definition of the wing planform and the fuselage. It should be noted that both stability and control requirements are dependent on the tail-arm l_h - the distance between the aerodynamic centre of the horizontal stabiliser and the main wing. This is kept as a variable throughout up until the design integration process, alongside with the sweep angles of both horizontal stabiliser and the main wing, and the taper and aspect ratios of the horizontal tail. Once the dependent parameters have been fixed, the required surface area of the horizontal stabiliser can be obtained to comply with both stability and control requirements for a given X_{cg} range, as illustrated in Figure 9.4.

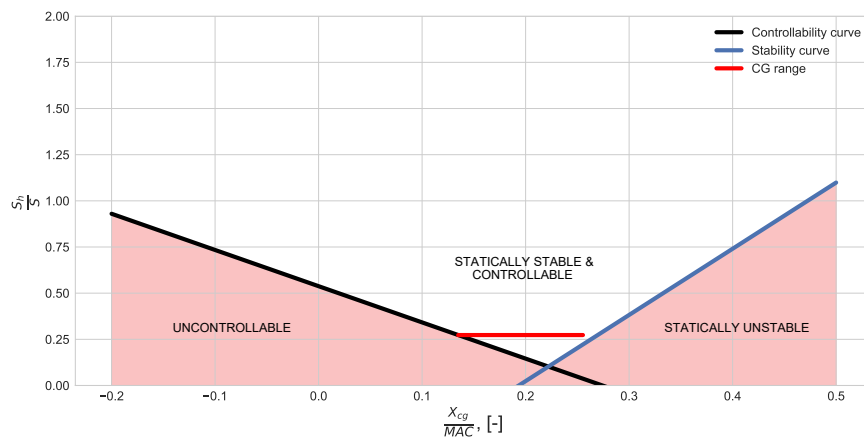


Figure 9.4: Illustration of the "scissor" plot for horizontal stabiliser sizing for stability and control.

9.4. Stability and Control in Vertical Flight

Even though the majority of the flight-phase is in forward flight, the aircraft's ability to hover is a key design feature which will be used extensively during its service as emergency vehicle. Therefore it is of vital impor-

tance that the vehicle can be manoeuvred safely and accurately in the VTOL flight phase. This section will discuss a methodology to assess what performance can be extracted from the propulsion system combined with a control system and other aircraft parameters such as mass and moments of inertia. The developed tool can also be used to analyse if the installed propulsive system delivers satisfactory performance in terms of noise and motor saturation.

9.4.1. Modelling the Aircraft

To determine if the aircraft is controllable and stable to a point where it is as good as the current emergency helicopter, an accurate model of the aircraft is used to determine what certain inputs to actuators do to the state of the vehicle as well as to establish a control strategy that can be used to manipulate the aircraft to respond to pilot inputs as the pilot would expect. From now on the aircraft model with its actuators is referred to as the 'plant' which is conventional in control theory.

Reference Frames

Representing motion and orientation is always done with respect to a certain observer. Translation and rotation of the plant are defined in the inertial frame which has its X_n and Y_n axis pointing at the north and east directions of a flat-earth. To complete the right-handed coordinate system, Z_n must point downwards to the ground. Describing the dynamics of the plant is however much easier when a body-fixed reference frame is considered where the propeller thrust is always pointing in the same direction and the force of gravity depends on the attitude with respect to the inertial reference frame. The body-fixed reference frame consists of three axes, b_1 , b_2 and b_3 pointing forward, through the right wing and down respectively. In Figure 9.5 it can be seen how these body axes are pointing and what distances are used that are relevant for setting up the control problem.

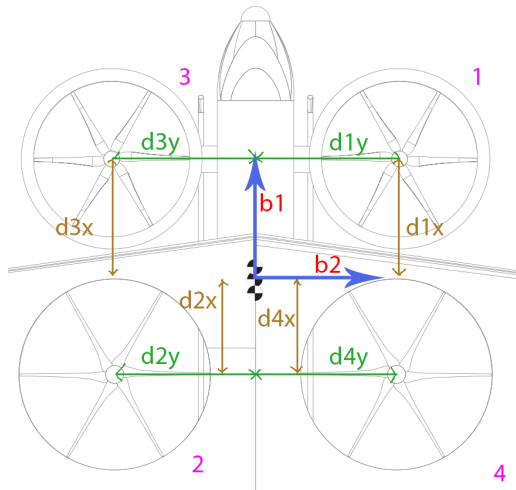


Figure 9.5: Body coordinate system axes and propeller distances relative to c.g.

To transform a vector from the inertial frame to the body-fixed frame, a rotation matrix is used. This matrix is the combination of a rotation about the yaw axis, pitch axis and roll axis in that order. These rotations can be mathematically written as shown in Equation 9.10. The resulting transformation matrix can also be inverted and used to transform vectors from body-fixed frame to inertial frame. Because the matrix is orthogonal, inverting is the same as transposing which is a very fast operation. Besides that, this way of representing attitude is intuitive.

$$\begin{bmatrix} b_1 \\ b_2 \\ b_3 \end{bmatrix} = \begin{bmatrix} 1 & 0 & 0 \\ 0 & \cos(\phi) & \sin(\phi) \\ 0 & -\sin(\phi) & \cos(\phi) \end{bmatrix} \begin{bmatrix} \cos(\theta) & 0 & -\sin(\theta) \\ 0 & 1 & 0 \\ \sin(\theta) & 0 & \cos(\theta) \end{bmatrix} \begin{bmatrix} \cos(\psi) & \sin(\psi) & 0 \\ -\sin(\psi) & \cos(\psi) & 0 \\ 0 & 0 & 1 \end{bmatrix} \begin{bmatrix} X_n \\ Y_n \\ Z_n \end{bmatrix} \quad (9.10)$$

Important Variables

Important variables to keep track of when simulating motion are the linear velocities of the body: $\mathbf{v}^b = [u \ v \ w]^T$, angular rates of the body: $\boldsymbol{\omega} = [p \ q \ r]^T$, forces $[F_x \ F_y \ F_z]^T$ and moments $[L \ M \ N]^T$. Gravity is always pointing along the Z_n axis and appears in the equations of motion as described in the body-fixed reference frame. Therefore it is important to keep track of the euler angles as well to properly model the force of gravity. This results in three additional state variables: $\Phi = [\phi \ \theta \ \psi]^T$.

Assumptions

Several assumptions have been made for this model to simplify the analysis without losing its relevance to the design work. In future design work when more parameters of the aircraft are known (such as an elaborate propeller model and motor dynamic model) the model can be improved to resemble reality even more closely. The most important assumptions are listed below.

- The plant is assumed to be a rigid body without any deformations.
- Motor and drivetrain component dynamics are not taken into account. This means that the RPM of the motor changes instantly when commanded by the flight controller.
- The plant is assumed to have its principal axes aligned with its c.g. meaning that the product moments of inertia are zero.
- A flat non-rotating earth is assumed with a constant acceleration of gravity independent of altitude.
- Gyroscopic effects of propeller inertia are neglected. Gyroscopic effects of the body itself are modelled however.
- The propeller thrust and torque are quadratic functions of the motor RPM.
- Propeller and body forces as a result of aerodynamic loads are assumed to be negligible because of the low speeds in VTOL mode.
- Differences in rotational acceleration of the propellers cause a yaw counter torque to be generated which is not modelled.

Equations of Motion

The equations of motion describe the dynamics of the plant. The goal is to use these equations to their full extent in non-linear form to improve model accuracy. To start, from Coriolis' theorem the following holds:

$$\dot{\mathbf{v}}_{\text{inertial}}^b = \dot{\mathbf{v}}^b + \boldsymbol{\omega}_n^b \times \mathbf{v}^b = \begin{bmatrix} \dot{u} \\ \dot{v} \\ \dot{w} \end{bmatrix} + \begin{bmatrix} 0 & -r & q \\ r & 0 & -p \\ -q & p & 0 \end{bmatrix} \begin{bmatrix} u \\ v \\ w \end{bmatrix} = \begin{bmatrix} \dot{u} + qw - rv \\ \dot{v} + ru - pw \\ \dot{w} + pv - qu \end{bmatrix} \quad (9.11)$$

Above equation describes the acceleration components of the body as seen from the inertial frame. The force components in the body-fixed frame are simply the gravity force multiplied by the rotation matrix from inertial to body-fixed and the sum of the four propeller forces acting in negative b_3 direction due to the assumption of a rigid body. The equations for translational motion are then found through $\mathbf{F} = m\mathbf{a}$:

$$\begin{bmatrix} -mg \sin(\theta) \\ mg \sin(\phi) \cos(\theta) \\ -F_1 - F_2 - F_3 - F_4 + mg \cos(\phi) \cos(\theta) \end{bmatrix} = m \begin{bmatrix} \dot{u} + qw - rv \\ \dot{v} + ru - pw \\ \dot{w} + pv - qu \end{bmatrix} \quad (9.12)$$

In similar fashion the moments are related to body angular accelerations through $\mathbf{M} = \mathbf{I}^b \ddot{\boldsymbol{\omega}}_n^b + \boldsymbol{\omega}_n^b \times \mathbf{I}^b \boldsymbol{\omega}_n^b$. This system written out, including the assumption that the product moments of inertia are zero leads to the following equations for the roll, pitch and yaw moment:

$$\begin{bmatrix} L \\ M \\ N \end{bmatrix} = \begin{bmatrix} I_{xx}\dot{p} \\ I_{yy}\dot{q} \\ I_{zz}\dot{r} \end{bmatrix} + \begin{bmatrix} -I_{yy}qr + I_{zz}qr \\ I_{xx}pr - I_{zz}pr \\ -I_{xx}pq + I_{yy}pq \end{bmatrix} \quad (9.13)$$

An important note is that the body angular rates p, q and r are not the same as the time rate of change of the euler angles ϕ, θ and ψ . This is due to the fact that the euler angles represent a sequence of rotations

while the body rates are instantaneous (as they would come out of for instance a sensor on the body). This gives three additional equations that can be used in two ways: calculating angular body rates from Euler angle time derivatives and vice versa. Because the order of rotation with the Euler angles is yaw, pitch, roll the following applies:

$$\begin{bmatrix} p \\ q \\ r \end{bmatrix}^b = \mathbf{R}(\phi)\mathbf{R}(\theta) \begin{bmatrix} 0 \\ 0 \\ \dot{\psi} \end{bmatrix}^{b''} + \mathbf{R}(\phi) \begin{bmatrix} 0 \\ \dot{\theta} \\ 0 \end{bmatrix}^b + \begin{bmatrix} \dot{\phi} \\ 0 \\ 0 \end{bmatrix}^b \quad (9.14)$$

For simulation purposes it is useful to determine an earth reference frame which only differs by flipping the sign of the Z_n component of the inertial reference frame. The result is that now upwards is positive and the new coordinate axis is called h_E . In this new coordinate system, $X_n = X_E$ and $Y_n = Y_E$ still. The final equations of motion are shown in Equation 9.15.

$$\begin{aligned} \dot{u} &= -g \sin(\theta) + r v - q w \\ \dot{v} &= g \sin(\phi) \cos(\theta) - r u + p w \\ \dot{w} &= \frac{1}{m} (-F_z) + g \cos(\phi) \cos(\theta) + q u - p v \\ \dot{p} &= \frac{1}{I_{xx}} (L + (I_{yy} - I_{zz}) qr) \\ \dot{q} &= \frac{1}{I_{yy}} (M + (I_{zz} - I_{xx}) pr) \\ \dot{r} &= \frac{1}{I_{zz}} (N + (I_{xx} - I_{yy}) pq) \\ \dot{\phi} &= p + (q \sin \phi + r \cos \phi) \tan \theta \\ \dot{\theta} &= q \cos \phi - r \sin \phi \\ \dot{\psi} &= (q \sin \phi + r \cos \phi) \sec \theta \\ \dot{x}^E &= c_\theta c_\psi u^b + (-c_\phi s_\psi + s_\phi s_\theta c_\psi) v^b + (s_\phi s_\psi + c_\phi s_\theta c_\psi) w^b \\ \dot{y}^E &= c_\theta s_\psi u^b + (c_\phi c_\psi + s_\phi s_\theta s_\psi) v^b + (-s_\phi c_\psi + c_\phi s_\theta s_\psi) w^b \\ \dot{h}^E &= -1 * (-s_\theta u^b + s_\phi c_\theta v^b + c_\phi c_\theta w^b) \end{aligned} \iff \begin{aligned} F_z &= F_1 + F_2 + F_3 + F_4 \\ L &= -F_1 d_{1y} + F_2 d_{2y} + F_3 d_{3y} - F_4 d_{4y} \\ M &= F_1 d_{1x} - F_2 d_{2x} + F_3 d_{3x} - F_4 d_{4x} \\ N &= T_1 + T_2 - T_3 - T_4 \end{aligned} \quad (9.15)$$

9.4.2. Actuator characteristics

There are four actuators which can manipulate the state of the vehicle. These four propellers are used to generate a thrust force and moments about the body axes of the vehicle. If one would like to control the states of the vehicle in a simulation using these actuators, knowledge about the characteristics of these actuators is essential. Propellers are complex actuators with performance depending on many variables such as airspeed (3 directions), air density, rotational velocity and blade design. A common method to model these dynamics in a simple way is to assume that the thrust force only depends on a constant and the rotational velocity through $T = C_t \omega^2$ [7]. The propulsion department was able to provide the values for these C_t 's based on their calculations with the two propeller types used for the VTOL phase. In similar fashion, the torque can be described as $\tau = C_d \omega^2$ [7]. The values for C_d were also provided by the propulsion department.

9.4.3. Control system design and pilot interaction

From Equation 9.15 it can be seen that there are four possible forces and moments that can be directly controlled by changing the thrust forces of the four propellers: upward thrust and the roll moments about the three body axes. Therefore this system is underactuated: not every state can be directly controlled. There is no way to move forward without also pitching forward. This is not a problem in itself, it just requires a good controller (pilot or electronic system) to manoeuvre. If a certain combination of these thrust and moments is desired, there exists only one solution for F_{1-4} that satisfies these force and moments. A method to find these forces (and the motor RPMs they relate to) is presented in Equation 9.16. Values for C_t and C_d are taken per pair of propellers because they are identical.

This method can be used to calculate the motor commands based on desired force and moments by solving this linear system and taking the square root of the solution vector entries. It would theoretically be possible to let the pilot directly control the force and moments, however this would feel unnatural to the pilot because he controlling the second derivative of position. This control strategy would also not take full

advantage of the possibilities of disturbance rejection and c.g. shift compensation that a control-system assisted pilot would have. One last advantage of changing the control strategy is that the aircraft can be more silent by carefully tuning the controller to reach desired setpoints quickly without spiking the noise levels to unbearable levels.

$$\begin{bmatrix} C_{t13} & C_{t24} & C_{t13} & C_{t24} \\ -d_{1y}C_{t13} & d_{2y}C_{t24} & d_{3y}C_{t13} & -d_{4y}C_{t24} \\ d_{1x}C_{t13} & -d_{2x}C_{t24} & d_{3x}C_{t13} & -d_{4x}C_{t24} \\ C_{d13} & C_{d24} & -C_{d13} & -C_{d24} \end{bmatrix} \begin{bmatrix} \omega_1^2 \\ \omega_2^2 \\ \omega_3^2 \\ \omega_4^2 \end{bmatrix} = \begin{bmatrix} T_{des} \\ L_{des} \\ M_{des} \\ N_{des} \end{bmatrix} \quad (9.16)$$

Therefore, a control architecture as in Figure 9.6 is proposed which allows the pilot to command altitude, pitch angle, roll angle and yaw rate. This allows the pilot to select an altitude which the control system will work towards, or a pitch and roll angle which correspond to moving forward/backward and sideways. Instead of yaw angle it is decided to control yaw rate. This means that the pilot does not have to keep pushing the pedals (which control yaw) if it is desired to hold a non-zero yaw angle with respect to the earth reference frame. All these controls are similar to what is currently used in the EC135, except for that here the altitude is held at a certain level automatically. If the pilots desire to have manual control over thrust instead of altitude, this could easily be implemented in the control software. A different possibility is to have two different modes which the pilot can choose from. Then the 'manual' thrust mode can be used in normal flight and the automatic altitude keeping mode can be engaged if a long period of hover in presence of disturbance winds is required.

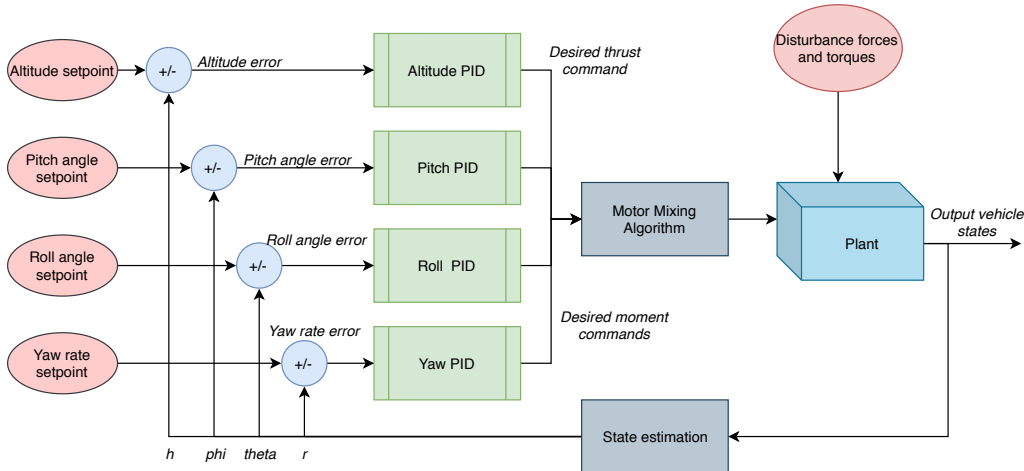


Figure 9.6: Control architecture for the vehicle in vertical flight mode.

PID Controller Design

From Figure 9.6 it can be seen that a total of 4 Proportional Integral Derivative (PID) controllers have to be tuned. As time goes by, the controller aims to reduce error between desired setpoint and vehicle state to zero. The PID controllers consist of three paths which combine elements from the logged error terms using numerical integration and differentiation to come up with a thrust or moment command. Before feeding this command to the motor mixer, the output is limited so that if a sudden change in setpoint is given, the derivative term in the controller does not demand extreme accelerations. The controllers are all manually tuned to exhibit desired behaviour such as low to none overshoot and short rise times. An example of this experimental tuning can be seen in Figure 9.7. The rise times could be even lower than they are in the current controller design but this would mean that the propeller RPM's would be much higher for short periods of time, which breaks the noise requirements of the aircraft. One could possibly design a third flying mode where these restrictions are not in place and the (more noisy) aircraft is more agile and uses the full capabilities of the propulsion system.

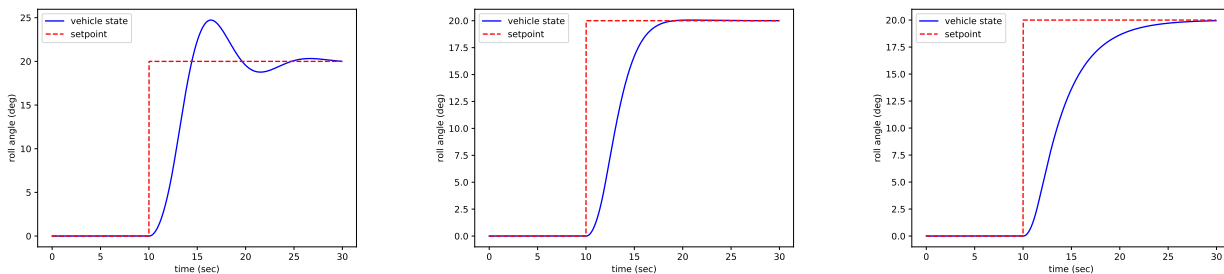


Figure 9.7: Effects of controller tuning. From left to right: underdamped, critically damped and overdamped response to a change in roll angle setpoint.

9.4.4. Simulation

Once the controllers are tuned the system can be analysed through a simulation where different realistic pilot inputs are given. By tracking the vehicle states and propeller RPM's an analysis about the system's (noise) performance is made.

Simulation Setup

For the moments of inertia, experimental data of an Avro 707B is used [41]. This aircraft has a similar mass and shape and is therefore considered a good first estimate for the values. The equations of motion are numerically integrated using the classic Runge-Kutta (RK4) method. Currently there is no simulator environment where pilot inputs are given through a joystick thus the pilot inputs are predetermined and abruptly changing setpoints.

Simulation Results

The results of a simulation run are shown in Figure 9.8. The simulation results show that pitch and roll angles are very easily commanded and reach their setpoint quickly without generating too much noise. The altitude controller is properly tuned so that the noise limit (1600RPM for the big propeller) is almost met. The result of this noise limit is that the vertical acceleration is limited at about 0.3g. Unfortunately the yaw rate command causes the RPM to rise above the loudest RPM that is allowed. Therefore, the controller has to be adjusted further to not allow yaw rates in this range to occur. This means lower manoeuvrability however, which is not desirable for the pilot. However, the pilot said during the interview that yaw is the least important motions to happen fast, 'as long as it turns'. The simulation result thus shows that this type of vehicle is difficult to yaw because it relies on propeller counter-torques which are not very free to choose throughout the flight.

The simulation has been performed at three c.g. locations: the most forward, the middle and the most aft position. In all three positions the aircraft is controllable and responds quickly to pilot inputs.

9.4.5. State Estimation

For the control system, four states have to be fed back: altitude, roll angle, pitch angle and yaw rate. Altitude can be measured using standard altitude measuring devices used in other aircraft based on pressure. For flight close to the ground, a more precise altitude measurement is helpful if good hover performance is required. For this purpose, the accelerometer is used to provide accurate altitude measurements by integrating its output twice with a certain initial condition that is periodically reset using GPS. This is done to remove the effects of sensor drift. Correcting these first two sensors is done through a third sensor: the GPS. The three sensors can be fused together to output a single altitude estimate using a Kalman filter. The Kalman filter is an established method used for state estimation that can resolve system states from other state measurements, as long as the system is observable. It does this while also correcting for noise and errors in the sensors [60]. The other three states can all be obtained from the inertial measurement unit (IMU) data through use of an extended Kalman filter [28].

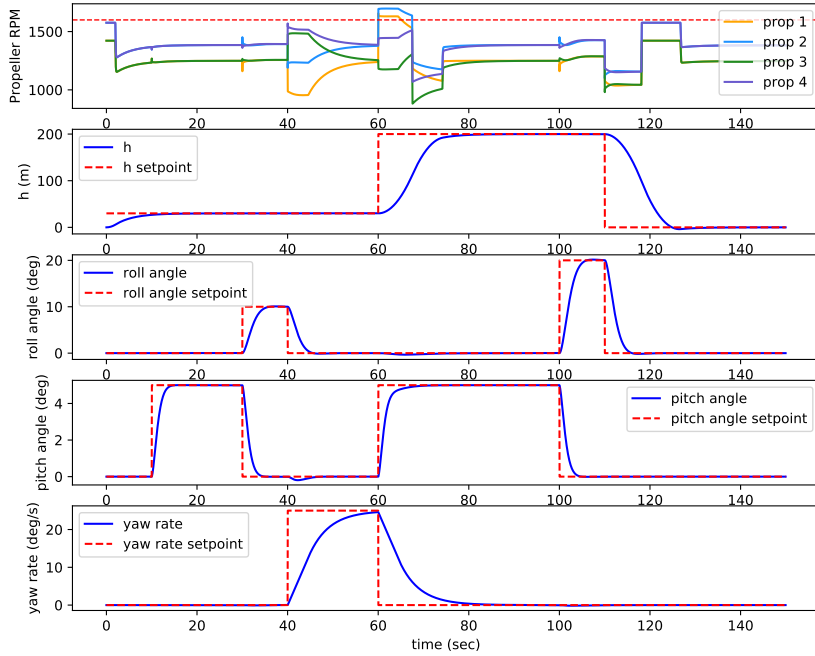


Figure 9.8: Simulation results from a single simulation with multiple changing pilot inputs. Xcg is halfway the calculated excursion range.

9.4.6. Safety

Safety during vertical flight is a very important consideration for the design. The control system must always work, otherwise the aircraft cannot be manoeuvred. Therefore, a redundant system is used where a second flight computer can take over if the first one fails. The same is done for the measurement devices. IMU's are light devices and taking multiple of them onboard is not a problem. There are many existing aircraft that require a control system to operate and they get certified and fly safely for years already.

If a motor fails, a sensor in the motor gives a signal to the flight computer which then disables all four motors to prevent the aircraft from spinning uncontrollably. The flight controls have to be changed to the horizontal flight setting instantly as well to give the pilot the option to make a gliding landing. As the aircraft starts to fall down, the propellers will autorotate and slow the aircraft down resulting in a hard, but not fatal landing which will heavily damage the undercarriage which is designed to take up the impact energy and save the lives of the passengers. If the pilot thinks the altitude is high enough he can first pitch the nose down, gain speed and then pull the nose up and do a gliding landing. This is much preferred over the first option, but as with many rotorcraft there is often no choice close to the ground. Important is to note that if the altitude is high enough, a quick switch towards forward flight can still be made by changing flight modes and engaging the rear propulsion system. This is always a better option than an autorotation landing, but only possible if there is sufficient airspeed and altitude.

9.5. Control Surfaces Actuators

In order to move the control surfaces an hydraulic system will be used. The hydraulic system is composed by different parts. As presented in Figure 9.9, the different components are: the pilot inputs, the amplification mechanism, the electrical system, the hydraulic storage / conditioning and the actuators.

The hydraulic system works as follows. The pilot inputs are passed through the hydraulic storage and conditioning. The hydraulic pump draws energy from the electrical system (directly from the fuel cell with the proper voltage converter) as specified in chapter 6. Finally, the liquid in the hydraulic storage is carried through tubes to the actuators in the elevators, rudders and ailerons. These actuators push the control

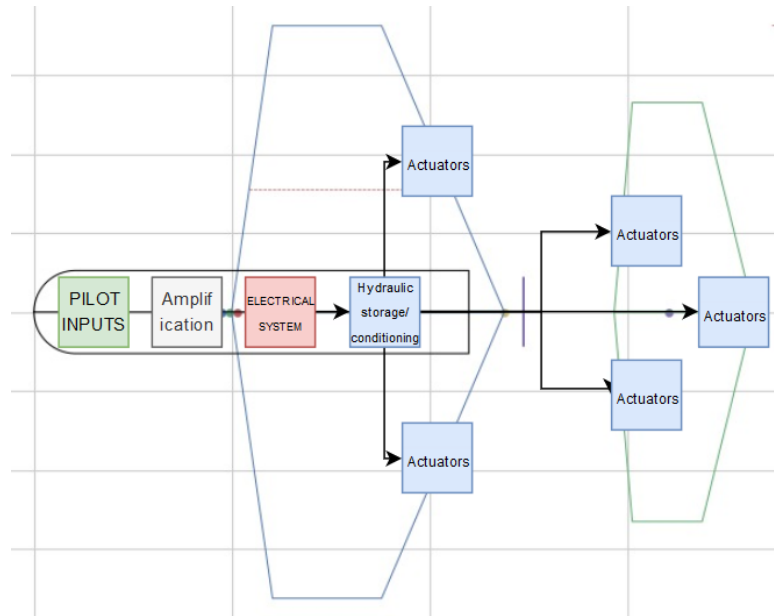


Figure 9.9: Hydraulics system position determination.

surfaces to acquire the required deflection.

A more specific design can be made in the actuators and hydraulic storage components. The actuators will depend on the liquid used in the system, since this will specify the required diameter and pressure on the actuator. The hydraulic storage is composed of: the reservoir, the pump, a filter, the pressure regulator, an accumulator, and some valves.

9.6. Requirement Compliance & Feasibility

Table 9.4: Overview of the requirements regarding the stability & control subsystem.

Code Identifier	Requirement	Type	Verification	Compliance
EVTOL-SRSC-221	The yaw rate provided by the S&C subsystem shall be greater than 45 deg/s.	Regular	Analysis	In Progress
EVTOL-SRSC-222	The pitch rate provided by the S&C subsystem shall be greater than 30 deg/s.	Regular	Analysis	Met
EVTOL-SRSC-223	The wing control surfaces shall not interfere with integration of propulsive system of the wing.	Regular	Inspection	Met
EVTOL-SRSC-224	The S&C subsystem shall provide stability and control for changes in centre of gravity of 0.773 m.	Driving	Inspection	Met
EVTOL-SRSC-225	The rotor angular velocity of the S&C subsystem shall not exceed 1600 RPM in order to meet noise requirements.	Driving	Analysis	Met
EVTOL-SRSC-226	The S&C subsystem shall provide for stability during vertical take-off and landing	Driving	Analysis	Met

As discussed in the vertical flight control subsection, the yaw rate requirement is hard to meet due to the nature of the control methodology used for yaw control. Analysis was used to prove that yaw control is still achieved but to a lower extent, which is not a big problem according to the pilot the team consulted. The pitch rate requirement is easily met as discussed in this chapter. The control surfaces interference is validated by inspection of the CATIA model. The c.g. range requirement is validated through inspection of the design output code. Rotor RPM is shown to be limited by proper controller design and this requirement is therefore validated. Stability in vertical flight is validated through analysis and the methodology is explained in this chapter.

As all but one of the subsystem requirements are met, the control and stability subsystems, as described in the chapter, are considered feasible. A more thorough analysis should be made to investigate the directional stability and control of the aircraft to size the vertical tail of the aircraft appropriately for the directional stability and control requirements, instead of using statistical estimates from reference aircraft. The sizing of the elevator, rudders and ailerons right now is only performed based on recommendations of an aircraft design handbook. For future design, requirements on the roll, pitch and yaw rate should be established before the control surface design, and perform the control surface sizing based on a dynamic analysis of the aircraft in order to achieve the prescribed rate requirements. The control system implemented for vertical flight phase is considered to be feasible, as there are already existing prototypes existing that make use of similar control system, hence also considered feasible.

Detailed Design: Structures and Materials Subsystem

This chapter focuses on the structural reinforcements in the wing and fuselage and on the materials for each structure of the H₂ERO. First the wing design will be discussed in section 10.1. The cabin design and fuselage design will be elaborated in section 10.2 and section 10.3 respectively. Materials will be discussed in section 10.4 and lastly, the requirements compliance & feasibility is concluded in section 10.5.

10.1. Wing Design

Designing the wing was set to be one of the challenges of interest for the H₂ERO. The wing will fully support a large rotor for vertical flight embedded within the wing structure on each side, which will mean two considerably big holes in the structure of the wings. It is chosen to use two I-beams right beside the propellers to cover the bending moment acting on the wing. Furthermore, a wing box with a hole for the propellers is implemented in the wing to cover the torsion and shear acting on the wing.

First free body diagrams are drawn in four different stages of the operation. The first is stationary on the ground. This is the state with the most negative moment, since only the weight of the rotors and wing structure itself act on the wing. The second is for VTOL when only the propellers are creating forces upwards, which will create a positive moment. The third is a special moment in the transition phase. After hovering vertically up, the horizontal speed is increased and so the wing surface starts to create lift. Once the stall speed is reached the main propeller can be shut down and covered. At this point both the propellers and the wing produce lift. Therefore, the vertical shear force and moment are positive in this state. Finally there is the horizontal flight with all propellers shut down and the integrated propellers covered so that the entire wing produces lift. During this phase the torsion is assumed to be highest because the entire wing produces the lift and therefore an aerodynamic moment will torque the wing box. Furthermore, it is assumed that this phase will have the highest bending moment for the same reason. It can be argued that the VTOL or transition phase has the highest bending moment, however then the lifting forces of the propellers is divided over the four propellers alleviating the forces on the wing.

Now a structural concept has to be found. While doing so it is important to keep in mind what inputs to use for the program. Most useful parameters come from a combination of aerodynamic output parameters and geometric properties. For example the leading and trailing edge sweep come from parameters such as root chord, quarter chord sweep and taper ratio.

A couple of assumptions are made. The wing is assumed to be trapezoidal. Meaning root and tip chords are parallel and connected by straight lines which are the leading and trailing edge. Also the wings are assumed to start at the side of the fuselage with the vertical rotor circumferences directly next to the fuselage. To counter the moment created by the lift and vertical thrust, two I-beams are placed adjacent to the rotors. The locations of these beams are dependent on the location and diameter of the rotors and the distance between them. It is decided that the position of the beams with respect to the chord is fixed throughout the wing span. The skin then connects the I-beams in order to

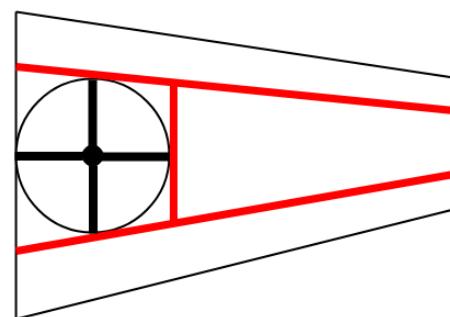


Figure 10.1: Sketch of the wing planform with struts placed in the rotor hole in black and the beams in red.

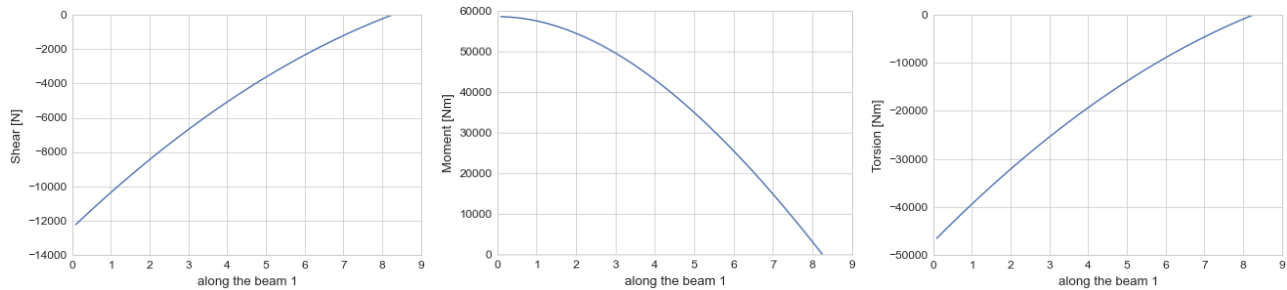
carry the shear and torsional loads. Another assumption made regards the struts with which the rotors are attached to the wing box. At this point it is yet unknown how the rotors can be attached in the most efficient way in terms of aerodynamics. Therefore the assumption is done that a cross-like structure holds up the axes of the rotors. In this way one quarter of the rotor loads are carried by the cabin and one quarter is carried by each I beam in front and aft of the rotor at the distance of one rotor radius from the fuselage. The last quarter will be carried by a boom parallel to the cabin, connecting the two nearest I beams. Meaning these I beams carry an additional one eighth of the rotor loads at a distance of two rotor radii. All together the structure looks like Figure 10.1.

A program is created to plot the loading diagrams. A choice in the program is given to include or exclude the loads on the wing. This is done so that the three aforementioned states can be described and designed for the critical one. A mesh of one hundred increments of the wing is made. The influence of the loads on the increments is added together for each increment. Then the reaction force or moment is subtracted from all increments in order to make sure that the internal load is zero at the wing tip. The formula's that are used for the shear, moment and torque diagrams can be seen in Equation 10.1, Equation 10.2 and Equation 10.3 respectively. Furthermore, the loading diagrams can be seen in Figure 10.2 and Figure 10.3 for beam 1 (near the leading edge) and beam 2 (near the trailing edge) respectively.

$$V = \frac{1}{2} \rho V^2 C_L c_{root} \left(y + \frac{\lambda - 1}{w_l} \frac{y^2}{2} \right) \quad (10.1)$$

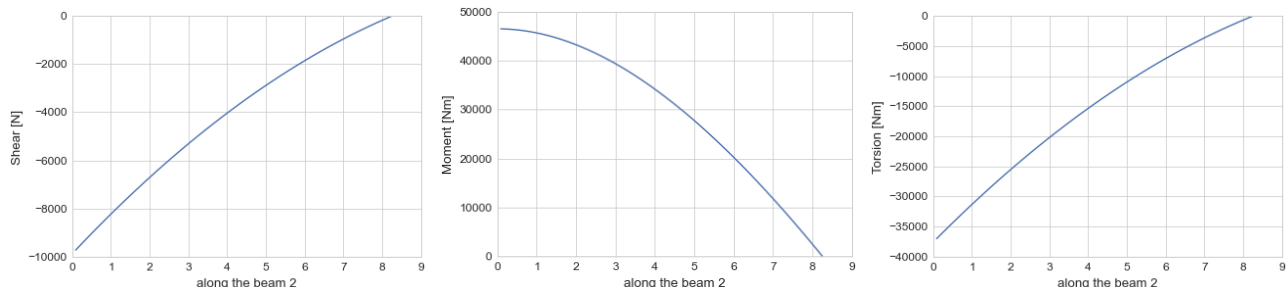
$$M = \frac{1}{2} \rho V^2 C_L c_{root} \left(\frac{y^2}{2} + \frac{\lambda - 1}{w_l} \frac{y^3}{6} \right) \quad (10.2)$$

$$T = \frac{1}{2} \rho V^2 C_m c_{root}^2 \frac{1 + \lambda}{2} \left(y + \frac{\lambda - 1}{w_l} \frac{y^2}{2} \right) \quad (10.3)$$



(a) Shear diagram acting on beam 1 along the wing span. (b) Moment diagram acting on beam 1 along the wing span. (c) Torque diagram acting on beam 1 along the wing span.

Figure 10.2: The shear, bending moment and torque diagrams acting on beam 1 along the span.



(a) Shear diagram acting on beam 2 along the wing span. (b) Moment diagram acting on beam 2 along the wing span. (c) Torque diagram acting on beam 2 along the wing span.

Figure 10.3: The shear, bending moment and torque diagrams acting on beam 2 along the span.

Now that a program can find the loads on any location on each beam. The I-beams can be designed. The height h of the beam is set by geometry and aerodynamic parameters. The chord length at any place in the wing span is given by Equation 10.4.

$$c(y) = c_{root} + \frac{\lambda - 1}{w_l} y \quad (10.4)$$

Here, c is the chord length, λ the taper ratio, w_l the wing length and y the position on the wing. When the local chord length is multiplied by the thickness-to-chord ratio of the location in the cross section, the thickness of the wing follows and therefore the height of the I-beam. The width of the two beams is found through an iterative process. For simplicity and easy manufacturing the beam dimensions will vary linearly throughout the wing span. The way this is done is building an iterative program that calculates the moment of inertia of multiple combinations of t_1 , t_2 and b , which are made visible in Figure 10.4. Using the root moment load, root height and a 1.5 safety factor of the allowable yield stress, a requirement moment of inertia is found, which can be seen in Equation 10.5. If one of these iterations leads to a sufficient moment of inertia, the area of the cross section is calculated. The sufficient cross section with the least amount of area will be the lightest solution.

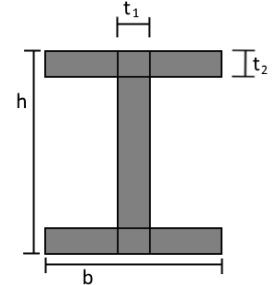


Figure 10.4: I-beam dimension definitions.

$$I_{xx_{required}} = \frac{M \cdot \frac{1}{2}h}{1.5 \cdot \sigma_{yield}} \quad (10.5)$$

Here I_{xx} is the moment of inertia around the x-axis, M the bending moment, h the height and σ_{yield} Ratio's of the root cross section are found and kept constant throughout the wing span. With the set $h(y)$ function, $\frac{b}{h}$, $\frac{t_1}{h}$ and $\frac{t_2}{h}$ it is possible to describe the beams, find the volume of each beam (and therefore the mass) and their centre of gravity. Results of the dimensions of the beam can be found in Table 10.1.

Table 10.1: Dimensions of the two I-beams given in mm.

Values are in mm.	Root				Tip			
	Height	Flange Width	Flange Thick.	Web Thick.	Height	Flange Width	Flange Thick.	Web Thick.
Beam 1	579	193	35	1.2	233	4	0.5	0.5
Beam 2	771	257	14.5	1.6	311	5.5	0.6	0.6

10.2. Cabin Design

The design of the cabin is of importance for the fuselage and thus aircraft dimensions. In this section, the design process of the cabin is given, as well as the final lay out.

10.2.1. Requirements on Cabin Design

In order to design a cabin, certain requirements have to be analysed to make sure all components and dimensions are thought of. This is done by creating a list, based on the current EC-135 [cite some document here] and requirements set by pilots and doctors received during a visit to the base of the emergency helicopter at Rotterdam airport. These requirements and desirable dimensions are listed below.

- Cockpit dimensions: minimum width of 1.2 meter, minimum height of 1.2 meter and a minimum length of 1.5 meter.
- Medical cabin dimensions: minimum width of 1.2 meter, minimum height of 1.2 meter and a minimum length of 2.5 meter.
- There should be a minimum of 4 seats and 1 stretcher.

- The cabin door should be big enough to get a stretcher in the cabin. Preferably there is a separate door for the cockpit.
- The pilot should be able to have a clear view to the front and side. The pilot should be able to have some kind of view up and down and there should be a system to watch backwards.
- The doctor should be able to operate necessary procedures and should have proper access to the head and torso of the patient. Medical equipment should all be within reach.
- There should be enough space in the rest of the cabin or fuselage for the fuel cell, motor, battery, tanks, avionics, cooling system and other necessary systems.

10.2.2. Cabin Design Options and Selection

For above stated requirements, several designs and lay-outs were considered. It should be noted that the fuselage creates drag and no lift, and should therefore be minimised.

The most restrictive requirement on the cabin design is found to be the door for the cabin, as the stretcher should fit through and concentration of loads due to a cut-out should be minimised. Multiple options for the doors were considered and the feasibility of each of them is analysed. They are listed below, including their advantages and disadvantages.

- A side door, which needs to be at least 1.1 meter wide and 0.8 meter high. Advantages mostly come from the ease of the location for the door, which can be almost anywhere along the fuselage. Disadvantages is that it requires a big cut out, as the length of the stretcher is most likely more than the fuselage width, so it has to be transferred into the aircraft with a turn around the doorpost. This increases the stress in the surrounding parts of the fuselage.
- A door opening up underneath the cabin. This door can fit in any configuration, however, the door needs to be larger as the patient cannot be brought in under a high angle, especially not when there is head trauma.
- A door at the rear of the aircraft. This is only possible if the horizontal rotor is not located at the rear of the aircraft, when the tail consists of two booms connected to the fuselage and if the horizontal tail lies sufficiently high that a medic with a stretcher fits underneath.
- A door at the front of the aircraft, for example by lifting the cockpit up, as is done with the Antonov An124 for example. This means there will be a sufficiently large door, however, this requires a strong rotating mechanism to lift the cockpit and the pilot has to get out, lift the nose, wait, put the nose back and then get in again, which is not very time efficient.

Looking at the four options for a door, a door underneath the cabin and at the front seems not very feasible, meaning there are two options left: a side door or a rear door. Since the propeller used for horizontal propulsion is located at the rear, this option is not feasible anymore either. The door will thus be at the side of the aircraft.

Looking at the other requirements, there should be enough space for four persons and a patient on a stretcher. Stretchers are generally 0.5 meter wide and 2 meter long. From the four other passengers, one is the pilot and it is thus needed to have at least one chair in the cockpit. Since he is helped by the medic for directions when flying to the site of the accident, a second chair is needed in the cockpit. This means there will be two chairs in the medical cabin, one for the doctor and one for an extra passenger.

The pilot has to have a clear view to the side, as well as 90 degrees up for taking off vertically and some view on the ground for vertical landing. The back can be viewed by making use of one or multiple camera's, as is done in the EC-135 as well.

Finally, the height, width and length of the fuselage has to be estimated. Using dimensions from current emergency helicopters, the width will be around 1.5 meter, with a height of at least 1.5 meter, since the fuselage will be most like circular or elliptical. The minimum length required for the cockpit and medical cabin combined is $2.5 + 1.5 = 4$ meter. More needs to be added to this to fit the energy systems and other subsystems. Therefore, using the size estimations described previously for the energy sources and the propulsive system, a minimum length of 7 meters is assumed.

10.2.3. Lay-out Cabin

The cabin should have enough space for all parts. A list of all parts that should be in the cabin is given below.

- A stretcher
- Two seats
- Two medical bags
- Three oxygen tanks
- Four medical displays
- Defibrillator, oxygen mask, a surgery set, straps, blanket and other medical sets
- At least three closets to store all equipment

In Figure 10.5, the lay-out of the cabin is given. Top, front and side views are shown with dimensions, as well as an isometric view to get an insight on the three dimensional view. All parts are labelled in the exploded view and are shown in the bill of material. The cabin as a whole is 2.9 meter long, 1.3 meter wide and 1.2 meter high. In this space, all components are fit in such a way that the stretcher can be loaded in and out of the cabin and that all medical equipment is accessible during flight.

The stretcher, which is indicated in the exploded view by number 3, can get into the aircraft through a door with a width of 1.2 meter and a height of 1 meter from the left side. The closets are designed in such a way that the stretcher fits through the door and into the designed space, as shown in Figure 10.6. With the dimensions shown, it is clear that the door is wide enough for the doctor and medic to fit a patient on a stretcher through, while having some room to manoeuvre around as well. It should be noted that the stretcher shown here is only for visualisation, the actual stretcher will have wheels and a structure to lift it up, as the current stretchers in most ambulances and emergency aircraft have. The dimensions shown are the dimensions all stretchers have in reality.

As can be seen in Figure 10.7, the left chair can be moved along the rails. The chairs are indicated in the exploded view by number 1. This translation and rotation enables the doctor to have access to the whole upper torso during flight, as was required. Furthermore, by moving and rotating the chair 90°, the doctor has access to all medical equipment, which is stored in the three closets shown on the exploded view by number 5, 6 and 11. Monitors for heartbeat, oxygen stats and more are shown by bullets number 7, 8 and 9. The oxygen tanks are within reach if needed and are indicated by number 2.

The medical bags, indicated by number 10, of which there are always two in the cabin, have their own storage space. When flying to the site of accident, the bags can be placed on the stretcher, as is currently done with the EC-135. However, with a patient on board, the bags have to be placed on the ground in the current emergency helicopter, which is impractical as it might block access to medical equipment. It is therefore that the bags placement is designed for. They can be stowed on the two top shelves of closet number 6, as shown in the isometric view.

Currently, some medical kits in the EC-135 can only be accessed via the door in the back. These kits can be stored in closet number 5 here, enabling access and saving some time which is now needed to walk around the helicopter to open the back doors. The remaining kits, consisting of smaller equipment, can be stored in closet 11. Contrary to what is shown here, all closets will have a door or drawer, ensuring no parts will fall out during flight. A final render of the cabin is shown in Figure 10.8.

10.2.4. Restriction on Aircraft Design due to the Cabin Design

As a final thought of the cabin design, it is useful to find all the restrictions set on the aircraft design due to the cabin. First of all, the fuselage should contain a cabin with a minimum overall height of 1.2 meter, width of 1.3 meter and length of 2.9 meter. Furthermore, there should be enough space for a door of 1 meter high and 1.2 meter wide, meaning if there is a wing or rotor at the same location, the fuselage should be higher. Furthermore, the first 1.5 meter of the fuselage is needed for the cockpit, which has a minimum of 1.2 meter for both width and height at 1.5 meter from the nose of the aircraft.

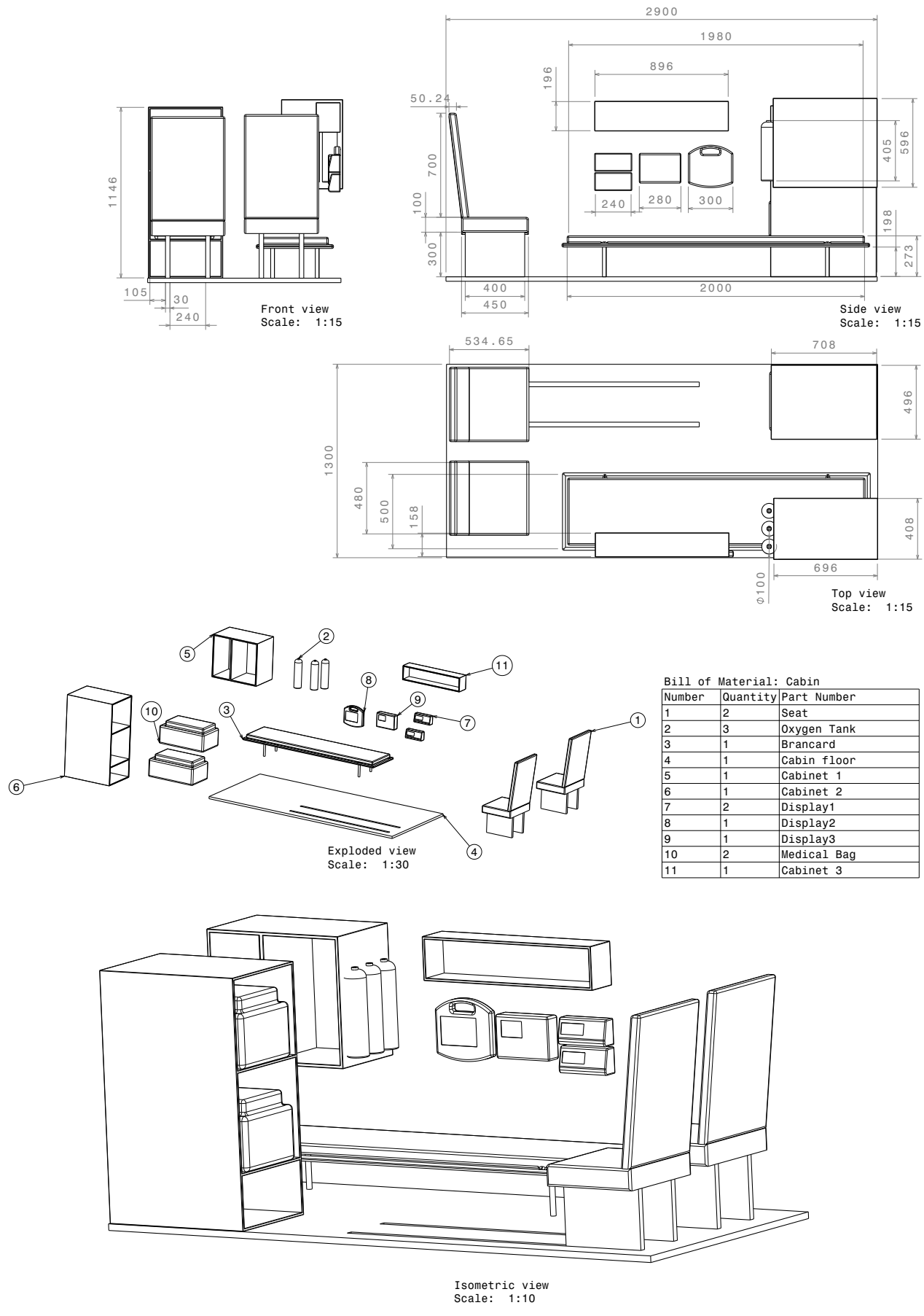


Figure 10.5: Lay-out of the cabin.

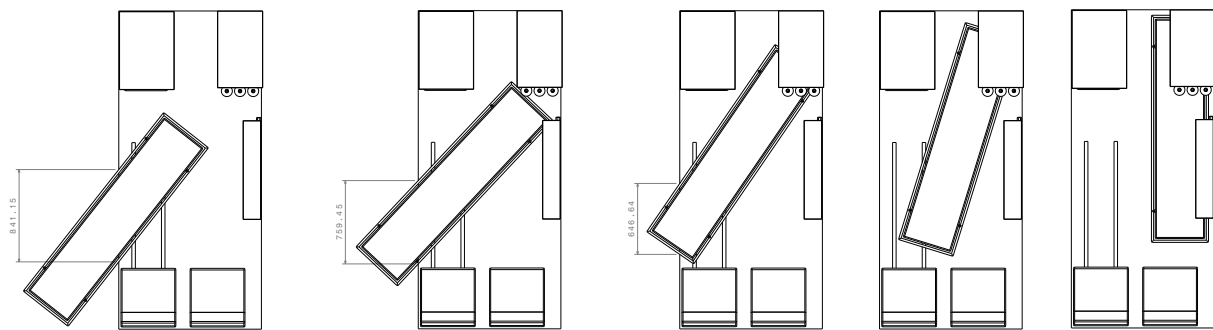


Figure 10.6: Stretcher loading through the door.

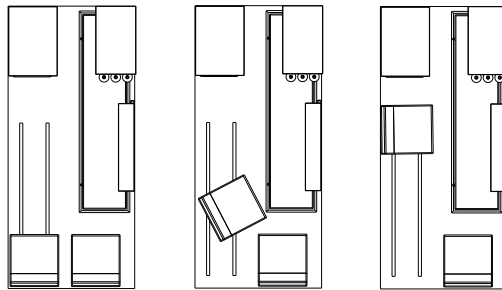


Figure 10.7: Chair movement along the rails for extra access to the patient and equipment.

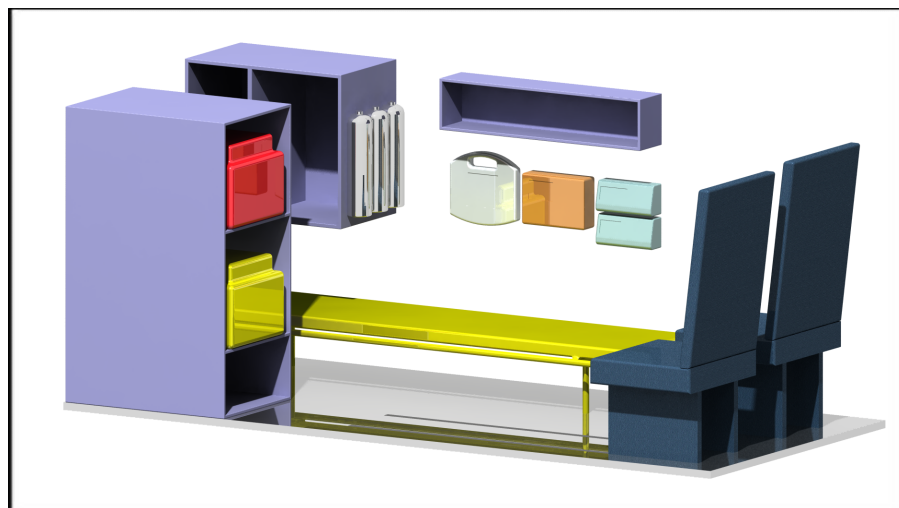


Figure 10.8: A render of the cabin design.

10.3. Fuselage Design

In order to design the fuselage, all loads acting on it have to be determined. Four main types of loads were found: bending moments, axial loads, shear and torsion. To compute the stresses in the fuselage, the method as described in Aircraft Structures by T.H.G. Megson [30].

10.3.1. General Fuselage Design

To start off with a design, a general lay-out of the fuselage is to be chosen. It was chosen that the wing box will be carried through the fuselage, which will help with the loads transmission. The extended wingbox-like structure will have a elliptical part before it, where the cockpit and energy systems are positioned in. The medical cabin will be positioned under the wingbox. After the wing, there is space for other subsystems. Furthermore, the fuselage is assumed to have a constant cross section reinforced with stringers.

From this design, a few properties can be calculated. For simplification, the fuselage is assumed to consist of two half circles with two vertical plates in between, instead of an elliptical cross section. The centroid location of the cross section can be determined, as well as the moments of inertia for both the cross section and side view. These are needed to compute the stresses and shear flow in the following sections. For this design, a python script was made in which the lengths and thicknesses of all the plates and stringers, as well as the number of stringers, could be set. Then, the location of each part is computed and stored before the centroid is calculated. The general equation for the centroid is given in Equation 10.6. The centroid location in both Y-direction and Z-direction is on the line of symmetry.

$$\bar{z} = \frac{\sum A_i z_i}{\sum A_i} \quad \bar{y} = \frac{\sum A_i y_i}{\sum A_i} \quad (10.6)$$

Furthermore, the moments of inertia I_{xx} and I_{zz} could be computed. This was done by taking the moments of inertia of every plate and stringer around the centroid. For the stringers on the circular bottom, the angle with respect to the arc has to be computed to generate the moment of inertia. For the stringers, Equation 10.7 was used. The theory for moment of inertia for rotated plates is applied for the stringers on the lower and upper circular plate, using Equation 10.8. In both equations, t_1, h, b and t_2 are defined in the same way as depicted in Figure 10.4. $A_{stringer}$ is the area of the stringer and $z_{stringer} - \bar{z}$ and $y_{stringer} - \bar{y}$ are the distances between the z or y-location of the stringer and the centroid, respectively. The angle that the stringer makes due to the curvature is depicted with α . In Equation 10.9, the formula to compute to moment of inertia for the upper and lower half circle is given, with t_{top} being the thickness of the top sheet and r_{top} being the radius of the top sheet. All dimensions are in meter or radians.

$$I_{zz} = t_1(h - 2t_2)^3/12 + 2wt_2^3/12 + A_{stringer}(y_{stringer} - \bar{y})^2 \quad (10.7a)$$

$$I_{yy} = t_1^3(h - 2t_2)/12 + 2w^3t_2/12 + A_{stringer}(z_{stringer} - \bar{z})^2 \quad (10.7b)$$

$$I_{zz_{strtop}} = t_1(h - 2t_2)/12 + t_1^2(\cos \alpha)^2 + (h - 2t_2)^2(\sin \alpha)^2 + 2(wt_1/12 + t_1^2(\cos \alpha)^2 + w^2(\sin \alpha)^2 + A_{stringer}(y_{stringer_{top}} - \bar{y}))^2 \quad (10.8a)$$

$$I_{yy_{strtop}} = t_1(h - 2t_2)/12 + t_1^2(\sin \alpha)^2 + (h - 2t_2)^2(\cos \alpha)^2 + 2(wt_1/12 + t_1^2(\sin \alpha)^2 + w^2(\cos \alpha)^2 + A_{stringer}(z_{stringer_{top}} - \bar{z}))^2 \quad (10.8b)$$

$$I_{zz_{halfcircle}} = \pi r_{top}^4/8 - \pi(r_{top} - t_{top})^4/8 + A_{top}(top - \bar{y})^2 \quad (10.9a)$$

$$I_{yy_{halfcircle}} = \pi r_{top}^4/8 - \pi(r_{top} - t_{top})^4/8 + A_{top}(top - \bar{z})^2 \quad (10.9b)$$

10.3.2. Loads

As can be seen in Figure 10.9, the free body diagram in the z-x plane are drawn, with x defined as positive towards the left and z as positive downwards. For every beam in the wingbox, there will be a point load and moment, as well as for the front propellers and the tail. The fuselage as a whole has a constant distributed load due to the weight of the structure. All major components inside the fuselage, such as the passengers, medical equipment, fuel cells, batteries, tanks and motors are represented with a point load in positive Z-direction. It should be noted that they are not drawn at the correct position as of yet, since this will be done during the subsystem integration with the centre of gravity determination. Therefore, the load and moment diagrams will be given in subsection 11.7.1 well. With these loads, the internal loads are computed. These are used in the following sections to compute the stresses and shear flows for every step from the front of the fuselage to the back.

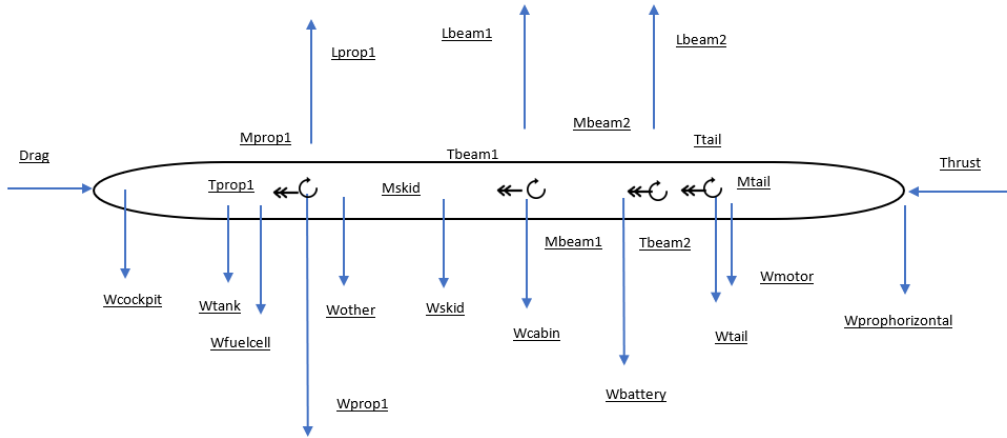


Figure 10.9: Free body diagram of the fuselage.

10.3.3. Assumptions

A few assumptions have to be made in order to analyse the fuselage. First of all, as stated before, the cross section is assumed to be constant. When boom idealisation is used, it is assumed that the booms only carry the bending and axial stresses. The stringers are assumed to be sufficiently close to consider constant shear throughout the sheet. The shear is assumed to be carried by the skin. For all computations, the stress is computed at every stringer location. This is done in small steps from the front of the aircraft to the back, resulting in a list with stresses for every stringer for every part of the fuselage.

10.3.4. Bending

For bending, the general bending formula is applied. Since the cross section is symmetrical, I_{xy} is zero and therefore neglected. The formula used for bending is given in Equation 10.10. Here, M is the moment created by both moments and loads that do not act through the centroid. $z_{stringer}$ and $y_{stringer}$ are the z and y location of the stringer relative from the centroid. This equation is applied to every stringer location for every step.

$$\sigma_{bending} = \frac{M_y z_{stringer}}{I_{yy}} + \frac{M_z y_{stringer}}{I_{zz}} \quad (10.10)$$

With these stresses, the boom area can be computed per stringer per step, which replaces the stringers in the shear calculations. The boom area is calculated using Equation 10.11, where $A_{stringer}$ is the area of the stringer, t_D the sheet thickness, b the width between the stringers and σ the stress induced by bending.

$$B_n = A_{stringer} + \frac{t_D b_{n+1/n}}{6} \left(2 + \frac{\sigma_{n+1}}{\sigma_n} \right) + \frac{t_D b_{n-1/n}}{6} \left(2 + \frac{\sigma_{n-1}}{\sigma_n} \right) \quad (10.11)$$

10.3.5. Normal stress

Since the horizontal propulsion is attached to the back of the fuselage and drag has to be taken into account, there will be normal stress within the stringers. This is computed using Equation 10.12. This is computed with the internal normal force S_x and the total area of the stringers $A_{total, stringers}$, as the stress will be distributed along all stringers. The stringers were assumed to take all axial stresses.

$$\sigma_{axial} = \frac{S_x}{A_{total, stringers}} \quad (10.12)$$

10.3.6. Shear

For the shear calculations, the sheets are assumed to have zero thickness and the loads are assumed to be applied through the shear centre. Using the boom idealisation, the shear flow can be computed with Equation 10.13.

$$q_s = q_b + q_{s,0} = -\left(\frac{S_z}{I_{yy}}\right) \sum B_n y_n - \left(\frac{S_y l}{I_{zz}}\right) \sum B_n z_n + q_{s,0} \quad (10.13)$$

$q_{s,0}$ is computed while using the shear centre and the assumption that the loads are applied through the shear centre. This is done using Equation 10.14, where A_m is the area of the whole cross section and d is the distance between the shear flow and the shear centre.

$$V_z \eta + V_y \xi = 2A_m q_{s,0} + \oint d \cdot q_b ds = 0 \quad (10.14)$$

10.3.7. Torsion

Finally, the torsion is computed. This is done by using the general torsion equation, Equation 10.15, since the skin carries all the shear from this type of loading.

$$q_t = \frac{T}{2A_m} \quad (10.15)$$

10.3.8. Total Stress and Shear Stress

After computing all the aforementioned load cases, the normal and bending stress can be added together to get the total stress in the booms. This is done by a simple summation, $\sigma_{total} = \sigma_{bending} + \sigma_{axial}$, where special attention should be paid to the sign convention. The total shear stress due to shear and torsion combined is computed by adding both up as well. After the system integration, all loads and distances will be known, as well as the material used for the fuselage and a proper analysis of the thickness and amount of stringers will be done.

10.4. Materials

Besides the mathematical designs regarding loads throughout the various structures of the aircraft is the selection of the materials used for these structures. Each section of the aircraft is designed for a different task. Hence, each section also requires a distinct selection for the materials used for it. One can imagine that the loads taken by the wing are different than those loads one can find within the fuselage section. These material choices will be considered below.

10.4.1. Wing

Starting off with the material selection for the wing. The wing can be regarded as one of the most important load carrying structural component within the aircraft. The loads throughout the wing are most dominant during the cruising phase as this is when the wing produces lift, and hence has to distribute loads. In comparison, the wing creates zero to very nominal lift during the VTOL phase. The wing will have to take loads in all possible directions. The main forces will be due to the bending moment. However, the wing should

also not buckle on the upper side of the wing and should not rip on the lower side of the wing when it is subjected to these bending moments. Hence, a material should be chosen that shows promising strength in all directions. Also, it should be noted that the wing entails the largest area of the aircraft. Hence, it is of utmost importance that a good selection is made between the strength to weight ratio to not make the aircraft too heavy but also the price to area ratio should be taken into account as well. Furthermore, the material needs to be able to sustain many different types of weather situations and hence terms as corrosion resistance should also be considered as important design choices.

Possible Materials

For the wing of aircraft nowadays many different materials are used. Depending on the location of the wing a different material is used. Aircraft wings mainly consist of a combination of skinned aluminium for the outer skin and consist of better stress resistant materials like steel for the heavy stress areas around joints.

However, there has been a decline in the use of metals in the aerospace industry due to the increase in the use of composites like carbon fiber reinforced resins. These composites can be laminated in the direction that a load carrying path is required. The main advantage of composites is their high strength to weight ratio. These composites are the most researched and most promising new material for the future. They are starting to be implemented in many various applications which greatly accelerate their research.

One of the greatest promises for the future is the new material called Flexfoil by the company FlexSys. Flexfoil is an innovative new technology which researches the use of an adjustable flexible material for the wing airfoil. This completely allows the designers of aircraft to eliminate the gap between the wing structure and any control surfaces at the trailing edge of a wing. According to FlexSys, this can increase the efficiency of a wing and hence the fuel use by 3% to 5% and reduces the overall noise produced by the wing by a staggering 40%. The way it works is that the control surfaces are embedded within a material. Due to the flexibility of the material, the control surfaces can introduce a twist, and angle deviation of the wing.

Material Selection

With the eye on the future and noise reduction of this aircraft it seems promising to further investigate the use of Flexfoil for the outer skin of the wing. Hereby, still considering the use of steel, aluminium and composites for the overall structural strength within the wing structure. The material design choice of this will be further explained in subsection 10.4.2

10.4.2. Wing Box Structure

The wing suffers the biggest loads acting on the aircraft. The wing box is the structural path that these loads follow and it is embedded inside the wing. The wing box of an aircraft must be rigid and strong enough to support the lift, the propellers weight, the propellers thrust and the weight of the wing itself. It is therefore important to choose the appropriate material in terms of strength and weight.

Possible Materials

Two main material possibilities exist for the development of the wing box. One is the Aluminium 2024. It is a metal which is easy to machine and work. It has high strength and a low weight, which fits perfectly in the requirements for the aircraft. The second material is the composites. Composites structures are becoming more common in the aerospace sector. This is due to its low weight compared to metals and its high strength. Thus composites must also be investigated as a possibility into the design. A study made in the university of Embry-Riddle [4], compares the different materials used in the aerospace sector. The Figure 10.10 represents the comparison between these.

Material Selection

It can be observed in Figure 10.10 that the best material for the wing box application must be either the Graphite/Epoxy, the Glass Epoxy or the Kevlar. Aluminium does not perform as well as the composites structures due to its higher weight, but not only performance must be accounted for. Manufacturing, sustainability and cost must also be considered. Aluminium performs better in such a complicated structure,

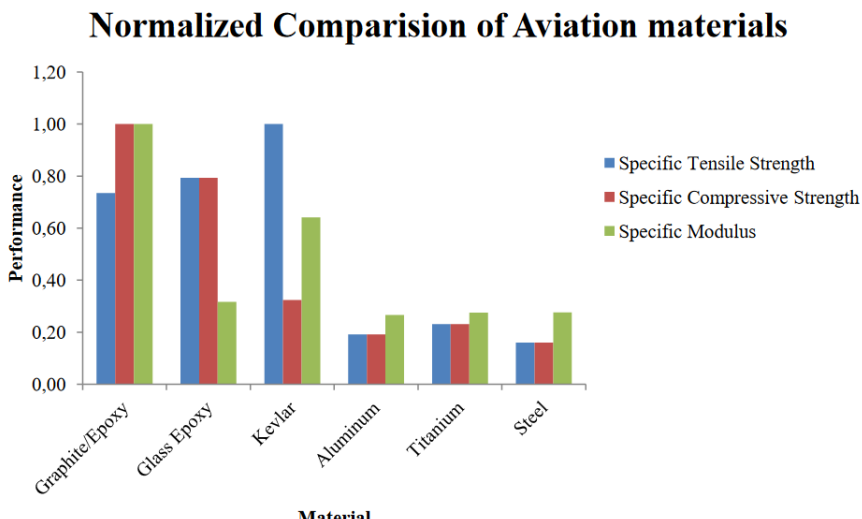


Figure 10.10: Different aerospace materials for the wing box design. [4]

since the attachments and the production are easier to manufacture. The cost is therefore lower. In terms of sustainability, most of the composites have a bad recycling cycle (except for the Natural Fiber Polymer Composites), and aluminium can be reused once the life-span has been ended.

10.4.3. Fuselage

The fuselage is the ending point of the aircraft loads. This means that all the loads acting on the wings, landing gear and tail will eventually affect the fuselage, since these structures are attached to it. Other loads affecting the fuselage are: the airflow, that creates distributed loads around it and the impact loads on landing must be considered as well, since these are high loads in a close time range. Since the flight altitude is low, there is no need for a pressurised cabin, thus pressurisation loads do not have to be taken into account.

Possible Materials

The fuselage must be able to sustain all kind of loads, from impacts, to torsional, to compressive and tensional. Thus, a material with good isotropic characteristics and good impact loads must be used. Aluminium is an isotropic material able to resist impact loads. The main drawback is the high weight compared to the composite material. As explained in the wing box design, manufacturing and sustainability were key advantages.

A composite concept can also be used, it should be quasi-isotropic and must be able to resist the loads stated above. The main advantage of the composites is the low weight and the high stiffness, since the airflow must not be able to deform the fuselage skin. The impact performance is not as good as aluminium, but it can be improved using GLARE.

Material Selection

While in the wing box design the easy manufacturing and low cost was considered as an advantage the fuselage is easy to design as a single monocoque structure. This means that manufacturing the fuselage with composites would be easier than manufacturing the wing box. It would also save a great amount of weight since connections are not required as in the aluminium fuselage. Furthermore, in places where impacts can be expected GLARE will be used (since it is light and has better impact properties).

The sustainability of the material will have to be improved. As a company, keeping the aircraft as sustainable as possible is very important. Therefore, recycling techniques must be improved to guarantee a proper polymer re-utilisation. The manufacturing method must be optimised for less energy consumption and the material waste must be limited.

10.4.4. Tail

[htbp] For the tail surface of the H₂ERO, the loads that it should be able to deal with are shown in Figure 10.11. The tail helps make the aircraft stable by producing a counter moment to any alteration in the angle of the aircraft. This counter moment increases the aircraft's stability but also increases the trim drag.

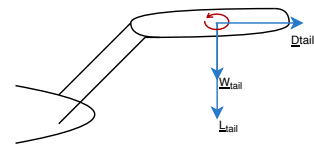


Figure 10.11: Loads in the tail.

Possible Materials

The same materials as were described for the main wing surface in subsection 10.4.1, have been analysed to use for the tail surface. This included the use of aluminium, Flexfoil and composites.

Material Selection

Like the wing material, it seems logical to experiment and research the Flexfoil as a possible material to be used as the surface material of the tail due to its increase in efficiency. Hence, Flexfoil is considered to be used as the material for the tail surface as well.

10.4.5. Propellers

The propeller of the H₂ERO, is subjected to many forces. It needs to sustain large centrifugal, bending, tangential and axial forces. It also needs to be designed to sustain the various weather implications in which it operates. Hence, the propeller is expected to be a complex system and needs multiple materials to be able to withstand these forces. An overview of the material selection is given in the following section.

Possible Materials

Conventional propeller materials are made up of various different types of materials depending on the location and function of the propeller. For instance, conventional main rotors of helicopters like the EC135, consist of glass (fiber) reinforced plastic or GRP for the blade skin. The core is filled with a hard foam material which provides the propeller with its structural shape and stabilises the skin material on top. The bending and tension forces are absorbed by the propeller spar which is also made of GRP. Finally, since the VTOL blades of a conventional helicopter are subjected to high speeds, wind, sand, rain, debris and other weather conditions, they are sensitive to erosion. Hence, the leading edge of conventional rotors are also covered with an erosion protection material which is two parts metal and one part cermet. This material is called tungsten carbide cobalt [53].

Material Selection

For the material selection of the H₂ERO propeller a difference is made between the VTOL and the cruising horizontal propeller. For the VTOL propeller the same material will be used as the EC135 main rotor blade for the core (which is a foam material), skin (glass fibre composite) and erosion protection (titanium). It should be noted that the erosion protection for the VTOL is located at the leading edge of the propeller. Also, even though the VTOL propellers are ducted for the H₂ERO, the propellers still require erosion protection as the air coming through them can still contain all of the debris. However their impact loads will be less severe than an open rotor at cruise speed.

Regarding the horizontal propeller, also the same set up has been chosen as for the VTOL blades. However, there is one alteration. Because the horizontal propeller functions at a different angle than the VTOL propellers, the entire top of the propeller will also be coated with the erosion protection material.

10.4.6. Landing Gear

The landing gear must be able to sustain high impact loads, when the aircraft does a forward flight landing or an emergency landing the loads are greater than on a VTOL landing. Thus the design must account for all.

Possible Materials

One of the main materials used for landing gears in aviation is the steel. Steel has a high weight but it accounts with great ultimate tensile strength and good fracture toughness. This makes of steel a good candidate for the landing gear material [33].

Titanium alloys are also utilised in the landing gear, it accounts with a similar specific strength than the steel. It is also good for fatigue and fracture toughness. The main difference with steel is that titanium is better at handling corrosion.

Material Selection

Aluminium can not be used due to its lower strength and stiffness. And composites materials are not the best at impact resistance. This is why directly steel and titanium were evaluated. The main difference is on corrosion. While steel suffers hydrogen embrittlement [33], the titanium alloy is able to handle the corrosion better. Hydrogen embrittlement reduces the material impact resistance when in contact with hydrogen.

10.5. Requirement Compliance & Feasibility

Code Identifier	Requirement	Type	Verification	Compliance
EVTOL-SRST-231	The structure shall be able to sustain a minimum of 45,000 N originated from the rotor loads	Regular	Test	
EVTOL-SRST-232	The structure shall be able to sustain a minimum of 110,000 N originated from the aerodynamic loads	Regular	Test	
EVTOL-SRST-233	The structure shall be able to sustain a minimum of 50,000 N originated from the ground loads	Regular	Test	
EVTOL-SRST-234	The structure shall be able to sustain a minimum of 80,000 N originated from impact loads	Regular	Analysis	
EVTOL-SRST-235	The structure shall be able to sustain a minimum of 100,000 N originated from the centrifugal loads	Regular	Analysis	
EVTOL-SRST-236	The structure shall be able to sustain a minimum of 100,000 N originated from the tail loads	Regular	Analysis	

Table 10.2: Overview of the requirements regarding the structural subsystem

Some of the above mentioned requirements can easily be tested for on the ground, however, for some this is not the case, as crashing due to the skids or tail not being strong enough is not desired. Therefore, these will be verified by analysis. All requirements are complied with.

Subsystem Integration Method

The subsystem integration accounts with three main branches. The **first branch** makes sure that, when designing, all the subsystems use the same initial values. This means that, all of the subsystem must use the same Maximum Take Off Weight (MTOW), the same power, the same airspeed etc. The **second branch** must make sure that, once of one of the designs has initiated the design and has calculated the intermediate parameters, these are transmitted to the other groups. Finally, the **third branch** makes sure that all the subsystems finally match each other, they fit all in the design and are able to perform both independently and together the design objective.

This chapter will start defining how the first two branches were taken care of in section 11.1 and section 11.2. Then, the subsystem design will be carried out. Finally, the third branch will be evaluated, to make sure that the final design of all the subsystems can be implemented together.

11.1. Initial Parameter Integration

All subsystems must use the same initial parameters. To confirm that this is the case, an excel list and a code was developed. In the excel file the initial parameters were written, parameters mostly obtained from the previous design phases [2]. These parameters are extracted from the excel file and implemented in each of the subsystems using a code, which was able to read and import the values. Thus, making all the subsystems use the same initial values.

11.2. Continuous Integration

The continuous integration is a very critical part of the design. All of the subsystem must use outputs of other subsystems. To take care of this, an excel file was created. In the file, each subsystem writes the required inputs for their program which are outputs from other subsystems. Thus, when developing the code for each subsystem, the required outputs for other subsystems must been taken care off. As an example, if in the stability and control subsystem requires the torque coefficient from the propulsion subsystem, when the propulsion subsystem is developing the code, one of the outputs must be the torque coefficient. This list of requirements was updated constantly during the subsystem design.

Once each of the subsystem design codes were ready, the departments got together to integrate the subsystems. This started with iterations, all the subsystems wrote the initial output values in the excel file. Then, the design was checked for feasibility, the main issue consisted on the propellers fitting in the wing. If the design was not feasible, new parameters were inputted until the design converged.

11.3. Propulsion Subsystem

As mentioned in section 5.4 the blade design will be done now. The XROTOR use explanation was given in section 5.4. Thus, only the results will be displayed next.

To finalise the propulsive system the propeller blade airfoil geometry design and structure need to be determined. Different blades are used for the VTOL and the cruise phase as both phases require different performance properties. The propeller blade design of the VTOL phase will also be divided into front and back propellers, since the thrust required for each of the propellers is different due to the centre of gravity location.

11.3.1. Propulsive System Configuration

In the Midterm Review of the design process, a propulsive system configuration separating the VTOL propulsion and the forward flight propulsion was chosen. A change in the forward flight propulsive system con-

figuration was made after the midterm review - instead of having two rotors for forward flight mounted on the horizontal tail, a single pusher propeller mounted at the back of the fuselage was chosen. A single pusher-propeller configuration allows, firstly, for a lower noise levels, as a single, large-diameter propeller requires lower RPM to achieve the same thrust as two, smaller-diameter rotors, hence making a single-rotor configuration more quiet. Additionally, the tail-mounted two rotor concept was initially chosen in order to provide additional thrust during take-off by having a rotating tail. Firstly, this option proved to be challenging to balance and control during vertical flight, especially due to the large difference in available power (hence thrust) between the VTOL propellers and the forward flight ones. Secondly, implementation of a rotating tail mechanism and together with a propulsive system mounted on it is a lot more structurally demanding, requiring a heavier, more complex structural design to facilitate it, if you compare it to the rear fuselage-mounted, single pusher propeller.

11.3.2. VTOL Blade Design

As explained in chapter 5 a series of possible propeller combinations was given. Once the integration started, the biggest problem was to fit the propellers inside the wing. Also there were problems with the MTOW of the aircraft. Therefore, the best option was to select the combination of parameters that lead to the lowest propeller diameter. This yielded to the following results. The results shown next are also the inputs for the program XROTOR

- Flight Altitude: 365.8 m. The highest altitude is used because the design is made for the worst case scenario, which means that we are still taking off at the cruise altitude.
- **Number of Propellers:** 4. Two in the front and twin in the back.
- **Number of Blades:** 6
- **Propeller Radius Back:** 1.795 m
- **Propeller Radius Front:** 1.465 m
- **Hub Radius:** Which is defined as the part where the actual blade starts, considered to be 10 percent of the radius: 0.18 m and 0.14 m.
- Airspeed: Its the upwards speed of the aircraft. From the performance parameters equals 1.5 m/s.
- Revolutions per Minute: Is the number of revolutions that the propeller does in a minute: 1250 rpm.
- **Power Required:** This is the power required : 259.610 kW.
- Ducted or Unducted Propellers: The program allows for the introduction of ducted propellers. In this case the propellers are ducted.

All the values are inputs in the XROTOR program and the final results are shown in Figure 11.1 and Figure 11.2. β_{twist} is the twist angle at the root of the blade and β_{tip} is the twist angle at the tip of the blade. The blade efficiency is represented by η , it is the green line on the graph. It can be observed that the efficiency is very low because of the high induced speed vs the low airspeed. It can also be observed in the graph that the Mach does not exceed 0.9 which is good for performance and noise.

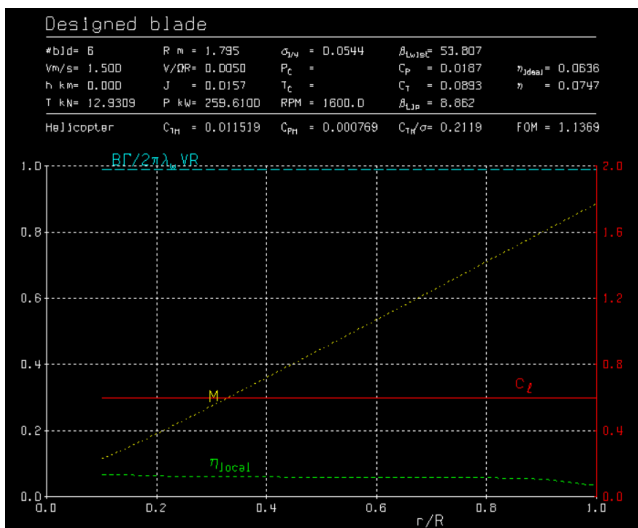


Figure 11.1: VTOL back propeller and blade design.

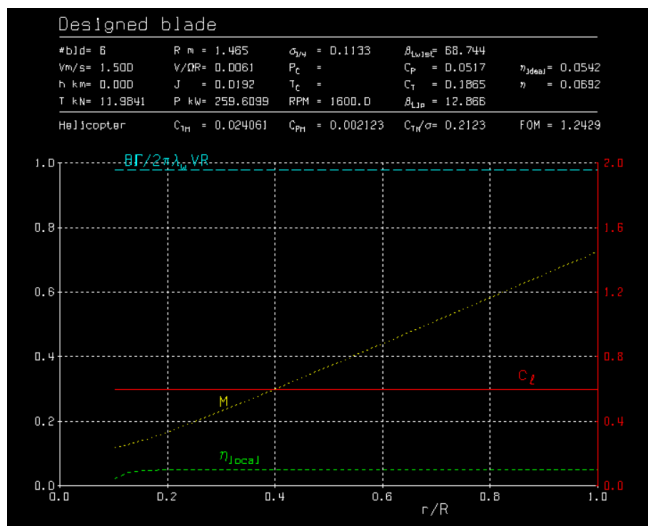


Figure 11.2: VTOL front propeller and blade design.

Some other propeller values can be extracted from the program. For example, the thrust coefficient C_t and the torque coefficient C_p . The final propeller design is shown in Figure 11.4 and Figure 11.3, which includes all the 6 blades.

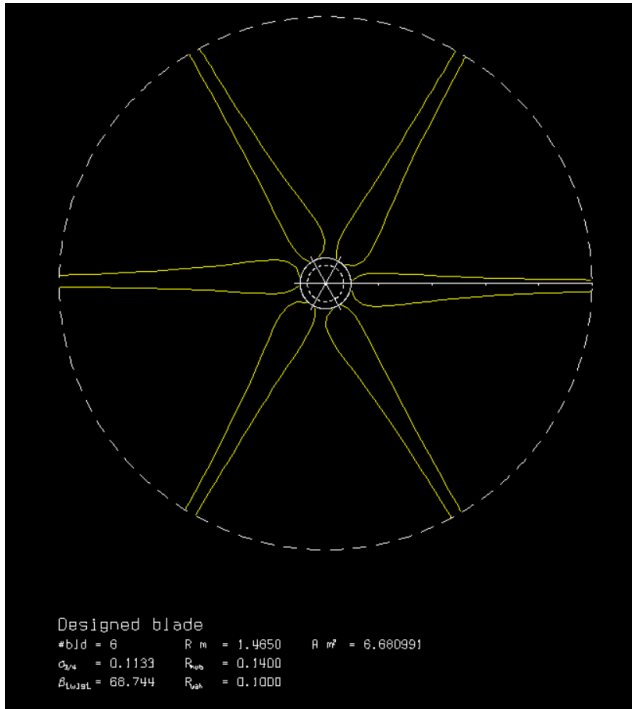


Figure 11.3: VTOL front propeller design.

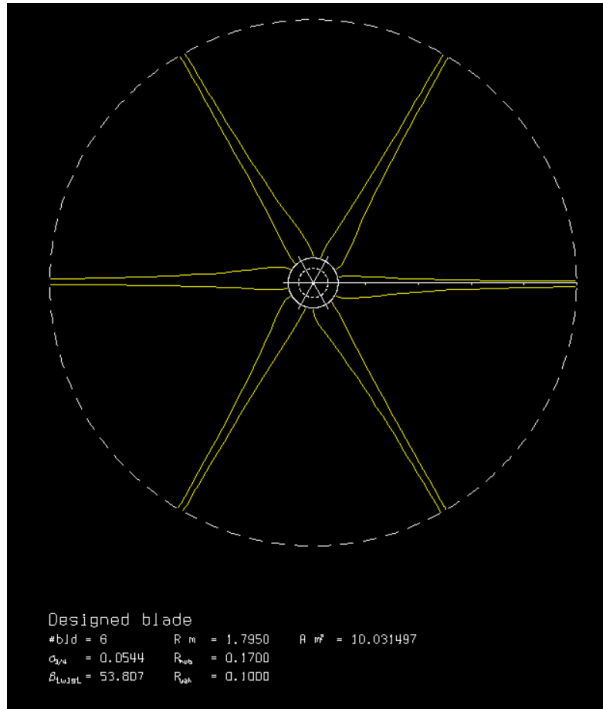


Figure 11.4: VTOL back propeller design.

Controllability Systems of VTOL Propellers

The EC135 helicopter, and many helicopters in general, use two systems incorporated in the main rotor design to help control the aircraft. These are the use of a swash plate through which the the helicopter moves left, right, forwards and back and the variable pitch settings of the entire rotor system which are used for the lifting force of the helicopter. For this design, the swash plate is removed fully. This is because for this design, control surfaces and the horizontal cruise propellers account for the various movements in the horizontal plane. Also, this reduces the complexity and weight of the main rotor system.

Furthermore, the variable pitch system has been considered. A great advantage of the variable pitch system is its responsiveness and consistency. A variable pitch allows the pilot to change the angle of attack of each blade simultaneously which increases their collective lifting force and hence results in an upward, or downward, motion of the aircraft dependent on the angle. Also, since the pitch variation can be done instantaneously and can be set to any required effective pitch angle the engine can stay at a constant RPM throughout the entire mission. A disadvantage of the variable pitch is the added mass and complexity of the system to each propeller. For a large number of propellers this can result in a significant increase of the overall empty weight of the aircraft.

For the VTOL propulsive system it has been decided that a variable pitch system is not required. Hence, a fixed pitch propeller system will be used. Main reasons for this is that the multiple propellers used in the design can provide the yaw, pitch and roll control of the aircraft by delivering varying thrust levels. As a counter argument, one could argue that using a fixed pitch propeller decreases the responsiveness of the design to a change of pilot inputs. This is true. However, initial mass determinations in designing for the various configurations in section 5.6 showed a relatively low mass of 24-39 kg for each propeller when only taking the blades and hinge point, and hence no variable pitch system or swash plate, into account. Also, most mass of the propeller blade is close to the root. Hence, when considering the moment of inertia, a propellers urge to resist angular acceleration, being low, one can conclude that each propeller is also relatively responsive to a change in power and RPM of the motor. Therewith, using a fixed pitch is argued to be logical.

Cruise Blade Design

Almost the same process as in the design of the VTOL propellers is followed. Instead of selecting the propeller based on minimum diameter, the propeller is selected based on the minimum Power Required times Weight, yielding to the lowest propeller weight at the lowest required power. This improves the efficiency of the propeller and thus of the aircraft. The following results were exported from the combinations. The results shown next are also the inputs for the program XROTOR.

- Flight Altitude: 365.8 m
- **Number of Propellers:** 1
- **Number of Blades:** 2
- **Propeller Radius:** 0.865 m
- **Hub Radius:** Which is defined as the part where the actual blade starts, considered to be 10 percent of the radius: 0.08 m.
- Airspeed: Is the cruise speed of the aircraft. This speed is selected to improve the performance in cruise flight: 69.44 m/s.
- Revolutions per Minute: Is the number of revolutions that the propeller does in a minute: 3000 rpm.
- **Power required:** The power required in cruise is: 428.16 kW.
- Ducted or Unducted Propellers: The program allows for the introduction of ducted propellers. In this case the propellers are non ducted.

Same as before, the values outputted from the program XROTOR are depicted in the Figure 11.5 and the propeller design in Figure 11.6.

```
Free Tip Potential Formulation Solution: Saved blade
                                            Wake adv. ratio: 0.33711
no. blades : 2      radius(m) : 0.8650      adv. ratio: 0.25553
thrust(N) : 0.459E+04    power(W) : 0.428E+06    torque(N·m): 0.136E+04
Efficiency: 0.7441    speed(m/s) : 69.440      rpm : 3000.000
Eff induced: 0.7580    Eff ideal : 0.8739      Tcoef : 0.6603
Tnacel(N) : -14.7705    hub rad.(m): 0.0800      disp. rad. : 0.0500
Tvisc(N) : -18.9986    Pvsc(W) : 0.613E+04
rho(kg/m³) : 1.22600    Vsound(m/s): 340.000      mu(kg/m·s) : 0.1780E-04
-----
Sigma: 0.22775
          Ct: 0.16711      Cp: 0.18029      J: 0.80277
          Tc: 0.66032      Pc: 0.88743      adv: 0.25553
-----
i r/R c/R beta(deg) CL Cd REx10^6 Mach effi efffp na.u/U
1 0.099 0.5099 77.46 0.600 0.0049 2.26 0.218 1.112 0.972 0.000
3 0.160 0.5550 69.25 0.600 0.0046 2.69 0.239 0.853 0.981 0.000
5 0.250 0.6127 58.39 0.600 0.0041 3.52 0.283 0.793 0.986 0.000
7 0.345 0.6131 49.35 0.600 0.0039 4.22 0.340 0.777 0.987 0.000
9 0.438 0.5757 42.49 0.600 0.0037 4.69 0.402 0.770 0.987 0.000
11 0.528 0.5221 37.33 0.600 0.0036 4.93 0.466 0.766 0.987 0.000
13 0.613 0.4635 33.41 0.600 0.0036 4.95 0.528 0.765 0.986 0.000
15 0.691 0.4046 30.38 0.600 0.0037 4.80 0.586 0.763 0.985 0.000
17 0.763 0.3473 28.02 0.600 0.0038 4.50 0.640 0.763 0.983 0.000
19 0.826 0.2921 26.15 0.600 0.0039 4.07 0.688 0.762 0.982 0.000
21 0.880 0.2389 24.68 0.600 0.0042 3.53 0.730 0.762 0.980 0.000
23 0.924 0.1874 23.54 0.600 0.0055 2.90 0.764 0.762 0.972 0.000
25 0.959 0.1376 22.69 0.600 0.0091 2.20 0.791 0.761 0.954 0.000
27 0.983 0.0895 22.11 0.600 0.0139 1.47 0.809 0.761 0.929 0.000
29 0.997 0.0456 21.79 0.600 0.0187 0.76 0.820 0.761 0.906 0.000
New rotor geometry created
```

Figure 11.5: Blade and propeller design of the forward flight propulsion system.

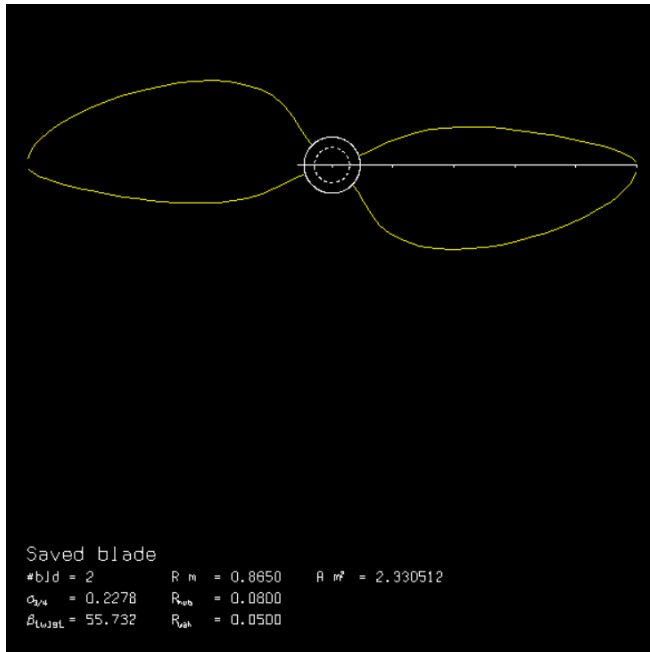


Figure 11.6: Propeller design of the forward flight propulsion system.

From the values, some of them as the efficiency and the blade twist were explained before. It can be observed that this time, the efficiency η is higher than the VTOL propellers. This is due to the higher aircraft speed on flight, which compared to the VTOL speed is almost 50 times bigger. There is some extra information in Figure 11.5. Some parameters change along the radius of the blade. These are, the chord length c/R , the blade twist β , the drag coefficient C_d , the Reynolds Number RE and the Mach speed over the blade. It can be observed that the mach does not go over 0.82 (which is good for noise and performance), and it increases towards the tip of the blade. This is due to the higher linear speed of the blade due to the angular speed. C_t and C_p are also extracted from the program, and are calculated as shown before.

If the propeller diameter is plotted against the Maximum Take Off Mass (MTOM) the following graph is

extracted in Figure 11.7. It can be observed that the propeller diameter vs mass is not linear, this is due to the combination jumps in diameter, since for different MTOM the optimum diameter might differ. Once the MTOM goes over 5100 kg the design stops converging, this is due to the requirements in forward flight, since one motor alone can not produce more than 560 kW. The first iterations converged to 4600 kg. With some weight reducing methods, the design point came down to 4200 kg, which decreased the diameter of the propellers by 1 m each.

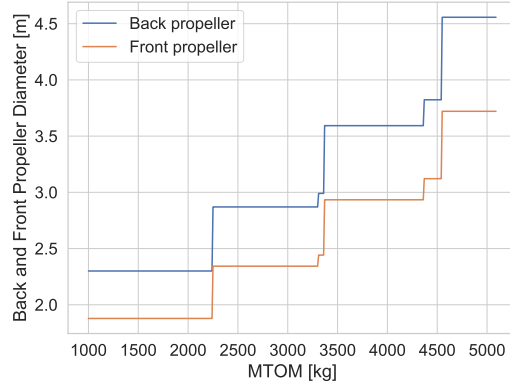


Figure 11.7: Diameter of front and back propeller vs MTOM.

11.4. Fuel Subsystem

The fuel system sizing method explained in chapter 6 has been integrated into the other subsystems of the aircraft. The power required to drive the rotors in the different flight phases and the power required for other subsystems such as electronics and avionics have been used as an input for the method described. In Table 11.1, an overview of all final volume and weight parameters for the fuel subsystem is given.

Table 11.1: System weights and volume overview.

System	Mass [kg]	Volume [m^3]
Fuel Cell	410.1	0.512
Battery	87.7	0.0762
Fuel Tank	90.86	0.54
Air Intake	15	0.0437
Hydrogen Transport	25	0.045
Cooling	20	0.050
Total:	648.7	1.263

However, the volumes and masses do not say anything without geometries and the physical integration into the body of the aircraft. The fuel cell consists of a rack of cubical smaller cells as discussed previously. The geometry of the fuel cell therefore is a rectangular block of 0.85m x 0.6m x 0.6m. The fuel tank has a cylindrical shape with a radius of 0.89m and a length of 0.85m to withstand the internal pressure efficiently. The fuel system is integrated in the body starting from 1.5 meters from the nose to 2.346 meters. The fuel tank and cell will be located next to each other. The oxygen intake system and cooling system will be altered to fit as they are not of noticeable volume.

11.5. Electrical Subsystem

As every subsystem in the H₂ERO is important, so is the electrical subsystem. The electronics interconnect all of the systems together and power the entire aircraft. Remembering Figure 7.1, an overview was shown on how all electrical systems in the aircraft are connected. This section will explain the relative locations of these systems and their integration throughout the aircraft. It should be noted that, as was calculated in chapter 7, the weight of the electronics subsystem is negligible to the overall aircraft weight. Hence, the respective masses and center of gravities of the components in the electrical subsystem are not regarded

as influencers of the overall center of mass. Hence, their location is only mentioned as a general location within the aircraft.

The avionics system of the aircraft is located in the front of the cabin of the aircraft where the pilot's seat is also located. This is an obvious location as the pilot requires the avionics system to successfully control the aircraft during each mission.

The cabelling of the electronics system is located throughout the entire aircraft as it connects each system with each other and the necessary power that the respective system requires. For instance, the cabelling can run from the battery to the medical equipment in the cabin or from the battery all the way to the front of the aircraft to power the avionics system. Hence, there is no mass concentration of the cabelling in the aircraft.

The electronics subsystem contains many smaller, but not less important, systems as well. The detailed design and integration of these smaller electrical systems are regarded as beyond the scope of this project. However, they are noteworthy. These are systems like airconditioning, pitot tubes, aircraft lights, radio antenna's, aircraft sensors, communication systems, navigation systems. Furthermore, the fuel cell and batteries integration have been elaborated on more in section 11.4.

11.6. Aerodynamics Subsystem

11.6.1. Fuselage Design

After considering the cabin dimensions and fuselage section, it is decided to not make a configuration for which the fuselage shape consists of an airfoil as well. The most important reason for this is the elongation of the fuselage height that was necessary to allow a sufficient height for the cabin underneath the wing. The front view of the fuselage will resemble a elliptical shape fuselage with a flattened out bottom, far from a wing cross-sectional shape. In addition, the width of the fuselage is only 1.5 meters and this small additional lifting surface area will not contribute much to the lift generation. Also, manufacturing of such a design is more complicated and more costly than conventional fuselage design. Therefore a conventional fuselage design is chosen for a non-pressurised vehicle. The rear part of the fuselage should converge (like the rear of an airfoil) to allow for the airflow to stay attached more easily. However, the forward flight rotor is placed here and therefore the design of the rear part of the fuselage is dominated by the propulsive subsystem and not the aerodynamic subsystem. The nose of the fuselage is designed to enhance the aerodynamic efficiency. However, no detailed aerodynamic analysis and design of the fuselage is done at this stage in the design process.

11.6.2. Lift and Drag Curves

After all calculations and estimations have been performed, the lift curve and drag polar have been constructed. These can be seen in Figure 11.8 and Figure 11.9 respectively. In Figure 11.8 one can see the lift curve based on the wing calculations as described in chapter 8. It can be seen that the stall angle is at 12.8 degrees, however as it is only based on the calculated C_{L_a} and the intersection on the $C_{L_{max}}$ it is expected that the stall angle will be slightly above 12.8 degrees. In Figure 11.9 one can see that the drag polar has a parabolic shape and does not resemble a drag bucket as is the case for the airfoil. This is caused by the approximation method that is used. In this approximation the induced drag is quadratically scaled with the lift coefficient and as no other parameters change in the approximation, the increase in the lift coefficient resembles the increase in the drag coefficient. In Table 11.2 all other important aerodynamic characteristics are listed. One can see in the first column of Table 11.2 that certain parameters have the subscript corrected, this is the case as the results of XFOIL needed to be scaled to resemble reality as typically to high values for $C_{l_{max}}$ and C_{l_a} are obtained. This has been performed by comparison with experimental data provided in "Theory of wing sections" [3]. More detail about this procedure can be found in chapter 13. From the figures it becomes abundantly clear that the methods used are a preliminary estimation of the aerodynamic characteristics of the system. Unfortunately, CFD modelling was not possible in the limited time span. However, because of the limitations of the used approximations, it is highly favourable and recommended to perform these CFD analysis in further design stages.

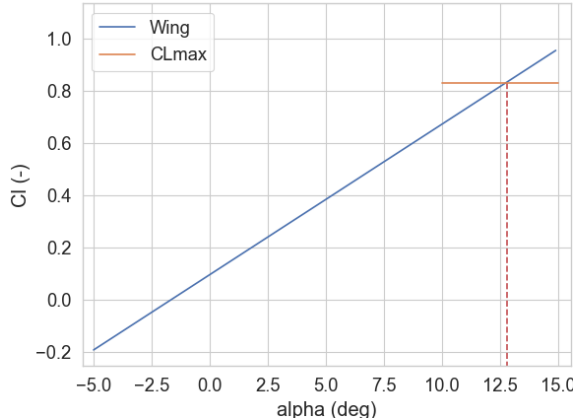


Figure 11.8: Lift coefficient versus angle of attack of the wing.

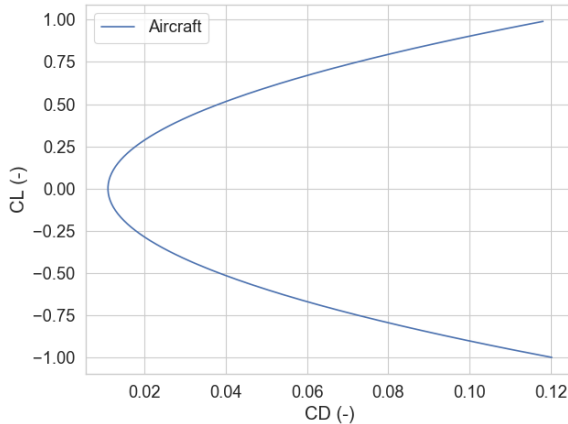


Figure 11.9: Drag polar of the aircraft.

Table 11.2: Aerodynamic characteristics.

Airfoil data			Wing geometry			Wing characteristics		
$C_{l_{des}}$	0.25	[\cdot]	$Sweep_{c/4}$	0	[rad]	C_D at $C_L = 0.25$	0.0169	[\cdot]
$C_{l_{max}}$	1.65	[\cdot]	AR	3	[\cdot]	C_{D_0}	0.0011	[\cdot]
$C_{l_{max\ corrected}}$	1.47	[\cdot]	taper	0.4	[\cdot]	$C_{L_{max}}$ calculation	1.43	[\cdot]
C_{l_α}	6.6842	[1/rad]				$C_{L_{max}}$ calculated	0.83	[\cdot]
C_{l_α} corrected	6.0123	[1/rad]				C_{L_α}	3.3001	[1/rad]
Cm_{ac}	-0.04	[\cdot]				Cm_{ac}	-0.04	[\cdot]
α_0	-0.027	[rad]				α_0	-0.027	[rad]
C_l_0	0.181	[\cdot]				C_l_0	0.0962	[\cdot]

11.7. Structures Subsystem

Just as for the subsystem designing, two separate sections are made for the fuselage and the wing

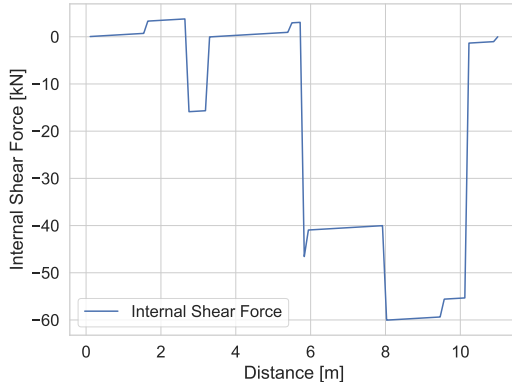
11.7.1. Fuselage

Since all distances, loads and materials are known, proper load and moment diagrams can be made. Since the most important loads are all in z-direction, Figure 11.10a displays the internal shear force in z-direction only. It can be seen that there are two big drops in shear force, which is for the first one, where the first vertical propeller is located and for the second one, where the first beam for the wing is located.

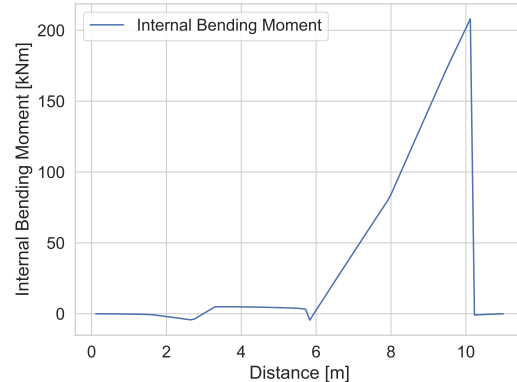
Figure 11.10b displays the internal bending moment around y, which is due to both moments from the wing, propellers and tail. All forces in z-direction affect the internal bending moment as well, which can be seen in the moment diagram.

The material for the fuselage is carbon fibre reinforced polymer with a tensile and compressive strength of 120 MPa while having the fibres with an angle of 45° to the loading axis, a shear strength of 310 MPa and a density of 1600 kg/m³¹. With both the material and loading diagrams, the stress and shear stress in each part of the fuselage can be computed using the equations described in subsection 9.2.2. Inputs for this are the type of material, the number of stringers and their geometry, as well as the thickness of the skin of the fuselage. For safety, a margin of 1.5 is applied to the outputted stresses. It was found that for stress, a minimum skin thickness of 1.2 mm is needed. For shear stress, multiple combinations are possible. It is therefore chosen to find the solutions with the lowest weight. It was found that for a skin of 1.2 mm thick, 4 stringers at both the top and bottom as well as 2 stringers at both sides is needed. The stringers will have a height h of 10 mm, width w of 5 mm and a thickness t₁ and t₂ of 1.5 mm. The stress that the

¹[http://www.performance-composites.com/carbonfibre/mechanicalproperties\\$_2.asp](http://www.performance-composites.com/carbonfibre/mechanicalproperties$_2.asp) [Accessed 2019-06-23]



(a) Internal shear force diagram for the fuselage in z-direction.



(b) Internal bending moment diagram for the fuselage around y.

fuselage can withstand is 2.5% higher than 1.5 times the tensile strength. The shear strength is 4.9 times lower than the composite can withstand. This is rather high, however, due to the nature of the equations, the number of stringers or booms greatly determines whether the structure is strong enough or not and reducing the number of stringers gives a shear strength that is about 1.5 to 2.5 times higher than the material can withstand.

11.8. Configuration Iterations

11.8.1. Sizing Process

Once the stability and controllability requirements have been established through methodology described in subsection 9.3.2, the horizontal tail surface area can be determined to satisfy control and stability requirements for the given centre of gravity range. However, a change in the surface area of the horizontal tail, in turn, will alter the maximum take-off weight of the aircraft, therefore, all of the other subsystems have to be re-sized for the new maximum take-off weight, again, leading to a new weight distribution of the aircraft, and, hence, a new X_{cg} range, characterising a simplified version of the full, multi-disciplinary iterative process of aircraft design optimisation to define the final geometry. Convergence of the process leads to a size of the horizontal tail - sufficient to satisfy control and stability requirements for the given range of longitudinal centre of gravity range. An illustration of the sizing process can be seen in Figure 11.11. The number

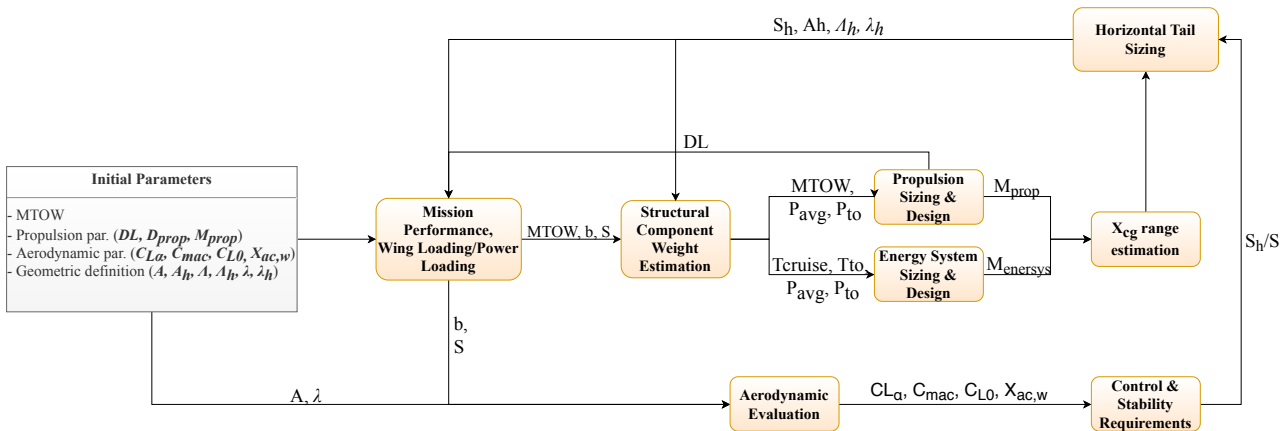


Figure 11.11: Aircraft balance and sizing process through iteration.

of iterations were set to 40 to ensure convergence, which was verified by performing an additional manual iteration after the automated cycle had been completed. The results of the iterative process yields the final, fully-integrated configuration. A visualisation tool was developed in order to visually validate the output of the iteration process, yielding a preliminary visualisation of the aircraft, that can be seen in Figure 11.12. A preliminary visual verification of the integrated aircraft is necessary to check feasibility of the aircraft con-

figuration resulting from process illustrated in Figure 11.11 - whether the given propulsive system can fit within the wing, how the horizontal stabiliser is sized with respect to the main wing, as well as allowing for quick re-positioning of the propulsive system, as well as longitudinal positioning of other subsystems, and immediately see the design implications thereof, hence proving to be a vital tool in design process before full Computer Aided Design (CAD) model development. The configuration iterations can be summarised

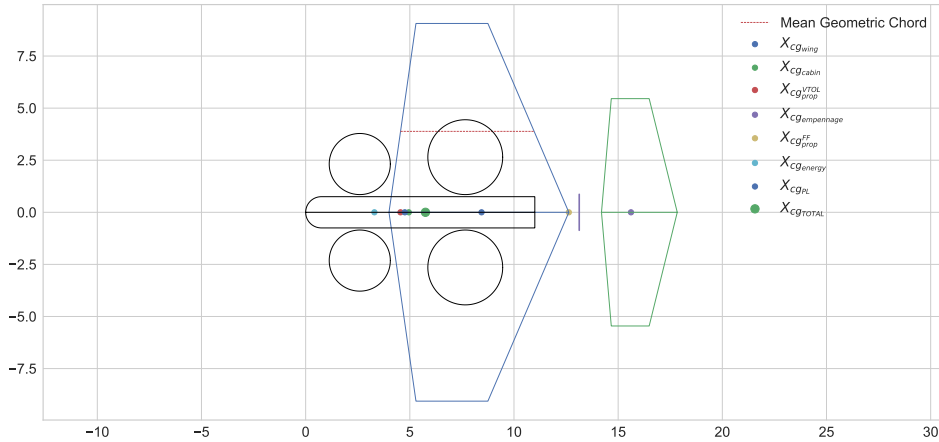


Figure 11.12: Visualisation of preliminary fully-integrated aircraft.

as follows. After converging all the different subsystems it is concluded that the four rotors needed for VTOL cannot be fitted in the wing surface area. Solutions to this without changing the configuration were tried, and include:

- Increasing the aspect ratio up to 5 in order to create more clean wing area (not influenced by the integrated rotor). This turned out not be feasible with the rotor dimensions.
- Pushing the boundaries of the wing span up to 18 meters in order to increase the wing surface area. This increased the weight as well, however, which influences the rotor dimensions. This way a snowball effect is initiated. In the iterations done, it could not converge to a feasible design with the rotors integrated in the wing.
- The rotor dimensions are automatically updated in each iteration in the range specified in Figure 11.7. They have to stay within the optimisation bounds in order to meet the noise requirements. It was not possible to decrease their diameter enough to make them fit into the wing as they would be too noisy.

The conclusion from this phase was that the configuration would need to be changed and not all four VTOL rotors could be integrated in the wing.

Next, different configurations were analysed with rotors not integrated in the wing. The challenge here is to keep sufficient space and accessibility for the door, to not block the visibility of the pilot and to keep the wing out of the wake of the VTOL rotors. Three main configurations were considered:

- To move the two smaller rotors right in front of the wing (so at the same height as the wing). However, the wing will be positioned in the wake of the ducted rotors, which is very unfavourable aerodynamically. Hence another configuration was considered.
- To change to a low wing configuration and move the front two ducted rotors before the wing. This will be a little better aerodynamically, however will pose problems for a door position. The door will not fit underneath the rotor and can also not be placed above the wing. Therefore, another configuration was looked into.
- To move the front two rotors down and in front of the wing. Now the door must be placed under the wing. In order to allow for enough space, the fuselage needed to be elongated, and changed from 1.5 to 2 meters. This change in configuration proved to be most feasibly and was therefore chosen.

11.9. Final Design

11.9.1. Final Parameters

Table 11.3: Initial parameters used for the sensitivity analysis of the propeller.

Paramater	Value	Unit	Paramater	Value	Unit
Wing aspect ratio	3,00	-	MTOW	4150	kg
Wingspan	18,13	m	Back Propeller Diameter	3.59	m
Wing surface area	109,53	m ²	Forward Propeller Diameter	2.93	m
Wing taper ratio	0,40	-	FF Propeller Diameter	1.73	m
Wing Δc/4	0,00	deg	Power Required VTOL	1038	kW
Root chord [m]	8,63	m	Power Required FF	377	kW
Tip chord [m]	3,45	m	Noise VTOL	83,14	dB
XLECr	4,00	m	Noise FF	52	dB
t/c	0,1	-	Payload Mass	628	kg
Tail surface area	29,77	m ²	Number of Passengers	4	-
Range	346	km	Number of pilots	2	-
Speed	82,72	m/s	MAC	6,41	m

11.9.2. Mass and Power Budget

From the detailed design and subsystem integration chapters, the mass and power budgets were estimated. The mass budget is described in the following table:

Table 11.4: Mass and Power budget of the initial design.

Subsystem	Mass [kg]
Wing	335
Cabin	1511
Empennage	133,92
VTOL Propulsion	467
Energy Source	485
FF Propulsion	187
Flight Controls	48
Electrical	110
Avionics	116
Furnishing	24,7
Hydraulics	43,46
Payload	628
Total	4151

The power budget is described in chapter 11. The mass and power budget are necessary to be able to understand where the different weights and power consumers come from. With a power budget the information is easily available in Table 11.4 and it can be compared to the available power.

11.9.3. Mission Implications

For the final design configuration, an analysis and discussion was performed for the initial flying capabilities of the H₂ERO. A typical mission profile, as will be further elaborated on in section 17.1, contains a VTOL, transition and cruising phase. The aircraft subsystems have been designed mainly regarding the VTOL and the cruising phases as these are the critical driving phases of the design. However, once the final configuration was set, frozen and documented at the end of the design phase of the project a discussion started regarding the possible unfeasibility of a successful transition phase between the VTOL and cruising phase. Discussion recommendations for the transition phase will be further elaborated in section 16.2 and has only been mentioned here for clarity.

11.9.4. Impression and Technical Drawings of Final Configuration

After that the configuration was determined and the calculations had been run, a CAD model was made. This was made to ensure that all relevant subsystems or parts would fit together and that nothing was forgotten. Additionally, it gives the ability to present a clear overview of all important dimensions and the general shape of the aircraft. In Figure 11.13 and Figure 11.14, the technical drawings of the front and top view are given respectively. The technical drawing of the side view is not given as only little new information

can be provided in this drawing. The only new information regards position and dimension the door which grants access to the cabin. The width of the door is 1.41 meters and the height of the door is 1.25 meters. From the nose the distance is 6 meters and the door is located on the left hand side of the aircraft. To give

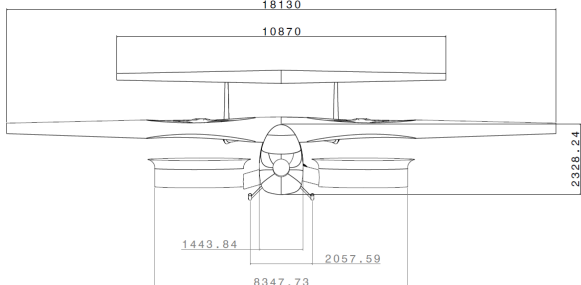


Figure 11.13: Technical drawing of front view of the aircraft.

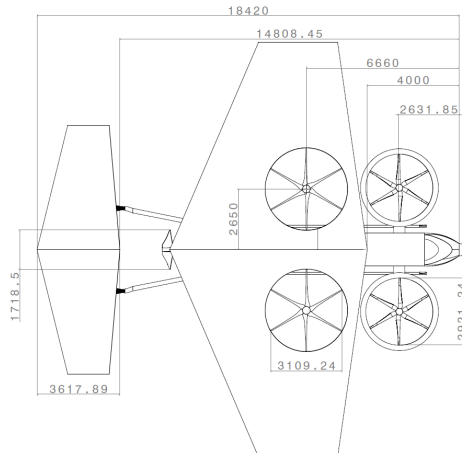


Figure 11.14: Technical drawing of top view of the aircraft.

a more visual overview of the aircraft Figure 11.15 and Figure 11.16 are provided. In Figure 11.16 it is also clear that the vehicle is very accessible. This has been an important factor in the design as passengers need to be (un)loaded as fast as possible when necessary.

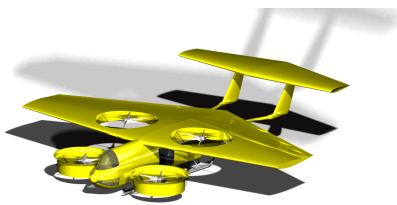


Figure 11.15: 3D render of the aircraft.

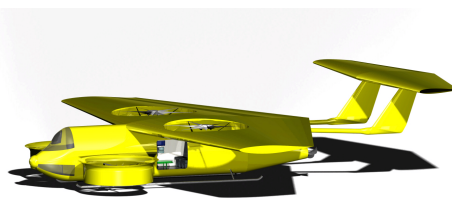


Figure 11.16: Render with clear view of the door.

11.9.5. Requirement Compliance & Feasibility

The aircraft has been designed to fit sufficient volume and area to fit pilots, passengers and medical equipment. In the cabin, which is placed underneath the wing, sufficient space is allocated for the passengers and the medical equipment. Therefore, all requirements in Table 11.5 are met.

Table 11.5: Overview of the requirements regarding the area and space usage within the aircraft cabin.

Code Identifier	Requirement	Type	Verification	Compliance
EVTOL-GNVO-131	The aircraft shall have enough inner surface area to transport five persons, including one patient and at least one pilot	Key	Analysis	
EVTOL-GNVO-132	The aircraft shall have enough inner volume to transport five persons, including one patient and at least one pilot	Key	Analysis	

The two requirements that have been set for the weight requirements have been the base of the design of the H₂ERO. Therefore, the requirements in Table 11.6 have been met.

Table 11.6: Overview of the requirements regarding the weight of the aircraft.

Code Identifier	Requirement	Type	Verification	Compliance
EVTOL-GNWE-121	The aircraft shall be able to transport five persons of 90 kg each	Key	Analysis	
EVTOL-GNWE-122	The aircraft shall be able to transport 208 kilograms of medical equipment	Key	Analysis	

12

Performance

A performance analysis of the aircraft is performed in order to estimate its technical performance capabilities and operational limits. This entails a payload-range, power-airspeed, climb-performance, endurance, load factor analysis. Additionally, the performance will be compared to the EC-135 where applicable and relevant.

12.1. Payload Range

The payload range diagram, depicted in Figure 12.1, displays the effect of payload on the maximum range of the aircraft. If the payload decreases, the take-off weight decreases, requiring less energy during the mission flight phases. As a result, if the fuel weight is kept constant, the maximum range of the aircraft increases. The total hydrogen mass is only 37.4 kg, therefore the mass decrease during flight is considered to be irrelevant to the range performance.

As can be seen, the maximum range with total payload is 264 km, while the maximum range, without payload, is 303 km. The EC-135 has a range with maximum payload of 620 km. The difference lies in the fact that the EC-135 was not specifically designed for emergency operations, but rather for a wider field of application. Equation 12.1 is used to construct the diagram.

$$R = \eta_{tot} \frac{L}{D} \frac{E_{spec}}{MTOW} M_{HydrogenCruise} \frac{1}{g} \quad (12.1)$$

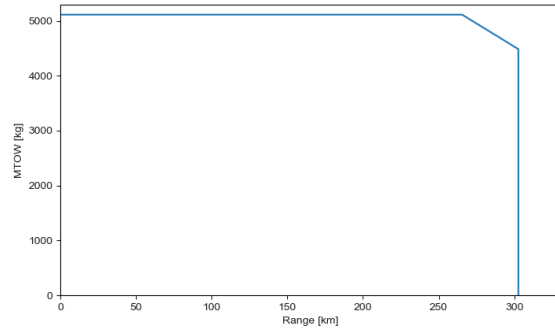


Figure 12.1: Payload-Range Diagram.

Where E_{spec} is the hydrogen fuel system energy density. The η_{tot} is the whole-chain efficiency (from the energy source until the propeller energy output) during cruise and $M_{HydrogenCruise}$ is the fuel mass that is used for cruise.

12.2. Power-Airspeed

The Power-Airspeed diagram in Figure 12.2 displays the P_{req} and P_a versus TAS (for cruise conditions with TAS ranging between V_{stall} and V_{max}) [2].

For steady flight at a certain airspeed, the power required is scaling proportionally with the drag. The power available is equal to the maximum power available from the propulsion system. From Equation 12.2, the power required required can be calculated [2].

$$P_{req} = \frac{1}{2} \rho V^3 \cdot \left(C_{D_0} + \left(\frac{MTOW}{\frac{1}{2} \cdot \rho \cdot V^2 \cdot S} \right)^2 \cdot \left(\frac{1}{\pi \cdot e \cdot AR} \right) \right) \quad (12.2)$$

Here, ρ is the density at cruise altitude. Excess power, indicative of ROC_{max} for certain airspeed, as well as the optimal airspeed points for maximising range and endurance can all be deduced from Figure 12.2. The maximum range is achieved at the most aerodynamically efficient condition, at optimum L/D . The point of maximum range is indicated by a blue dot [2]. From the diagram, the maximum rate of climb can be

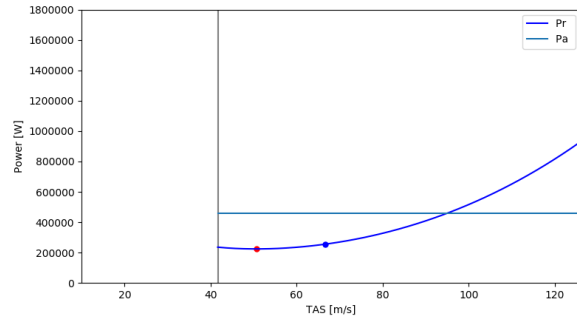


Figure 12.2: Power-Airspeed Diagram, The blue dot indicates optimum speed for maximum range. The red dot indicates optimum speed for maximum endurance.

deducted. The velocity of maximum rate of climb is the velocity where the margin between P_a and P_r is the largest.

12.3. Endurance

The optimal endurance condition is attained at minimum P_{req} , indicated by a red dot in Figure 12.2. After selecting a flight velocity, the endurance can be determined using Equation 12.3.

$$\text{Endurance} = \frac{E_{\text{spec}} \cdot M_{\text{hydrogen}}}{P_{r_{\text{endurance}}}} \quad (12.3)$$

The optimal endurance, reached at 50 m/s, is equal to 5.5 hours.

12.4. Manoeuvre and Gust Load Diagram

The load factor per airspeed are represented in the flight envelope for the operational range of the aircraft. Equivalent airspeed is applied, hence sea level density is used.

The manoeuvre limits are plotted using Equation 12.4 [19], which is based on $n = \frac{L}{W}$. The positive and negative load factor limits require $C_{L-\max}$ and $C_{L-\min}$ as inputs. The variables needed to make the gust diagram are calculated using the equations below [19]. Equation 12.5 computes the lift curve slope.

$$n = \frac{0.5\rho V^2 C_L}{W/S} \quad (12.4)$$

$$C_{L_\alpha} = 2\pi \frac{AR}{AR + 2} \quad (12.5)$$

The correction factor for the gust loads is computed using Equation 12.6. The change in load factor is equated using Equation 12.7.

$$K_g = \frac{0.88\mu}{5.3 + \mu}; \quad \mu = \frac{2W}{g \cdot \rho \cdot S \cdot MGC \cdot C_{L_\alpha}} \quad (12.6) \quad n_{gust} = 1 \pm \Delta n; \quad \Delta n = \frac{\rho V_{cruise} C_{L_\alpha} K_g u}{2(W/s)} \quad (12.7)$$

The European regulations specify the limit load factors, which are used for this design as well. Since there is no VTOL fixed wing aircraft category yet, two categories are considered: the CS-23 is used for normal aircraft¹ and CS-29 is used for large rotorcraft². The maximum limit results from CS-29 and is 3.5; the minimum limit is the same for both categories and is -1.0. The maximum additional gust load velocity is usually higher for aircraft than for large rotorcraft. For the latter it is 9.1 m/s in all flight conditions. For aircraft this value is not stated in the European regulations, but is stated in the American regulations: 15.4 m/s³.

The strictest regulations are considered for now, which means that for the H₂ERO a value of 15.4 m/s for gust load at cruise speed is used as a initial estimate. The regulations state that the value for gust load at dive speed can be lower than they are for cruise speed, hence this value is kept at 9.1 m/s.

¹<https://www.easa.europa.eu/sites/default/files/dfu/CS-23%20Amendment%205.pdf> [Accessed 2019-5-20]

²<https://www.easa.europa.eu/sites/default/files/dfu/CS-29%20Amendment%206%20v1%20%282019-05-20%29.pdf> [Accessed 2019-5-20]

³<https://www.law.cornell.edu/cfr/text/14/part-23/subpart-C> [Accessed 2019-05-20]

The first part of the load factor curve changes quadratically with velocity, as seen in Equation 12.4. The stall speed can be read from the graph at $n=1$, since here the aircraft is flying at minimum speed and maximum C_L , hence $L = W$. The horizontal edges of the curve, where the load factor is constant with increasing velocity, indicate the minimum and maximum load factor defined by regulations. For all concepts the limits are +3.5 and -1.0. V_D is the diving speed, which is the absolute maximum speed that can only be achieved by a diving manoeuvre. The minimum speed at which the maximum load factor can be reached is called the manoeuvre speed, V_A .

In Figure 12.3 the filled, green area indicates the minimum envelope that needs to be designed for, as specified by regulations. Either the manoeuvre or gust load is leading and show the minimum load factor the aircraft must sustain.

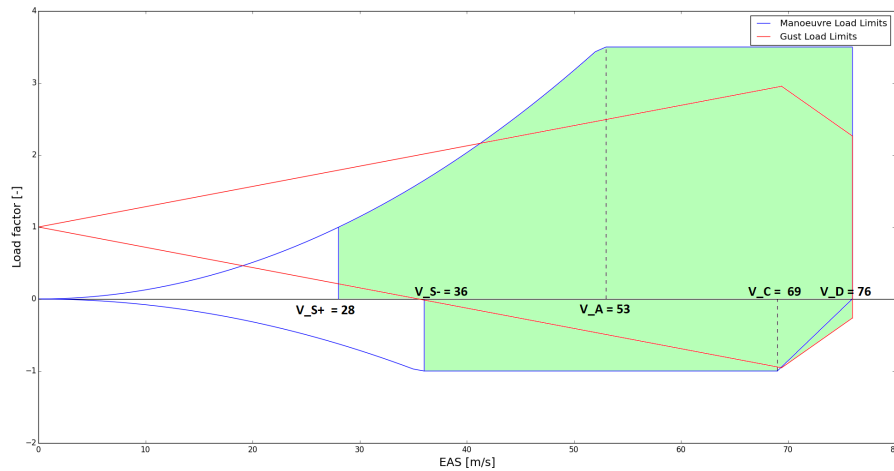


Figure 12.3: Manoeuvre and Gust Load Diagram; all airspeeds indicated in [m/s].

The cruise and dive speed follow from requirements and are thus fixed values. The stall speed for full use of wing surface area is 28 m/s. This is beneficial for the design as it delays the need for hovering instead of flying forward.

This load diagram is now constructed for MTOW at cruise conditions. It gives a preliminary input for the structural engineer and also an indication on the limitations of the aircraft. Generally several diagrams are made for different weights, flaps/slats extension and different altitudes. For this analysis, only the flight envelope for MTOW at cruise conditions is considered. This will be the design driving envelope, since the maximum weight and maximum speed will result in the largest load factors. Also, the load factors represented in the graphs are limit loads. In order to know the ultimate loads, they should be multiplied with a safety factor of 1.5.

As already explained before, the aircraft regulations specify a higher gust load factor than for helicopters. Therefore, the limit load factors may be a little higher for the H₂ERO than for the EC-135. Also, a helicopter's stall speed is the speed for which the blades will stall and is indicated by the maximum speed. The stall speed is therefore defined by the maximum speed for the EC-135 of 260 km/h, slightly below the 274 km/h of the H₂ERO.

Verification and Validation

In this chapter the tools used to develop and design the aircraft will be verified and validated. In verification, section 13.1, it must be made sure that the tool does the work that is intended to do. While in validation, section 13.2, it must be made sure that the tool gives results that approximate reality. It is important to note the difference between verification and validation since different processes will be followed in both sections.

13.1. Verification

The methodology for verification consists in three different techniques, namely **unit testing**, **system testing** and **full scale testing**.

Unit testing, as its name indicates, consists of making sure that the individual values are correct, and that they are correctly inputted in the tools. The following techniques can be used to maintain a coherent unit testing for the subsystems:

- Some of the functions can be computed manually before introducing them in the code. This means that the result of the function is known prior to the code result. Meaning that after running the code, the same result should show.
- Evaluating every line in the code. With this technique, it can be made sure that each code line does what is supposed to do, without interfering with each other.
- Substitute the variables by the units, to make sure that the result has the expected units. This method is used to make sure that, for example, no kN are inputted where N should go, or similar errors.
- Check that the individual results make sense, in terms of value, size and comparing it to other existing or calculated values.
- Check for single numbers in the code. Many times to accelerate the process instead of linking values to variables the value is directly added into the program. It can be possible that this value changes as a function of something, and in loops and iterations it might cause problems.

System testing, here larger blocks of code are tested. This is necessary since the interaction between functions must be made correctly. Some examples include:

- Separating different functions in the code by creating independent functions. With this technique, it can be made sure that each function does what is supposed to do, without interfering with each other.
- It is good to have at the same time of the python code an excel file that performs the same calculation. This is used to make sure the relationships between the different formulas are made correctly.
- More than one method can be developed to find the same result, this allows for comparison of the results at the end, and see if there is any divergence factors. Improving the quality of the code.
- Check for inputs and outputs. If it is known that a certain change in an input should produce a scalar change in the output this must be checked. In case that the output does not change accordingly, some input is not properly interacting with the output.
- Make sure that, in the iterations, the level of detail is accurate enough. When designing for a range, that the step on that range is small enough to find the possible solutions.

Finally, **full scale testing** can be performed, including the full check of the code. Some of the techniques are:

- The subsystem integration is done by combining all the different tools together to calculate the subsystems. During this integration, all team members try to understand each other's codes, this cross-control checking serves as full scale testing.

- Most of the system tests can be reproduced in the full scale tests, but instead of being for individual functions it will be for the whole code.
- Making final plots, creating plots help visualising the information and it is easier to detect errors in the code. A sudden jump in a graph, or missing some values could mean that something in the code is not working well.

The next subsections will use the previously explained methodology to verify the tools used for each of the subsystem designs.

13.1.1. Propulsion

The main tools used for the development of the propulsion system were: the blade design tool (XROTOR) and the Propeller design tool (Group 11 development). The XROTOR program is widely used and many papers verify and validate the results. Thus, it is already an accepted program with no need of verification nor validation.

The propeller design tool however needs to be verified, it must be made sure that the tool does the work that is intended to do. Three different verification techniques can be used as explained in section 13.1.

During unit testing several errors were discovered in the code:

- Many of them were mistakes related to units. In the program, the power required and available was of major importance and many times Watts were used where kW should be used. Some errors due to the units of the RPM were also corrected, since sometimes the rad/s had to be used.
- Moreover, due to misunderstandings in formulas, the log10 were confused with natural logarithms. Creating unfeasible solutions that were corrected at the spot.
- Misspelling of variables was a problem, since a part of the code was duplicated to calculate the propeller diameter in VTOL and in cruise. With some inspection, the errors were spotted and corrected.

As explained before, system testing consists on comparing blocks of code. Errors such as the following were corrected:

- As explained in chapter 5 the code was set up to satisfy certain constraints. This constraints were modified to make sure a feasible solution was achieved. Surely, the constraints were modified only if it was still possible to satisfy the.
- Initially, only the power to hover was considered in the VTOL phase. This was wrong because the design must also be able to lift off, what requires extra power or diameter.
- Using different power required decreased sometimes the comprehension of the program. On some occasions the power required was compared wrongly to the maximum power to satisfy noise, which gave wrong solutions.
- When exporting results from this code to the others the values of disk loading were fundamentally wrong. Since the disk loading was given per propeller and not as an overall value with the summation of all propellers. Which was required as such by the other subsystems.
- Some other errors were corrected during system testing but they had a lower impact than the ones presented above.

Finally, during the full scale testing, some errors were discovered:

- The program calculated the weight of the propulsive system. Initially, some parameters (used for calculating weight) were not linked to the final solution. This lead to a wrong mass estimation.
- When the program was used by other team members during subsystem integration some methods were explained and altered, for example instead of using just the cruise requirement for the forward flight propeller, the climbing power required was used.

With all these errors corrected the propulsion system code was verified.

13.1.2. Fuel System

The python programme written to size the fuel system has been verified starting with unit tests. The program, which sizes the fuel system based on the mission power profile and duration, consists of individual

blocks of code accounting for sizing a part of the system such as the tank and the fuel cell. Each individual block of code has been checked to make sure known inputs would result in expected outputs. Two small mistakes were filtered out of the program. The first one made a mistake while calculating the average power supply of the fuel cell, mixing up the cruise power with the peak power. The second one got a value in kW as input, while it expected W. Both have been solved.

Then, to test the system, two separate methods were used to size the fuel system ([61] and [62]). The difference in outcome between both was within 5%. This margin was considered to be small enough to verify the program and the method.

13.1.3. Stability and Control

Verification of longitudinal stability and control assessment tools for forward flight can be split up in verification of stability and control criteria (for sizing of the horizontal tail), and verification of the component weight estimates, and the subsequent X_{cg} range calculation.

During unit testing, the main errors found were predominantly originating from unit conversion: as the statistical relationships used for component weight estimation require inputs in the imperial measurement system, conversion factors had to be applied for each input variable, which was not done correctly on all variables. Additionally, errors related to coordinate system transformation were discovered in generation of the so-called "scissor" plot (Figure 9.4) - the actual X_{cg} range of the aircraft was calculated in the aircraft global reference frame, however, the tail sizing procedure through generation of the "scissor" plot requires to convert it to the wing frame of reference, defined with respect to the mean aerodynamic chord.

On a system-level, larger blocks of code - determining stability and control requirement curves, centre-of-gravity determining algorithm, selection of the correct tail-to-wing area coefficient - were tested for correct and logical functionality. For an example, to verify the X_{cg} -location determining algorithm, the weight of one of the propulsive system was artificially increased, which, logically, lead to the centre of gravity shifting towards the centre of gravity of the propulsive system. Similar tests were also ran in control and stability requirement generating curves - e.g. if the aerodynamic centre of the aircraft is moved more aft, the stability curve shifts towards the right side of the "scissor" plot, indicating positive contribution to the aircraft longitudinal static stability, hence similar tests allowed verifying the effect of each variable in Equation 9.9 and Equation 9.8 on the longitudinal stability and control requirements.

Full scale tests were done by going through a single iteration of horizontal tail surface area sizing calculations (determining X_{cg} range, determining control and stability requirements on X_{cg} range, and determining the required $\frac{S_h}{S}$) by hand, and comparing the results with the ones obtained from the programmed tool. No discrepancies between the two methods were found, as the same model was used in both manual calculations and the programmed tool.

13.1.4. Aerodynamics

All the steps described in the general approach for verification are performed for the tools used for the aerodynamic subsystem as well. Some highlights of the verification process are described in this section.

As has already been mentioned in chapter 8] the airfoil selection has been based on preliminary selection and the analysis of each individual airfoil in XFOIL for different Reynolds numbers. As XFOIL is a widely used and globally accepted tool no verification procedures regarding the software are necessary. However, the method that is used to model viscous effects makes generally the approximation near or past stall inaccurate. Therefore, the results of these analysis have to be validated, which will be explained in section 13.2.

The script that was written to convert the 2D airfoil characteristics into the 3D wing characteristics was verified in several manners. First of all, unit and system checks have been performed. When available examples calculations used in books (such as in [18], [26], and [27]) were put into the scripts to check if each calculation gave the correct answer. If these examples were not available or found, common used values were used as input and the output of the calculation was recalculated by hand. This resulted in the correction of several typos, such as a plus or minus sign, forgetting factors of 0.5, etcetera.

Before the complete script was ran with all the small functions coupled, unit consistency was checked. It

was checked whether all variables were put into the function with the unit they required. The result of this was there were especially the unit of the angle inconsistency. Some functions had an input in degrees while it required the input in radians and vice versa. This issue has been resolved by using the convention of a input in radians. If a function required an angle in degrees, the unit was converted inside the function before the respective input was used. At the end of the functions the result was than again converted to radians for the sake of consistency.

Some full scale tests and diagram verification include to check the graphs for sensibility. For example, the $C_L - \alpha$ curve is expected to progress linearly up to stall and intersect the y-axis at positive y-values since a cambered airfoil is used. As can be seen in Figure 11.8, this is indeed the case. Also, a typical range of lift coefficients is from -1.5 to 1.6 (without flaps and slats) where the maximum lift coefficient is reached well before 20 degrees angle of attack. Also this makes sense. The order of magnitude for drag coefficients should be 10^{-2} , which is true. In addition the $C_l - d$ curve should show the typical drag bucket curve and show a parabolic graph. Also this is true as seen in Figure 8.1.

The aerodynamic polars were also checked for their consistency with a change in Reynolds number. For higher Reynolds numbers the maximum lift coefficient should increase, whereas the lift curve slope is unaffected [39]. This is indeed shown in the graphs as well, as seen in Figure 8.1. The friction and form drag decrease with higher Reynolds numbers, resulting in lower values for the drag coefficient [39]. Also this effect is shown in Figure 8.1. Therefore, it can be concluded that the general method, implementation of the relevant equations and order of magnitude of the aerodynamic coefficients is correct. However, the numerical values cannot be verified, but will be validated.

13.1.5. Structures

The fuselage designing can rather easily be verified, as most computations on the whole structure can be done by hand or with Excel. Verification is first done by performing unit tests, in which some errors were found. These errors were mainly due to switching from calculations done with z-locations to calculations with y-locations. After thorough inspection, it was verified that all blocks have to correct dimensions. Furthermore, single outputs of code were printed and compared to simple hand calculations, in order to check whether the output was in the right order of magnitude. After unit testing, systems were looked into and it was checked if all functions interact in the right way. It was found that for several cases, the function did not take the right number from a list created in a previous function. Finally, a full scale test was performed. It was found that beside being confusion in terms of units, the program worked as it should.

13.2. Validation

Validation is slightly more challenging than verification. As explained in the introduction of the chapter, validation compares the results to real values, to make sure that the final solution is correct. Due to the conceptual nature of the design, it is hard to compare values directly to existing similar aircrafts but some techniques can be used:

- Not only comparing the final solution is validation, the results of functions of code can be compared with existing values. Since it is a conceptual design, this part of the process will be a bit harder, but there are some values that can be found from reference.
- Moreover, estimations based on MTOW and existing aircraft can be compared different values of each subsystems. For example, the power required, the propeller diameter, etc.
- In future stages of the design, models that simulate reality can be created and tested. This will give validity to the results obtained during the design. For example, engine tests, windtunnel tests and prototype testing.

13.2.1. Fuel System

To check if the system sizing method was actually the right method to use for real life sizing applications, first two methods from separate sources ([61] and [62]) were compared. Both methods' sizing results only differed only 5% from each other, verifying the method. To also validate the sizing method used, the results are compared to other hydrogen aircraft concept designs. Multiple missions were mapped and the relative fuel systems were compared to the system designed for this aircraft. According to this analysis, the fuel

system is in line with the expected dimensions expected for such mission requirements. Therefore, the fuel system is considered validated.

13.2.2. Balancing and Weight Breakdown

In order to validate the obtained values of sub-system weight that have been based on the statistical methods described in section 9.2 that were used in aircraft longitudinal balancing, the mass of the H₂ERO was broken-down into 6 main weight groups - structures, propulsion, energy system, payload, crew, and others (which include avionics, engine controls, hydraulics mass, etc.), and then compared to an reference aircraft. The reference aircraft was chosen to be a Short Take Off and Landing (STOL) concept, described in the study performed by Legresley et. al, firstly, due to availability of component-level weight breakdown information, and, secondly, due to the aircraft being classified as cargo/transport aircraft. As it is visible in Figure 13.1, the propulsion, payloads, crew and "other" component groups show somewhat similar range of values for their relative contribution to their respective maximum take-off weights, maximum difference between the aforementioned existing between the propulsive system groups - limited to less than 4%, indicating a potentially valid weight estimates for these subsystems. The two largest discrepancies - between structure and energy system subgroups are also believed to be a logical consequence. Firstly, the relatively heavier energy system on the STOL reference aircraft can be purely explained by the use of the different energy source - liquid hydrogen fuel cell system, even with the required complex systems accompanying it, is still more energy-dense than a typical, kerosene-driven internal combustion engine system. Secondly, the heavier structural subsystem of the H₂ERO can be explained by the relatively large surface area of the wing, when compared to the size of the other structural subsystems. Due to the relatively high stall-speed of the aircraft, the wing-loading of the eVTOL emergency aircraft is a lot smaller than for a typical aircraft within the same category, leading to a higher wing surface area needed, hence increasing the relative weight of the structural subsystem. By taking the aforementioned information into account, it is believed that the obtained weights of each subgroup are sufficiently accurate to be used for longitudinal stability and control assessment, as the relative weights have been validated with a reference aircraft.

13.2.3. Aerodynamics

Only a limited amount of empirical data is available at this stage in the design process. Therefore, most of the aerodynamic subsystem cannot be validated yet. For future validation, CFD analyses are advised in order to validate the 2D analyses, translation from 2D to 3D (and how this affects the assumptions and design choices made), post stall behaviour and stability dynamics. In addition, wind tunnel tests are advised in order to validate the CFD data, as also explained in section 16.6.

One element that can be validated already is the airfoil data by means of Abbott and Von Doenhoff's Theory of Wing section [3]. This is for subsonic aircraft data, so is applicable to the H₂ERO as well. However, the windtunnel data available for the airfoils selected only go up to Reynolds numbers of 6 million, far less than the 14.25 million the airfoil was analysed for in XFOIL. Still, these empirical data provide a way of validation, as illustrated in Figure 13.2. A quantitative comparison is illustrated here for one airfoil, the NACA64210, for the sake of completeness. The same approach and analysis was taken for the other airfoils entering the trade-off as well. As can be seen, the minimum drag coefficient range from 0.004 to 0.009 for increasing Reynolds numbers in the windtunnel data. For XFOIL this range is from 0.004 to 0.0075, which is slightly below. Therefore, it should be considered that the real drag coefficient is higher than estimated by XFOIL. This may have caused an underestimation of the drag, hence an underestimation of the wing surface area. The drag bucket length is slightly larger for the XFOIL data as well. However, the windtunnel data still allows for the design lift coefficient to be well within the drag bucket limits, so this is not expected to show

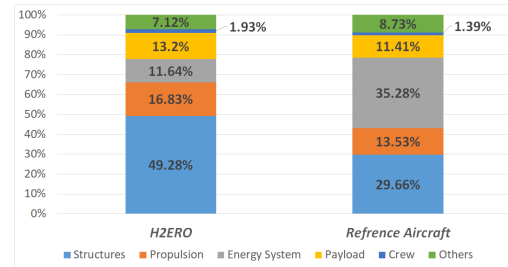


Figure 13.1: Electric Vertical Take-Off and Landing (eVTOL) emergency aircraft MTOW breakdown relative to a reference aircraft.

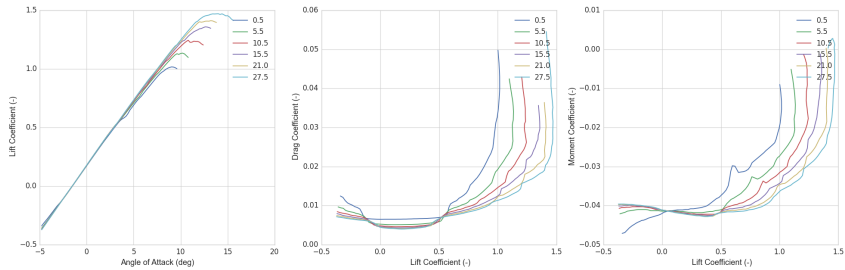


Figure 13.2: Xfoil data for NACA64210 at a range of different Reynolds numbers at $M = 0.2$.

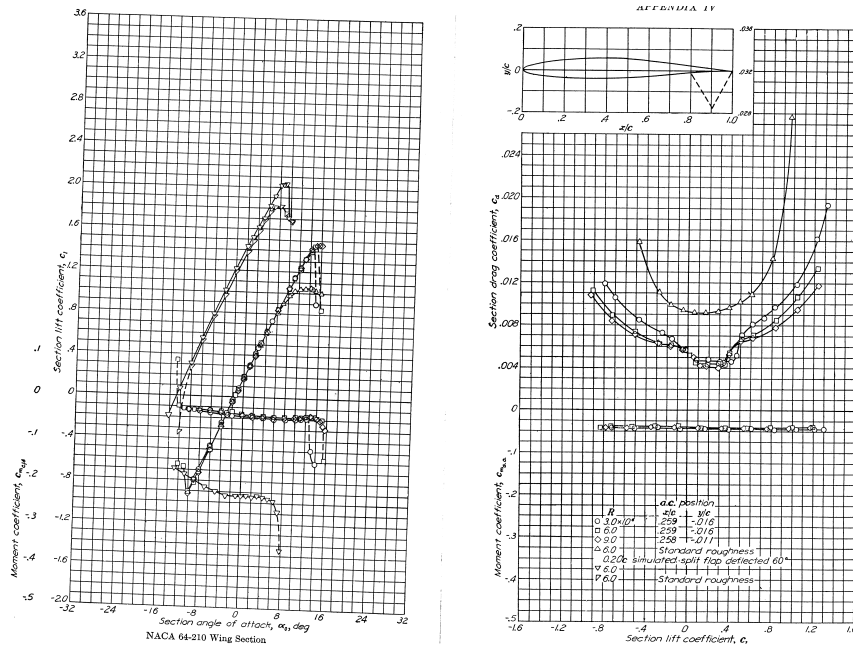


Figure 13.3: Windtunnel data for NACA64210 at a range of different Reynolds numbers from Abbott and Von Doenhoff's Theory of Wing section [3].

significant differences.

The maximum lift coefficient given by Xfoil at higher Reynolds numbers is actually the same as the one for the lower Reynolds numbers in the windtunnel data. Although the maximum lift coefficient does not increase infinitely with increasing Reynolds numbers, it may be the case that it is underestimated in the current analysis. As a result, the wing surface area may be over designed as well. It cannot be concluded straight away whether the underestimation of the drag and the underestimation of the lift compensate for each other. The wing surface area is still expected to change for optimisation after further analysis (including CFD).

The graph of the moment coefficient versus lift coefficient shows a linear line for the windtunnel data, but a parabola for the Xfoil data. Therefore, only the (semi-)linear part of Xfoil should be considered and the data for lift coefficients above 0.5 should be discarded. Also, for the windtunnel data the moment coefficient stays the same for different lift coefficients and Reynolds numbers, with a numerical value of from -0.03 to -0.04 . For Xfoil this is just below -0.04, which will result in a slight overestimation of the tail surface area. From the three coefficients, the moment coefficient is the least reliable from Xfoil data, because of its graph not resembling windtunnel data, and should therefore be used with caution.

Sensitivity Analysis

A sensitivity analysis can be performed to see how a change in some of the input parameters alter the output solution of any of the tools used for the design. This sensitivity study is carried out because the design parameters might vary continuously during the design phase and might not be accurate enough to predict well the aircraft performance. The obtained information is used to check for the most relevant parameters, and, in case that is necessary to change the design, it gives information about which parameters to alter and in what percentage.

The sensitivity study methodology is performed as follows. First the main inputs and outputs of the program must be defined. The inputs are defined as the values that you can modify and optimise, or parameters where the uncertainty is big. The outputs to evaluate are mainly the values that serve as inputs for the design integration or the other subsystems. Once the inputs and outputs are defined, the tool is ran with some initial parameters and the program outputs are appended. The input parameters are then altered by the same percentage (10 %) individually. For example, in the case of XROTOR, first the airspeed was changed by 10% and the outputs were appended, then the radius, then the airspeed, and so on. Finally, the outputs with the 10% input change are compared to the initial outputs. If the results are plotted (for example in Figure 14.2), the inputs influence on the outputs can be observed.

In this chapter, the sensitivity study will be carried out for each of the tools used during the subsystem design. When all the subsystems are analysed, the output value ranges will be known. Then, this ranges will be inputted in the final integration tool to check for requirement compliance.

14.1. Propulsion Subsystem

The propulsion system design uses two design tools, namely the propeller design tool and the blade design tool (XROTOR). In the following two subsections a sensitivity study for both tools will be described. But first, the initial values used are presented below.

Table 14.1: Initial parameters used for the sensitivity analysis of the propeller.

OUTPUTS	Initial Value	Output	Initial Value	Output	Initial Value	Output	Initial Value
RPM_vtol	1600	DL_total	4826	D_prop_small	2.93	N_blades_vtol	6
RPM_ff	3000	D_prop_big	3.59	D_prop_ff	1.73	N_blades_ff	2
W_propulsion	698.44	Power_vtol	1038980	Power_ff	377330		

14.1.1. Propeller Design Tool

The propeller design tool was investigated with a sensitivity analysis. The general process was followed and the results can be seen in Figure 14.1. Where the inputs are on the vertical axis and the outputs on the legend. The horizontal axis represents the change of the output in percentage.

It can be observed that many of the parameters do not influence the final design. This is due to the "step" method for calculating the diameter of the propellers, based on noise and revolutions per minute, explained in chapter 5. Since the output of this program will serve as input for the blade design tool in the next section, the ranges must be specified. This is depicted in Table 14.2. MTO (More Than One), means that more than one input change generates that minimum or that maximum. ALL means that all of the inputs generate the same value. This happens for example in the **maximum RPM**, since if this number increases **the design will not satisfy the requirements**. Some of these results will also be used in the final integration tool sensitivity analysis.

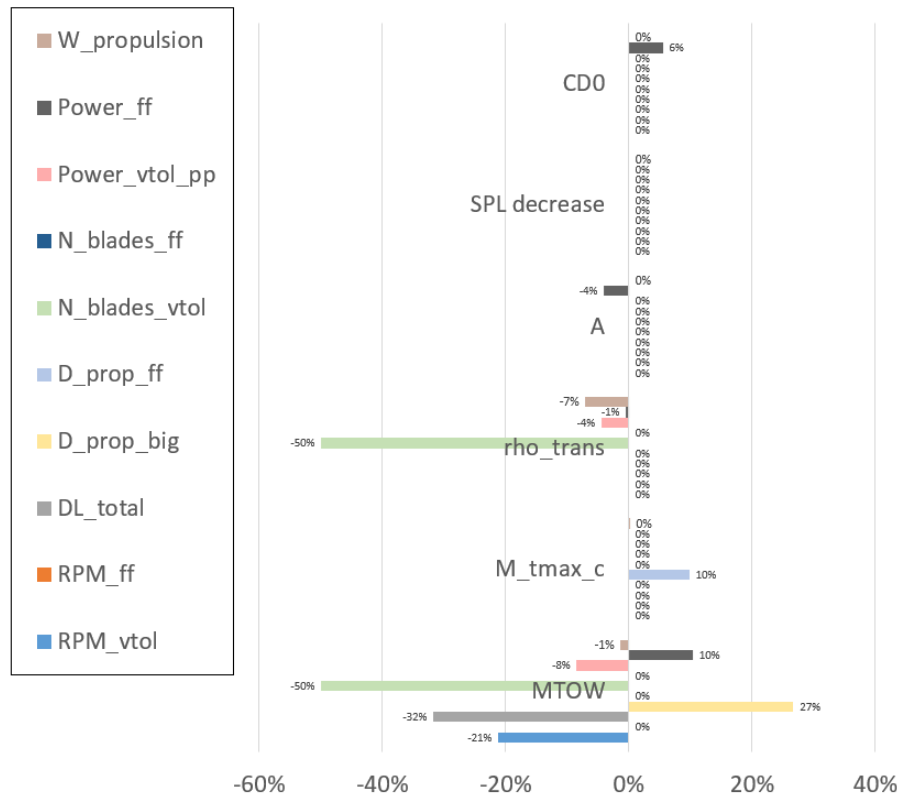


Figure 14.1: Propeller design tool sensitivity analysis.

Table 14.2: Sensitivity study for the propeller design tool.

OUTPUTS	Input	Input value	Change	Min	Input	Input value	Change	Max
RPM_vtol	MTOW	4247.97	4672.767	1260	MTO			1600
RPM_ff	ALL			3000	ALL			3000
DL_total	MTOW	4247.97	4672.767	3292.78	MTO			4826.88
D_prop_big	MTO			3.59	MTOW	4247.97	4672.767	4.55
D_prop_small	MTO			2.93	MTOW	4247.97	4672.767	3.72
D_prop_ff	M_tmax_c	0.8	0.72	1.55	M_tmax_c	0.8	0.88	1.9
N_blades_vtol	rho_trans	1.221	1.0989	3	MTO			6
N_blades_ff	ALL			2	ALL			2
Power_vtol_pp	MTOW	4247.97	3823.173	888720	MTO			1093290
Power_ff	MTOW	4247.97	3823.173	338120	MTOW	4247.97	4672.767	416560
W_propulsion	MTOW	4145.92	3731.328	648	M_tmax_c	0.8	0.88	699.43

The ranges represented in Table 14.2 will be used in the Blade Design Tool and in the subsystem integration tool.

14.1.2. Blade Design Tool: XROTOR

Since XROTOR uses the values produced by the Propeller Design Tool, the output ranges of the previous sensitivity study must be used. The Figure 14.2 was extracted from XROTOR, it depicts the sensitivity study for the back VTOL propeller for the low end input value. The inputs are on the vertical axis and the outputs on the legend. The horizontal axis represents the change of the output in percentage.

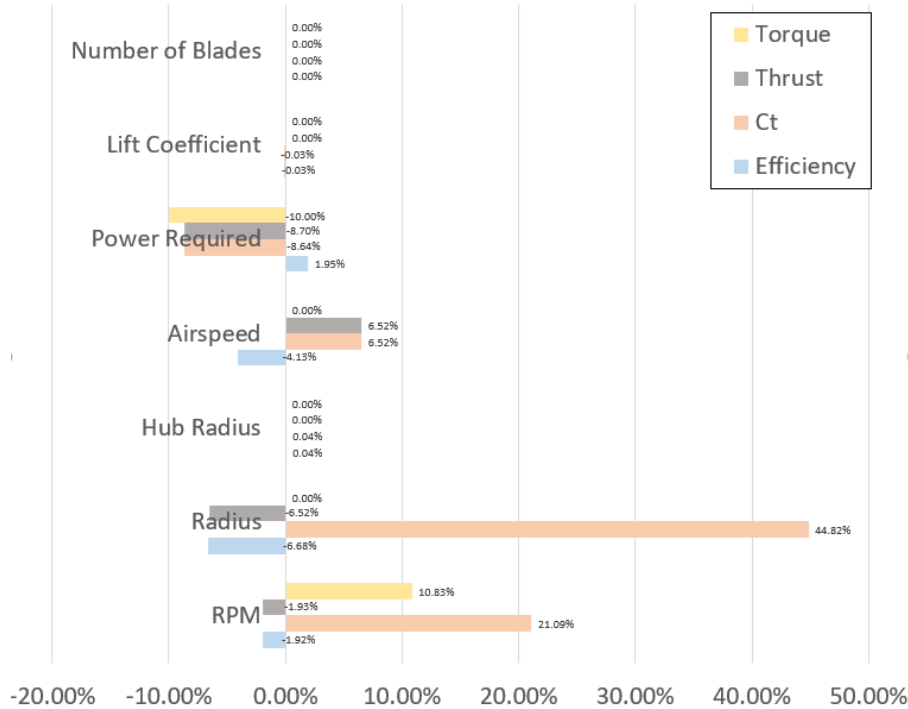


Figure 14.2: Sensitivity study for the XROTOR program for a 10% increase on the inputs.

As it can be observed, the most susceptible inputs are the revolutions per minute, the power required, the airspeed and the radius. While, an increase in lift coefficient or hub radius does not affect greatly the outputs. Although it is not depicted in Figure 14.2, a change in number of blades would affect considerably the outputs. This is not shown because the lower end range of the number of blades does not change compared to the original number of blades, as observed in Table 14.1 (since it is still 2 blades, it can not be higher or lower).

14.2. Fuel Subsystem

As depicted in Figure 14.3, changing governing inputs such as battery energy density, base power and peak power by +10% and -10% results in a change in hydrogen fuel mass, battery mass, PEM mass and their respective volumes. The ranges of the fuel mass are exported to Table 14.6.

If the Battery density increases, the battery volume and mass have to decrease to keep similar performance. If the required base power increases, there needs to be more hydrogen to be able to perform the mission. Additionally, the battery can be smaller as the additional power the battery has to be able to deliver during take-off is smaller than before. The PEM fuel cell mass also increases, as the average power it has to produce increases. Finally, if the peak power increases, the fuel cell, the battery and the hydrogen tank all have to increase to still perform the mission. Namely, the average power increases, the gap between the average and peak power increases and the total power required increases.

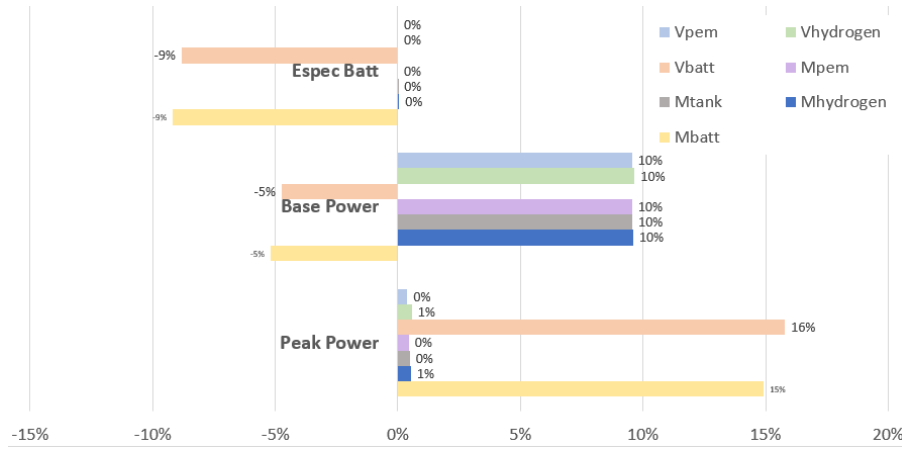


Figure 14.3: Fuel sensitivity study.

14.3. Aerodynamics Subsystem

For the aerodynamics department, 2 tools have been build. The first tool calculate the aerodynamic wing characteristics based on airfoil data while the second tool calculates what the area required is for both cruise and the transition phase and what the available area is. In Table 14.3 the increase or decrease of the wing characteristics can be seen by an increase of a certain parameter. It is clear that the aspect ratio has a considerable effect on the characteristics as it accounts five time for the maximum deviation form the current characteristics. The same data is plotted in Figure 14.4 but than only for increase of the parameters and the result is plotted in percentage of change. In this graph it can be seen that an increase in C_L has a very big influence on the drag coefficient. This is caused by the squared influence of the lift coefficient on the drag coefficient. In Table 14.3 one can also see the change in $C_{L_{max}}$ even though the calculation is not used in the design iteration. It has nevertheless been added to illustrate the theoretical influence of different parameters.

Table 14.3: Sensitivity study for the wing characteristics for a 10% increase on the inputs.

OUTPUTS	Input	Input value	Change	Max	Input	Input value	Change	Min
C_{L_a}	AR	3.0000	3.3000	3.4840	AR	3.0000	2.7000	3.1128
C_{L_0}	C_{l_a}	6.2070	5.5863	0.1022	AR	3.0000	2.7000	0.0908
C_{D_0}	C_{root}	6.9000	6.2100	0.0112	C_{root}	6.9000	7.5900	0.0108
C_D	Cl	0.2500	0.2750	0.0175	Cl	0.2500	0.2250	0.0148
$C_{L_{max}}$	AR	3.0000	3.3000	1.4445	AR	3.0000	2.7000	1.4250

For the required and available surface area the same sensitivity procedure has been used. The results of this can be found in Table 14.4 and Figure 14.5. From these results it can be concluded that a span increase has the biggest influence on the available surface area when taper ratio is set to be constant. Therefore, an increase in span would be beneficial for the transition phase as more effective area would be available to produce lift. However, it also has some downsides as will be explained in section 14.5. Furthermore the required cruise area is most influenced by the cruise speed due to the quadratic relation. The MTOW influences the required transition surface area. Preferably, this transition area is as small as possible and therefore the aim should be to decrease the MTOW as well.

Table 14.4: Sensitivity study for the surface area available and required by a 10% increase on the inputs.

OUTPUTS	Input	Input value	Change	Max	Input	Input value	Change	Min
S_{cruise} required	V_{cruise}	69.4	62.46	79.19478837	V_{cruise}	69.4	76.34	53.01469304
S_{trans} required	MTOW	40652.64	44717.904	33.77624314	MTOW	40652.64	36587.376	19.70615187
S_{cruise} available	span	18.13	19.94	107.822758	span	18.13	16.317	85.98300196
S_{trans} available	span	18.13	19.94	41.957618	span	18.13	16.317	23.35523667

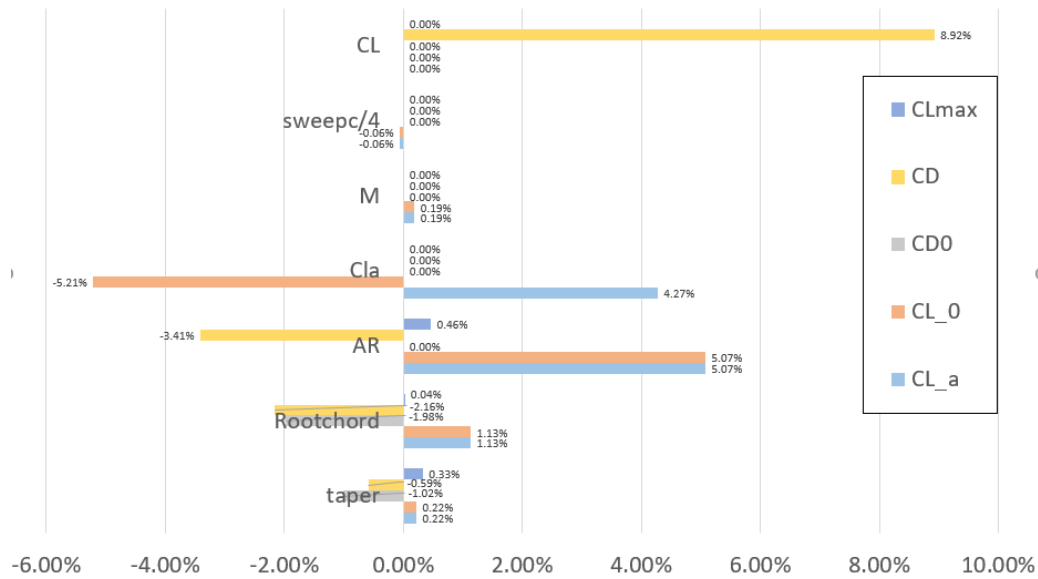


Figure 14.4: Increase of aerodynamic characteristics per 10% parameter increase.

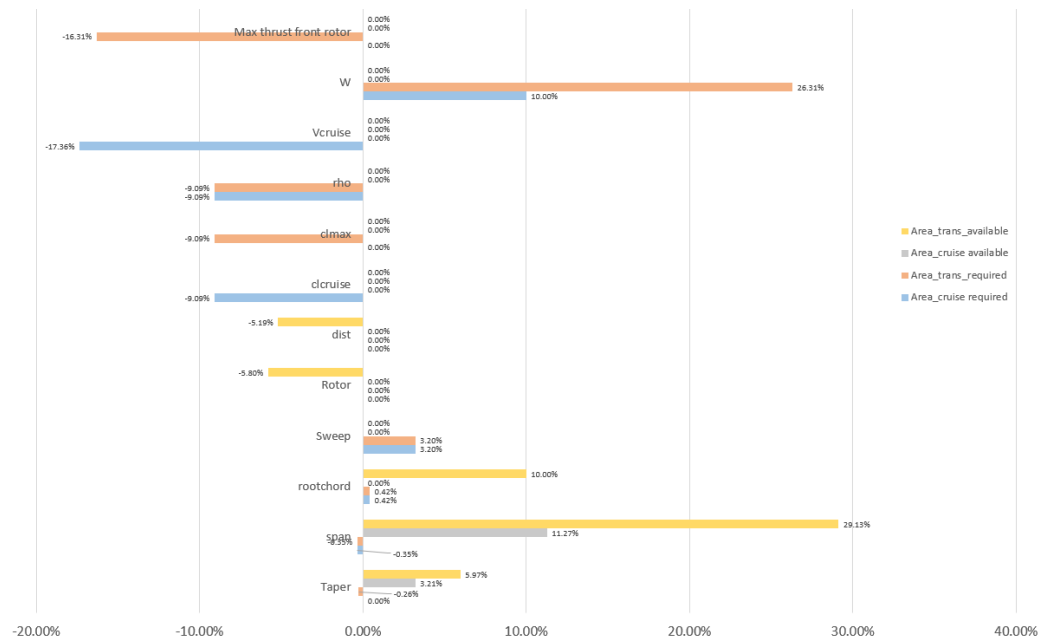


Figure 14.5: Surface area available and required change per 10% parameter increase.

14.4. Structures Subsystem

Since the structural analysis of the aircraft is split up into a wing design and a fuselage design, both will be analysed here separately.

14.4.1. Wing Design

The wing box is designed in a way that it should be able to bare the given and following loads. Therefore the main output that influences the aircraft is structural weight of the wing. In Figure 14.6 the weight increase is as a result of a 10 percent increase and decrease. Looking at the sensitivity of the wing box design, it is important to keep in mind that the design point for the wing is the cruise phase. Even with a 10% increase of the rotor thrust, the cruise phase still constrains the thickness. This can be seen in the zero mass increase in the table. The largest influence on the weight of the wing box are wing span, cruise speed and wing thickness. The wing span doesn't only change the physical volume of the wing box but it also increases all aerodynamic loads therefore the dimensions increase. These loads obviously increase quadratically with the cruise speed. The wing thickness increases the wing box resistance to moment with a power of 4. This makes it one of the largest weight reducing factors of the program. It can be noticed that the mesh density is sufficient since a change in increments isn't followed by large changes in weight.

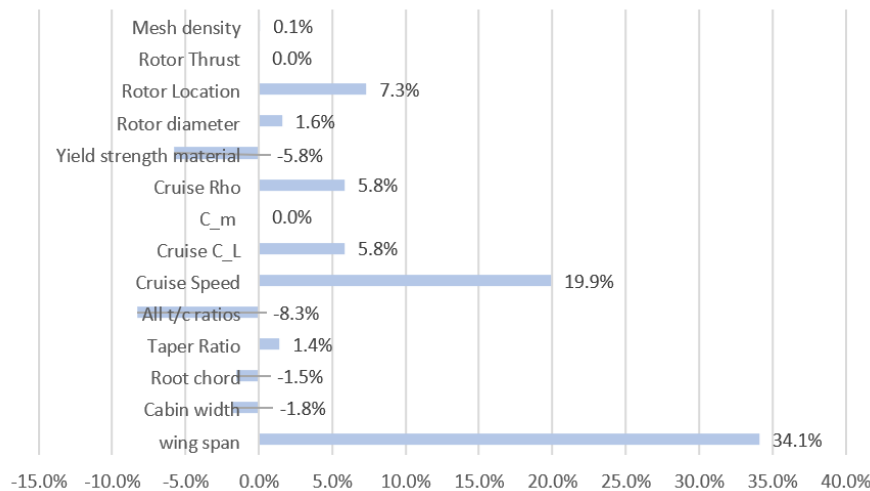


Figure 14.6: Sensitivity study of the wing weight adding 10% on the inputs.

Some unbalanced parameter scaling of interest are rotor location and root chord. Moving the rotor more aft increases the torque and places the front beam more to the centre of the wing, making it the main carrying element and increasing all its dimensions. Decreasing the root chord does essentially the same with the side effect of decreasing the thickness as well¹. This decreases the bending resistance, which has to be compensated for. The final remark of interest is the fact that the aerodynamic moment coefficient does not influence the weight. This is due to the fact that the thickness of the wing box is set to be 1 and .5 mm, due to production requirements. Therefore no optimisation loop is needed, the structure can hold the shear load and torque with these small values. With increased torque it is checked if the skin would experience more than the allowed shear stress. This was not the case, thus the wing box doesn't need to be strengthened.

Table 14.5: Table with the output ranges for the wing weight calculation.

Output	Input	Original Value	Input Value	Output Value
MTOW	wing span	18	16.2	740.56
MTOW	wing span	18	19.8	1294.68

14.4.2. Fuselage Design

The fuselage is designed with length, width, thickness, number of stringers and the loads as input and the stress, shear stress and fuselage mass per meter as output. All these inputs influence the outputs. With

¹Since the t/c ratio is set

this sensitivity analysis, all inputs are increased and decreased by 10% and their influence on the outputs is analysed. In Figure 14.7 the increase in stress, shear stress and mass in percentage is given as a result of the increase in the input.

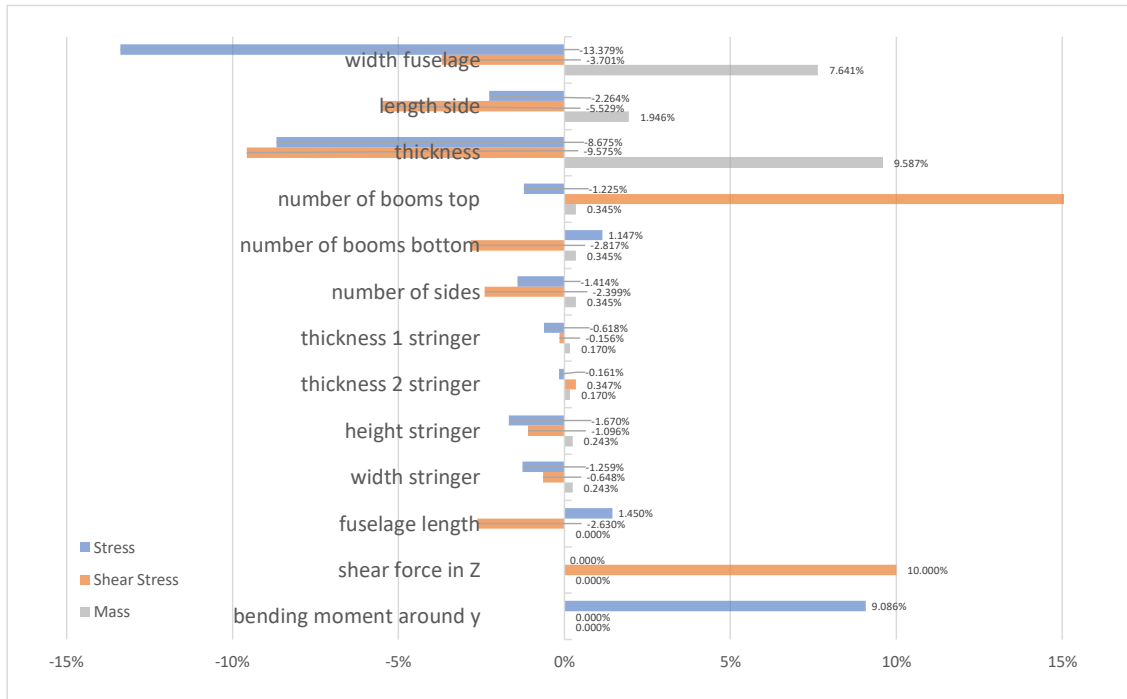


Figure 14.7: Sensitivity study of the stress, shear stress and mass of the fuselage when 10% is added on the inputs

As can be seen in the figure, increasing or decreasing the number of booms at the top has the most influence, especially decreasing the number of booms at the top influences the shear stress greatly. This is mostly due to the fact that the forces and moments in x and y direction are assumed to be applied halfway the beams of the wing. Furthermore, increase in the total shear force or bending moment influences the design, which is quite logical looking at the formulae given in subsection 9.2.2. The width of the fuselage greatly influences the output as well, as this changes the area, moment of inertia and stringer spacing as well. The thickness of the skin is of importance as this influences the area and moment of inertia greatly as well.

14.5. Integration Sensitivity Analysis

Once all the previous subsystems have been analysed, the sensitivity study can be done for the final subsystem integration. The outputs of each subsystem are fed into the final integration tool. Ultimately, the outputs of the integration tool will be compared to the key requirements, to see in which conditions these will be met. The Figure 14.8 depicts the final outputs in relation to the ranges specified in Table 14.6.

It can be observed in the graph that the most influential parameter is the mass of the wing, this is due to its high mass compared to the other inputs. The same happens with the mass of the propulsion subsystem and the mass of the fuselage. Finally, the inputs can be compared to the requirements. It is important to note that, during the design of the aircraft, the requirements were incorporated in the code as constraints. Meaning that, as long as the design is feasible, some requirements such as the span and noise will always be met. The key requirements that can be verified by analysis are compared to the output values in Table 14.7. Where, if the square is green, the requirement is met. It can be observed that, the maximum noise in VTOL is met in all of the input changes, since it is always lower than 88.5 dBA.

Table 14.6: Input ranges for subsystem integration sensitivity analysis.

Input	Min	Original	Max	Input	Min	Original	Max
Mfuel [kg]	445.8	483.2	520	Mprop [kg]	648	655	699
Mwing [kg]	258.15	335.3	449.2	CD0 [-]	0.0108	0.011	0.0112
Diameter Prop Back [m]	3.59	3.59	4.55	Mfus [kg]	1346	1511.4	1678
Diameter Prop Front [m]	2.93	2.93	3.59	Mtail [kg]	120.5	133.92	147.3
Diameter Prop FF [m]	1.53	1.73	1.9	Mhydraulic [kg]	38.7	43	47.8
Melectronics [kg]	99.72	110.8	121.9	Mavionics [kg]	105	116.73	128

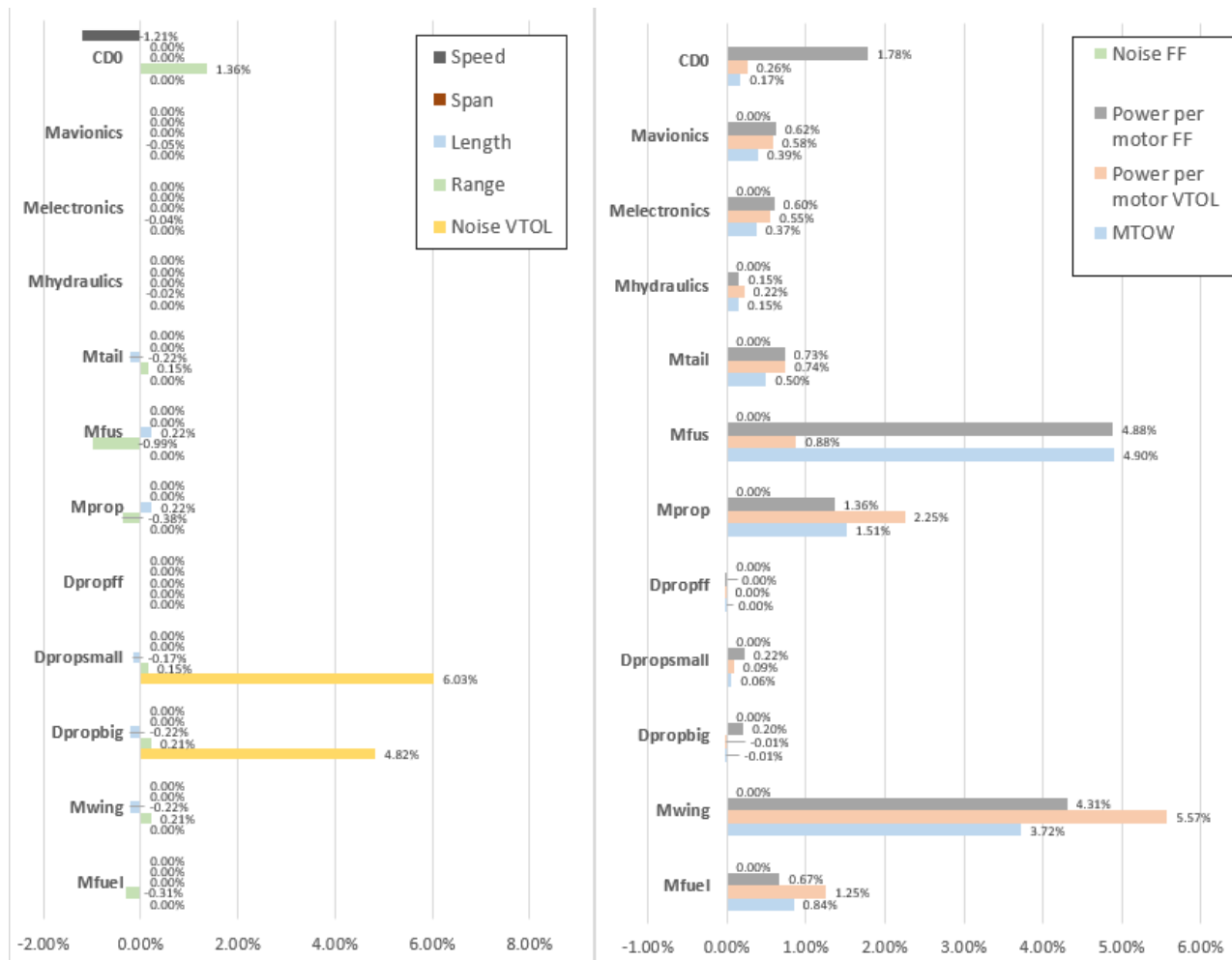


Figure 14.8: Sensitivity analysis of all integrated systems

Table 14.7: Requirement compliance after sensitivity study.

General Requirements Compliance and Feasibility

In most of the chapters that have preceded this one, a requirement compliance and feasibility analysis has been done regarding the respective subsystem or non-technical system like the safety, maintenance, costs and schedule. However, besides these requirements, requirements have also been determined for the more general overall part of the aircraft and its design as stated in chapter 2. The compliance of these requirements can be found in this chapter and have been divided into the remaining technical requirements in section 15.1 and the non-technical requirements in section 2.5.

15.1. Remaining Technical Requirements

Transport Requirements

The H₂ERO's initial mission will be to perform medical emergency missions. These will be from the aircrafts base to the emergency site where in a few cases a patient is picked up to transfer to a nearby hospital. In the case a patient is taken on board, their safety and health needs to be assured. Also, once the decision is made to take a patient along, the aircraft is required to be quicker than transport by a land vehicle. This results in the two requirements EVTOL-GNTR-101 and EVTOL-GNTR-102 tabulated in Table 15.1.

During the subsystem design and final design integration in chapter 11 safety has always been a main focus. The aircraft has been designed to be able to provide stable VTOL ascent and descent and the cruising phase does not require a dangerous range of angle of attack. Furthermore, all initial necessary medical equipment to stabilise a patient for transport is available in the H₂ERO. Therefore, a patient would be in just as good hands as they would be in a ground vehicle. Hence, it is expected and argued that the patients health can be kept stable and will not deteriorate during transportation to a hospital.

Furthermore, regarding EVTOL-GNTR-102, the decision at an emergency site should be made if a patients transport will be through use of the H₂ERO or through ground transport. This is mainly due to the distance and location of the emergency site to the hospital. In a busy city centre with lots of traffic or an accident in a field far away from a big city the H₂ERO is expected to be quicker. However, an accident within a range of 1 kilometer, ground transport is of course expected to be quicker. So, the compliance of EVTOL-GNTR-102 is location dependent but for now will be argued to be compliant.

Table 15.1: Overview of the requirements regarding the transporting capabilities of the aircraft.

Code Identifier	Requirement	Type	Verification	Compliance
EVTOL-GNTR-101	The aircraft dynamics during take off, flight and landing shall ensure that the state of the patient will not deteriorate during transport	Regular	Analysis	
EVTOL-GNTR-102	The aircraft shall provide faster transportation from accident site to hospital than an ambulance	Regular	Analysis	

Noise Requirements

The main initial set up of this project has been to reduce the noise produced by emergency aircraft in the Netherlands. This is because they constrain the amount of commercial aircraft that are allowed to take-off and land in the Netherlands since they take up a lot of the noise. Hence, noise was one of the main aspects that has been taken into account throughout the entirety of this project. This already started with the trade-off for the various initial design concepts determined in [2].

Hence, it seemed logical to continue addressing the noise as the main component to design the aircraft for. According to the subsystem design the aircraft does comply with all of the noise requirements. This is

due to the fact that, for instance, the propulsive system was actually backward engineered from the noise requirement. Hence, any configuration that was considered already complied with these requirements. This also resulted in many somewhat unfeasible or unlogical initial designs as this constraint was rather tight with a significant noise increase. It should be noted that the propulsive system, containing the propellers and motors, was considered as the largest noise producer on the aircraft.

Table 15.2: Overview of the requirements regarding noise.

Code Identifier	Requirement	Type	Verification	Compliance
EVTOL-GNNO-110	The aircraft shall reach a noise reduction of at least 25% in loudness compared to the EC135	Key	Analysis	
EVTOL-GNNO-111	The close range EPNL shall be a maximum of 88.5 dB	Driving	Analysis	
EVTOL-GNNO-112	The cruise altitude EPNL shall be a maximum of 80 dB	Driving	Analysis	

Design Recommendations

As there was a limited amount of time available for the design, there are numerous future design recommendations that would be worth looking into. Many of these recommendations come from results and conclusions made after the design process. Additionally, the recommendations contain possible configurations alteration or problems with the general concept itself.

16.1. Full Aircraft Configuration

The current design does not fit both of the propellers in the main wing. This will increase the induced drag and the performance in forward flight. However, it gives more design freedom in terms of stability and control. It is recommended however, for future research, to keep the propellers inside the wing. This can be done in two ways; either reducing the size of the VTOL propellers, or modifying the wing area and shape. The second option is the most feasible one, but further analysis has to be made regarding different planform designs and accessibility to the vehicle.

Another possible configuration that is recommended for further research is to rotate the two front rotors with 90 degrees during cruise flight, which will reduce the drag.

16.2. Transition Phase

As mentioned in subsection 11.9.3, there was some concern regarding the transition phase from VTOL to cruise for the H₂ERO. This section will elaborate more on the reason for this concern and will also give recommendations for further research and possible solutions.

Starting off with the reason for concern. To be able to perform a successful transition phase, a few problems need to be overcome. Firstly, at the end of the VTOL phase, the aircraft has zero horizontal ground speed. Hence, the wings create zero lift as well. If the rotor doors are closed at this instant, the aircraft would fall back to earth like a rock. Therefore, it is required to achieve at least the stall speed of the aircraft before the VTOL rotors are turned off and closed. The second problem is the wing surface area during transition. Since the VTOL are required to stay operative and open until the wings produce enough lift to carry its own weight, the gaping holes of the VTOL constrain the total lifting capability of the wing. Hence, even when the full wing stall speed is achieved, there is a period of time in which the VTOL rotors need to be turned off and the doors closed. Until this process is successfully done the wing is missing a large part of its lifting capability due to the rotor holes. Hence, the transitioning phase can only be completed once the wing, including the holes, generates enough lift to sustain its own weight. Therefore, this increases the aircrafts stall speed as the effective wing area is 30.6 m^2 when the rotors are open and 93.8 m^2 when the rotors are closed. This is a ratio of 0.326 between open rotor effective wing surface and closed rotor effective wing surface. Since the stall speed and the wing area are related quadratically ($V^2 = \frac{1}{S}$) in the general lift formula, this results in a stall speed increase of 75.1%. Given the full wing stall speed being $28.1 \frac{\text{m}}{\text{s}}$, the stall speed with the rotors open and off becomes $49.2 \frac{\text{m}}{\text{s}}$.

The significant stall speed increase with the VTOL rotors open raises the question if the transitioning phase is feasible. A few options have been discussed and thought of that should be researched further.

Ideally, a system should be found that allows the rotors to be closed linearly according to the aircrafts speed at that given moment. The gradual horizontal speed increase results in more lift being generated by the wing, hence less VTOL rotor lift required, hence the VTOL rotor door can decrease the rotor area in size and hence give more surface area and lift again. This continues until the rotor is completely closed.

Another option that was discussed was the possibility of having a closing system that works hydraulically.

These can close the rotor doors instantly and hence increase the effective wing surface area from 30.6 m^2 to 93.8 m^2 instantly as well. However, initially this option was not considered due the large amount of forces that are expected to the structure. Also, the VTOL rotors will still be running so instantly closing the rotor doors could create a problem with the propellers as they would still be producing some sort of thrust.

Added to the option just stated was then to implement brakes that can also instantly stop the rotors from spinning. However, due to the size of the VTOL rotors and their moment of inertia, an instant stop of their motion could result in an overall devastating torque to the aircraft. Hence, this option did not seem very feasible.

Regarding all of the options mentioned in this section, further research should be done on the possibilities regarding the transitioning phase. For now, this phase has been regarded as beyond the scope of this project as it was not possible to initiate an elaborate research and design process for it. The main focus was set on the VTOL and cruising phases of the H₂ERO.

16.3. Propulsion

The propulsion system can be further improved if more time and resources are available. Studies have shown that an uneven spacing of the blades decrease the noise even further [23]. Moreover, a decrease in noise of 4db would allow to further decrease the propeller diameter.

In the current design the power delivered by the VTOL motors is limited to 280 kW. If a better engine with the same mass would be available in the market, higher thrust and manoeuvrability could be achieved.

16.4. Fuel System

The techniques used for the fuel system design are the most efficient tested and verified on the current market. However, there is a lot of research being done to further improve the different components. The current best fuel cell is the PEM (Proton Exchange Membrane) Fuel Cell, which consists of 7 plates where oxygen and hydrogen react. In the near future, the plates can be made of other materials, increasing the power density of the cell and increasing the efficiency with approximately 10% [61]. Furthermore, one of the major drawbacks of using liquid hydrogen is the insulation of the tank. The hydrogen needs to stay cool to stay liquid. As described earlier, a part of the hydrogen turns into a gas because the temperature in the tank rises. In future designs, better tanks need to be created to keep the hydrogen in liquid state.

16.5. Electronics

In terms of electronics, the design is quite evolved. For future designs, the cabling and on-board computer can be lighter and more energy efficient compared to the current techniques. Additionally, the battery energy density used is 350 kW/h, which is high for modern standards. In the future, battery densities up to 700 kW/h are expected to be produced, which would make the electronics lighter and more efficient.

16.6. Aerodynamics

As briefly mentioned in chapter 8 more research should be done and considerations should be taken for the more detailed design of the aerodynamic subsystem. They include the following items:

- The interaction between the integrated rotors in the wing and the airflow should be investigated on its aerodynamic effects (like lift, drag and moment coefficient).
- The effect of front two ducted rotors on fuselage, wing and tail surface air flow should be analysed and designed for. The same accounts for the effect of the forward flight rotor on the airframe.
- The dynamics of the moving mechanism to cover up the rotors in flight should be assessed. This includes the movement of the shutter mechanism, the effective wing surface area producing lift, the airflow disturbance, time duration and altitude change.
- A CFD model for the full aircraft design should be made in order to analyse the lift and drag in 3D properly, how it differs from the 2D analyses (and how this affects the assumptions and design choices made), stall behaviour, the effect of noise reduction techniques, and stability behaviour.

- Wind tunnel experiments of the wing section and perhaps a scaled down prototype of the aircraft should be made in order to validate the CFD data for this specific mission profile.
- If from the CFD and windtunnel experiments it can be concluded that the wing does not perform as well as it should, a more elaborate airfoil selection can be made. For this, also specially tailored airfoils can be designed instead of the standard NACA ones.
- A more detailed design and aerodynamic design of the aircraft nose can be made to reduce drag and hence enhance efficiency.

16.7. Structures and Materials

The wing box and I-beams masses, calculated in chapter 11, are fairly high because of the two big rotors in the wing. The two rotors imply two relatively big holes in the wing box, which means that the I-beams have to carry almost all the loads near the root of the wing. For future designs, more research can be done on lighter and stronger materials for the wing box and I-beams. Also, the use of stiffeners and stringers for the wing box which would relieve some loads for the beams should be researched. Other considerations for a more detailed design are the connections of the two front propellers to the fuselage, the tail connection to the main fuselage, and the moving mechanisms that will cover the propellers in forward flight.

16.8. Stability and Control

16.8.1. Vertical Flight

The simulation can be improved by implementing additional effects that were first assumed to be negligible such as propeller drag, airframe drag and propeller gyroscopic effects. The control software can be improved by further tuning the PID gains with real test-flight data to feel more natural to the pilot. If the pilot trusts the system he will also extract more performance out of it by pushing the system to its boundaries. Another improvement to the control software would be to add a measure against integral windup. Because the actuator inputs are limited to never exceed certain values, the integral term in the controller might keep growing, demanding a higher RPM than is allowed by the saturation limit. The issue here is that when the error term switches signs, the integral term has kept growing and needs a long time of negative error to finally start being useful again. This can be avoided in multiple ways and clamping is a popular method which essentially turns the integrator off when the demanded command is higher than the saturation limit. The last recommendation for the control software is to add some logic that prioritises certain state setpoints more than others. For example, if the pilot is doing a yaw manoeuvre at constant altitude and a different aircraft approaches, he would want to quickly gain altitude. However, because the yaw motion is already demanding the propellers to spin at the noise limit, there is no possibility to gain altitude without becoming unstable. Ideally, altitude would always be the setpoint with priority followed by pitch, roll and finally yaw. Whenever there is a problem with motor RPM's becoming too high, priority should be given to the commands in this order.

16.8.2. Horizontal Flight

As briefly already mentioned in chapter 9, an improvement for the design would be closer investigation in the directional and lateral stability and control characteristics of the aircraft, coupled with a dynamic analysis of the aircraft motion, in order to size the control surfaces, as well as the rudders and ailerons of the aircraft more accurately and tailored for specific requirements. Additionally, a more accurate aerodynamic analysis of the aircraft (e.g. CFD analysis) would greatly benefit in the analysis of the effectiveness of the aerodynamic surfaces, as well as would allow to investigate the stability and control derivatives of the aircraft. This would allow to perform a dynamic analysis of the aircraft, and assess the dynamic stability characteristics of the aircraft, such as its eigenmodes and their characterisation.

16.8.3. Hydraulics

The hydraulic system is not fully designed yet, the first step for future research would be to calculate the required force to move the control surfaces. From here, calculate the dimensions of the actuator, the hydraulic liquid and the required pressure. Once the pressure and the liquid are known, the pressure regulator, the reservoir and the valves will be designed.

Operations and Logistics

Having a good overview of the day to day logistics and operations of the aircraft is important before making a design. Before determining the concept in the midterm report [2], a preliminary analysis has been carried out. Now, as all subsystems are designed and integrated, a fully detailed analysis can be made. First, a mission profile will be presented. Then an operations diagram, a functional breakdown structure and a functional flow diagram are given.

17.1. Mission Profile

The general mission profile the aircraft is designed be able to perform is depicted in Figure 17.1. The mission can be generalised in three separate phases: the aircraft takes off from base, cruises to the location of the accident and lands at a open spot of at least 25mx25m; The aircraft takes off, cruises to the hospital and lands at the hospital's helicopter pad; finally the aircraft takes off from hospital flies back to base.

Once the aircraft lands at the location of emergency, there are two options: 10% of the time, the helicopter takes the patient to the hospital; the other 90% of the time, they only take a specialised doctor to the location to stabilise the injured. Then, the doctor and the pilot fly back to base straight away.

Every mission is subject to change; while in the air on the way to the place of an emergency, the control room may decide to cancel the mission or divert the aircraft to another accident. Even on the way back from an emergency, they can be sent on another mission. The limiting factor however is the amount of fuel onboard. For this reason, the pilot always takes off with maximum fuel (MTOW) on board.

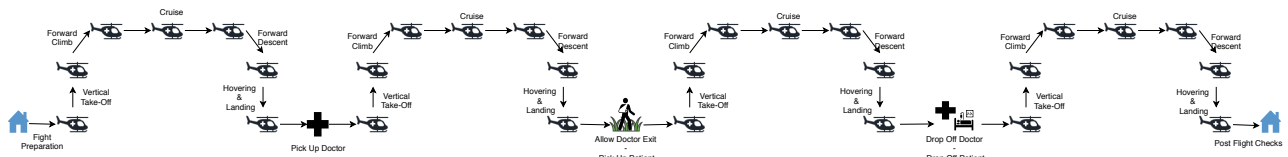


Figure 17.1: Mission Flight Profile [2].

Table 17.1 summarises the relevant mission parameters. These parameters are based on the customer requirements and the interview with a real emergency helicopter pilot.

Table 17.1: Mission performance parameters used in preliminary calculations.

	Vertical Take-Off	Climb	Cruise	Descend	Vertical Landing
Height change [m]	500	414.4	0	-414.4	-500
ROC [m/s]	3.5	$0.9 \cdot 2.5$	0	$0.9 \cdot 2.5$	3.5
Forward Velocity [m/s]	–	69.4	69.4	69.4	–
Time [s]	142	184	832	184	142

17.2. Operations Analysis

The operational analysis mainly focuses on the ground operations part of the mission cycle. As can be seen in Figure 17.2, the flight phase is summarised in one block and will be elaborated on in section 17.3.

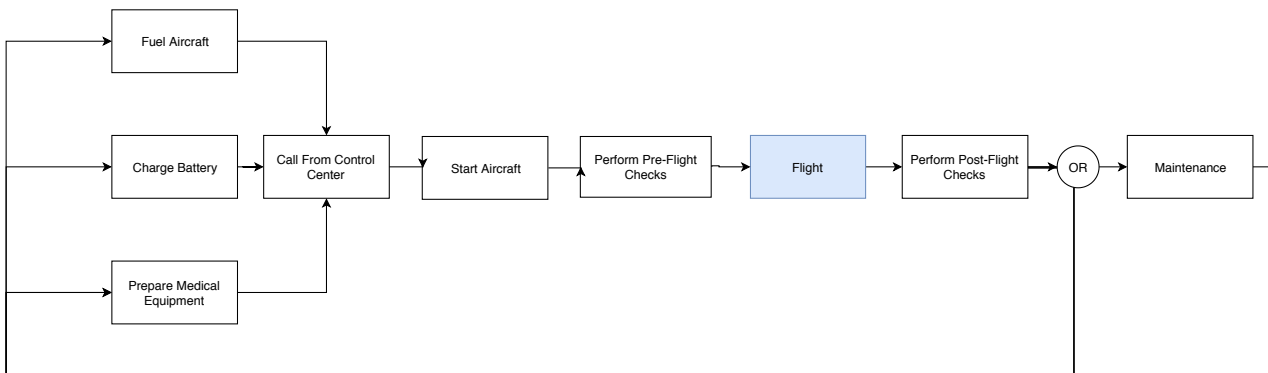


Figure 17.2: Operations Diagram.

As clearly indicated in the diagram, before flight the aircraft has to be refuelled with liquid hydrogen and the battery has to be charged by an external power source. A turnaround time of maximal 10 minutes is desired, as the regular helicopter needs ten minutes to fully tank after landing. In practice, this never causes problems. We use 37.4 kg of Hydrogen. The tank rate thus needs to be at least 0.063 kg/s to match the acceptable fuel time. As described before, charging is not necessarily required as technically the hydrogen fuel cell produces plenty of power to charge the battery during cruise. However, it is more efficient to charge the battery before take-off as the electrolysis of hydrogen is less efficient than electricity generated by, for example, the sun or wind.

Then, after a call comes in from the control center, the doctors rush to get the bags with medical equipment required for the specific mission. Simultaneously, the pilot enters the aircraft, unplugs the charger and starts the autopilot and board-computer, which takes up to two minutes maximum. During this start-up, the pilot does pre-flight checks and looks up a possible location to land close to the place of emergency. After all checks have been performed, the pilot takes off. After the mission, post-flight checks are performed. Depending on the amount of flights made since the last maintenance and the post-flight checks, additional or scheduled maintenance is performed.

17.3. Functional Analysis

A mission consists of a pre-flight phase, three airborne phases and a post-flight phase. In order to analyse the hierarchy of functions that the aircraft has to perform during this mission, a functional breakdown structure has been created. The ground operations part is depicted in Figure 17.3 and the airborne operations part in Figure 17.4. Next to the functional breakdown diagram, the logical order of functions that the aircraft has to perform during the mission is given in the functional flow diagram, depicted in Figure 17.5. This is an And/Or diagram. The three airborne phases are indicated by an option (OR), because either the patient gets picked up or the patients gets dropped off at the hospital or the post-flight checks are performed. Each individual airborne phase consists of taking-off, climbing, cruise, descend and landing. Both diagrams have only slightly changed from the midterm report [2], as the mission and its functions were already clearly defined back then.

17.4. Requirement Compliance & Feasibility

As explained with the content in this chapter, all requirements regarding the operations and logistics are met.

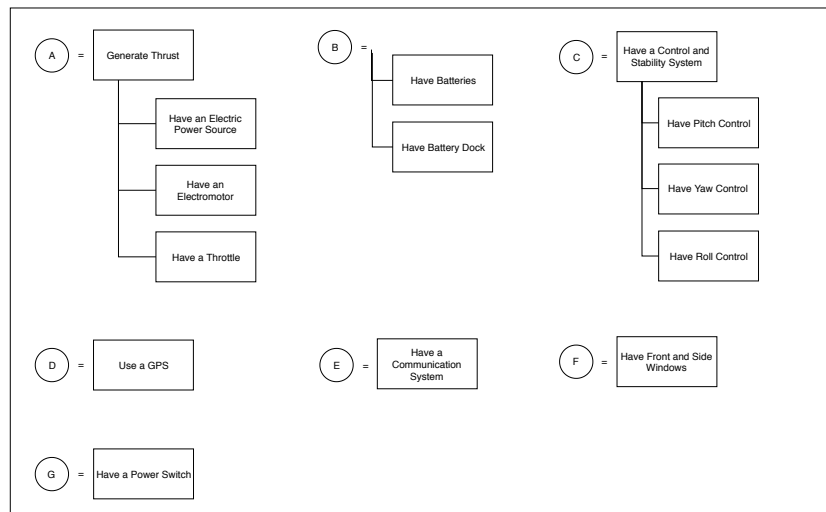
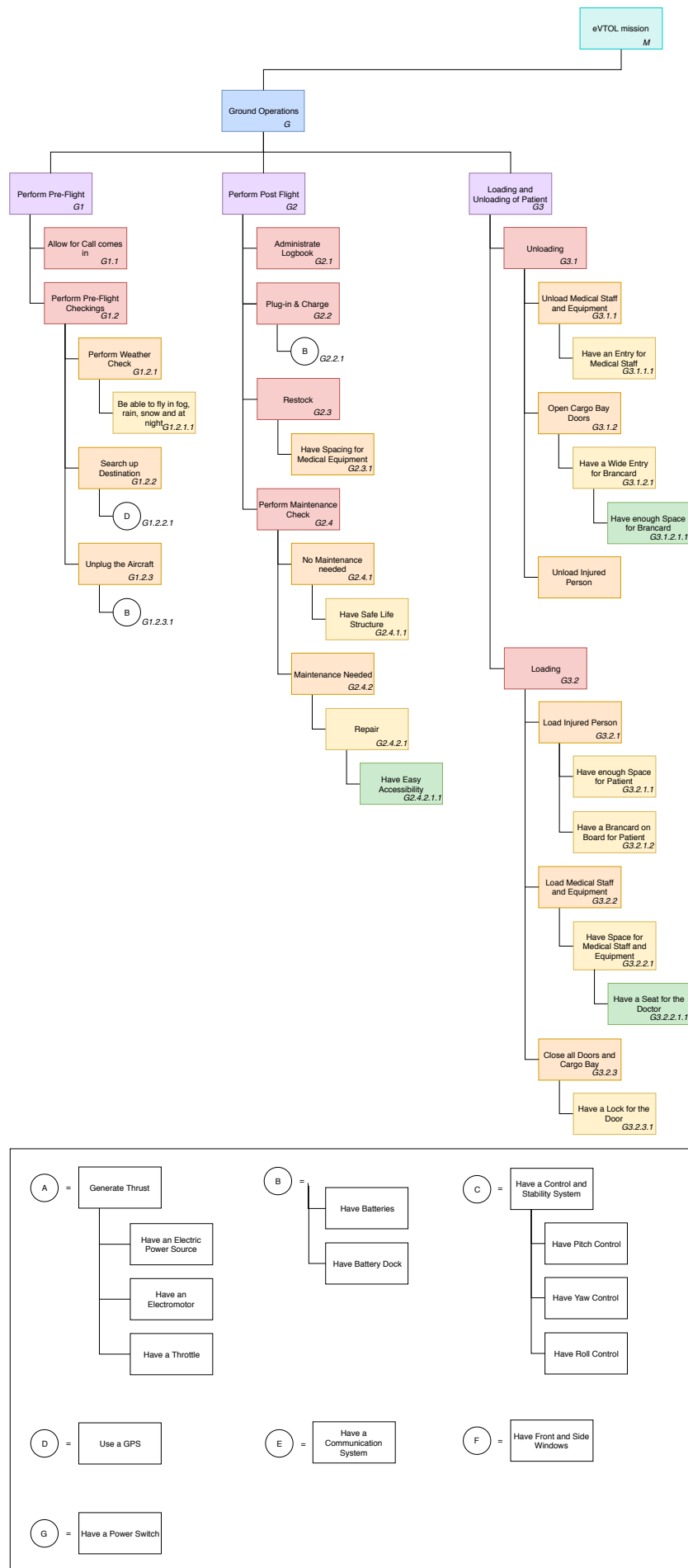


Figure 17.3: FBS Ground Operations.

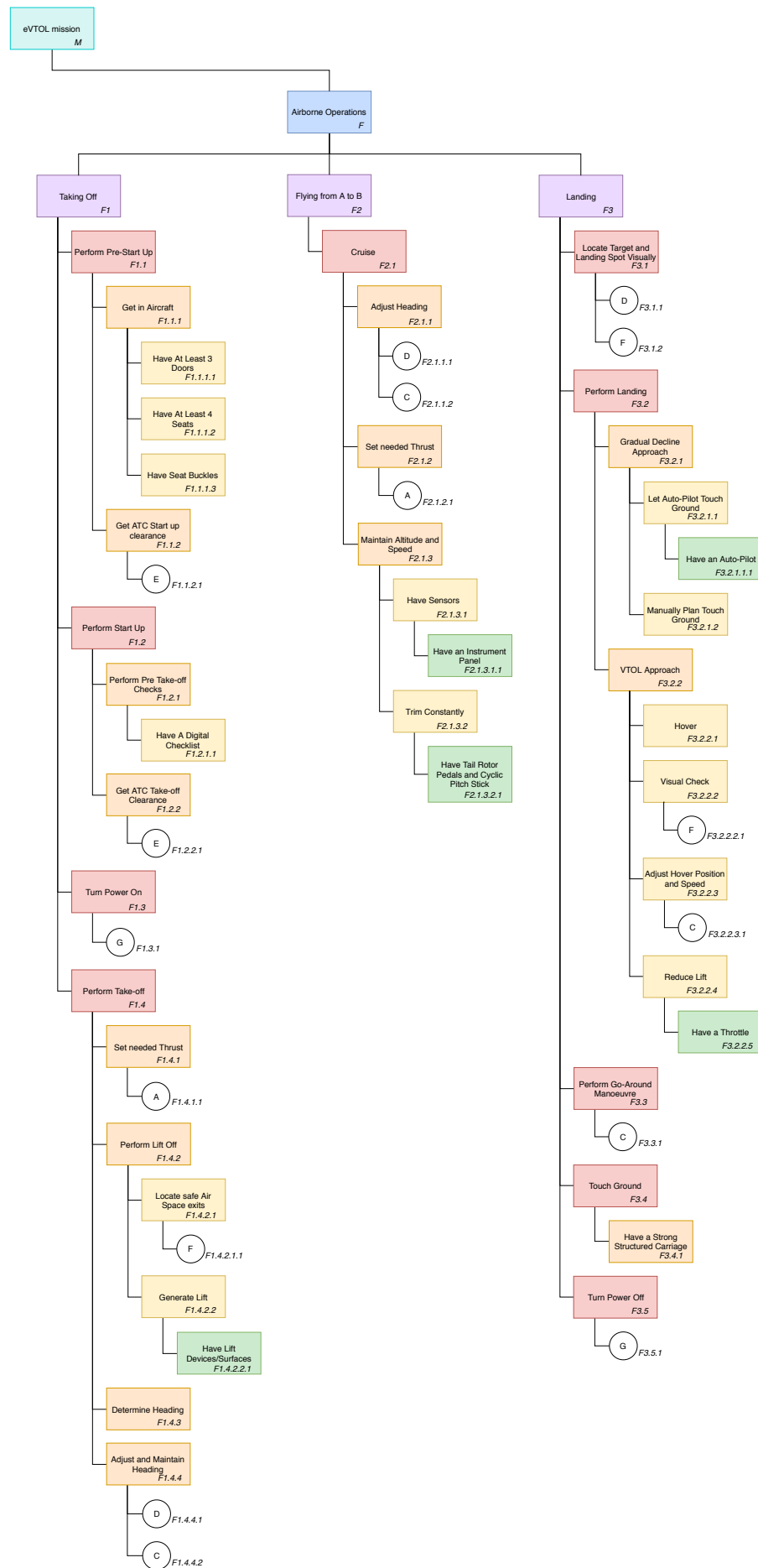


Figure 17.4: FBS Airborne Operations.

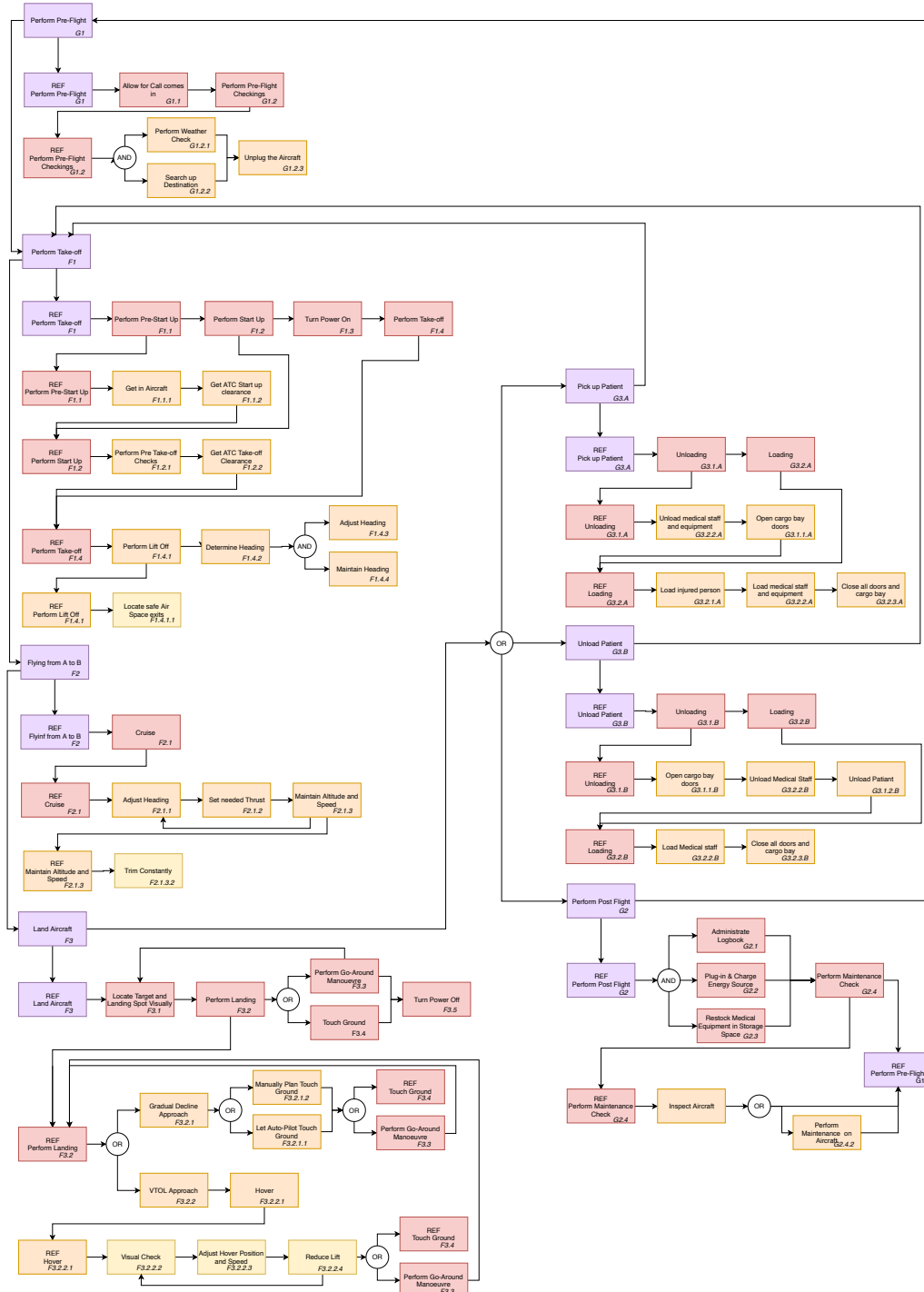


Figure 17.5: Functional Flow Diagram.

Manufacturing, Assembly and Integration Plan

The Manufacturing, Assembly and Integration (MAI) plan is developed to give a chronological outline of the activities that have been performed to construct the product. This plan is of great importance for many aspects of the design as well as project planning. The production timeline is shown in Figure 18.1. First the divisions made to break up the assembly process are discussed, then the work done in each block of Figure 18.1 is discussed. Finally, an overview of the practical aspects of the production line such as labour hours, manufacturing location and logistics is given.

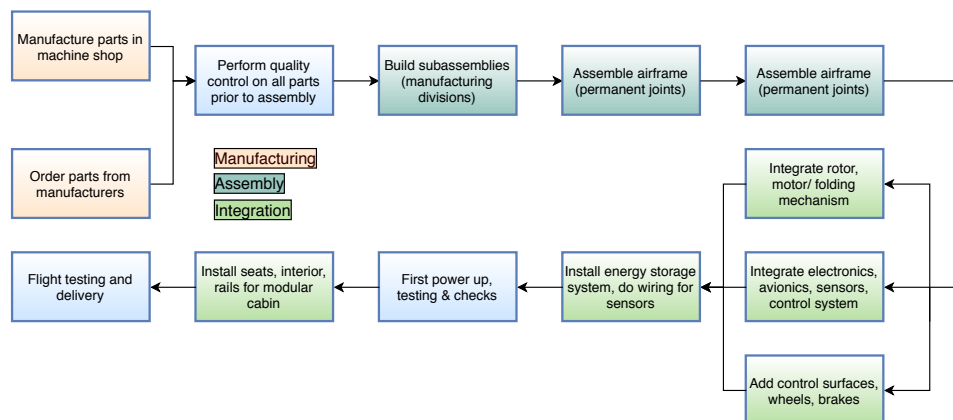


Figure 18.1: Production plan for the aircraft.

18.1. Divisions

Manufacturing the whole aircraft at once from a single piece is clearly impossible because it is highly impractical, expensive and impossible due to different materials that are suitable for certain applications. Therefore the product is divided into divisions which has some key advantages:

- Increased production efficiency, parallel manufacturing of parts
- Accessibility during production and assembly allowing for easy access by workers
- Less issues with handling impractically big parts that require increasingly expensive manufacturing processes such as huge autoclaves
- Maintainability is increased when certain parts can be replaced easily without scrapping the whole product
- Improved structural efficiency by combining parts made of different materials in a single product

Table 18.1: Assemblies and their groups and materials.

(a) Manufacturing divisions

Division	Material
Cockpit	GLARE
Front door	CFRP
Large door section	CFRP
Main fuselage section	CFRP
Wing leading edge	GLARE
Wing-fuselage connection	Titanium alloy
Tail main struts	CFRP
Windows	Plexiglass

(b) Mounting divisions

Division	Material
Landing gear	Titanium alloy
Wing main structure	Aluminium alloy
Propellers	Titanium leading edge, glass fiber reinforced polymer main body, foam filling
Control surfaces	CFRP

To divide the aircraft into divisions, two types of divisions are considered: mounting and manufacturing divisions. Mounting divisions are used for parts which require replacement such as landing gears and motor mounts. Manufacturing divisions are used to indicate permanent connections, for instance the wing and fuselage connection. These divisions shall be made at logical positions, for instance when two different materials are used for different parts or when the shape drastically changes (wing-fuselage) or divisions are impossible (not in the middle of the door). Table 18.1 shows the group each division of the main frame belongs to. This table only includes the main parts of the structure so items such as the energy system are not included.

18.2. Production Process

This section explains the different steps taken during the production of the aircraft until delivery to the customer. It starts with laying out the different manufacturing techniques employed to manufacture parts and then the assembly process of these parts is explained. The final part of this section is about the integration and testing of the aircraft before delivery.

18.2.1. Manufacturing and Ordering

All individual parts of the aircraft have to be manufactured either at the factory itself in the machine shop or at factories elsewhere and then transported to the factory where they are stored until needed for assembly. This subsection discusses the manufacturing processes used for different parts of the aircraft.

Aluminium Components

The stringers and spars used in the wingbox are generic profiles that are extruded and then cut to length. This is a very cheap production process and these parts are readily available from manufacturers.

The ribs have more complex shapes with flanged edges and holes. These holes are punched in the sheet metal first and sharp edges are removed. After this, the sheet metal is rubber-formed in the machine shop which is a common manufacturing technique in the aerospace industry due to the relatively low number of parts made.

The skin of the wings (except for the leading edge curves) is shaped by stretch forming it over a mould. The leading edges of the wings and the cockpit are made of GLARE because of its excellent damage tolerance. Birdstrikes are a serious issue with emergency aircraft that fly in urban environments according to the pilot consulted by the team and therefore an airframe that can safely withstand impacts in places where they are common is important. Manufacturing parts from GLARE is difficult because the glass fibers have a small failure strain meaning that forming is almost impossible. Machining is also not possible due to the abrasive nature of the glass fibers which damage the tooling. Therefore a lay-up technique is used which allows for the desired shapes to be manufactured [50].

Titanium Components

The titanium components are produced by milling them out of large blocks of titanium, followed by heat treatments to even out residual stresses. Then the material is treated with corrosion resistant materials.

CFRP Components

Tape laying over a mould is used to produce the large CFRP structures which allows for integration of many structural reinforcements directly into the structure without any additional material for joining required. Stringers can be adhesive bonded onto the shells and afterwards the entire structure is cured in an autoclave. The long booms of the tail section are produced through filament winding.

The CFRP components that will directly face the outside environment must be further processed to provide sufficient electrical conductivity. The reason for this is that when a lightning strike hits the aircraft, a current of up to 200.000 Amps has to be discharged to the electrical ground to prevent damage. To achieve this conductivity, a metal mesh is placed over the CFRP parts with a thin layer of glass fiber composite in between

the two to prevent current flow as well as galvanic corrosion. An adhesive film is applied over the metal mesh to smoothen the (aerodynamic) surface again, on top of which the paint can be applied¹.

Plexiglass Windows

Poly(methyl methacrylate) or Plexiglass is produced through cell-casting the raw material into a mould. Afterwards the material toughness can be improved through rubber-toughening which makes this an excellent material for the windows in the cockpit. The current EC135 also uses this material for its windows according to the pilot.

Propeller Blades

The propeller blades have their own production method description due to the complicated structure and different materials used together. First, the spar of the blade is produced through moulding of carbon fibre filament layers impregnated by a thermoset resin. The rear part of the blade is made of a lightweight cellular material which is moulded into the right shape. To combine the two they are covered by an envelope of fibres pre-impregnated with polymerisable synthetic resin. Finally the machined titanium erosion protection devices are adhesive bonded to the leading edge of the blades [15].

18.2.2. Assembly

After the individual parts are produced and checked for any defects they are assembled into subassemblies. The wing structure is created by joining stringers, skin panels, spars, GLARE parts and ribs together using rivets [50]. The large doors are reinforced with frames and stringers to account for the concentrated loads occurring due to the missing material in the door itself. These additional components will be adhesive bonded and the bonds are inspected using non-destructive testing to ensure a reliable connection. The cockpit section are constructed in similar fashion as the main door section with reinforcements around the large windows that are adhesive bonded to the outer shell. The entire fuselage is then assembled as one large composite structure.

To connect the wings to the fuselage a strong and compact part is used to join the aluminium and CFRP structures. The choice of titanium for this part is based on avoidance of galvanic corrosion. When materials of different electrical potentials are connected to each other and an electrolyte (such as water) is present, corrosion occurs which deteriorates the mechanical properties of the metal. Besides this, the CFRP suffers from galvanic blistering, the formation of hydrogen bubbles within the material due to the chemical processes related to reaction taking place. To avoid this issue, titanium is used as a barrier between the two materials. Titanium does not react with any of the two by means of such a reaction and is therefore safe to use as a barrier². The titanium connection bracket is bonded to the CFRP fuselage section while the wings themselves are bolted together with the connection bracket. This allows for more efficient storage options with wings detached and increased maintainability.

Once the wing is connected to the frame, the tail is added to the structure. Then the titanium landing gear can be bolted to the CFRP frame by sandwiching the CFRP in between titanium connection plates. This way there is no large point load applied to the composite frame. At this stage the entire load-carrying airframe is built and the integration phase can begin. [picture of how this works.. maybe a bunch of pictures to show how it all works]

18.2.3. Integration

The propeller, motor and folding mechanism form one subassembly together. This subassembly will be integrated in the main wing structure and on the booms in the front of the aircraft. It is helpful to assemble and install this as a single unit because this gives workers full access to all small parts of the subassembly.

The wiring for electronics, avionics, sensors, antenna's and control system is installed in the airframe before adding more components now because there is still space to access all parts where wiring needs to be

¹<https://www.sciencedirect.com/topics/engineering/conductive-filler> [accessed 2019-06-20]

²<https://www.corrosionpedia.com/galvanic-corrosion-of-metals-connected-to-carbon-fiber-reinforced-polymers/2/1556> [accessed 2019-06-19]

that are filled up with interior panels later. After this, the windows are glued in place using cyanoacrylate (superglue) which works very well with plexiglass.

The control surfaces are installed and connected to their hinges and actuators. The actuator wiring is connected to the flight control system. After this wiring is done the energy system cabling, radiators, refuelling system and other equipment that is positioned outside of the cabin is installed. Then the interior is installed within the load-carrying airframe. This interior is the only part of the aircraft that passengers will interact with and turns the oval floor into a flat floor that allows for mounting of chairs and rails. Once the interior structure is installed the final parts of the energy system can be added and the first power-up testing can be done. During these tests all electronic devices onboard of the aircraft are verified to be in working condition, although their full performance can only be tested during the test-flights.

If everything is working properly, the final interior components are added such as the seats, cockpit interior and communications hardware. Once the aircraft has passed quality control it will be flown to a different facility that specialises in fitting aircraft with medical equipment depending on customer requirements. This is the type of work that is not covered by the aircraft manufacturer but the customer will do themselves.

18.3. Labour Hours and Learning Curve

An initial estimate for the labour hours is made based on several data sources. First of all the parts that will be ordered from outside manufacturers have to be excluded from the labour hours done by the workers in the factory. The labour hours required by factory staff is the sum of part production work in the factory's shop and the total man-hours required to assemble and test the aircraft. The estimated number of man-hours required is between 16 and 22 hours per pound of aircraft weight for the first aircraft in the series based on internal research at aircraft manufacturer Embraer. They also report that the learning curve slope is generally around 80%, meaning that consecutive units require 80% less time than the previous unit [17]. The required man-hours per pound is estimated to be 16 and is most likely lower due to modern manufacturing techniques and automation in certain parts of the factory such as automated drilling and riveting. With a series length similar to that of the EC135, the learning curve looks as shown in Figure 18.2. It can be seen that the initial effort is well over 140.000 man-hours and production efficiency increases rapidly.

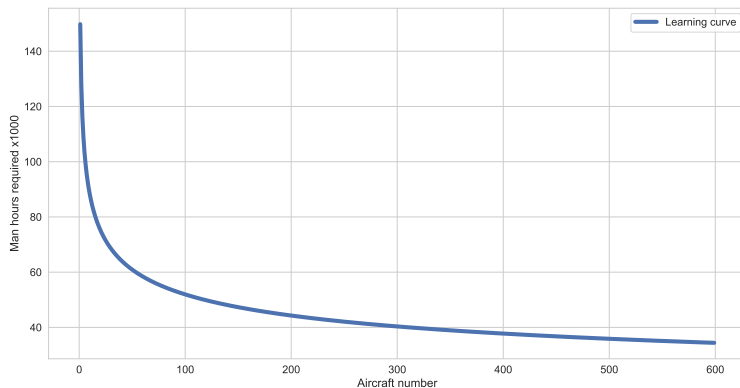


Figure 18.2: Learning curve.

18.4. Requirement Compliance & Feasibility

The requirements regarding the production methods are all satisfied. The production plan is feasible because all manufacturing techniques used are already widely implemented in industry today.

Table 18.2: Overview of requirements regarding the manufacturing phase.

Code Identifier	Requirement	Type	Verification	Compliance
EVTOL-GNMF-171	All designed parts shall be manufacturable with existing manufacturing techniques	Regular	Inspection	
EVTOL-GNMF-172	All designed parts shall allow for assembly with existing assembly techniques	Regular	Inspection	

Aircraft Interface Definition

In this chapter the aircraft interface will be described using of four different diagrams. These include the hardware diagram showing the components of the aircraft and their interactions, the software diagram showing the working principle of the aircraft, the communication flow of data through the system, and finally the data handling block diagram illustrating the components of the data handling system of the aircraft.

19.1. Hardware Interface

The hardware diagram, which shows all the components of the aircraft and their interactions, is illustrated in Figure 19.1. Each block that is included in the diagram represents a type of component. This is illustrated by using different colours. The energy system is in green, the power distribution unit is in red, all sensors are in yellow, the flight controls are in blue and the lift producing components including the Electronic Speed Controllers (ESC) are in purple. These main components are further explained below and can be seen in Figure 19.1.

1. The battery and fuel cell system (explained in section 6.4), are included in the energy source. This system generates and stores the power for the aircraft.
2. The power distribution unit converts all the powers to the other main components of the aircraft.
3. The sensors provide the pilot and onboard computer information to safely control the aircraft. The sensors include an Inertial Measurement Unit (IMU), which itself consist of an accelerometer, a gyroscope, a magnetometer and a barometer, ground communication which is also further explained in section 19.3, a pitot tube for airspeed measurements, and a navigation system using GPS.
4. The flight controls enable the pilot to safely control the aircraft. This component consist of the throttle, cyclic stick, pedals, collective stick and the auto pilot.
5. The lift producing elements consist of the high lift devices and the Electronic Speed Controllers (ESC) which drives the propellers.

19.2. Software Interface

The software interface, which can be seen in Figure 19.2, concerns the software components that are working onboard of the aircraft to fly it. The check flags block makes sure that if any system error was logged during the last flight or any problems with subsystems are detected, the aircraft mentions this to the pilot and does not allow take-off. Furthermore the pilot flight mode choices are shown. The pilot can choose two vertical flight modes and one horizontal flight mode. The flight controller will control the vertical flight system or the horizontal flight actuators based on selected flight mode.

19.3. Communication Flow

The communication flow diagram graphically displays all external communications between the aircraft and ground control. The goal of the diagram is to understand what equipment is needed on board to communicate with all necessary external services and workers to safely and efficiently operate. The diagram partially displays the operational structure and how the medical team in the aircraft communicates with the outside world. The diagram is shown in Figure 19.3.

The emergency and secret services use the C2000 network in the Netherlands. C2000 delivers safe and reliable encrypted communications between all emergency workers with an Ultra High Frequency (UHF) of 385 MHz. C2000 operates at a different frequency than the ATC tower, which operates at a Very High Frequency (VHF) of 121.5 MHz, and the GPS satellites, which operate at a Ultra High Frequency (UHF) of

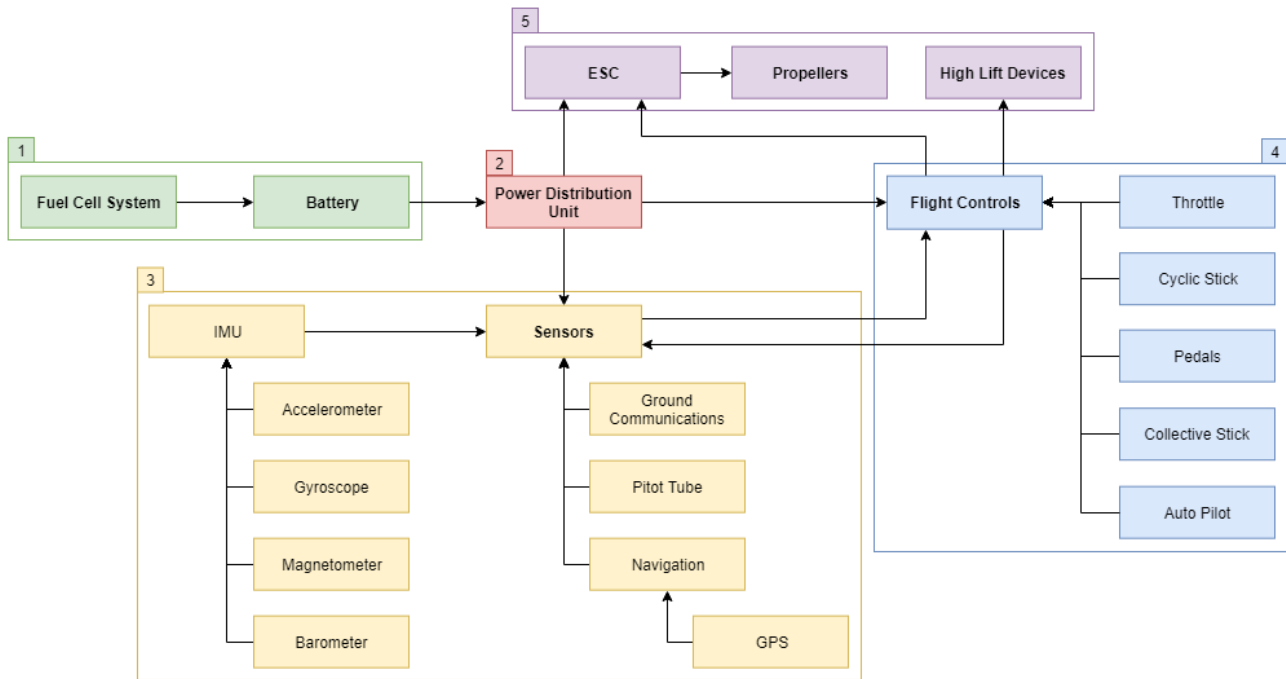


Figure 19.1: Hardware Diagram.

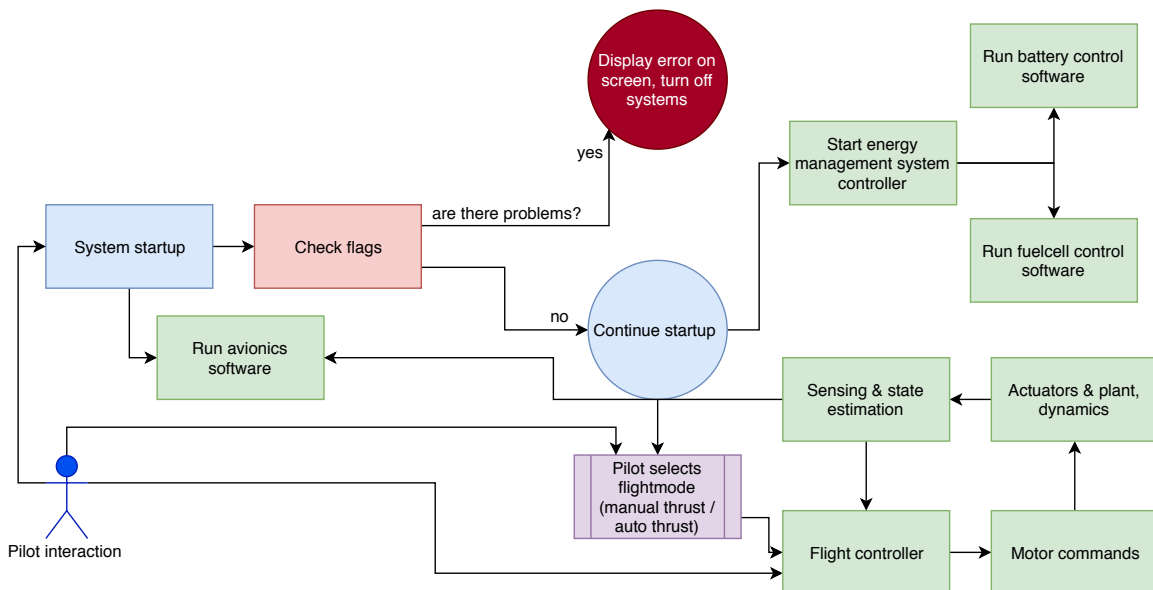


Figure 19.2: Software diagram for the main aircraft systems.

1575.42 MHz, so different antenna's are needed on board of the aircraft. The data handling system has to be sized such that all data streams can be processed.

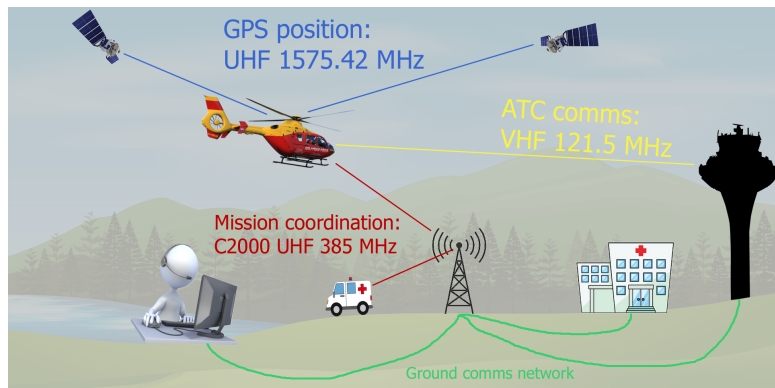


Figure 19.3: Communication flow diagram.

19.4. Data Handling

The data handling diagram illustrates the way data is used in the aircraft and it could give insights on what systems are needed. The diagram is shown in Figure 19.4. As can be seen the Inertial Measurement Unit (IMU) is responsible for both the attitude indicator and navigational display in the cockpit. For the attitude control it uses its gyroscope and magnetometer and for the navigational display it uses its accelerometer. Furthermore, the Automatic Dependent Surveillance-Broadcast (ADS-B) and GPS are necessary for the navigational display. The ADS-B system will send out signals about its position and possibly its registration and flight number, speed, height, direction and intentions to other nearby aircraft. This way a clear picture of the airspace is visible. Lastly, the GPS is needed for navigation but also to work with the ADS-B as this is 'Dependent' on data from the aircraft's navigational data.

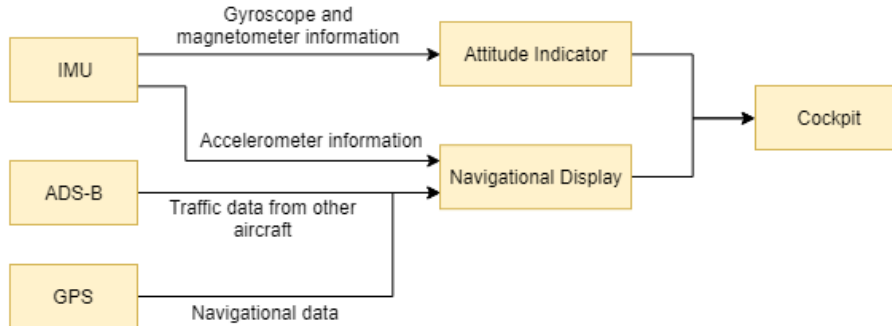


Figure 19.4: Data Handling Diagram.

Cost Estimate and Market Analysis

20.1. Cost Estimate

To estimate the cost of the aircraft, the entire aircraft has to be taken apart in different subsystems. The cost analysis is divided into three different categories. Firstly the development cost consisting of engineering cost, designing and building tools, support costs, scaled tests and quality control. Secondly the cost of production is assessed. Some subsystems can be purchased from a manufacturer, some subsystems have to be specially designed for the H₂ERO. For these subsystems, manufacturing tools have to be designed and build. Also the manufacturing of the aircraft itself is costly. After development and producing cost, the operating cost is addressed in terms of fuel cost, electricity, maintenance, insurance and overhaul cost.

Inflation

Healthy economies always endure price inflation, meaning that the value of the used currency deteriorates. Historically the golden zone for the inflation rate is between 1 and 3 percent, meaning that services and goods go up in value by 1 to 3 percent. Right now the price inflation of the dollar is 1.9% and is estimated to rise due to politic economic tension between the United States and China. The forecasts roughly state the same estimate of 2.24%.¹ As a first price indication this will be sufficient. It is assumed that the aircraft can be build and tested in 10 years. So all expenses in these years have to be multiplied by their corresponding factor. For the euro it is a bit less. According to the European Central Bank the current rate of inflation (June 2019) is 1.4 %². The forecasts predict 1.8% for the coming years. In the table below the expense multipliers are listed.

Table 20.1: Design Costs

	2019	2020	2021	2022	2023	2024	2025	2026	2027	2028
Euro \euro	1.000	1.018	1.036	1.055	1.074	1.093	1.113	1.133	1.153	1.174
Dollar \$	1.000	1.022	1.044	1.067	1.091	1.115	1.139	1.165	1.190	1.216

20.2. Development Cost

Under development cost one can find everything related to research, design and testing costs. Basically everything up until the factory can start their jobs. The costs lie mostly in engineering salaries, tool development, support cost (everything related to but not about the production of the aircraft such as administrative cost, HR, logistics etc.), testing costs of all the subsystems and scale models and finally the quality control. Firstly a couple of parameters have to be set. According to the method by Gudmundsson [18] these parameters are the structural air frame weight, the maximum level airspeed and number of produced aircraft. Each expense can be estimated with these base factors and a couple of specific factors, which will become clear in a moment. Then a time slot is needed. As will be discussed in more depth in the market analysis, a time slot of 15 years until operation is given. Therefore, to create some margin, the process is designed to take 12 years.

The salaries of the engineers are one of the highest expenses of the entire project. The man hours are dependant on frame weight, maximum speed and number of aircraft along with factors that take a complex

¹<https://www.statista.com/statistics/244983/projected-inflation-rate-in-the-united-states/> [accessed 2019-06-23]

²[https://www.ecb.europa.eu/stats/ecb\\$_\\$surveys/survey\\$_\\$of\\$_\\$professional\\$_\\$forecasters/html/table\\$_\\$hist\\$_\\$hicp.en.html](https://www.ecb.europa.eu/stats/ecb$_$surveys/survey$_$of$_$professional$_$forecasters/html/table$_$hist$_$hicp.en.html) [accessed 2019-06-23]

flap system (F_{CF}), pressurised fuselage (F_{PRESS}) and weight fraction of composites in the air frame in to account(F_{COMP}). The values of these are given. For example there are no flaps on the H₂ERO since VTOL doesn't require it and because of the mission profile, no pressurised cabin is needed. Therefore both of these factor become 1. F_{comp} is determined to be 0.5 times the weight fraction of the structure made of composite plus 1. Therefore adding to the engineering cost.

$$H_{ENG} = 0.0396 \cdot W_{airframe}^{0.791} \cdot V_H^{1.526} \cdot N^{0.183} \cdot F_{CF} \cdot F_{COMP} \cdot F_{PRESS} \quad (20.1)$$

Knowing the man hours needed, the man hours in a year and the development time, one can easily calculate the amount of engineers needed. With Equation 20.2 each year the salary of the engineers(R_{ENG}) is multiplied by the inflation rate(INF), which can be found in Table 20.1.

$$Cost_{ENG} = 2.0969 \cdot H_{ENG} \cdot R_{ENG} \cdot INF \quad (20.2)$$

The same is done for the tool design and developers. With new factor Q_m , the production rate in units per month. This comes down to project length in months divided by number of aircraft. F_{TAPER} is equal to 1 for tapered aircraft.

$$H_{TOOL} = 1.0032 \cdot W_{airframe}^{0.764} \cdot V_H^{0.899} \cdot N^{0.178} \cdot Q_m^{0.066} \cdot F_{TAPER} \cdot F_{CF} \cdot F_{COMP} \cdot F_{PRESS} \quad (20.3)$$

$$Cost_{TOOL} = 2.0969 \cdot H_{TOOL} \cdot R_{TOOL} \cdot INF \quad (20.4)$$

Support cost is given by Equation 20.5. N_p stands for the number of prototypes used, which is chosen to be five.

$$Cost_{SUPPORT} = 0.06458 \cdot W_{airframe}^{0.873} \cdot V_H^{1.89} \cdot N_p^{0.346} \cdot INF \cdot F_{CF} \cdot F_{COMP} \cdot F_{PRESS} \quad (20.5)$$

The cost of the different tests used to validate the design is given with Equation 20.6.

$$Cost_{test} = 0.009646 \cdot W_{airframe}^{1.16} \cdot V_H^{1.3718} \cdot N_p^{1.281} \cdot INF \quad (20.6)$$

The cost for quality control is found with Equation 20.7 in which $Cost_{MAN}$ stands for the manufacturing costs.

$$Cost_{QC} = 0.13 \cdot Cost_{MAN} \cdot F_{COMP} \quad (20.7)$$

In total this results in the following table.

Engineering Cost	Tool Development	Validation Tests	Quality Control	Support Cost	Total Design Cost
2610 k	3317 k	2854 k	368 k	1067 k	10.2 M

20.3. Product cost

By product cost is meant the cost of producing aircraft once the research and development is finished. It consist of the materials used, the manufacturing of the structure, the avionics, the five electric motors, the 12 motor controllers, a cooling system, battery, a fuel cell, the five rotors, cabling and assembly. This chapter will assess these expenses in this order.

Firstly for the structures an equation is found for the cost [18]. Together with the required manufacturing man hours and the manufacturing costs, it is possible to estimate the structures cost.

$$H_{ENG} = 0.0396 \cdot W_{airframe}^{0.791} \cdot V_H^{1.526} \cdot N^{0.183} \cdot F_{CF} \cdot F_{COMP} \cdot F_{PRESS} \quad (20.8)$$

$$H_{MAN} = 9.6613 \cdot W_{airframe}^{0.74} \cdot V_H^{0.543} \cdot N^{0.524} \cdot F_{COMP} \cdot F_{PRESS} \quad (20.9)$$

$$Cost_{MAN} = 2.0969 \cdot H_{MAN} \cdot R_{MAN} \cdot INF \quad (20.10)$$

The avionics are found to be 15000 dollars and can directly be added to the analysis [18]. The entire propulsive system has been chosen to be bought from electric motor company *MagniX*. It has been decided that for each VTOL rotor a MagniX250 motor is needed and one MagniX500 motor is required for the forward propulsion. In order to manage the thrust 12 MagniDrive Motor controllers are needed. Yet the company isn't willing to share the price of such an order. Therefore an estimation has to be made. The following linear regression model of NASA's Cost Estimating Handbook is used for the propulsion system, battery, hydrogen tank, rotors, wiring and assembly.

Linear Regression Model for Subsystem Cost Estimation

In order to determine the cost of the to be designed subsystems, a parametric cost estimation is done. The method is taken from NASA's Cost Estimation Handbook part C [34]. For each sub(sub)system similar sub(sub)systems have to be found, which create a reliable data set to base the cost on. Also a main performance parameter has to be determined in order to scale the subsystems. For example the hydrogen tank will more likely go up in cost with increasing volume as opposed to mass. In Table 20.2 all the estimated subsystems and their main parameter are listed.

Subsystem	Propulsion system	Battery	H^2 Tank	Rotors	Wiring	assembly
Scaling parameter	Output Power	kWh/kg	Volume	Disk Loading	Total cost	MTOW

Table 20.2: Cost estimation parameter Table

In order to create the most efficient linear estimate of the data set, two special formula are used to set up the right $ax + b$ the following formula are used:

$$a = \frac{n \sum XY - (\sum X)(\sum Y)}{n \sum X^2 - (\sum X)^2} \quad (20.11)$$

$$b = \frac{\sum Y - a \cdot \sum X}{n} \quad (20.12)$$

With this linear estimate the cost of most subsystem can be found. The values found of in multiple manners can be found in the table underneath. When possible the R^2 value of the regression is placed underneath. It can be seen that the propulsive system and the structure are the main costs. These complex systems are

Propulsion System	Structures	H_2 Tank	Rotors	Wiring	Assembly	Battery	Total
1900 k	2815	150	65 k	861 k	80 k	15 k	6.54 M
0.65	N/A	0.76	0.91	N/A	N/A	0.89	N/A

also the main cost in other aircraft and on top of that, this is where the H_2 ERO really innovates with respect to current aircraft. Hydrogen aircraft have yet to be developed in at this scale and two separate propulsion systems for VTOL and cruise was not expected to be cheap. As for the structures it is believed to be quite costly provide enough space for this large power plant and to mount all five rotors to the fuselage in a safe manner. Due to these complexities is very hard to predict the costs. The design would benefit from a more comparable data and more detailed subsubsystem analysis.

The cost can be reduced by developing technology in the hydrogen aircraft industry. Also it has to be taken into account that the product analysis is done for five aircraft over the course of 12 years. The production cost greatly reduces with increasing productions. Tools become relatively cheaper and craftsman get more experience with the construction, which has the potential to save lots of time and money.

20.4. Operation Cost

The operational cost consists of maintenance costs, fuel cost, insurance cost and overhaul cost. [18] Maintenance cost are dependant on maintenance to flight hours ratio, the flight hours and the mechanics salary. The average flight takes 15 minutes and the aircraft takes off 10 times a day. The Lifeliners currently have to be available 98% of the time. This gives the yearly flight hours. Finding the right flight hours to maintenance ratio consist of multiple checks which all add to or relieve maintenance cost. Internal fuel tank, complex

flap system, accessibility of the motor, retractable landing gear and VFR and IFR radio are all factors that contribute. It is found that for every thousand flight hours, 250 hours of maintenance are necessary. This results in the fact that 2.6% of all hours in a year the aircraft will be under maintenance, so an availability of 97.4%. If this is unacceptable the maintenance cost hourly will have to be doubled in order to hire 2 mechanics to speed up the process.

2.6 % unavailability	12 500 Dollar/Year
2 % unavailability	19 250 Dollar/Year

Table 20.3: Maintenance cost as a result of availability

Fuel cost is the largest operating cost. With a cost of 8.29 dollar per kg of liquid hydrogen³ it is much higher than kerosene of 0.61 dollar per kg⁴. This fuel price of hydrogen is found to be accurate given that a concentration solar power plant is used to produce the LH₂. These types of power plants are hard to realise in the Netherlands. It is assumed that even though this technology might not be available, the technology available 15 years from now⁵ will have similar cost reducing effect. So this price will be used for this preliminary estimate. The aircraft consumes 35 kg/hour. The battery will be mostly charge from the hydrogen fuel cell, but in between missions the aircraft will be plugged in to save hydrogen. It is assumed that on a daily basis the battery will not have to be recharged entirely since the battery will be nearly full every time the aircraft lands. It is therefore assumed that on average one tenth of the entire battery capacity is added in this passive phase on a daily basis. One kWh cost 20 cents on average in the Netherlands. Overhauls have to be done every x flight hours and are set by the motor manufacturer. During an overhaul the motor is removed, disassembled and cleaned. The overhaul effort of an electric motor is probably lower since it doesn't make use of chemical reactions and has less moving parts, but because of lack of cost estimation methods the same value is used. This makes use of an average of 5 dollars per engine per flight hour[18]. Insurance is estimated with a yearly interest rate of 1.5% of the aircraft value and an administration fee of 500 dollar [18].

Hydrogen	Battery	Maintenance	Overhaul	Insurance	Total Operational Cost
261.4 k	229 k	125.5 k	22.8 k	89 k	624.4 k

20.5. Market Analysis

Now that the product has been realised it possible to say something about its utility in the market. First and foremost, the H₂ERO aircraft is an emergency aircraft designed to operate in the Netherlands. Therefore this chapter will firstly touch upon the current emergency helicopter business. Then it will elaborate on a PESTEL analysis. This analysis sketches the stance of the H₂ERO's within the macro economy from a Political, Economical, Social, Technological, Environmental and Legal point of view. Finally, since the H₂ERO currently has one opponent in the market, the EC-135, an extensive comparison will be made between the old EC-135 and the new H₂ERO.

The current situation in the Netherlands as explained by the Lifeliner Station 2 of the MAA-ANWB in Rotterdam is as follows. The Netherlands government subsidises four large hospitals in the country to enable them to hire an aerial medical service. Together they host a tender for which multiple companies apply. Each operating company chooses their desired aircraft and operation policy for the job. The large hospitals together decide which company is most capable and affordable. The winning company gets to sign a 15 year contract. This contract contains the operating rights of the four zones the Netherlands are divided up into. Each zone makes use of one emergency aircraft and nationally there is one spare aircraft.

Just recently the latest tender has taken place and the winner was the "Algemene Nederlandse Wielrenners Bond" or ANWB, using Airbus' EC-135 as their vehicle of choice. For this market entry to succeed, the H₂ERO

³<https://clipair.epfl.ch/wp-content/uploads/2018/08/FullReportMA3.pdf> [accessed 2019-6-23]

⁴<https://www.iata.org/publications/economics/fuel-monitor/Pages/index.aspx> [accessed 2019-6-23]

⁵As discussed earlier the first opportunity to replace the EC-135 will be 15 years from now

team has 15 years to develop and produce the aircraft while convincing the ANWB or rivalling companies that the H₂ERO is the best choice for the task as medical air support vehicle.

20.5.1. PESTEL Analysis

It strengths and weaknesses on macro economic scale can be systematically addressed with a PESTEL analysis. This tool provides certainty on the completeness of this analysis. The six aspects will now be addressed in the of the acronym.

Political

An important aspect of the design process is the fact that building aircraft this large is quiet an operation. This will create jobs in the locations where parts are produced. Politicians might want to attract parts of the production or assembly to their districts. Therefore politicians often feel the incentive to alter policies regarding production in order to attract the production of an aircraft. This could reduce the production cost. What might become an opportunity is that politicians get pressured by the public into restricting airbases even more when it comes to noise. This will make a quiet (emergency) aircraft even more relevant.

Economical

Looking at the economic environment for this design, it can be split into trends in electric or hydrogen driven vehicles, eVTOL aircraft and emergency aircraft.

It is commonly known that the electric vehicle market is in a monumental lift. This growth is represented in the development of eVTOL aircraft. This suggests that the market is looking for ways to use eVTOL technology. Some research suggests that emergency aircraft are losing cost effectiveness in densely populated areas. Due to the high hospital density and good infrastructure in the Netherlands, it could be that the time it takes to take off is too long to compensate with the great speed. Making ambulances in some cases more cost effective [?]. Other research contradict this conclusion. More consistent research has to be done, using methods that take population density and infrastructure into account. It can be concluded however that the advantage of emergency aircraft is larger in countries like Australia and Norway.

Social

The market is getting more and more sustainable. Businesses are pursuing a green perception by the public. Therefore the government or emergency aircraft operating companies could boost that image vastly with such a eye catching grand piece of equipment. It sets a good and effective example if the health care sector is linked to a high tech, quiet, zero emission aircraft that roams the skies for 10 times a day to save lives.

Technological

The main aspect that is important for the technological factor of this analysis is the use of a new energy source in the form of hydrogen. This technology transition can boost the air transportation business. Furthermore, the H₂ERO can be used for multiple intentions besides the emergency aircraft option. Therefore, the H₂ERO (emergency) aircraft will be more relevant.

Environmental

Nowadays, more and more attention is brought to environmentally friendly transportation vehicles. The car industry is already very far in this transition, so air transportation could not be excluded from this transition. As the new design of the emergency aircraft will be electric, this will have a serious positive effect on the environment and therefore the eVTOL will be more relevant. Important is to keep in mind that the energy used for electrolysis has to be green in order to reduce the carbon emission of the operation.

Legal

The legal part of this analysis will mostly concern noise reduction and safety. The purpose of the H₂ERO is mainly about the reduction of noise because noise is becoming more and more of a problem. Therefore, the new aircraft will go in the right direction concerning these noise restrictions. Legal restrictions contain the allowed noise emission of the airbases, the noise threshold the aircraft may exert and the quantity carbon

dioxide it may emit. The exact quantities mostly depend on weight, passenger number and configuration. During production there will be a lot of regulations regarding producing, trading, importing, assembling etc. This is, however, beyond the scope of this project.

20.5.2. Comparison

Because the goal of the design is to replace the EC135, a comparison between the H₂ERO and EC135 is done. The three main categories in which they can be compared are cost, performance and sustainability. In 15 years these two aircraft will compete for the position of the emergency aircraft of the Netherlands.

Comparing the cost is the most obvious and direct drive criterion of the three. Using the same estimation method on the operation costs it is concluded that the H₂ERO costs about 525 thousand dollars per year while the EC-135 only costs 178 thousand per year. As for total aircraft cost for a new trauma helicopter one pays 4.2 million dollars⁶. The H₂ERO cost is previously calculated and comes in at 6.54 million dollars. Meaning that for now, with the current estimation, the costs of using an EC-135 are significantly lower than the H₂ERO. This is mainly due to the big batter

For sustainability there also is a clear winner which is elaborated on in chapter 23. The H₂ERO doesn't have direct emissions, the noise is by design 25% less and the ability to operate solely on renewable energy source are valued high. The H₂ERO loses sustainability point on operation cost and technology readiness level. The advantage of noise reduction is seen in the number of flights possible and the reachable area's. Hydrogen production cost is expected to further decrease as the technologies used mature.

20.6. Requirement Compliance & Feasibility Analysis

Table 20.4: Overview of requirements regarding cost analysis.

Code Identifier	Requirement	Type	Verification	Compliance
EVTOL-COST-001	The total costs of the production of one aircraft shall not exceed €4.000.000,-	Regular	Demonstration	
EVTOL-COST-002	The total costs for the structures department shall not exceed 35 % of the total maximum costs	Regular	Demonstration	
EVTOL-COST-004	The total costs for the electronics department shall not exceed 20 % of the total maximum costs	Regular	Demonstration	

It can be seen that the total product cost requirement is far from met. The structures can be a good first start to reduce the cost. The bulkiness of the design and the embedded rotors drive up the cost. The main cost excess is the propulsion system. Two separate propulsion systems will always cost more than one. The biggest contributor to the cost overshoot however is the hydrogen power plant. With relatively low technology readiness level and high volume compared to transitional power sources, it greatly drives up the cost. More research has to be done on this technology to reduce the cost. A more detailed structural and propulsive analysis has to be done in order to estimate the total cost more accurately.

⁶https://www.helicopterinvestor.com/articles/eurocopter_ec135_buyers_guide/ [Accessed 2019-06-24], [Data from 2009-06-20]

Risk Management

At the beginning of each project a set up is done of the schedule, cost and technical performance that is expected of the final product. Regardless of the amount of time and work that is invested in determining and perfecting this plan, changes and unexpected events are inevitable. To minimise the effect of these unexpected events, the possible risks that come with these events can be predetermined. This helps understand which risks should be monitored more than others and for which events some preparational measures should be taken.

This chapter is split into the risk analysis of the technical performance, schedule and cost of the project. First, in each section, the risks are identified. After this, a risk map is created in which an overview is created of the risks. In this risk map one can determine the risks that should be monitored more significantly than others. For the most significant risks a risk mitigation plan will be set up.

21.1. Technical Risk Identification Process

At the start of the project a risk manager was assigned. The task of the risk manager has been to identify, discuss, evaluate and continuously alter or take action regarding possible risks. This entire process has been done in co-operation with the team manager to help ensure his overview of the entire team is continuously up to date. The end responsibility is held with the risk manager. As identifying and mitigating risks are a live process, weekly meetings were held to discuss alterations. This helped obtain the required level of design to ensure customer satisfaction, to decrease the possibility of schedule delays and to decrease the chance of going over budget.

21.2. Technical Performance Risks

21.2.1. Identification

The risks that have been identified regarding the technical performance are tabulated in Table 21.1.

21.2.2. Risk Map

In Figure 21.1, the risk map is shown which provides an overview of the level of significance of each risk regarding technical performance. Green identifies a risk as acceptable, orange indicates a risk that requires more extensive monitoring throughout and red requires more research and a mitigation plan.

For this phase, no risks have been identified that require an extensive risk mitigation. This is due to the fact that most risks have been identified as having an unlikely probability of occurrence. The risks that have a severity level that is catastrophic are risks for which a deeper level of design has been performed during the subsystem design. Hence, although being catastrophic if it happens, these risks are unlikely to happen as these were the main focus of the designing phase.

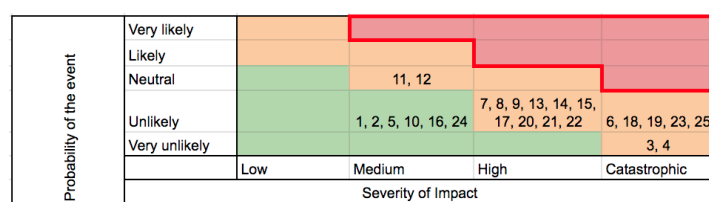


Figure 21.1: Risk map before mitigation of the technical performance risks.

Table 21.1: Technical risks activity regarding the technical performance of the project.

ID	Risk Explanation	Subsystem	Occurrence Probability	Severity
1	One propeller system fails	Propulsion	Unlikely	Medium
2	One electromotor fails	Propulsion	Unlikely	Medium
3	Two or more engines fail	Propulsion	Very Unlikely	Catastrophic
4	Two or more motors fail	Propulsion	Very Unlikely	Catastrophic
5	Engine performance sensors read faulty measurements	Propulsion	Unlikely	Medium
6	Overall lift from propellers is insufficient for VTOL	Propulsion	Unlikely	Catastrophic
7	Fuel tank failure	Fuel system	Unlikely	High
8	Fuel pump failure	Fuel system	Unlikely	High
9	Fuel system sensors read faulty measurements	Fuel system	Unlikely	High
10	Fuel storage shows fatigue stresses	Fuel system	Unlikely	Medium
11	Batteries are fatigued	Fuel system	Neutral	Medium
12	State of Charge level below 50%	Fuel system	Neutral	Medium
13	Wiring of aircraft is short circuited	Electrical	Unlikely	High
14	Engine door does not close after transition	Aerodynamics	Unlikely	High
15	Engine door does not open during approach	Aerodynamics	Unlikely	High
16	Control surface does not return to required angle	Aerodynamics	Unlikely	Medium
17	Bird strike	Aerodynamics, Structural	Unlikely	High
18	Wing surface area insufficient to ensure lift during cruise	Aerodynamics	Unlikely	Catastrophic
19	Control system fails	Stability & Control	Unlikely	Catastrophic
20	Control surface fails	Stability & Control	Unlikely	High
21	Material fatigue	Structures	Unlikely	High
22	Corrosion	Structures	Unlikely	High
23	Load of magnitude greater than elastic yield range	Structures	Unlikely	Catastrophic
24	Avionics system fails resulting in fly on sight	Avionics	Unlikely	Medium
25	Noise requirement below expectation	Overall Design	Unlikely	Catastrophic

21.2.3. Mitigation

As explained in subsection 21.2.2 no risks need to be mitigated for at the moment. However, the greater part of the risks have a medium combination of occurrence probability and severity. Hence, these require constant monitoring.

21.3. Schedule Risks

21.3.1. Identification

The risks that have been identified regarding the schedule are tabulated in Table 21.2.

Table 21.2: Technical risks activity regarding the schedule of the project.

ID	Risk Explanation	Risk type	Occurrence Probability	Severity
26	Product material not delivered on time	Schedule	Neutral	High
27	Production delay in main process line in the factory delaying all other processes	Schedule	Neutral	High
28	Unhappy workers resulting in a strike	Schedule	Unlikely	High
29	Final product does not pass validation tests resulting in design revisit and delays	Schedule	Neutral	High
30	Undereducated Employees	Schedule	Unlikely	High

21.3.2. Risk Map

Like for the identified technical performance risks, no immediate mitigation is required for any of the risks regarding the project schedule. Green identifies a risk as acceptable, orange indicates a risk that requires more extensive monitoring throughout and red requires more research and a mitigation plan.

As can be seen, there is no major schedule risk. However, all risks regarding the schedule of the project should be continuously monitored as these can change in short periods of time.

21.3.3. Mitigation

It should be noted that risk number 26 and 27 are risks that are related and dependent on third party organisations. Therefore, it is difficult to interpret their overall risk. Hence, although not considered as a most important risk in the risk map, a mitigation plan will be determined. Good communication with these third



Figure 21.2: Risk map before mitigation of the schedule risks.

parties should be maintained to ensure these risks not occurring. In the event that communication with a supplier becomes more difficult or disappears, immediate action should be taken to possibly consider a different supplier. Also, a mitigation for this problem could be to increase the amount of stock for certain or all parts. However, this does increase the cost so this trade off should be taken into account.

21.4. Cost Risks

21.4.1. Identification

The risks that have been identified regarding the cost of the design are tabulated in Table 21.3.

Table 21.3: Technical risks activity regarding the cost of the project.

ID	Risk Explanation	Risk type	Occurrence Probability	Severity
31	Aircraft cost budget underestimated	Cost	Neutral	High
32	Aircraft mass budget underestimated	Cost	Neutral	High
33	Aircraft power budget underestimated	Cost	Neutral	High
34	Employee wage increases	Cost	Unlikely	High
35	Investor(s) leave(s) project	Cost	Neutral	Catastrophic
36	Schedule delays result in extra costs	Cost	Neutral	High
37	Full scale model does not pass validation tests, redesign required	Cost	Neutral	High

21.4.2. Risk Map

In the figures underneath, the risk map can be seen for the risks regarding costs. Figure 21.3 indicates the risk map before the mitigation plan, whereas Figure 21.4 indicates the risk map after the mitigation plan which is elaborated on in subsection 21.4.3. Green identifies a risk as acceptable, orange indicates a risk that requires more extensive monitoring throughout and red requires more research and a mitigation plan.

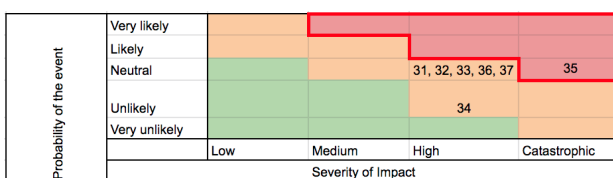


Figure 21.3: Risk map before mitigation of the technical cost risks.

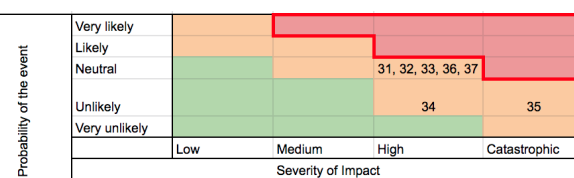


Figure 21.4: Risk map after mitigation of the technical cost risks.

21.4.3. Mitigation

For the cost risks, risk ID 35 in Table 21.3, investor(s) leave(s) project, has been identified as a risk that needs to be mitigated. Without money, there is no research, design and production. Therefore, this risk is identified as catastrophic. However, the risk is considered to be neutral for the occurrence probability. This is because the risk can be mitigated and controlled well. Mainly due to good communication from the design team and its investors. As long as the investors are kept up to date with all of the project changes and general progress there should not be a large consequence. However, once it has been determined that the project idea in general is unfeasible, then this risk could still occur but this seems logical for any project as an unfeasible design will end any project. Therefore, risk ID 35, has been mitigated to unlikely but still catastrophic should it occur. Furthermore, other risks are identified as risks that need to be continuously monitored but no immediate action is required.

RAMS Analysis

The following chapter contains the reliability, availability, maintainability and safety analysis of the H₂ERO, better known as a RAMS analysis. The RAMS analysis indicates the operational performance of the aircraft. These characteristics are also an important indication for customers, stakeholders and users in what to expect when having this aircraft in operation.

The chapter is set up with an analysis in the order of the acronym, RAMS. First, the reliability will be assessed in section 22.1, next, the availability is analysed in section 22.2, following this will be the maintainability in section 22.3 and safety will finalise the chapter in section 22.4.

22.1. Reliability

Starting off with the analysis regarding the reliability of the aircraft with reliability being considered as the degree of consistency of a design meeting its performance standards throughout its life. This, hence, closely relates reliability with the probability of failure for certain components within the aircraft. The strive for the reliability of an aircraft should be close 100% to ensure aircraft satisfaction by users, stakeholders and customers.

The failure modes, which were also described as risks in section 21.2, are shown in Figure 22.1. A failure of any of these subsystems shall effect the reliability of the total aircraft. However, it should be noted that all of these subsystems are designed to last for the operational lifetime of the aircraft keeping in mind certain scheduled maintenance for smaller parts within the subsystems.

Also, an unreliable aircraft does not refer to an aircraft that will crash but it means that the aircraft should not be used until repaired or it should land immediately. For instance, a failure of the control surfaces, due to the two OR statements would result in an unreliable aircraft. However, the aircraft can still land using its VTOL propulsive system.

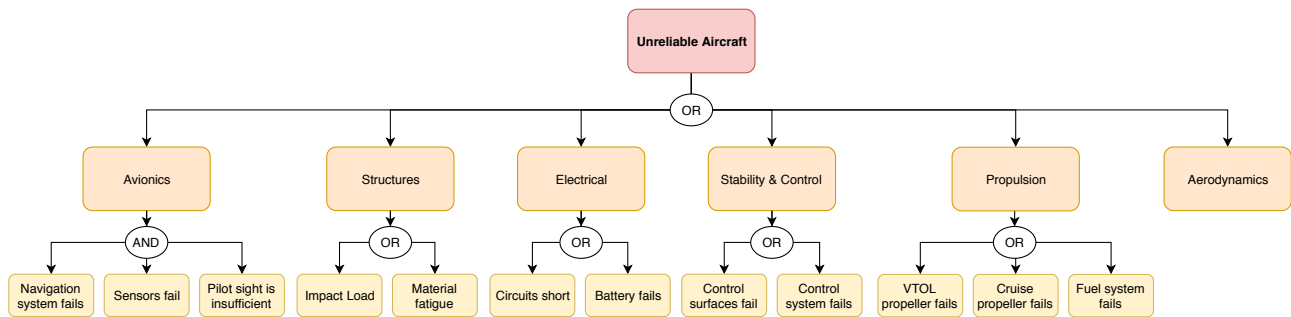


Figure 22.1: Subsystem failure reliability overview.

As mentioned before, all subsystems are designed to last during the entire operational lifetime of the aircraft and a reliability within a few percentages of 100% is strived. However, how is this achieved? Reliability can be continuously improved. For instance, a simple improvement is performing pre- and post-flight checks. A visual inspection can greatly improve the reliability of the structures and control surfaces group by spotting small fragmentations, dents or other irregularities. Furthermore, a good organisational methodology regarding historical data of certain equipment failures can provide a better understanding of each components reliability and optimise maintenance intervals. Also, in flight data can increase reliability by correlating certain data changes with possible maintenance required.

To conclude reliability, it is evident that reliability comes forth from good understanding of the components of the aircraft and maintenance, which will be described in section 22.3.

22.2. Availability

Availability is defined as the percentage of time that the aircraft is deployable. To ensure user, stakeholder and customer satisfaction, the availability of the aircraft should also strive to be within a few percentages of 100%. Factors that influence the availability of the aircraft are scheduled maintenance, unscheduled maintenance, refueling, crew delays, air traffic control influences. The last two factors are not aircraft specific factors but however, do influence the availability. The availability can be determined according to the simple formula presented in Equation 22.1 where the total amount of unavailable time is shown in Equation 22.2.

For the availability of the aircraft, scheduled maintenance is expected to be done every 1440 as will be explained in section 22.3. Unscheduled maintenance is taken as an average of 1944. The refueling station will be placed at the emergency control station where the aircraft is situated. To go from completely empty to full is expected to take a maximum of 10 minutes. For the missions that the aircraft will perform it is required that the aircraft is always fully fuelled. Hence, performing 10 missions every 24 hours, this will take 100 minutes per day of the availability of the aircraft. Regarding crew delays and air traffic control influences the availability is expected to be 0 minutes. This is because the crew is situated in a room next to the aircraft 24 hours, 7 days a week and the aircraft gets priority over other aircraft at the airport for take off and landing.

$$\text{Availability} = \frac{T_{\text{year}} - T_{\text{Unavailable}}}{T_{\text{year}}} \cdot 100\% \quad (22.1)$$

$$T_{\text{unavailable}} = T_{\text{Sch.Main}} + T_{\text{Unsch.Main}} + T_{\text{Fuel}} + T_{\text{Crew Delay}} + T_{\text{ATC}} \quad (22.2)$$

$$T_{\text{unavailable}} = 1400 + 1944 + 36500 + 0 + 0 = 39844$$

$$\text{Availability} = \frac{365 \cdot 24 \cdot 60 - 39844}{365 \cdot 24 \cdot 60} \cdot 100\% = 92.4\%$$

Hence, the aircraft is available for 92.4% of the time.

22.3. Maintainability

To ensure reliability, availability and safety, the maintainability of the aircraft needs to be well documented and easy to be performed. This includes a clear overview of maintenance periods, accessibility, procedures and standards.

Therefore, three different phases regarding the maintenance have been determined. These are the daily or every flight pre- and post-checks, the periodical check and the unscheduled maintenance period.

The daily checks contain a visual inspection of the aircraft and an analysis of the data recorded by pilot and instruments during the previous flight. If there are irregularities in the visual check or data analysis, the extent of the irregularities will be determined and documented in the aircraft logbook. To be able to determine the degree of severity of the irregularities each pilot is trained. This will be touched upon later in this section. The overall time period of the checks performed each day is estimated to be around 50 minutes. This is based on an estimated 5 minutes required per flight.

The second phase is the periodical mandatory full service check. The periodical check should happen every 12 months or every 800 flight hours. This periodical check is done by a trained aircraft mechanic with expertise on the H₂ERO. These periodical checks have a 10% allowable margin. Each periodical check is expected to take 24 hours or 1440 minutes. The periodical checks will happen at a specialised facility specifically tuned to maintain the H₂ERO. It is expected that this facility can replace and repair any significant damage within 24 hours as well due to the fact that the facility is well equipped with all necessary tools, parts and expertise. Maintenance will take longer for larger damages that are related to the unscheduled maintenance scheme.

The unscheduled maintenance scheme is difficult to apprehend. Unscheduled repairs can result in signifi-

cant availability loss of the aircraft. Often, these damages restrict the aircraft returning to the maintenance hub explained in the paragraph above. Hence, the aircraft needs to be transported over land or mechanics need to come to the aircraft itself with the necessary parts. From [55] a ratio has been determined between the amount of unscheduled maintenance versus the amount of scheduled maintenance as a function of the aircraft age. This relationship is shown in Equation 22.3.

$$\frac{T_{unsch.maintenance}}{T_{sch.maintenance}} = 0.0487 \cdot age_{aircraft} + 0.8397 \quad (22.3)$$

This results in a ratio ranging from 0.88 to 1.81 for an aircraft age of 1 year to 20 year respectively. On average, this ratio is 1.35 and results in an unscheduled maintenance time of 1.35 days or 1944 minutes a year.

22.3.1. Maintenance Requirement Compliance & Feasibility

Table 22.1: Overview of the requirements regarding the maintenance.

Code Identifier	Requirement	Type	Verification	Compliance
EVTOL-GNMA-161	Parts that require maintenance shall be accessible for inspection	Regular	Analysis	
EVTOL-GNMA-162	Parts that require maintenance shall be accessible for maintenance operations	Regular	Analysis	
EVTOL-GNMA-163	Part that require maintenance shall be replaceable or allow for maintenance operations to be performed	Regular	Analysis	

22.4. Safety

Regarding the high level of conceptuality that the design of the H₂ERO brings with it, safety has been a main focus throughout the entire period of the project. In this section the main risks regarding safety will be discussed. The focus is also mainly on the more unconventional sections of the design.

First, the fuel system. The H₂ERO is powered through a combination of batteries and liquid hydrogen fuel cells. As mentioned before, the liquid hydrogen is under pressure and highly explosive if its storage facilities malfunction. Therefore, the fuel tank wall thickness is greatly over designed for the fuel it is required to hold. Furthermore, the tank structure is checked periodically and the tank is separated from the passengers in its own protective compartment as mitigation actions.

Next, the design of the propeller systems was mainly designed for the noise reduction. However, the ducts around the VTOL propellers also protects bystanders from coming into contact with the propeller blades. The horizontal propeller at the rear of the fuselage is unducted. However, it is located between two tail boom struts and not close to any access door of the aircraft.

For the control redundancies, the H₂ERO makes use of various control surfaces. It has two rudders, two ailerons and two elevators. Furthermore, the H₂ERO can glide with its VTOL propeller system closed in the case the horizontal propeller malfunctions with the control surfaces still functioning.

One of the main points of safety that was regarded in the design is the passenger and patient safety within the aircraft. If a patient is transported within the aircraft, the medical stretcher is locked to the fuselage floor to keep it in place. Furthermore, the aircraft is designed too not require too large flight angles which ensures the transportation satisfaction of the patient during flight. The aircraft is also equipped with all necessary equipment to monitor and help the patient until the aircraft arrives at a hospital. Furthermore, there is space for a doctor and a passenger in the cabin to come along.

22.4.1. Safety Requirement Compliance & Feasibility

Table 22.2: Overview of the requirements regarding safety.

Code Identifier	Requirement	Type	Verification	Compliance
EVTOL-GNSA-151	The aircraft shall allow for safe storage of the medical equipment	Regular	Analysis	
EVTOL-GNSA-152	The aircraft shall be able to safely land and take off in populated areas	Driving	Analysis	
EVTOL-GNSA-153	The aircraft shall be controllable in every stage of flight	Driving	Analysis	
EVTOL-GNSA-154	The passenger shall be transported safely	Regular	Analysis	
EVTOL-GNSA-155	The aircraft shall be able to take off and land on all paved and unpaved surfaces with a minimum hardness of TBD	Regular	Analysis	
EVTOL-GNSA-156	The aircraft design shall allow for safe entering and exiting of the crew	Driving	Analysis	
EVTOL-GNSA-157	The aircraft design shall allow for safe loading and unloading of the patient	Driving	Analysis	
EVTOL-GNSA-158	The medical equipment shall not interfere with the aircraft avionics	Driving	Analysis	

Sustainability Analysis

This chapter discusses the application and results of the sustainable development strategy for the three main categories: environmental, economic and social, as explained in chapter 4. For these an analysis is done on the sustainable approach in the subsystem design. Finally, a result of the aircraft's sustainability in comparison with the existing emergency aircraft (EC-135) will be shown.

The final analysis is visualised in a radar chart for which a scale from zero to five is used. In the paragraphs below a score is given for each criterion in the plot for both the H₂ERO and the EC-135.

The analysis is performed as if the aircraft is ready for operations. This is considered to be in 15 years, 2034, because of further research and testing that still needs to be done.

23.1. Environmental Sustainability

Increasing Life Time

Increasing the life time of the aircraft benefits environmental sustainability, because it decreases the amount of aircraft (replacements) needed in the long term and hence reduces mining of raw materials and waste production. The technological life can be elongated easily, as long as there are spare parts available and proper maintenance is done to keep the aircraft airworthy. However, the economic life of the aircraft is very limited. Maintenance will get more difficult and expensive with increasing life and aircraft with newer technology will have a higher demand and are more profitable. Therefore, a way should be found to optimise maintenance and implementation of new technologies in order to elongate the life time as much as possible. Thus, the aircraft is designed for easy and effective maintenance and replacement procedures. An example of this is the use of advanced software and sensors to monitor the condition of engines. These diagnostics allow for fast data collection which will reduce the amount of physical checks needed and therefore make the maintenance program easier.

Reconditioning of the aircraft also elongates the life span, as will be explained in the section below.

Both the EC-135 and the H₂ERO will require extensive maintenance as they get older and will need upgrades, which is included in both designs. However, more focus on this maintenance and possibilities is included in the design of the H₂ERO and it is included in its operations plan. Therefore, H₂ERO gets a higher score than the EC-135: 4 and 3 respectively.

End of Life Procedures Reducing Waste

An important element of environmental sustainability is to minimise the waste produced (and reduce the mining of new raw materials as well). This can be done by repairing, reconditioning, remanufacturing and recycling the aircraft parts and/or materials. The difference between them and the cycle is illustrated in Figure 23.1.

Repair is the best option for environmental benefit, since less energy is needed and all material is reused [?]. AELS (Aircraft End-of-Life Solutions) provides an extensive list of aircraft parts they sell after having disassembling ¹. They range from motor

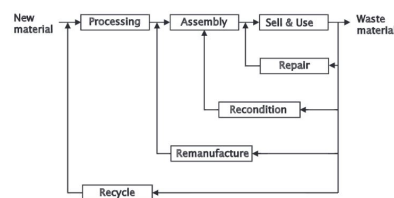


Figure 23.1: Visual cycle of repairing, reconditioning, remanufacturing and recycling [24].

¹<https://www.aels.nl/search-stock> [accessed 2019-06-18]

elements, GPS antenna's, valves, fuel pumps, rudders, elevator surfaces, joysticks, gearboxes and sensors to smoke detectors, (cockpit) microphones and seats. However, generally the quality is significantly reduced and there is no or little warranty. For this reason reusing aircraft's parts should be done with care and expertise, in order to always guarantee safety. Airlines can part out an aircraft and gain much profit, especially if the spare parts are in high demand. Life limited parts (parts that have a mandatory replacement deadline), including the auxiliary power unit, brakes, emergency escape slides, flap carriage, landing gear and RAM air turbine can hardly be reused in other aircraft.

Reconditioning involves rebuilding or replacing parts that failed or are close to failing to allow for extended use. The same issue as with repair occurs, namely the reduced quality and little warranty compared to the original new product. This can be done after disassembling or on the current aircraft to increase the life span. Reconditioning is not just maintenance, but involves more intensive and detailed upgrades. An example of exterior reconditioning is surface wash which extensively cleans the surface of debris and impact spots. Also, brightwork metal polishing can be done, which restores scratches and gouges in engine inlets, propeller elements and leading edges. Also, De-ice boot refurbishment conditions and seals the boots, extending their life.

Contrasting to repair and reconditioning, remanufacturing does result in products that are at the same performance level as the original product and is thus given similar warranties. It is an often used practise in the aerospace industry. It dismantles the product, retrieves the core and perform restorations or part replacement were needed. After reassembly and proper quality testing, the product can safely be used again. Hence for the benefit of environmental sustainability, remanufacturing preserves the energy that has been used to make the components originally and reuses the material. Remanufacturing only requires about 20-25% of the energy used in its original production [?]. An additional advantage of remanufacturing is the feedback on reliability and durability obtained from the dismantled components. Remanufacturing is also a term used for integrating new systems and sensors in existing airframes. Challenges for remanufacturing lie in legislation limits and its time consuming process. An example of a high level remanufacturing process is replacing skin sections suffering from fatigue in the existing airframe. Other aircraft remanufacturing examples include placing a new avionics system, changing the interior cabin design and installing new engines.

Parts that cannot be reused are recycled after dismantling. They are sorted, processed and used for making new products. Issues for recycling involve uncertain quality and supply. The energy used in production of the original product is lost, because energy is required to shape the new product with the recycled materials. Thus, it benefits to environmental sustainability the least, but is still a more environmentally sustainable solution compared to burning fuel or filling land sites. Aircraft materials can be recycled. After breaking down the shell with an These include the materials used for the H₂ERO: glare, carbon fibre, aluminium, titanium and plexiglass as explained in section 10.4. The hydrogen tanks can either be made of monolithic metal or tailored composites [62]. All of these materials are usually downcycled, and are used as raw material for new products². Also the key materials of the fuel cell can be recycled using a efficient and environmentally friendly approach using a sulfuric acid treatment. About 95% of the platinum and nearly all of the Nafion can be recycled. The performance of the recycled Nafion is close to that of originally used Nafion [63].

A similar score is given to both the H₂ERO and the EC-135, since for both the disassembling and dismantling procedures can be defined in such a way that waste production is minimised. This results in a score of 4.

Design Choices in Material Selection and Production Plan

Environmental sustainability is an important factor in material selection and production plan and is discussed in the relevant chapters (chapter 18 and chapter 10). Therefore, this analysis will not be repeated here but is mentioned for the sake of consistency.

The production plan for the EC-135 and the H₂ERO are similar as well, so both aircraft would receive the same score for this one. They also use the same materials: titanium, glass reinforced plastic, aluminium and carbon composites. However, the H₂ERO is larger and will use more material than the EC-135. Therefore, the EC-135 gets a score of 4 and the H₂ERO gets a score of 3.

²<https://www.aels.nl/sites/aels/files/original/news/file/atemparticle.pdf> [Accessed 21 June 2019]

Emissions and Energy Sources

Apart from noise reduction, the most important aim for the H₂ERO is to design for the absence of harmful emissions. The only emissions present is water vapour.

Water vapour is less polluting for the environment than the emissions from fossil fuels, which include CO₂, SO₂, Pb, AS, Hg and Cd [35]. The EC-135 emits 780 kg CO₂ emission per hour [45], whereas the H₂ERO emits zero CO₂.

Apart from direct emissions, the supply of the energy carrier should be investigated as well. The energy sources used are hydrogen (input for the fuel cell) and electricity from the grid (to charge the battery when on the ground). In order to analyse the environmental sustainability for those, the emissions and energy required to produce 1 kWh of electrical energy are analysed [2]. The emissions are expressed in grams of carbon dioxide per kWh for all different processes.

For the electricity source two cases are considered: the average European electricity mix (29% renewables, 26% nuclear, 20% gas and 25% coal) and a 'green mix' (90% renewables, 10% gas). The emissions and energy consumed to create 1 kWh for the average electricity mix are 404 gCO₂/kWh and 1.73 kWh/kWh. In the green scenario this would be 85 gCO₂/kWh and 0.34 kWh/kWh respectively [29]. For the hydrogen, the liquefaction process is analysed. When electrolysis is used on the European average electricity mix, the liquefaction process emits 915.4 gCO₂/kWh and consumes 4.51 kWh/kWh in energy. When steam methane forming is used to liquefy the hydrogen, it emits 463.8 gCO₂/kWh and 1.16 kWh/kWh energy is consumed [29]. The fuel cell are estimated to require 9.9 kgCO₂/kWh to be produced and the hydrogen tanks 7.9 kgCO₂ per kg tank mass [29].

In Figure 23.2 an overview is given on the emission for different powertrains. Here it can be seen that hydrogen emits far less compared to kerosene fuel.

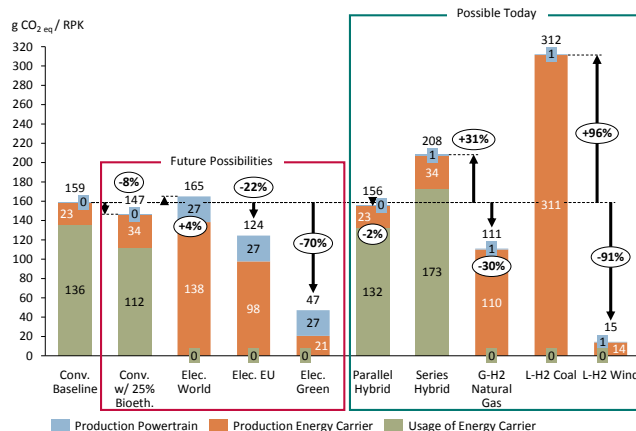


Figure 23.2: Summary of emissions from different powertrains fitted to a small propeller aircraft [29].

Therefore, the H₂ERO scores much better in terms of emissions compared to the EC-135. A score of 5 and 1 is given on emissions respectively.

23.2. Social Sustainability

Noise

The most important goal of H₂ERO is to reduce the noise level compared to the current emergency aircraft. Currently, the emergency aircrafts based at airports have to compete against commercial flights. Especially during the night this is an issue, since the emergency aircraft accounts for 25% of the maximum allowed noise in Rotterdam Airport, as stated by the emergency aircraft pilot interviewed. Other solutions such as the feasibility of moving the base from the airport to a new location have not been successful, yet it is pleaded that the emergency aircraft is of vital importance to society³. Therefore, a new aircraft reducing

³<https://www.ad.nl/politiek/traumaheli-in-de-knel-door-geluidsregels-ziekenhuizen-eisen-maatregelen~a6fb85db/> [accessed 2019-06-19]

the noise will be a good solution for the current noise problems. As stated in chapter 5 the noise reduction of H₂ERO is 25% less than the EC-135.

Therefore, the final scores are 5 and 2 for the H₂ERO and EC-135 respectively.

Technical Readiness Level

The Technology Readiness Levels (TRL) is another important factor in the acceptance of H₂ERO in the society it operates in. The customers and users need to trust the aircraft before they will buy or use it. Currently the TRL of H₂ERO is lower than the EC-135, because of the use of a fuel cell on hydrogen, the VTOL lift + cruise aircraft configuration and the rotors integrated in the wing. As can be seen in Figure 23.3, the H₂ERO is between level 1 and level 2 whereas the EC-135 has reached level 9. This will be improved after a more detail design is done and complete prototypes are made, which will require much research and investments. An overview of research and developments that need to be done in order to increase the TRL to the same level as currently flying aircraft is presented in chapter 24.

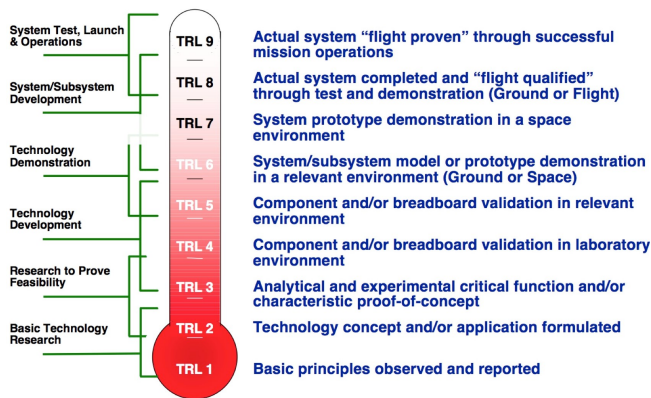


Figure 23.3: Definition of Technology Readiness Level created by NASA and adopted by EU [13].

Now the H₂ERO lacks far behind the EC-135 in terms of TRL. However, since this aircraft sustainability analysis is done as if it is 2034, when the H₂ERO is ready to be operated, both the EC-135 and H₂ERO will have a TRL of 9. The EC-135 will have decades more of experience, so will receive a slightly higher score than the H₂ERO for TRL: 5 and 4 respectively.

Regulations

When design choices were dependent on regulations, a combination of both helicopter and aircraft EASA legislation were used. However, regulations are constantly adapted to technological advancement, and it is therefore expected that in 15 years, when H₂ERO is ready to fly, the regulations will have been adapted or created accordingly. New regulations must be made or adapted from current ones for VTOL configuration in general and the use of hydrogen fuel cells. Already EASA is working on a special condition for small VTOL aircraft ⁴.

When the H₂ERO is ready to enter service, the regulations are expected to be fully up to date. Therefore, both the EC-135 and H₂ERO will adhere fully to the regulations, indicating an equal score of 5 for both.

Renewable Energy and Emissions Reduction

Because the H₂ERO only emits water vapour, it will contribute positively to air quality and will therefore benefit the quality of life for society. Also, the use of renewable energy, namely the hydrogen fuel cell, will ease the acceptance of this new aircraft by the public, because a general shift from fossil fuels to renewable energy has become the norm [48]. The H₂ERO has the potential to replace other missions as well next to the emergency aircraft. The emergency aircraft's medical air assistance service makes it a visible and sympathetic mission to the public. Therefore, it is the perfect vehicle to show the change from fossil fuels to renewable energy and the possibilities to reduce noise significantly in the aerospace industry.

⁴<https://www.easa.europa.eu/sites/default/files/dfu/SC-VTOL-01%20proposed.pdf/> [accessed 2019-06-19]

Because the H₂ERO performs much better in terms of renewable energy and acceptance in society in terms of emissions and noise, it gets a score of 5 whereas the EC-135 gets a score of 3.

23.3. Economic Sustainability

The two main factors for economic sustainability are costs and risks. The detailed cost analysis can be found in chapter 20 and the detailed risk management in chapter 21. In the paragraphs below a summary will be given and a comparison to the EC-135.

Design and Production Costs

The H₂ERO is designed based on the new lift + cruise concept without any prior experience with similar vehicles. In contrast, the EC-135 was an iteration on an already existing helicopter design (the BO-108 by MBB, later Eurocopter)⁵. Therefore, the design costs for the H₂ERO will be much more than the EC-135, because new techniques that are used, more research that needs to be done and the absence of prior experience. Production costs will also be higher due to the fact that the H₂ERO is bigger and will thus require more material, hence more costs.

Therefore, the EC-135 scores 4 and the H₂ERO scores 2 on design and production costs.

Operational Costs (Including Maintenance)

The operational costs will be less for the EC-135, mainly because kerosene is cheaper than hydrogen. The cost of Jet A-1, the kerosene currently used for helicopters, is about 0.61 \$/kg⁶. The fuel consumption at economical cruising speed is 205 kg/h at maximum weight for the EC-135. So for one hour at cruise, this adds up to \$125.1 of kerosene. The costs for liquid hydrogen are 8.29 \$/kg⁷. As calculated in chapter 6, the H₂ERO has a fuel consumption of 35 kg/h for maximum weight and cruise speed. This adds up to \$290.15 for one hour cruise flight for the H₂ERO, significantly more than than the EC-135.

Compared to the EC-135 the H₂ERO does not have any complex gearboxes or combustion which will reduce the maintenance costs. However, the H₂ERO has five rotors and five motors whereas the EC-135 has two rotors and two engines, so the H₂ERO will require more expensive maintenance on its rotors and engines. The general maintenance done on inspection, cabin and landing gear are similar for both aircraft. Therefore, the costs for maintenance are estimated to be similar for both the EC-135 and the H₂ERO.

Thus the scores for operational costs are 4 and 3 for the EC-135 and the H₂ERO respectively.

Disassembly and Dismantling Costs

Disassembly is economically feasible since valuable components of the aircraft are removed and sold to be used as spare parts. Dismantling is economically feasible because of the metal and plastics reclamation which can generate some revenue [5]. Since the same materials are used for the EC-135 and the H₂ERO, they will both benefit. The H₂ERO has more material, however, so is expected to gain more money from end of life procedures.

Although the overall configuration of the H₂ERO is unconventional, the main components (fuselage, wing, tail, rotors, engines) are not different from existing aircraft. It is expected that similar procedures and tools as are used for other aircraft can be used to dismantle the H₂ERO as well. Additional challenges may lie in the hydrogen tanks and fuel cell, which is a new system. With adequate support from the manufacturer, it is expected that these challenges will not pose problems to the dismantling operators.

Thus, both the EC-135 and the H₂ERO are expected to have the same disassembly and dismantling costs and are therefore given the same score of 4.

⁵<https://www.helis.com/database/model/MMB-Bo-108/> [accessed 2019-06-19]

⁶<https://www.iata.org/publications/economics/fuel-monitor/Pages/index.aspx> [accessed 2019-06-21]

⁷<https://clipair.epfl.ch/wp-content/uploads/2018/08/FullReportMA3.pdf> [accessed 2019-06-21]

Risk Management and Contingency Plans

The detailed risk identification, management and contingency plans can be found in chapter 21. It will not be repeated here, but is mentioned for the sake of consistency, since it is a part of the economic sustainability.

The risk management and contingency plans will continuously be updated up to entry into service, the phase considered for this sustainability analysis. Therefore it will be expected to be well developed and at the same level as the EC-135 by 2034. Also, Airbus, the manufacturer of the EC-135 uses proper risk management and contingency plans which can be expected of a well established company with this large amount of resources, production scale and product sales. Both the EC-135 and the H₂ERO have adequate risk management and contingency plans, so score a 4.

23.4. Sustainability Overview and Conclusion

The results explained above are graphically represented in Figure 23.5. If all the scores are added H₂ERO scores 48 and the EC-135 scores 43 (where the maximum would be 12 categories times the maximum score of 5 equals 60). This indicates that H₂ERO is expected to be slightly more sustainable than the EC-135. The main reasons for this are the non-harmful emissions and noise reduction, resulting in a better score on environmental (and to a lesser extent social) sustainability, as visualised in Figure 23.4.

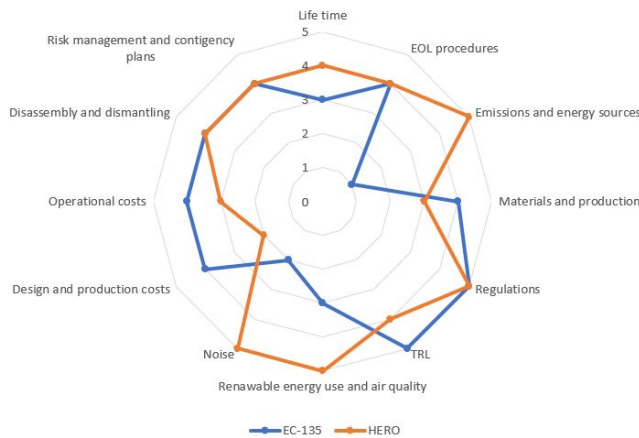


Figure 23.4: Overview of the sustainability analysis for H₂ERO and EC-135. Starting from the top, environmental, social and economic sustainability factors are indicated in clockwise direction respectively.

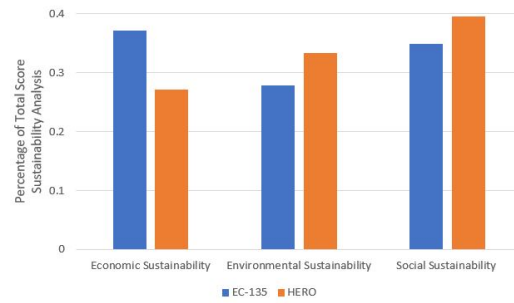


Figure 23.5: Overview of sustainability analysis for H₂ERO and EC-135 for the main categories.

Future steps

This chapter will elaborate on the steps that will follow the finalisation of the final design research. The first steps that can be researched and reviewed on the final design have already been elaborated on in chapter 16.

24.1. Future Project Development

Once we come to the end of the final design phase of this project, this is not where it all stops. The project will be further developed, improved, produced, tested, marketed and sold. Figure 24.1 shows an overview of the general way the next steps of this project are expected to be taken. Firstly, the team will review, present and publish its findings to their customer. Besides the customer, due to the research that has been done, it is expected that other individuals might be interested in the research as well. Hence, presenting at seminars or conferences is not left out as a possibility.

To further enhance the worldwide interests into the design and research that has been performed, the core team is expanded with a marketing and financial acquisition team. The marketing team should be able to create promotional materials to help the financial team acquire new customers, possibilities and further enhance the strength of Fokker-GKN in the aircraft industry.

Next, a prototype should be built to go along with the marketing and acquisition aspects of the project. For the prototype an assembly line is set-up with all relevant machines, personnel and materials.

Following the prototype production is the testing and validation of the prototype to see its potentials. During testing also new data can be acquired for which the aircraft can be altered and optimised. Therefore, the aircraft should be reviewed and improved after the prototype validation.

Before production of the actual aircraft can begin, the aircraft needs to be certified. This will happen with the help of the validation tests of the prototype. Should the aircraft not pass any certifications, the aircraft design should be revisited, improved and the testing and validation phase should be reperformed. This process should be repeated until the aircraft passes the certification tests.

Once the aircraft has received its certifications it can be produced in larger quantities in the final production phase. The prototype assembly line should be revisited to see if it works sufficiently for larger quantities. Any parts of the assembly line that are not sufficient should be updated with better machinery and personnel.

Finally, the aircraft can be distributed to their customer throughout the world. It should be noted that this can only happen with a good transport logistical plan. Hence, this will be set-up first before distribution starts. Once the aircraft is distributed and arrives at the customers the process is completed. However, this process is of course a continuous process for each aircraft that is ordered.

The future steps mentioned above are put on a time line in form of a Gantt chart, depicted in Figure 24.2. It is not detailed, but gives a broad overview of the timeline of future steps in the design project.

24.2. Expectancy

In general, the design process of commercial aircraft from drawing board to full scale production can take up to a decade or longer. For the H₂ERO, due to its conceptuality and hence higher amount of testing that will be required, it is expected to take around 15 years to be able to produce larger amounts of full scale products. Also, this 15 year expectancy is in line with current contracts that for instance, the ANWB has with Airbus for the EC135 helicopter. These contracts will end in 15 years. Hence, when the contract for the ANWB is won by the H₂ERO, the aircraft will be able to roll out of the assembly line.

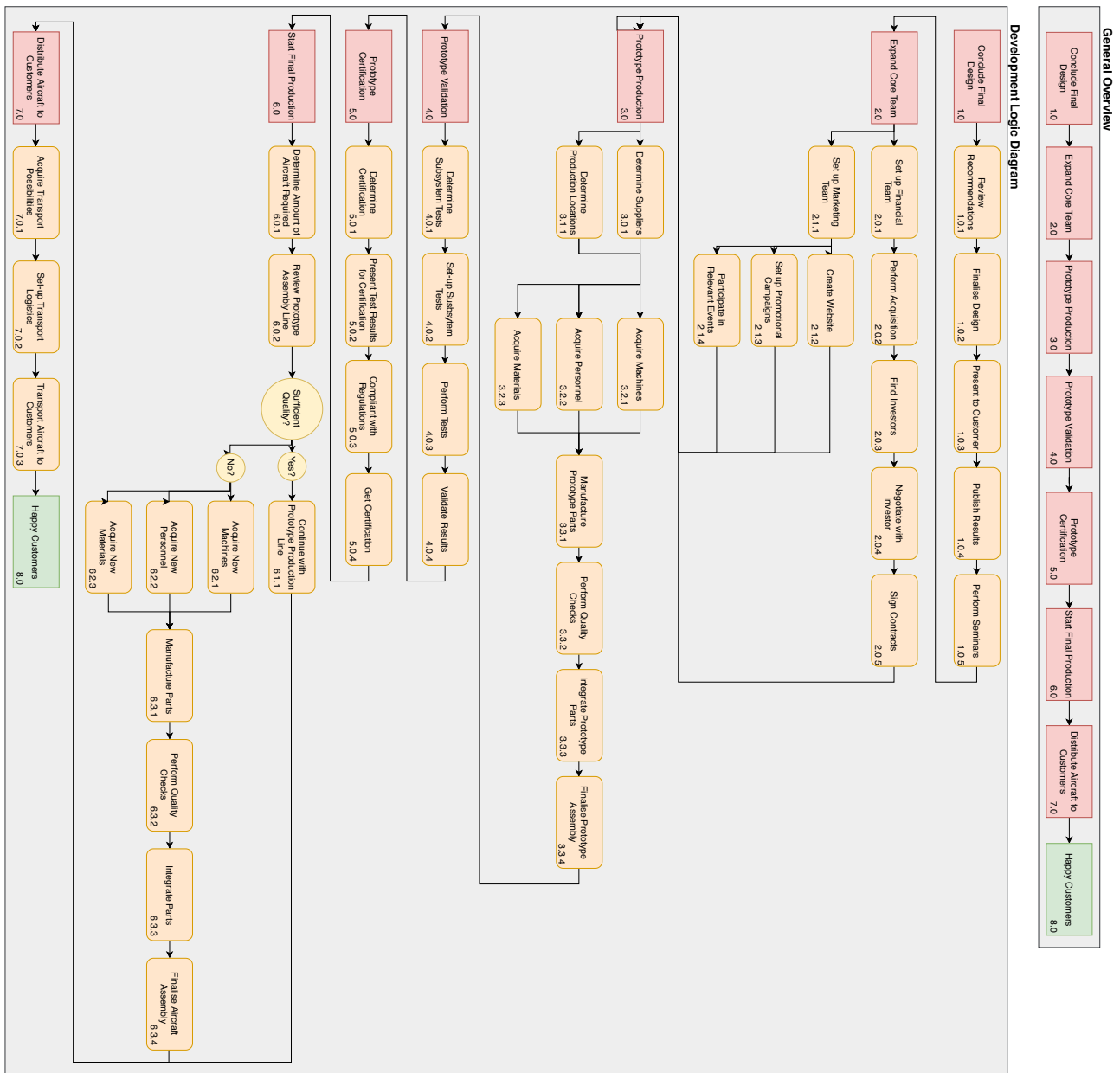


Figure 24.1: Project Future Development Overview.

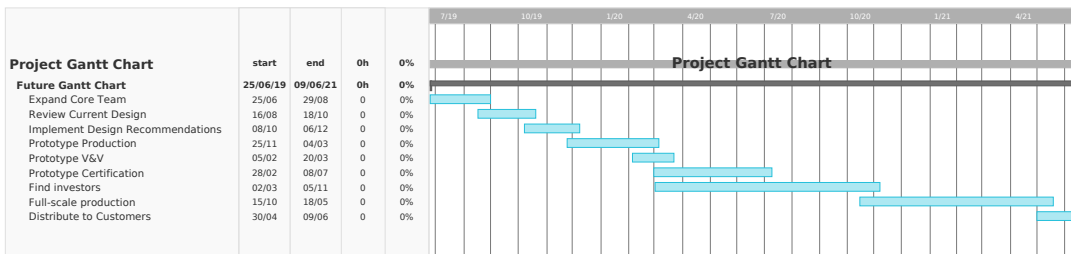


Figure 24.2: Gantt Chart for future steps.

Conclusion

The goal of this report was to generate a final detailed design for the H₂ERO. Besides subsystem design and the aircraft configuration design, costs, risks, operations and production were analysed for this. Furthermore, it was checked whether the requirements are met, which is a driving factor for successful designing the aircraft.

The propulsion group looked into the rotors and how to reduce the noise they produce, the fuel system and the electrical system were designed and sized for. For the aerodynamics subsystem, an airfoil with desired characteristics was chosen and the transition phase was analysed. It was chosen to not make use of a blended wing body, as this would not be very beneficial for the design, while it would make it harder to design. In the stability and control analysis, it was found that having both rotors inside the wing is impractical, which is why the front propellers are now outside the wing. Furthermore, the dimensions of the aircraft and the location of all subsystems was determined. In the structural analysis, the wing was designed to fit a propeller inside. The medical cabin was designed to be of minimum dimensions, while still providing enough space for the doctor to perform all necessary operations and for the patient to fit on a stretcher. Moreover, the fuselage design was looked into, which is somewhat different than for aircraft due to the extra vertical propellers. During the integration, all subsystems were put together and after several iterations, a final design was generated, with the most important parameters being four vertical propellers, of which the smaller front propellers are not integrated in the wing, one horizontal propeller for forward propulsion, a fuselage length of 11 meters, a span of 18.13 meter and a MTOW of 4150 kg.

Looking at the top level requirements and the performance, the range is met as this is 346 km, 96 kg more than required at a speed of 298 km/hour, which is 48 km/hour more than required as well as faster than the current emergency helicopter, the EC-135, which has a maximum speed of 259 km/hour. More importantly, the noise reduction of 25% compared the EC-135 is reached for the H₂ERO while being electrically powered.

From the cost analysis, it was concluded that the budget of 3.5 million\$ will most likely not be met due the innovative nature of the design. All requirements from the RAMS analysis are met due to the fact that the H₂ERO can take-off like a helicopter and fly like an airplane. From the sustainable analysis, it was found that although the economic sustainability of the EC-135 is better, the H₂ERO outperformed it in terms of environmental and social sustainability.

Finally, recommendations on the design were given. Most important is the recommendations to look into the transition from VTOL to forward flight, as the rotors in the wing have to be covered somehow while the wings already produce lift. Furthermore, the influence of the rotors in front of the wing has to be analysed.

Future steps will include looking into the above mentioned recommendations, after which the design can be further developed and a prototype can be made. After optimisation, the certification can start and finally, the aircraft can be put on the market. It will be setting an example for sustainable less noisy aircraft, which will be allowed to fly off from its base at any time to save lives, as only a H₂ERO can do.

Bibliography

- [1] Technical data. *Recent Waterscapes*, 2013.
- [2] TU DELFT DSE Design Group 11. evtol emergency aircraft midterm report. 2019.
- [3] von Doenhoff A.E. Abbott, I.H. *Theory of wing sections*. McGraw-Hill Book Company, 1959.
- [4] P.T. Arévalo. Design optimization of a composite wing box for high-altitude long-endurance aircraft. 2014.
- [5] SGI Aviation. Aircraft decommissioning study. 2018.
- [6] Boerner. Basic design of flying wing models. 2019.
- [7] T. Bresciani. Modelling, identification and control of a quadrotor helicopter, 2008. Student Paper.
- [8] Brett D.J.L. Browning D. Brandon N.P. Cai, Q. A sizing-design methodology for hybrid fuel cell power systems and its application to an unmanned underwater vehicle. 2010.
- [9] Stefanescu I. Ionete R. Ene H. Ingham-D. Ma L. Carcdea, E. Pem fuel cell geometry optimisation using mathematical modeling. *The International Journal of Multiphysics*, 2008.
- [10] Huicui Chen, Pucheng Pei, and Mancun Song. Lifetime prediction and the economic lifetime of proton exchange membrane fuel cells. *Applied Energy*, 142:154–163, 2015.
- [11] Liu H.J. Chen, D.Z. The design and construction of a liquid hydrogen transfer line. 1995.
- [12] L.U. Dadone. Design and analytical study of a rotor airfoil. *Office*, (May), 1978.
- [13] B. Dunbar. Technology readiness level. NASA, 2012.
- [14] J. Elkington. *Cannibals with forks: the triple bottom line of 21st century business*. 1999.
- [15] Beziac H.L. Gilbert F.A. Euler, A. Method of manufacturing a helicopter rotor blade, 1981.
- [16] Thring R.H. Fly, A. A comparison of evaporative and liquid cooling methods for fuel cell vehicles. *International Journal of Hydrogen Energy*, 41(32):14217–14229, 2016.
- [17] C.R. Frischtak. Learning and technical progress in the commuter aircraft industry: an analysis of embraer's experience. *Research Policy*, 23(5):601 – 612, 1994.
- [18] S. Gudmundsson. *General Aviation Aircraft Design - Applied Methods and Procedures*. 2014.
- [19] Snorri Gudmundsson. General Aviation Aircraft Design. pages 774–783, 2014.
- [20] D. Haynie. What is the working mechanism of the lens' aperture in dslr cameras? 2018.
- [21] Diepenhorst T. Lin R. Hulbert, D. Fuel cell air intake system. 2009.
- [22] Angilella A. Reddinger J.P. Howard A. Misiorowski-M. Pontecorvo M. Krishnamurthi J. Jacobellis, G. The emperor uav: Executive summary. 2013.
- [23] T. Kim. Reduction of tonal propeller noise by means of uneven blade spacing. 2016.
- [24] Burgess S.C. Ijomah W. McMahon C.A. King, A.M. *Reducing Waste: Repair, Recondition, Remanufacture or Recycle?* 2006.
- [25] P.C. Klein. Parametric modeling and optimization of advanced propellers for next-generation aircraft. *MSc Thesis, TU Delft*, 2017.
- [26] A.K. Kundu. *Aircraft Design*. Cambridge University Press, 2010.
- [27] Price M.A. Riordan D. Kundu, A.K. *Conceptual Aircraft Design: an industrial approach*. John Wiley Sons, 2019.
- [28] W. Liang. Attitude estimation of quadcopter through extended kalman filter. 2017.
- [29] Stumpf E. Lueckhof, J. *Well-to-Prop – A Holistic Analysis of Emerging Powertrain Concepts for On-Demand Air Mobility Vehicles*.
- [30] T.H.G. Megson. *Aircraft Structures for Engineering Students*. Elsevier Ltd, 2007.
- [31] Doolan C. Moreau, D. J. Noise-reduction mechanism of a flat-plate serrated trailing edge. 2013.
- [32] Hirose K. Mori, D. Recent challenges of hydrogen storage technologies for fuel cell vehicles. *International Journal of Hydrogen Energy*, 2009.
- [33] A.P. Mouritz. 9 - titanium alloys for aerospace structures and engines. In *Introduction to Aerospace Materials*, pages 202 – 223. Woodhead Publishing, 2012.
- [34] NASA. Appendix c : Cost estimating methodologies. *NASA Cost Estimating Handbook*, (February 2015):1–42, 2015.
- [35] Arcuri N. Nicoletti G. Bruno R. Nicoletti, G. A technical and environmental comparison between hydrogen and some fossil fuels. 2014.
- [36] Cha S.W. Colella W. Prinz F.B. O'Hare, R. Fuel cell fundamentals, 3rd edition. *The International Journal of Multiphysics*, 2008.
- [37] F. Oliviero. Aircraft weight balance. 2018.
- [38] F. Oliviero. Ae3211-i: Requirement analysis and design principles for aircraft stability & control. 2018.
- [39] F. Oliviero. Ae2111-ii: Aircraft aerodynamic analysis - lift & drag. 2018.
- [40] F. Oliviero. Ae2111-ii: Aerodynamic analysis: software tools. 2018.
- [41] Dr. V. H. Perry. Measurements of the moments of inertia of the avro 707 b aircraft. 1961.
- [42] Alley N.R. Phillips, W.F. Predicting maximum lift coefficient for twisted wings using lifting-line theory.
- [43] Kadrigama K. Vijayan S. Ramasamy, D. Design optimization air intake system of 1.6l engine by adding guide vane. *National Conference in Mechanical Engineering Research and Postgraduate Students*, II, 2010.
- [44] Hibma R. Heeg L. Scott H. Child-R. Owl G. Maier R. Mcgachan E. Robinson D. White S. Hoge H. Robinson M. Palmer G. Yang H. Swaim R. Sun C.T. Schmidt D. Reese B. Heiser W. Raymer G. Raymer, D.P. *Aircraft Design : A Conceptual Approach*.
- [45] T. Rindlisbacher. Division aviation policy and strategy guidance on the determination of helicopter emissions. *Director*, 2009.
- [46] Merino Martínez R. Avallone F. Ragni-D. Snellen M. van der Zwaag S. Rubio Carpio, A. Experimental characterization of the turbulent boundary layer over a porous trailing edge for noise abatement. *Journal of Sound and Vibration*, 2019.
- [47] G.J.J. Ruijgrok. *Analysis of a Contra-Rotating Propeller Driven Transport Aircraft*. 2004.
- [48] Grin J. Rotmans J. Schot, J. Governing the energy transition. 2012.
- [49] van den Brink J. Köhler-A. Silvius, A. J. G. The impact of sustainability on project management. 2012.
- [50] J. Sinke. Manufacturing of glare parts and structures. *Applied Composite Materials*, 10(4):293–305, Jul 2003.
- [51] R. Slingerland. Prediction of tail downwash, ground effect and minimum unstick speed of jet transport aircraft. 2005.
- [52] E. Torenbeek. Synthesis of subsonic airplane design, 2013.
- [53] M.D. Trexler. Development of a novel erosion resistant coating system for use on rotorcraft blades. 2012.
- [54] Nguyen N.V. Kim S. Lee J.W. Tyan, M. Comprehensive preliminary sizing/resizing method for a fixed wing – vtol electric uav. *Aerospace Science and Technology*, 2017.
- [55] M. Urdu. Aircraft maintenance cost modelling considering the influence of design parameters, 2015.
- [56] J. Van Craenbroeck. Boundary layer suction configurations with minimal pump requirements for multi-element airfoils.
- [57] J.J.A. van Kuijk. Analysis of swirl recovery vanes. *Delft University of Technology*, 2015.
- [58] Melkert J.A. Vos, R. Wing and propulsion system design. volume 6, page 103. 2017.
- [59] Horvath B.L. Wells, D.P. The flight optimization system weights estimation method. June 2017.
- [60] Wada C. Widodo, R.B. Attitude estimation using kalman filtering: External acceleration compensation considerations. *Journal of Sensors*, 2016:1–24, 2016.
- [61] Kadyk T. Bensmann B. Krewer U. Hanke-Rauschenbach R. Winnefeld, C. Modelling and designing cryogenic hydrogen tanks for future aircraft applications. 11, 2018.
- [62] Kadyk T. Bensmann B. Krewer U. Hanke-Rauschenbach R. Winnefeld, C. Modelling and designing cryogenic hydrogen tanks for future aircraft applications. *Energies*, 2018.
- [63] Mu S. Pan M. Xu, F. Recycling of membrane electrode assembly of pemfc by acid processing. 2009.